

Investigation into the Mechanisms and Consequences of Explosions of Premixed Gaseous Combustibles with Detailed Chemical Kinetics

JOSEPH OWEDE ADOGHE

M.Sc. FIRE SAFETY ENGINEERING (2014)

M.Sc. ANALYTICAL CHEMISTRY (1992)

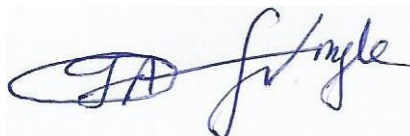
Submitted in partial fulfilment of the requirements for the degree of
Doctor of Philosophy

School of Engineering
University of Central Lancashire
2023

Statement of Original Authorship

The work contained in this thesis has not been previously submitted to meet requirements for an award at this or any other higher education institution. To the best of my knowledge and belief, the thesis contains no material previously published or written by another person except where due reference is made.

Signature:

A handwritten signature in blue ink, appearing to read "J.A. for myle". The signature is written in a cursive style with a large, stylized initial "J.A." followed by "for myle".

Date: 8th November 2022

Acknowledgements

I wish to deeply acknowledge my supervisors, Dr. Weiming Liu and Dr. Jonathan Francis for their awesome supervisions, and Prof. Champika Lasanthi Liyanage for her unalloyed support as well as Dr. Akinola Adeniyi for his role as my referee during my transfer. Also, I wish to deeply appreciate Petroleum Technology Development Fund (PTDF) for the scholarship awarded to me to study and complete this programme. I would like to appreciate the University of of Central Lancashire, Preston, UK for providing the AMROC tools that gave a unique basis for this study.

I also wish to acknowledge my beloved family - Mrs. Patience Odion Adoghe (wife), Favour Osahioria Adoghe (daughter), Joshua Enosakhonan Adoghe (son), Emmanuel Enosadeba Adoghe (son) and Deborah Enosamudianan Adoghe (daughter) for their love, understanding, prayers and encouragements.

Keywords

Adaptive mesh refinement, Direct numerical simulation (DNS), Deflagration, Deflagration-to-Detonation, Detonation, Combustion waves, Explosion, Flashover, Backdraft, Hugoniot curve.

Abstract

Detonation is a self-sustaining combustion wave with a rapid reaction process and a propagation speed. It is a central topic in combustion and serves a significant role in the theory and the application of combustion. The volatility of petroleum products and crude oil in the downstream and upstream sectors of the oil and gas industry constitutes a high degree of fire explosion risks and disasters thereby leading to losses of over 528 lives, more than 1,289 persons injured, over 1,280 nearby homes burnt, and numerous workshops destroyed, large quantities of barrels of crude oil spilled into the environment and billion dollar projects burnt down. The aim of this project is to explore the effects and influences of chemical kinetics and geometric configurations to the wave behaviours using computational fluid dynamics (CFD) approach. Mathematical models and numerical methods will be employed in solving the problems in this research work. This project report focused on numerical investigation of indirect initiation of detonation using direct numerical simulations (DNS). In this simulation, the chemical combustion reactions are ignited in a shock tube and then the processes of transition of deflagration to detonation (DDT) were explored. The DNS database provides a source to investigate the influences and effects of chemical kinetics of explosions on hydrogen-oxygen and propane oxygen combustion reaction processes were explored. For this work, the CFD programme employed is an Adaptive Mesh Refinement in object-oriented C++ (AMROC) tools which can be executed in parallel processes to obtain an accurate DNS database on the chemical kinetics of the elements.

From the simulation results, the influences, and the effects of chemical kinetics of explosions on hydrogen-oxygen and propane oxygen combustion reaction combustion reactions were investigated; and slow flame (called laminar flow), fast flame, DDT and Detonation data were obtained. When the concentration was low, the reaction rate was very slow, no DDT and no detonation were achieved, but when the concentration was high/large, the reaction rate was very fast, and thus DDT and detonation would be formed and consequently explosion occurred. Exploring the influence of free radical H on flame propagation, it was found that in each case study, as the concentration of the reacting species increases, the flame speed increases for each propagation for certain limited duration. The results showed that as the flame moves through more

volume, more fuel is thereby being burnt and so, less free radical, H around that is being burnt.

Moreover, in this research work, the influences and effects of geometric configurations on explosion of hydrogen-oxygen and propane -oxygen mixtures using numerical simulation method were equally investigated. Hence, when vent is created in the tube, DDT will occur and consequently detonation is achieved, and vent explosion took place. Moreover, for closed end tube such as that of case study with one Block, the block constituted an artificial obstacle, hence, FD, DDT, and detonation were formed, and explosion would consequently occur. Therefore, the main significance of this work showed that chemical kinetics and geometric configurations have influences and effects on explosion of hydrogen-oxygen and propane -oxygen reaction mixtures.

Table of Contents

| | |
|--|-----------|
| Statement of Original Authorship..... | ii |
| Acknowledgements..... | iii |
| Keywords..... | iv |
| Abstract..... | v |
| Chapter 1 Introduction..... | 1 |
| 1.1 Background..... | 1 |
| 1.1.1 Previous accidents in petroleum tank farm explosions..... | 4 |
| 1.1.2 Description of tank farm fire/explosion accidents..... | 4 |
| 1.1.3 Causative factors of tank farm fire/explosion accidents..... | 6 |
| 1.1.4 Consequences of accidents and socio-economic factors..... | 9 |
| 1.1.5 Prevention and protection of industrial explosions..... | 11 |
| 1.2 Statement of problem and originality..... | 15 |
| 1.3 Aim and objectives of this project..... | 16 |
| 1.4 Outline of this thesis..... | 16 |
| Chapter 2 Chemical Explosion Waves..... | 21 |
| 2.1 Overview of explosions..... | 21 |
| 2.1.1 Deflagrations..... | 22 |
| 2.1.2 Detonations..... | 22 |
| 2.1.3 Flashover..... | 25 |
| 2.1.4 Backdraft..... | 25 |
| 2.2 Explosion disasters in oil and gas industry..... | 25 |
| 2.2.1 Piper Alpha disaster..... | 26 |
| 2.2.2 The Deepwater Horizon explosion..... | 27 |
| 2.2.3 Petrobras P-36 Oil drilling rig explosion..... | 29 |
| 2.3 Explosion blast waves..... | 31 |
| 2.4 Deflagration and detonation..... | 34 |
| 2.4.1 Deflagration waves..... | 34 |
| 2.4.2 Detonation waves..... | 38 |
| 2.4.3 Hugoniot conditions..... | 39 |
| 2.4.4 Rankine-Hugoniot relations..... | 40 |
| 2.4.5 Chapman–Jouguet waves..... | 42 |
| 2.4.6 Upper CJ and Lower CJ Point curves of detonation..... | 43 |
| 2.5 Deflagration-to-detonation transition..... | 44 |
| Chapter 3 Basic Equations and Numerical Schemes..... | 51 |
| 3.1 Introduction..... | 51 |
| 3.2 Reactive Navier – Stokes equations..... | 51 |
| 3.2.1 Continuity equations..... | 51 |
| 3.2.2 Equation of momentum..... | 52 |
| 3.2.3 Equation for energy..... | 52 |
| 3.2.4 Equation for species mass concentrations..... | 55 |
| 3.2.5 Thermodynamical properties of the mixture..... | 56 |
| 3.2.6 Boundary and initial conditions..... | 59 |
| 3.3 Numerical methods..... | 60 |
| 3.3.1 Finite volume methods..... | 60 |
| 3.3.2 Calculations of various fluxes on the surfaces of control volumes..... | 60 |

| | | |
|-------|--|------------|
| 3.3.3 | Calculations of the sources | 62 |
| 3.3.4 | Explicit schemes | 64 |
| 3.3.5 | Explicit-implicit schemes | 64 |
| 3.3.6 | Method of fractional steps | 64 |
| 3.3.7 | Courant-Friedrichs Lewy (CFL) Condition | 65 |
| 3.4 | Adaptive Mesh Refinement | 66 |
| 3.4.1 | Adaptive mesh refinement strategies | 66 |
| 3.4.2 | Block structured adaptive mesh refinement..... | 68 |
| 3.4.3 | Object-oriented implementation | 70 |
| 3.4.4 | AMROC's DAGH | 72 |
| 3.4.5 | Capabilities of AMROC over other CFD software..... | 73 |
| 3.4.6 | Limitation of AMROC | 73 |
| 3.5 | Validation and verification of this research work | 73 |
| | Chapter 4 Chemical Kinetics | 74 |
| 4.1 | Introduction..... | 74 |
| 4.2 | Basic concepts on reaction rates | 74 |
| 4.2.1 | Law of mass action | 74 |
| 4.2.2 | Reversible and multistep reactions | 75 |
| 4.2.3 | Reaction equilibrium | 77 |
| 4.2.4 | Arrhenius law: theories of reaction rates | 78 |
| 4.2.5 | Rates of reactions and their temperature dependence..... | 80 |
| 4.3 | Chain reaction theory | 81 |
| 4.3.1 | Straight-chain reactions: the Hydrogen–Halogen system..... | 81 |
| 4.3.2 | Branched-chain reactions..... | 84 |
| 4.4 | Combustion mechanisms of hydrocarbon fuels | 87 |
| 4.5 | Oxidation mechanisms of hydrogen and carbon monoxide reactions..... | 88 |
| 4.5.1 | Hydrogen and carbon monoxide oxidation reaction | 90 |
| 4.5.2 | Detailed reaction mechanisms for H ₂ + O ₂ reaction | 92 |
| 4.5.3 | Calculations of reaction rates..... | 93 |
| 4.6 | Oxidation of hydrocarbons..... | 96 |
| | Chapter 5 Chemical Reaction Mechanisms of Explosions | 100 |
| 5.1 | Introduction..... | 100 |
| 5.2 | Setup of simulations..... | 100 |
| 5.2.1 | Domain mesh..... | 101 |
| 5.2.2 | Initial conditions and ignition sources | 104 |
| 5.3 | Comparison of numerical simulation with experimental results..... | 108 |
| 5.4 | Effects of kinetics of H ₂ -O ₂ combustion reactions | 110 |
| 5.5 | Brief Summary | 126 |
| | Chapter 6 Effects of Complex Geometric Configurations | 128 |
| 6.1 | Introduction..... | 128 |
| 6.2 | Setup of simulations..... | 128 |
| 6.2.1 | Domain mesh..... | 129 |
| 6.2.2 | Initial Conditions and ignition sources | 132 |
| 6.2.3 | Chemical kinetics..... | 133 |
| 6.3 | Effects of Geometric configurations of H ₂ -O ₂ combustion reactions | 135 |

| | |
|--|------------|
| 6.4 Brief Summary | 153 |
| Chapter 7 Conclusions/Limitations/Recommendations | 155 |
| 7.1 Conclusions..... | 155 |
| 7.2 Limitations of this research work..... | 157 |
| 7.3 Recommendations for the future researches | 158 |
| References..... | 159 |
| Appendices..... | 171 |
| Appendix 1 | 171 |
| Appendix 2..... | 172 |
| Appendix 3..... | 176 |
| Appendix 4..... | 179 |
| Appendix 5..... | 181 |
| Appendix 6 | 184 |
| Appendix 7 Publications and Presentations..... | 189 |

List of Figures

| | |
|--|-----|
| Figure 1.1: Incipient stage of Amuay Refinery fires, Venezuela | 2 |
| Figure 1.2: Final stage of Amuay Refinery fires, Venezuela | 2 |
| Figure 1.3: Fishbone diagram of Accident Causes | 7 |
| Figure 1.4: Fishbone Diagram of Accident Prevention | 12 |
| Figure 2.1(a): Piper Alpha Offshore Oil Rig, Britain prior to the incident..... | 27 |
| Figure 2.1(b): Piper Alpha Offshore Oil Rig after the incident | 27 |
| Figure 2.2(a): Deepwater Horizon Drilling rig prior to the incident..... | 28 |
| Figure 2.2(b): Deepwater Horizon Drilling rig after the incident..... | 28 |
| Figure 2.3(a): Petrobras P-36 rig, Brazil prior to the incident. | 30 |
| Figure 2.3(b): Last minute of P-36 rig after the incident..... | 30 |
| Figure 2.4: Blast wave generated by an explosion..... | 31 |
| Figure 2.5: Illustration of the structure of a laminar flame front in a premixed gas | 34 |
| Figure 2.6: Laminar burning velocity for methane-, ethylene- and hydrogen-air | 35 |
| Figure 2.7: Positive feedback loop causing flame acceleration due to turbulence | 36 |
| Figure 2.8: Detonation waves | 39 |
| Figure 2.9: Schematic identifying the Rankine –Hugoniot solutions | 43 |
| Figure 2.10: Position of deflagration and detonation in a combustion wave | 46 |
| Figure 2.11: Compressible flows within complex Geometries than Shock Tube | 49 |
| Figure 2.12: Velocities used in analysis of detonation problem | 50 |
| Figure 3.1: Unstructured refinement strategy | 66 |
| Figure 3.2: Mesh and local quadtree-tree of structured mesh refinement strategy..... | 67 |
| Figure 3.3: Block structured refinement grids of AMR method for sub grids..... | 68 |
| Figure 3.4: Object-oriented design of the AMROC framework | 71 |
| Figure 4.1: Potential energy diagram showing the concept of reaction activation | 79 |
| Figure 4.2: C-shaped pressure-tempt. Explosion limits by mechanisms and wall..... | 86 |
| Figure 4.3: Explosion Limits of a Stoichiometric H ₂ ---O ₂ Mixture | 90 |
| Figure 5.1: Computational mesh and its simulated results at a time instant. | 102 |
| Figure 5.2 Computational mesh and its simulated results at another time instant..... | 103 |
| Figure 5.3 Visualisation of a part mesh enlarged and refined in Figure 5.2 | 104 |
| Figure 5.4 Comparison of numerical results with experiments by Liberman et al..... | 109 |
| Figure 5.5 Comparison of numerical solutions and experiments of Urtiew et al | 109 |
| Figure 5.6: Concentration (kg/m ³ against flame speed (m/s) for case study R ₂ | 110 |
| Figure 5.7: Concentration (kg/m ³ against flame speed (m/s) for case study R ₃ | 111 |
| Figure 5.8: Concentration (kg/m ³ against flame speed (m/s) for case study R ₄ | 111 |
| Figure 5.9: Concentration (kg/m ³ against flame speed (m/s) for case study R ₅ | 112 |
| Figure 5.10: Concentration (kg/m ³ against flame speed (m/s) for case study Ra | 114 |

| | |
|--|-----|
| Figure 5.11: Concentration (kg/m ³) against flame speed (m/s) for case study R _b | 115 |
| Figure 5.12: Concentration (kg/m ³) against flame speed (m/s) for case study R _e | 115 |
| Figure 5.13: Concentration (kg/m ³) against flame speed (m/s) for case study R _d | 115 |
| Figure 5.14: Concentration (kg/m ³) against flame speed (m/s) for case study R _e | 116 |
| Figure 5.15: Concentration (kg/m ³) against flame speed (m/s) for case study R ₂₀ | 120 |
| Figure 5.16: Concentration (kg/m ³) against flame speed (m/s) for case study R ₂₁ | 121 |
| Figure 5.17: Concentration (kg/m ³) against flame speed (m/s) for case study R ₃₀ | 121 |
| Figure 5.18: Concentration (kg/m ³) against flame speed (m/s) for case study R ₃₁ | 122 |
| Figure 5.19: Concentration (kg/m ³) against flame speed (m/s) for case study R ₄₀ | 122 |
| Figure 6.1 Time is at 0.0001 second from ignition, ignition state..... | 129 |
| Figure 6.2: Time is at 0.000145 second, slow flame mode of combustion waves..... | 130 |
| Figure 6.3: Time is at 0.000195 second, fast flame mode of combustion waves..... | 130 |
| Figure 6.4: Time is at 0.00022 second at which the detonation is initialized | 131 |
| Figure 6.5: Detailed mesh structure for the detonation | 132 |
| Figure 6.6: Concentration (kg/m ³) against flame speed (m/s) for case – Block..... | 136 |
| Figure 6.7: Concentration (kg/m ³) against flame speed (m/s) for case - Step..... | 136 |
| Figure 6.8: Concentration (kg/m ³) against flame speed (m/s) for case - Wall..... | 137 |
| Figure 6.9: Concentration (kg/m ³) against flame speed (m/s) for case study A | 140 |
| Figure 6.10: Concentration (kg/m ³) against flame speed (m/s) for case study B..... | 140 |
| Figure 6.11: Concentration (kg/m ³) against flame speed (m/s) for case study C | 141 |
| Figure 6.12: Concentration (kg/m ³) of propane against flame speed for case R ₂₀ | 145 |
| Figure 6.13: Concentration (kg/m ³) of propane against flame speed for case R ₂₁ | 146 |
| Figure 6.14: Concentration (kg/m ³) of propane against flame speed for case R ₃₀ | 146 |
| Figure 6.15: Concentration (kg/m ³) of propane against flame speed for case R _{30x} | 147 |
| Figure 6.16: Concentration (kg/m ³) of propane against flame speed for case R ₃₁ | 147 |
| Figure 6.17: Concentration (kg/m ³) of propane against flame speed for case R ₃₁ | 148 |

List of Tables

| | |
|--|-----|
| Table 1.1: Tank Farm Explosion Incidents | 3 |
| Table 2.1: Qualitative differences between deflagration and detonations in gases | 23 |
| Table 2.2: Blast damage and personal injury pressures and impulses..... | 32 |
| Table 2.3: Relationship between deflagration and detonation | 47 |
| Table 3.1: Refinement after the last time step with AMROC's DAGH | 72 |
| Table 4.1: Heats reaction steps for the halogen-hydrogen systems at 300 K..... | 83 |
| Table 4.2: Oxidation of H ₂ ---CO mixtures | 90 |
| Table 5.1: Initial conditions of kinetics for 4 case studies of H ₂ -O ₂ combustion..... | 104 |
| Table 5.2: Initial conditions of kinetics for 5 case studies of H ₂ -O ₂ combustion..... | 105 |
| Table 5.3: Initial conditions of kinetics for 5 case studies of propane combustion..... | 105 |
| Table 5.4: Elements Considered for simulation | 105 |
| Table 5.5: Reacting species considered | 106 |
| Table 5.6: Reactions considered ($K = AT^b e^{-(E_a/RT)}$) | 106 |
| Table 5.7: Comparison of induction time for simulations and Experiments..... | 108 |
| Table 5.8: Effects and influences of kinetics on H ₂ -O ₂ combustion processes | 110 |
| Table 5.9: Effects of kinetics on H ₂ -O ₂ combustion of case studies 2, 3, 4 and 5..... | 112 |
| Table 5.10: Effects and influences of kinetics on H ₂ -O ₂ combustion processes..... | 114 |
| Table 5.11: Effects of kinetics on H ₂ -O ₂ combustion of cases a, b, c, d and e..... | 116 |
| Table 5.12: Effects and influences of kinetics on propane combustion processes..... | 119 |
| Table 5.13: Effects of kinetics on Propane for cases 20, 21, 30, 31, and 40 | 123 |
| Table 6.1: Initial conditions of complex geometry for 3 case studies | 132 |
| Table 6.2: Initial conditions of complex geometry for 3 case studies | 132 |
| Table 6.3: Initial conditions of complex geometry for 6 case studies of propane | 133 |
| Table 6.4: Elements Considered for hydrocarbon simulation | 133 |
| Table 6.5: Reacting Species considered | 134 |
| Table 6.6: Reactions considered ($K = AT^b e^{-(E_a/RT)}$) | 134 |
| Table 6.7: Effects of geometric configuration on H ₂ -O ₂ combustion | 135 |
| Table 6.8: Effects of geometric configuration for cases Block, step and wall..... | 137 |
| Table 6.9: Effects of geometric configuration with vent on H ₂ -O ₂ combustion..... | 139 |
| Table 6.10: Effects of geometric configuration for cases A, B, and C..... | 141 |
| Table 6.11: Effects of geometric configuration on propane combustion | 144 |
| Table 6.12: Effects of complex geometry on cases 20, 21, 30, 30x, 31, 31x..... | 148 |

Lists of symbols, abbreviations and their definitions

Table i: List of symbols

| s/no. | nomenclature | definitions of used formula symbols |
|-------|--------------|---|
| 1 | $K(T)$ | the chemical reaction rate constant that depends on temperature |
| 2 | R | universal gas constant (8.314 j/mol/k) |
| 3 | E_a | activation energy (j/mol) |
| 4 | b | index of T |
| 5 | A | pre-exponential factor (frequency of collision) |
| 6 | ΔH_c | heat of combustion (j) |
| 7 | q_r | radiative heat flux (kw/m ²) |
| 8 | V | velocity (m/s) |
| 9 | Pa | pressure (pascal) |
| 10 | Q | total heat release by fire (kw) |
| 11 | Q_r | total radiative heat release rate (kw) |
| 12 | ρ | density of fuel (kg/m ³) |
| 13 | Q_r | internal production rate for thermal energy |
| 14 | ω | reaction rate |
| 15 | λ | fraction of total radiant heat |
| 16 | X_i | mole fraction of species i |
| 17 | p | pressure pa |
| 18 | T | absolute temperature in kelvin at which reaction occurs |
| 19 | $M_{w,i}$ | molecular weight of species i |
| 20 | CFD | computational fluid dynamics |
| 21 | FDS | fire dynamics simulation |
| 22 | E | specific inner energy. |
| 23 | HRR | heat release rate (kw) |
| 24 | NFPA | national fire protection association |
| 25 | API | american petroleum institute |
| 26 | m/s | unity of flame speed in metre per second |
| 27 | ASME | american society of mechanical engineers |
| 28 | USEPA | united states environmental protection agency |
| 29 | USCSB | united states chemical safety board |
| 30 | USCSHB | united states chemical safety & hazard board |
| 31 | η | efficiency of combustion |
| 32 | T | transmissivity of air |
| 33 | q_j | heat flux (kw) of species j |
| 34 | CFL | courant-friedrichs-lewy |
| 35 | Δt | time step |
| 36 | Δx | the length interval |
| 37 | u | the magnitude of the velocity |
| 38 | ΔH_F | standard enthalpy of formation |

Table ii: List of abbreviations

| s/no | abbreviations | acronyms |
|------|---------------|---|
| 1 | LF | low flame |
| 2 | FD | fast deflagration |
| 3 | DDT | Deflagration-to-Detonation Transition |
| 4 | DD | direct detonation |
| 5 | DNS | direct numerical simulation |
| 6 | HRR | heat release rate (kw) |
| 7 | CFD | computational fluid dynamics |
| 8 | FDS | fire dynamic simulation |
| 9 | PMS | premium motor spirit |
| 10 | AMROC | adaptive mesh refinement in object-oriented C++ |
| 11 | DAGH | Distributive Adaptive Grid Hierarchies |
| 12 | Q | heat |
| 13 | BC | boundary condition |
| 14 | CFL | Courant-Friedrichs Lewy |
| 15 | ω | (omega) Reaction rate |

Chapter 1 Introduction

This chapter will cover background to this work, statement of problem, aim and objectives of this research, originality and the outline of this thesis. Explosions occasionally happen in industrial processes and in daily life. When they occur, they can produce big overpressures and associated fires which can usually make a great amount of damage and may be catastrophic.

Explosions have posed one of the greatest threats to the oil and gas Industry (in areas of human losses, environmental damages, economic/financial losses coupled with property loss such as storage tank damage) [1]. A good understanding of the mechanisms and consequences of explosion is a key for designing fire safety management programmes not only to protect the assets of an organization, but also to ensure the safe evacuation of all personnel present.

Explosions could be classified as either mechanical explosion (e.g. caused by mechanical failure of a pressure vessel), or chemical explosion that is driven by chemical reactions, i.e. by strong premixed combustion [2]. The combustion mostly takes place in gaseous mixture. When solid and liquid fuels undergo combustion, they are converted to gaseous state by the application of energy in the form of heat thereby breaking the molecules to form chemically reactive species called free radicals which then combine with oxidizer [3]. Usually, combustion occurs when the fuel is converted to vapour or gaseous state because the oxidizer occurs as a gas and its combustion involves both oxidizer and fuel in the gaseous state for recombination to occur [4]. A chemical explosion will be addressed in this project.

1.1 Background

Petroleum products are stored in downstream tank farms and their volatility poses explosion hazards. However, recent study [1] outlined over 85% explosion accidents, and of petroleum by-products, petroleum hydrocarbon gas is prone to explosions due to its low flash point. Researches have shown that tank farm explosions cost over £10 million [2] and loss of lives [3], [4]. Some works studied other gases [5], but no detailed study of hydrocarbon gases such as propane and butane. Other researchers investigated detonation combustion mechanisms and low Mach number [6], [7], [8].



Figure 1.1: Incipient stage of Amuay Refinery fires, Venezuela [9].



Figure 1.2: Final stage of Amuay Refinery fires, Venezuela [9].

Table 1.1: Tank Farm Explosion Incidents [9], [10], [11], [12], [13], [14], [15], [16], [17], [18], [19]

| Explosion Incidents | Causes | Cost Effects |
|--|--|---|
| Amuay Refinery fire explosion, Venezuela. 25/08/2012 | Sabotage | (i)48 deaths. (ii) 86 persons injured. (iii) 500 nearby homes burnt. (iv) 956,000 bbl/day lost. |
| Oil Field fire explosion, Mississippi, USA. 05/06/2006 | Fire explosion | (i)650 gallons of crude oil lost. (ii) 1 person killed. (iii) 3 contractors killed. |
| Exxon Mobil Oil Refinery Fire explosion, USA. 23/12/2021 | Gas leakage | (i)4 workers injured (ii) 561,000 barrels of oil spilled. |
| Chevron Oil Tank fire explosion, Escravos, Nigeria. 20/07/2002 | Lightning | (i)2 workers killed. (ii) 180,000 bbl/day lost. (iii) Billion dollars gas project burnt down. |
| Chemical explosion, Binhai Tianjin, China 12/08/2015 | Auto-ignition of chemical | (i)173 deaths. (ii) 801 people injured (iii) 1 bn pounds lost (iv) 8 persons missing |
| Buncefield fire explosion, Hertfordshire, UK. 11/12/2005 | Human failure/ instrumentation failure | (i)£10 million materials burnt. (ii) 630 nearby homes burnt. (iii) Nearby businesses burnt. (iv) 500 livelihoods of people affected. |
| Kaohsiung gas explosion, Taiwan, 31/7/2014. | Gas leakage | (i)32 Worker killed (ii) 321 workers injured |
| Refinery tank Fire explosion, Louisiana, USA. 3/9/2005. | Hurricane striking the refinery tanks (storm) | (i)25,110 barrels of oil spilled into the environment (ii) Crude oil tank of 65,000 bbl lost. |
| Lagos Seaport Tank Farm fire explosion, Nigeria. 9/01/2013. | Improper discharge of fuel into Tank | (i)4 wounds. (ii)Tank Farm burnt down |
| Oil Tank Fire Explosion Tokachi Japan 26/09/2003. | Earthquake/sparks | (i)166 deaths (ii) 14 Industrial complexes destroyed (ii) Several tanks burnt for 13 days (iii) Floating roofs dislodged and jamming |
| Gas explosion, Pottstown, Pennsylvania, USA. 26/05/2022. | 2 tanks exploded beside a welding operation unit. | (I)5 deaths. (ii) 2 injuries (iii) Nearby property destroyed |
| Pipeline Fire Explosion, Nigeria 11/10/2020. | Human failure – overflow of fuel during filling operation. | (i) 45 deaths (ii) 100 persons injured (iii) 276,000 people displaced (iv) 150 buildings burnt (v) 32 commercial shops destroyed (vi) 2 billion dollars gas project burnt down |
| Kentucky Gas Explosion, Kentucky, USA 01/08/2019 | Gas leakage | (i)11 death (ii) 5 people injured (iii) 5 Nearby homes destroyed |
| Oil & Gas explosion, Petromedia Refinery Platform, Romania 02/07/2021 | Open flames | 1 death 5 persons injured |

1.1.1 Previous accidents in petroleum tank farm explosions

The possible causative factors and preventive measures of Petroleum Tank Farm Explosion fire accidents are described as follows, and this is illustrated using the fishbone diagrams of Figures. 1.3 and 1.4 showed in Section 1.1.3, and also of Table 1.1 showed in Section 1.1

1.1.2 Description of tank farm fire/explosion accidents

Industrial fires have posed one of the greatest threats to companies/organizations in areas of human losses, environmental damages, economic/financial losses as well as losses of properties [3]. Figures 1.1 and 1.2 above explained the position of Venezuela Refinery fire explosion outbreaks at its incipient and final stages of the explosion, and Table 1.1 showed in Section 1.1 described globally some major fire explosion incidents that have occurred.

The accidents from oil and gas explosions in the Oil and Gas sector of the Nigerian economy are alarming and heart breaking and therefore call for urgent attention to remedy the urgent situation. A critical analysis of fire and gas explosion accident victims in Nigeria on a conservative estimate rose to about 45 deaths, 100 people injured, 45,347 pipeline explosions, 276,000 people displaced, 150 nearby homes burnt down, 32 workshops burnt, and 2 billion dollars gas project burnt between 21st March 2019 to 11th October 2020 [10]. This research work will immensely be of great importance to the Federal Government of Nigeria, most especially the Oil and Gas sector.

Furthermore, fire explosion disasters at storage tank farms do constitute many environmental damages most especially to the nearby host communities [9]. For instance, on 31/07/2014 at Kaohsiung gas explosion, Taiwan resulted from gas leakage leading to 32 deaths, 321 persons were injured which resulted in an explosion that metamorphous to cascading events of the release of several gallons of product into the environment causing the deaths of thousands of fishes and other wild animals [20]. In addition, on 15th March 2020, pipeline explosion due to human failure led to an overflow of fuel during filling operation and this singular human error led to 23 deaths, 25 people injured, 276,000 people displaced, 50 buildings destroyed, and 32 commercial shops burnt down [10]. On 3/9/2005 at a Refinery in Louisiana, USA, fire explosion resulted from hurricane storm striking the storage tank and this consequently

led to the release of 25,000 barrels of crude oil spilled into the environment leading to huge environmental damage [21], [22].

Nonetheless, on 11/12/2005 at the Buncefield, Hertfordshire, UK because of instrumentation failure during work operation, 10 million pounds worth of materials were lost to devastating fires [11].

Furthermore, it will equally alleviate the fears of the tank farm operators, the private and government officials of the time-bomb danger posed by the tank farm operations [23].

Fire explosion hazards at workplace and even in the homes, outdoors put people and properties at risk. These include: (i) Improper storage (ii) Maintenance and use of everyday items increase the risk of fire. Therefore, fire prevention is essential. Reduce the risk of fire with your choice of design, and by following fire safety recommendations for the home and offices. All workplaces contain chemical, electrical and other fire hazards that pose major health and safety threats if left unchecked. Objects that do generate heat such as computers are potential fire trouble spots [23]. Fire hazards at workplace would include:

Ignition Source

No fire can start without an ignition source such as open flames, sparks, static electricity and hot surfaces, but ignition temperature refers to the minimum temperature at which a substance burns without the application of external heat according to an analysis by Assured Fire and Security. Other office equipment includes computer monitors, microwaves, ovens used in staff kitchen/canteen. Even items like cigarettes and matches also create ignition sources especially if employees must immediately put out smoking materials [24].

Fuel Sources

Every fire does need a fuel source. Many workplaces are careless in dealing with materials that burn easily, such as cardboard and paper, according to Assured Fire Analysis. This type of hazards is unique to workplaces and industrial sites like factories and workshops that may contain flammable liquids, timber pallets and packaging materials such as polystyrene. In order to ensure safe handling, employers must check the specific Materials Safety Data Sheet (MSDS) for each substance [3].

Flammable Liquids and Vapours

Flammable liquids and vapours can burn once they mix with air and other oxygen sources and hence solvent containers should be properly sealed. In order to prevent static build-ups that do increase the risk of explosion, electrical equipment should be bonded or grounded along a conductive path [25].

Heat Producing Devices

The U.S Occupational Health and Safety Administration (OSHA) spells out numerous standards for dealing with fire hazards. One standard covers heat-producing devices and equipment such as boilers, burners, fryers, heat exchangers, ovens and stoves. Companies must provide for the proper storage and maintenance of equipment, while keeping them away from flammable liquids [24].

Electrical Hazards

Misused extension cords and multiple power strips are the most common causes of office fires. Using multiple fire strips to power large appliances can overload outlets and branch circuits. The same rule holds true for extension cords, which provide power when a regular outlet is not available. Moreover, extension cords should never be left coiled up and coiled extension cords can cause inductive heating which could damage insulation and ultimately cause a fire disaster [26].

1.1.3 Causative factors of tank farm fire/explosion accidents

The possible causative factors of Petroleum Tank Farm Explosion fire accidents are described as follows, and Figure 1.3 in Section 1.1.3 explained these factors using the fishbone diagrams.

Tank gauging/physicalisation: Manual gauging should be done at scheduled intervals in order to have the accuracy of the automatic systems. For manual gauging and sampling operations, the operator is required to climb to the top of the tank. During product reception, 30 minutes to 4 hours relaxation period should be followed depending on product thereby allowing any electrostatic built up to dissipate before conducting manual gauging or sampling. Explosion safety demands that entry onto tank farm roofs for gauging, sampling or other activities should strictly be avoided during lightning or thunderstorms [13].

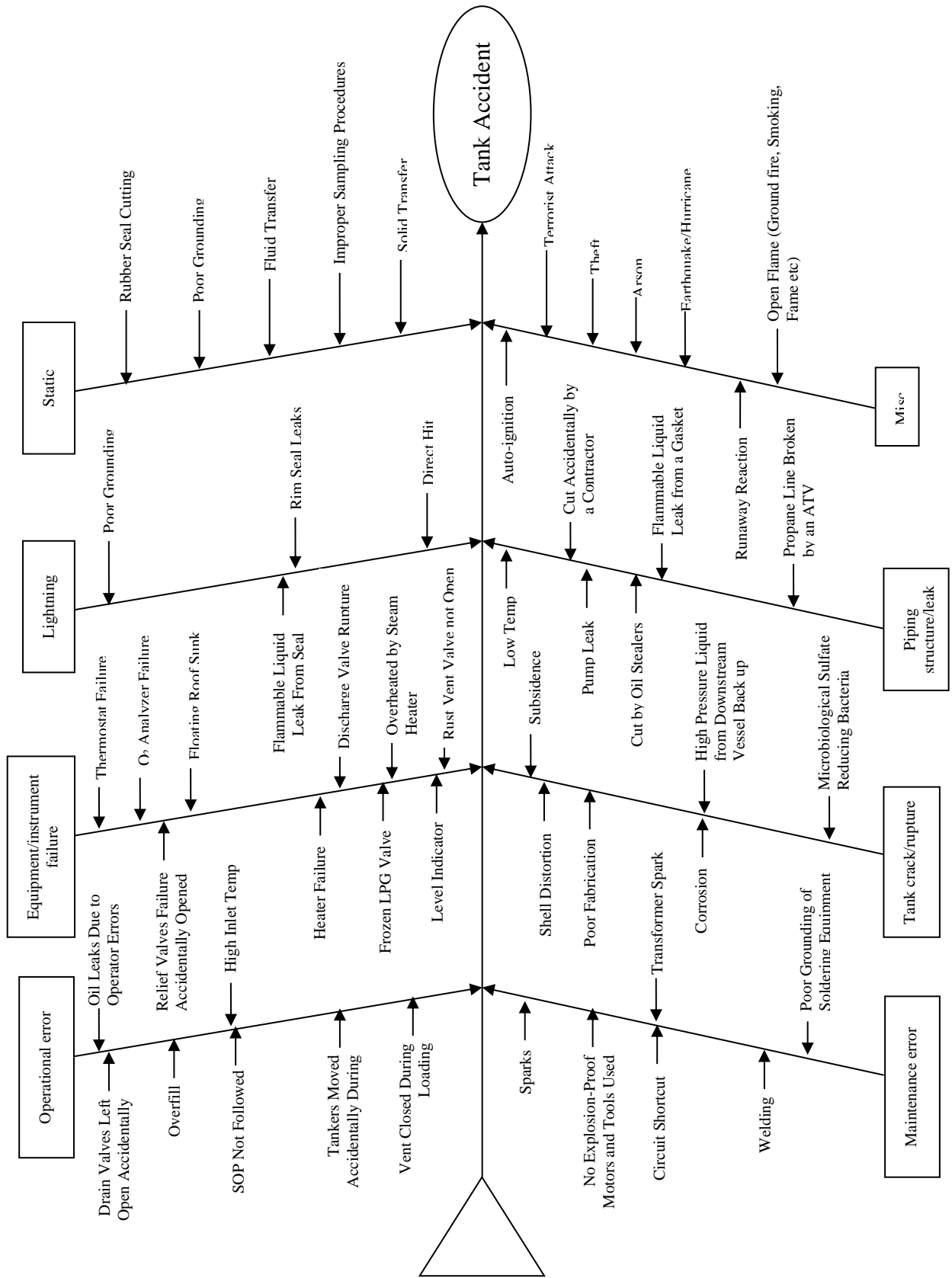


Figure 1.3: Fishbone diagram of Accident Causes [13].

Maintenance error: When tank contents are instantly released, thereby igniting the second tank, explosion can thus occur, and consequently damaging additional storage tanks. As ventilation continues and the vapour levels in the tank drop lower, entry work permits must be issued before allowing workers with appropriate personal safety equipment to clean tank. After tanks have been cleaned and dried, a final inspection and testing should be conducted before maintenance jobs commence. A catastrophic failure of aboveground atmospheric storage tanks can occur when flammable vapours in the tank explode. Electrical sparks/mechanical frictions can also ignite flammable vapours resulting in explosion [24].

Sabotage: Sabotage entails disgruntled workers and or arsonists maliciously set tank farms or workplaces on fires. The Amuay Refinery fires (2012) were caused by sabotage that eventually led to great mishaps and this is supported in Table 1.1 above. Also, the destruction of Agip Oil tank farm at Yenegoa, Bayelsa state, Nigeria was due to sabotage [13].

Operational errors: During a filling operation of petroleum products, fuel can overflow through the roof of a floating roof tank leading to several tons of fuel escaping into the environment. Thus, explosion can occur injuring several persons and storage tanks can be destroyed [21].

Equipment failures: At Brucefield, Hert Yorkshire, U.K. in 2005, a tank overfilled with product at an estimated rate of 550 m³ per hour for several hours overflowed into the bund generating vast quantities of vapours causing damages (see Table 1.1 above) [13].

Static electricity (static sparks): In reducing sampling hazard arising from static sparks, avoid operation at the open access port and if the operation at the open access port is unavoidable, sampling beakers and sampling gauges made of non-conductive materials should be used. Do not use any device made of metal. The containers should be bonded to each other and the one from which product is being dispensed should be grounded during product transfer [24].

Tank leakage: Any unwanted discharge may be considered a leakage however small. Moreover, petroleum tanks should be checked regularly for possible rust and leaks. Visual inspection for potential leaks and corrosion to be done weekly. However, Kaohsiung gas explosions occurred in Taiwan on 31st July 2014 leading to 32 deaths and 321 injuries [16], [21].

Naked/Open flames: Naked flames such as cigarette smoking, and hot particles can ignite flammable vapours around storage tanks. The Petromidia Refinery Platform, Romania involving oil and gas fire explosion incident which was caused by open flames on 2nd July 2021 led to one death and five severely injured [19], [27].

Lightning: During lightning strokes, sparks from one object to another are induced by nearby lightning stroke and induced surges in circuits and electrical equipment. The rim seal of a floating roof tank is the most likely place to be ignited in a thunderstorm. In July 2002 lightning strike in Chevron crude oil tank of 100,000 barrels ignited and the fire explosion lasted for about five days [27], [28].

Tank crack and rupture: In addition, most storage tank damage is attributable to age deterioration, corrosion and seismic motions. Most often, cracks usually occur at the bottom or the welding edges. The fire explosion incident at Kaohsiung, Taiwan refinery in 2002 occurred due to the crack at the bottom of the tank [28], [29].

1.1.4 Consequences of accidents and socio-economic factors

If a good survey of the various definitions of accident is taken, it would be observed that majority of them dwell on the fact that accident is an unplanned event that produces unintended injury, death and property damage. Therefore, whenever an accident happens, the following consequences arise, and they include the followings:

Loss of Time

This arises as a result of the accident and thus, there will be a stop in production in the event of trying to find out what led to the accident, level of severity, number of lives lost and trying to remedy the situation. In actual sense, much time would be spent rectifying the situation. For example, lost time by fellow crewmen at the time of the

incident, giving the victim the desired assistance such as lost time injury (LTI), lost time injury frequency (LTIF); Time lost by fellow workers discussing the accident; Time lost by supervisors during investigation and registration of the accident [29], [30].

Loss of money

When accident occurs, production falls due to time spent in assisting the victim(s) and this will lead to great fall in profit making. Accident thus can lead to financial loss. Money loss could be seen as direct cost of accident to the company such as money paid for medical treatment which could have been used for other vital needs. Money can also be lost through compensating victims of the accidents and money is also lost by spending money to train new workers to take the jobs of the victims mainly for accidents where there is fatality (Permanent Total Disability cases). Money can be lost owing to loss of efficiency arising from breakdown of crew and money spent for the investigation team. All these lead to fall in production which will invariably lead to loss of money [24], [31].

Loss of Lives

Whenever an accident happens, there could be loss of lives depending on the severity of the accident. It could lead to mental strain, suffering loss of earning power, extra expenditures, possibilities of a continuing disability e.g. permanent partial disability (PPD), Restricted workday cases (RWC), Fatality (F) etc., loss of talents to such industry were the accident happened. Moreover, loss of lives due to an accident would have adverse effects on families, friends, and colleagues especially if the victim(s) are the breadwinners of the affected families [29], [32].

Loss of properties

An occurrence of an accident in an area can lead to damage of properties and this might call for a huge sum of money to replace such properties. Whenever, there is fire explosion, there is high probability of damages to properties nearby [24].

Socio-economic consequential effects

Recent studies on combustion are extremely important as they greatly contribute in a firefighting scenario, and the huge economic cost implications to the company, to the

victims and the government is colossal. Other areas of socio-economic consequences include loss time by fellow crewmen at the time of accident through assisting the victims; time loss by fellow workers discussing the accident; damage to moral of crew; and some workers quitting their jobs when they witnessed terrible accidents on the job. Furthermore, other socio-economic consequences are loss of efficiency because of break-up crew leading to production decrease during such periods; wages paid to new workers as replacement for the injured workers; time lost by other workers visiting injured colleagues coupled with cost of damaged tools and equipment [24].

For example, money paid for medical treatment of accident victims, compensations paid to victims and their families coupled with wages paid to workers while off the job. Eventually, most explosions occurring in the industry result in deflagrations, but detonations are potentially more destructive than deflagrations [1],

1.1.5 Prevention and protection of industrial explosions

The classic basis of fire protection is to isolate one of these three components – cooling, smothering, and starvation or to inhibit the chemical reaction. Explosion can best be controlled by one or more of these methods- (i) Containment – Designing a container/vessel to withstand maximum pressure; (ii) Quenching – Withdrawal of heat or chemical inhibition to stop a reaction; (iii) Dumping- Release of the reaction mixture that will not stop the reaction, but transfer the reaction to an area that can withstand/handle it; (iv) Venting- Release of energy and gases from the explosion in a controlled manner; (v) Isolation- Separation of the process from surrounding areas affected by an explosion, and is achieved by physical separation or through the use of blast-resistant structures

Generally, the preventive measures in an organisation are adopted to prevent losses of human lives and properties due to fire explosions. A loss of just one major facility can have terrible severe negative financial impact on production activities. For instance, when a business that is a major employer of labour burns down, several people will be out of work and consequently the jobs may never be available again. It is even worse where there are numerous documented cases of oil and gas explosions which have led to major loss of lives attributable to preventable hazards, for instance locked, or inadequate fire exits [23], [24].

Figure 1.4 in Section 1.1.5 using the fishbone diagrams explained how to eliminate the causative factors of industrial explosions thus making industrial operations safe.

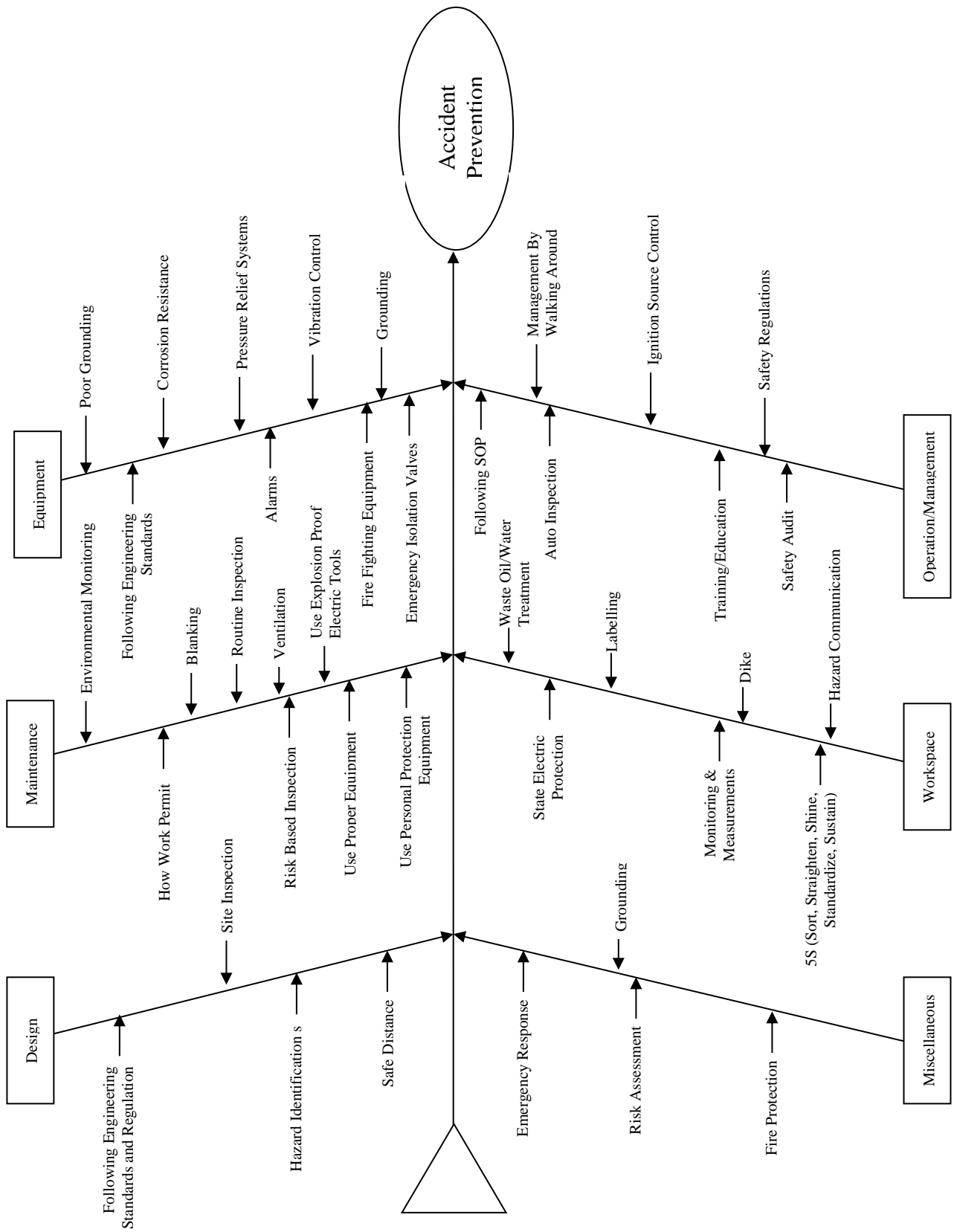


Figure 1.4: Fishbone Diagram of Accident Prevention [13].

A summary of the known reasons of an analysis of more than 25,000 explosions reported to the Mutual Engineering Corporation for a reasonable period of time is arranged in order of their frequency throughout industry, and thus the preventive and protective measures are employed to ameliorate fire explosions in the Oil and Gas Industry.

Electrical factors: Fire explosions resulting from wiring and motors can be prevented by more maintenance services, and special attention is needed for equipment at hazardous processes and in storage areas [23].

Incendiarism (sabotage): In the hydrocarbon environment like the petroleum storage tank farm, fire explosions maliciously caused by saboteurs, intruders, juveniles, disgruntled employees, and arsonists can adequately be protected and prevented by watch and guard service coupled with installation of fences and other security measures [24].

Smoking: This is the potential cause of fire almost everywhere. It is prevented by a matter of control and education. Smoking is strictly prohibited in dangerous areas such as those involving flammable liquids, combustible dusts of fibres and combustible storage areas [32], [33].

Heat: Heat from boilers, furnaces, hot ducts and flues, electric lamps, irons and hot-process-metal igniting flammable liquids and ordinary combustible which often result in explosions are preventable by design and good maintenance of flammable-liquid piping and by ample clearances, insulation and air circulation between hot surfaces and combustibles [31].

Friction: Hot bearings, misaligned or broken machine parts, choking or jamming of material, and poor adjustment of power drives and conveyors that can constitute fire explosions can be prevented by a regular schedule of inspections, maintenance, and lubrication [32].

Overheated Materials: Abnormal process temperatures, especially those involving heated flammable liquids and materials in dryers can easily be prevented by careful

supervision under competent operators, supplemented by well-maintained temperature controls [34].

Cutting and Welding: Usually, sparks, arcs and hot metal from cutting and welding operations which lead to fire explosions at Oil and gas production platforms are preventable using the permit system and other recognised precautions [24], [35].

Burner Flames: Improper use of portable torches, boilers, dryers, ovens, furnaces, portable heating units, and gas-or burner flames that cause explosions in petroleum tank farms are protected and prevented by proper design, operation, and maintenance through adequate ventilation and combustion safeguards; and keeping open flames away from combustible materials [27].

Spontaneous Ignition: In protecting and preventing oily waste and rubbish, deposits in dryers, ducts flues, materials susceptible to heating and industrial wastes which result in industrial explosion, good housekeeping and proper process operation are employed [34].

Combustion Sparks: Industrial explosions resulting from sparks and embers released from incinerators, furnaces, various process equipment and industrial trucks are technically protected and prevented using well-designed equipment and well-enclosed combustion chambers with spark arrestors [24].

Mechanical sparks: Sparks from foreign metals in machines, most especially in grinding and crushing operations that result in industrial explosions can be prevented by keeping stock clean and removing foreign material using magnetic or other separators [36], [37].

Static sparks: Ignition of flammable vapours, dusts, and fibres by discharge of accumulation of static electricity on petroleum storage tank which lead to industrial fire explosions can basically be prevented by methods of grounding, bonding, and ionization [27].

Chemical Action: Chemical processes getting out of control and chemicals reacting with other materials causing industrial explosions can be prevented by proper operations, instrumentation, controls and careful handling [36],

Lightning: Direct lightning sparks from one object to another induced by nearby lightning and induced surges in circuits and petroleum storage tanks can be prevented using arresters, surge capacitors and grounding [38].

1.2 Statement of problem and originality

Explosions in petroleum tank farms are complex combustion waves which have various forms. Understanding these combustion waves poses the important problems as follows: (i) Initiation of the combustion waves, (ii) Propagations of the combustion waves, (iii) Transition of different forms of the combustion waves and (iv) Consequences of the combustions [6], [7], [8]. However, experimental studies conducted by Liberman et al [39] and M. Kuznetsov et al [40] of hydrogen-oxygen mixtures in tubes using smooth and rough walls studied the reaction rates of hydrogen and oxygen mixtures, but did not examine the influences and effects of chemical kinetics and geometric configuration of hydrogen-oxygen mixtures as well as that of propane-oxygen mixtures on explosion. This work will primarily investigate the effects and influences of detailed chemical kinetics of hydrogen and oxygen mixtures coupled with that of geometric configuration on explosion processes and explosion protection of tank farms using CFD approach. This study intends to fill this gap. Previous work investigated fire spread due to inter-tank diameter and wind velocity using CFD approach [41]. Other relevant works studied the combustions of hydrogen gas, liquid hydrogen and natural gas [1], [14], [35], [42], [43], [44]. The gap between our understanding and observation to the real process which include (1) how the flame in the pre-mixed combustible mixture accelerates as well as how the accelerated modes are determined; (2) effects of different reaction kinetics to the processes; and (3) effects of geometric configurations to the deflagration and DDT will be addressed. The data will be produced by AMROC simulations using DNS level, and usually, detailed chemical kinetics and geometric configuration for deflagration and detonation will be implemented.

1.3 Aim and objectives of this project

(i) Aim:

To investigate the initiation of the combustion waves, the propagations of the combustion waves, the transition of different forms of the combustion waves, the consequences of the combustions, and the mechanisms and consequences of explosions of petroleum hydrocarbon gases.

(ii) Objectives:

1. To examine the aftermath of explosion to storage tanks in petroleum storage tank farm operations.
2. To examine the initiation of the combustion waves, the propagations, and the influence of combustion waves.
3. To investigate the mechanisms of deflagration to detonation transition (DDT) of hydrogen – oxygen combustions in shock tube using direct numerical simulations at the first stage.
4. To examine the mechanisms of combustion wave propagations produced by the hydrocarbon gases that will be applied in petroleum tank farm operations.
5. To investigate the effects of the geometric configurations on initiations and propagations of explosion waves.

1.4 Outline of this thesis

The numerical simulation of this research work attended to the problems posed by combustion waves in the petroleum tank farms through: (i) the initiation of combustion waves, (ii) the propagation of combustion waves, (iii) the transition of different forms of combustion waves, and (iv) the consequences of the combustion. The numerical simulation work showed that there are two parts, and they are: (a) the ignition stage of combustion waves, and (b) the flame development of the explosion waves. How can the above situation be achieved? In achieving the above, the combustion mixture is ignited by the application of an external energy input in the form of heat for substances like solids and liquids thereby breaking down the molecules in the fuel to form chemically reactive species called free radicals which then combine with the oxidizer.

The research findings of my numerical simulation work proved that complex configurations have effects and influences on explosion of combustible reacting mixtures of hydrogen-oxygen and propane-oxygen mixtures studied in this research. This research work also revealed that chemical kinetics have influences and effects on explosion of reacting mixtures of hydrogen and propane. From the research results of this work obtained in line with the contributing effects and influences of kinetics and geometric configuration, the problems of explosions associated with tank farm operations can be prevented and thus make petroleum tank farm operations safe.

Chapter 1 examined the series of tank farm explosion incidents mainly in the oil and gas sector, and the possible varying factors for such explosion in the oil and gas sector have constituted the driving force looking at the effects and influences of chemical kinetics and complex geometry on explosion. It was discovered that the oil and gas sector has suffered great losses in terms of manpower losses, production materials and infrastructures/facilities destroyed, nearby businesses and homes destroyed, and occupants of nearby homes suffered untold hardships. This informed the background for this work. This chapter explained the reasons for tank farm fire explosion disasters, as well as the consequences of tank farm fire explosion accidents and the socio-economic factors. In addition, it clearly described the prevention and the protection of industrial explosions.

Chapter 2 perused the relevant literature to the initiation of combustion waves, the propagation of combustion waves, the influences of combustion waves and the consequences of the combustion waves on explosion attributable to the chemical kinetics and the geometric configuration of petroleum tank farms. This chapter also explored the explosion disasters in the petroleum tank farms such as the Piper Alpha disaster 1988, United Kingdom; the Deepwater horizon explosion 2010, USA; and the Petrobras P-36 Rig explosion, Brazil; and the consequences of explosion blast waves to mention but a few. Moreover, previous works on tank farm explosion incident reduction in relation to other parameters like tank diameter and wind velocity using Computational Fluid Dynamics (CFD) were examined. However, this research work zeroed absolutely on the effects and influences of kinetics and geometric configuration on explosions caused by the combustible reacting mixtures of hydrogen and propane in tank farm to achieve safe tank farm operations.

Chapter 3 dealt with the basic equations and numerical schemes governing the four processes – the flows, heat transfer, mass transfer and chemical reactions. Moreover, it explained the equations controlling conservation principles of the laws for mass, momentum, and energy conservation. This chapter further treated the reactive Navier–Stokes equations for (i) continuity equations of mass conservation, (ii) equation of momentum conservation, (iii) equation for energy conservation and (iv) equation for species mass concentration. This is not all, this chapter also handled equations for thermodynamical properties of the mixture which include (i) the thermodynamical state of the mixture, (ii) mass and mole fractions, (iii) enthalpy and internal energy, (iv) specific gas constant and adiabatic exponent. Other areas covered include boundary conditions which consist of (a) symmetry planes, and (b) inlet and outlet. Furthermore, this chapter explained numerical methods which are employed to solve the reactive Navier–Stokes equations consisting of finite volume methods, calculations of various fluxes of control volumes and calculations of sources as well as explicit and explicit-implicit schemes. In addition, it treated AMROC software used for adaptive mesh refinement strategies of structured and unstructured approaches.

Chapter 4 treated the chemical kinetics of the whole processes which is central in this research. It covered the basic concepts of reaction rates which includes the law of mass action, reversible and multistep reactions, reversible equilibrium, the Arrhenius law, and rates of reactions. Also, this chapter explained Chain reactions which play fundamental roles in combustion reaction mechanisms, and they comprised three basic steps, i.e. chain initiating step, chain carrying or propagating step and chain terminating step. The most important chain reactions to combustion processes are two of them: - straight-chain and branched-chain reactions, and they were treated in detail individually. Furthermore, it described the chain reaction theory which consists of straight-chain reaction e.g., hydrogen-halogen reaction; and branched chain reaction for example, hydrogen-oxygen reaction. Also, this clearly explained the mechanisms for combustion reactions of hydrocarbon fuels; and the oxidation of hydrogen and carbon monoxide reactions which entails detailed reaction mechanisms for hydrogen oxygen reactions and the calculations of reaction rates as well as the oxidation of hydrocarbons.

Chapter 5 explored the influences and effects of chemical reaction mechanisms to generations, propagations, and transitions of explosion waves. To this end, two premixed combustible mixtures: - hydrogen-oxygen and propane-oxygen mixtures were selected and filled into two-dimensional tube domains, then the mixtures were ignited. However, this chapter carefully examined the effects and influences of kinetics on the combustion reactions of hydrogen-oxygen and propane-oxygen filled in a tube. The results obtained showed that chemical kinetics have effects and influences on the explosion based on the case studies investigated. However, no DDT and no FD were formed for case studies 2, 3, 4, and 5 and this was because it is an open-end tube and there is no limited gas expansion, and no artificial obstacle, and therefore, deflagration-to-detonation transition (DDT) and fast deflagration (FD) were not formed, but the ignition process moves straight to detonation, thus forming a single explosion. Comparing the different case studies of H₂-O₂ studied: a, b, c, d, and e showed that it was only case study e that formed detonation, DDT, and FD, and consequently explosion occurred, and that was because case study e had very high temperature. In addition, in comparing the case studies of the reactions of propane-oxygen mixtures investigated, it showed that it was only case study 20 that did not form detonation. However, the rest case studies 21, 30, 31 and 40 formed FD, DDT, and detonation flame forms, and this is because case studies 21, 30, 31 and 40 had high fuel concentration and high temperatures, and hence explosion occurred.

Chapter 6 investigated the influences and effects of geometric configurations on explosion waves. Therefore, the computational domain is not tube-shaped like one in the last chapter. In this chapter, two premixed combustible mixtures: - hydrogen-oxygen and propane-oxygen are chosen and investigated. This chapter will logically examine the influences and effects of geometric configurations of effectobstacle, vent and oneBlock on explosion involving the combustion reaction processes of H₂-O₂ and propane-oxygen combustible mixtures respectively. It was observed that complex geometry has great influences and effects on explosion and that there is a high delay induction time, hence for case studies step and wall of H₂-O₂ combustion processes, no FD and no DDT were formed, rather the ignition process moves straight to detonation. However, for case studies 20 and 21 of propane-oxygen combustion process, because of the influences of complex geometry on the propane combustion, no detonation was formed. For example, for case study Block, FD, and DDT and

detonation were formed, but for case studies Step and Wall, no FD and no DDT were formed, but the ignition process moves straight to detonation thereby forming single explosion. Hence, when vent is created in the tube, DDT will occur and consequently detonation is achieved, and vent explosion will take place. The simulated results agreed with the principles of the effects of complex geometry on explosion. A good comparison of the effects and influences of simulation results of case studies 20, and 21 showed that there was no Detonation formed, but concerning that of case studies 30, 30X, 31 and 31X, there was quantum jump from DDT to Detonation, hence, fast detonation occurred, and explosion suddenly resulted. Additionally, the beauty of Computational Fluid Dynamics (CFD) is that after the simulation of the whole process, one can capture more information [45].

Chapter 2 Chemical Explosion Waves

In this chapter, a general review of chemical explosion waves will be explored. First, a description of explosion, deflagration, detonation, flashover, backdraft, explosion blast waves, and deflagration-to-detonation transition (DDT) coupled with Hugoniot curves, upper Chapman-Jouguet (CJ) and lower Chapman-Jouguet (CJ) points will be explained. Then, an outline of some explosion disasters in the oil and gas industry and the lessons learnt will be discussed.

2.1 Overview of explosions

An explosion produces high-pressure gas into the environment, and as a result, it can lead to massive property damage. In simple term, explosion is an event leading to a rapid increase of pressure. The released high-pressure gas in an attempt to seek equilibrium with the pressure of the surrounding environment will thereby dissipate the energy from the shockwave into the environment thus causing damage. Forces producing the high-pressure gas can be various, for example, mechanical pressure releases mechanical explosion or chemical reactions chemical explosion).

Mechanical explosion is due to failure of a pressure vessel, in which the explosion occurs as the sudden release of pressure due to mechanical means. An example of this type of explosion is the release of energy resulting in the failure of a pressure vessel. In physical explosion, there is no chemical change in the substance involved [3], [46]. Chemical explosion is caused by chemical reactions. The reactions transfer chemical energy into heat, resulting in gas expansion and high pressure zone. It is always accompanied by shock waves.

The magnitude of the increased high pressure depends upon many factors which include the rate of the release; the quantity of the gas released; the directional factors governing the release; the type of explosive agent; the space in which the agent is detonated; and the degree of confinement of the explosion [47].

There are four forms of chemical explosions that are often seen in practices which are include the followings:

2.1.1 Deflagrations

In accidental gas explosions, the most common mode of flame propagation is referred to as deflagration. Deflagration is an explosion in which the combustion wave propagates at subsonic velocities that are relative to the unburnt gas just in front of the flame. In the deflagrative mode, the flame speed of deflagration process ranges from a few m/s up to 100 – 300 m/s, and depending on the flame speed, the explosion pressure ranges from millibar to several bar. Usually, the gas cloud and the geometrical conditions of the process equipment within the cloud determine the flame speed and explosion pressure. Even if the prevailing parameters such as cloud size, fuel concentration and ignition point are known, the prediction of the flame speed and explosion pressure for a deflagration process is a difficult task.

It is an exothermic reaction which propagates from the burning gases to the unreacted materials by conduction, convection, and radiation. Deflagration is the combustion of a gas or aerosol that is characterised by a shock wave. In deflagration, the combustion wave passes through the gas-oxygen, burning until all the fuel is used. In deflagration, the rate of travel of the combustion wave is less than the speed of sound. The maximum pressures of approximately eight times the initial pressure result from deflagration of stoichiometric gas-air mixtures. Eventually, most explosions which take place in the industry are deflagrations [47]. Furthermore, after deflagration, the next section will discuss detonation.

2.1.2 Detonations

Generally, the most devastating form of gas explosion is detonation and compared to deflagration, detonation does not require confinement to propagate at high velocity. However, the behaviour of a detonation is entirely different from that of a deflagration even in an unconfined environment (situation). Detonation as a supersonic combustion wave, the detonation front usually propagates into unburnt gas at a velocity higher than the speed of sound in front of the wave. Usually, the velocity of a detonation process in fuel-air mixtures is 1500-2000 ms⁻¹, and the peak pressure is 15-20 bar [48]. The reactivity of the gas cloud greatly determines the transition to detonation, the propagation and the transmission of detonation waves [48].

Detonation is a combustion wave propagating at supersonic velocity relative to the unburnt gas immediately ahead of the flame. In contrast, detonation is an exothermic

reaction characterised by the presence of a shock wave in the material which determines and maintains the reaction. Detonation as a unique combustion phenomenon is the /combustion of a gas or aerosol which is characterised by a shock wave. In detonations, the shock wave travels at a speed greater than the speed of sound and the shock wave is characterised by very high pressure initiated by a very rapid release of energy. If the flammability of the gas mixtures is greater than the flammability limits of the explosive gas, such gas mixtures (fuel and oxidizer) will not spread in a burning zone or combustion wave. The combustion wave whether it is deflagration or detonation, it is determined by the flammability limits of the gas mixtures [49]. Detonations are much more destructive than deflagrations. Eventually, the very high pressure which was created from the shock wave does serve as heat source for the ignition of other combustibles in the area [47].

Table 2.1: Qualitative differences between deflagration and detonations in gases [4]

| S/No. | Ratio | Usual magnitude Ratio | |
|--|-----------------|-----------------------|------------|
| | | Deflagration | Detonation |
| 1 | u_u/c_u^a | 0.0001 – 0.03 | 5 – 10 |
| 2 | u_b/u_u | 4 – 16 | 0.4 – 0.7 |
| 3 | P_b/P_u | 0.98 – 0.976 | 13 – 55 |
| 4 | ρ_b/ρ_u | 4 – 16 | 8 – 21 |
| <i>a_{c_u}</i> is the acoustic velocity in the unburned gases. <i>u_u/c_u</i> is the Mach number of the wave. | | | |

Explosion and detonation can easily be confused, but explosion does not definitely need the passage of a combustion wave through the exploding medium. For the occurrence of either a deflagration or a detonation, an explosive gas mixture must be present [50], [51]. This implies that though both deflagrations and detonations require rapid energy release; explosions equally require rapid energy release, but explosions do not involve the presence of a waveform. The differences between deflagration and detonation are qualitatively illustrated in Table 2.1 above [4].

Considering several conditions, a deflagration or a detonation wave can be supported by an explosive medium. Indeed, the most known conditions of deflagration or a detonation are confinement, mixture ratio, and ignition source. Besides, the flame that propagates with subsonic speed is the major result of a common thermal initiation. The flame can cause adiabatic compression of the yet unreacted mixture ahead of it when

the flame velocity increases. The speed of the flame appears to rise gradually until it is equal to that of a detonation wave depending on some early observations [49]. Usually, an irregular change of velocity is observed from the low flame velocity to the high speed of detonation [52]. However, the detonation wave has been observed to begin apparently and spontaneously at certain distance ahead of the flame front. Besides, the starting point seems to occur simultaneously (match) with the location of a shock wave sent out by the expanding gases of the flame. The observations in modern experiments and analysis are dependent on the mode of initiation. Two modes of initiation occur in detonation phenomena—the slower mode known as thermal initiation (self-ignition) is the mode in which there is transition from deflagration; and the fast mode called direct ignition is the mode caused by an ignition blast or strong shock wave [4]. For instance, if a tube with one or both ends opened is placed an explosive gas mixture, a combustion wave can thus spread when the tube is ignited at an open end. Therefore, the wave will have a steady velocity, but cannot accelerate to a detonation wave. Nevertheless, if the mixture is ignited at one closed end of the tube, a combustion wave is thus formed, but if the tube is long enough, the combustion wave can speed up to a detonation. The mechanism of the thermal initiation can be explained thus: for process of initial deflagration, the burned gas products have an exact volume at the rate of 5–15 times that of the unburned gases ahead of the flame. Furthermore, the preheating can likely increase the flame speed, and this will consequently accelerate the unburned gas mixture to a point that turbulence will be developed in the unburned gases even to greater velocity and acceleration of the unburned gases thereby obtaining compression waves [53]. Eventually, this sequence of events will form a shock which can be strong enough to ignite the gas mixture ahead of the front. Besides, the reaction zone at the back of the shock does send a continuous compression wave that prevent the shock front from decaying, thereby forming a detonation. When shock is formed, a detonation is thus formed, and it propagates back into the unburned gases [49]. Moreover, the reaction zone in a detonation wave is the same as in other flames because it provides the sustaining energy. A difference does exist in that the detonation front initiates chemical reaction by compression, by diffusion of both heat and species, and thus inherently maintains itself. Essentially, worthy to note is the difference in the reaction that take place with unusual speed in extremely compressed and preheated gases. For cases of extremely reactive fuels such as acetylene, hydrogen, and ethylene, the duration of transition for deflagration to detonation is in meter order, but the

duration of transition is larger for the majority of other hydrocarbon–air mixtures. Eventually, the duration of transition is governed by several physical and chemical features of the experiments. To this background, certain question may arise as to whether methane can even detonate. Furthermore, direct initiation of a detonation can only take place when a strong shock wave is produced by a source and the shock usually maintains a minimum strength for certain specified duration. It is obvious that reaction rates are involved in ascertaining the establishment of a detonation occurrence [52], [53]. Now that detonation has been reviewed, the next section will handle flashover.

2.1.3 Flashover

Flashover is a quick fire in an enclosed area that can foster the build-up of heat when the temperature gets to the ignition temperature of the majority of the combustibles in the area, and thus spontaneous combustion of the combustibles occurs in the area [31]. Moreover, after deflagration, detonation and flashover, the next part to be explored is backdraft.

2.1.4 Backdraft

Backdraft as unique combustion phenomenon is a fire in an enclosed area that consumes the oxygen supply and thus generates carbon monoxide and heat. Hence, it is seldom called smoke explosion and because the oxygen is used up, the fire tends to smoke a lot and consequently the carbon monoxide will burn rapidly with an explosive force [54].

Having reviewed tank farm incidents as well as explosions, the next section would consider some major oil and gas sector explosion disasters that caused many nations of the world great catastrophic disasters.

2.2 Explosion disasters in oil and gas industry

When flammable vapours of liquefied petroleum gas (LPG) and gasoline are released from various sections in oil and gas industry without immediate ignition, a heavy vapour cloud will be produced. Dispersion and shape of the heavy gas cloud is dependent on the size and location of the break in the containment as well as its molecular weight and low temperatures. During the dispersion, the gas mixes with the

ambient air to form premixed combustible mixture within the cloud. If it is ignited, the flash fire, fireball and vapour cloud explosion will take place [55], [56] The following gives three large explosion disasters historically.

2.2.1 Piper Alpha disaster

The volatile nature of the hydrocarbon at the offshore production platform was responsible for the piper alpha disaster which was caused by the kinetics of the hydrocarbons present and the geometry, and this is why this research is looking at this explosion disaster. The lesson learned from the piper alpha disaster are quite valid far beyond the offshore oil industry, cut across every hazardous industry and moreover, every aspect of the lesson is relevant in present day work operation. However, the changes include: the design issues changed by management; prioritised personal safety over process safety; permit to work system enforced; the handover process with inadequate transfer of information between crews, shifts and disciplines corrected; safety culture enforced; and emergency response and evacuation procedures changed. In addition, the living quarters for workers on board were separated from the production platform thus making the platform safer for operations [56].

In United Kingdom, an oil fire explosion happened on a production platform at the Giant Piper Alpha in the North Sea of Aberdeen, UK on 6th Jul 1988 killing 167 offshore oil rig workers. Today Piper Alpha disaster stands as one of the worst oil rig disasters in history [56]. The primary cause of the piper alpha oil rig explosion disaster was because of the maintenance work carried out on a high-pressure condensate pumps and safety valve which led to a gas leakage of condensate from platform pipe [56]. Prior to the shift change, a pressure safety valve had been taken off earlier in the day by the routine maintenance crew, and the incoming maintenance crew was not adequately informed not to turn on one of the affected pumps. Worst still, because of this improper handover, the incoming maintenance crew commencing their hot work coupled with the gas leakage, explosion resulted leading to series of explosions and consequently the oil rig platform caught fire [56]. The oil rig platform was completely burnt down and combating the fire lasted three weeks. Red Adair, the world-famous firefighter helped to put out the fire on the Piper Alpha Oil platform (see Figures 2.1(a) and (b) in Section 2.2.1) [56].

Furthermore, after the piper alpha disaster incident, the following resolutions were reached:- That every offshore operator to carry out immediate wide-ranging assessments of their installation and management systems which include:

- a) Permit to work management system to be improved.
- b) Some pipeline emergencies shut down systems have to be relocated
- c) Smoke hazards have to be strictly prevented
- d) Evacuation and escape systems to be properly improved.

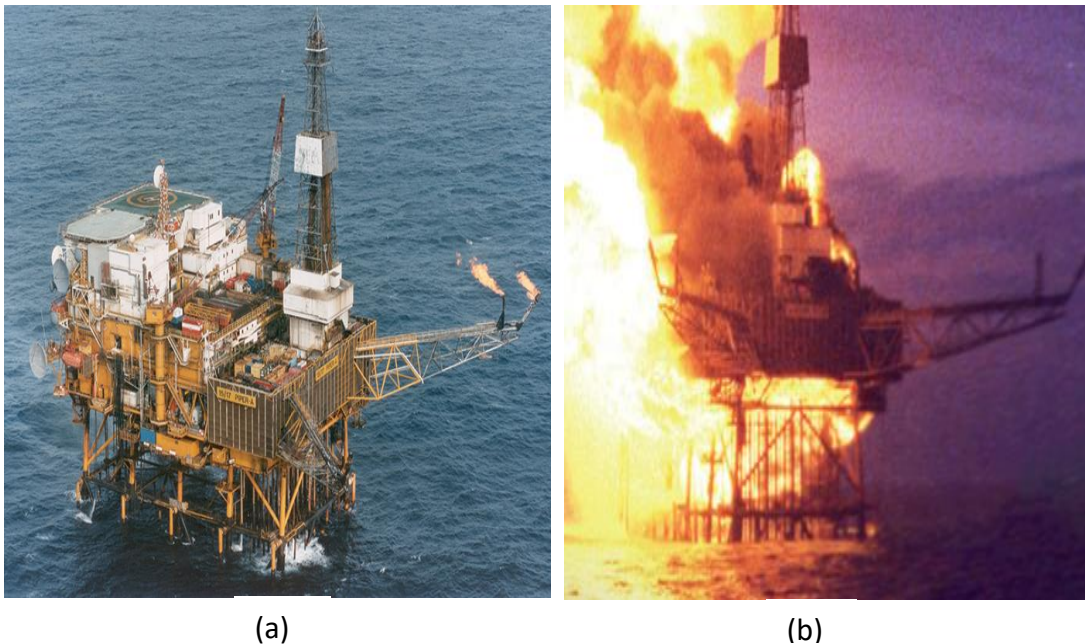


Figure 2.1 (a): Piper Alpha Offshore Oil Rig, Britain prior to the incident; (b): Piper Alpha Offshore Oil Rig after the incident [56].

In addition, after examining the causes, the lessons learnt and the resolutions reached concerning the piper alpha disaster, other unique explosion disaster which took place in the oil and gas sector with a global impact economically is the Deepwater Horizon explosion that occurred in USA in 2010 and the details of the explosion disaster will be treated in the next section.

2.2.2 The Deepwater Horizon explosion

The Deepwater Horizon drilling rig that was engulfed by fire resulted because of the kinetics and geometry of the volatile hydrocarbons at such oil drilling rig and for this reason, this work will at the explosion disaster. In United States of America (USA), the Deepwater Horizon drilling rig was dramatically engulfed by fire on 20th April 2010. On April 20, 2010, an explosion and ensuing fire occurred on the semi-

submersible mobile offshore drilling rig unit (MODU). It was owned and equally controlled by Transocean carrying out drilling jobs for BP in the Macondo Prospect Oil Field located at about 40 miles (64km) Southeast off the Louisiana coast [57]. The Deepwater Horizon drilling rig explosion was caused by well blowout and oil spill incidence, and it is the worst worldwide marine oil spill which ranked the most terrible environmental disaster in the U.S history [57]. This singular oil rig explosion killed 11 persons and 17 workers were injured and total crew was 126. After a thorough investigation was carried out, the U.S. government made BP to settle families with \$5.5 billion payable for a duration of 16 years because of the Deepwater Horizon oil spill [57]. Moreover, two BP rig supervisors responsible for overseeing the operational activities of the Deepwater Horizon rig were faulted. U.S. official report stated that out of the 126 people on board during the incident, 79 were Transocean employees, 7 BP staffs and 40 were contractors. During evacuation, 94 workers evacuated by lifeboat, 17 by helicopter and 4 evacuated by another vessel, thus bringing a total of 115 people that were safely evacuated as shown in Figures 2.2 (a) and (b) in Section 2.2.2 [57].

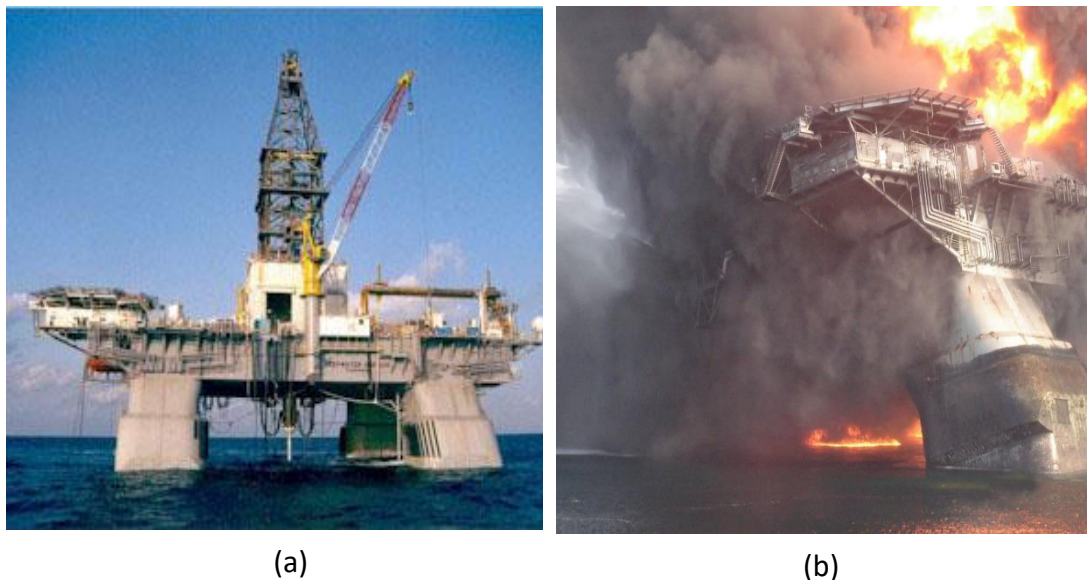


Figure 2.2 (a): Deepwater Horizon Drilling rig prior to the incident; (b): Deepwater Horizon Drilling rig after the incident [57].

The lessons learnt from the Deepwater Horizon oil spill is to do remote shutoff capability and they include amongst others include:

- a) Additional back up systems require to shut down offshore wells automatically.
- b) Relief well capability requirement needs to be adopted.
- c) Meaningful financial penalties for Deepwater spills to be imposed.

d) Energy legislation to be enacted [57].

Furthermore, after completing the review of the Deepwater horizon oil explosion, another explosion disaster that happened in oil and gas history which stands today as the world largest oil drilling rig production platform accident is the Petrobras-36 oil drilling rig, Brazil and the next section will examine the details of the disaster.

2.2.3 Petrobras P-36 Oil drilling rig explosion

The Petrobras P-36 rig, a semi-submersible came into operation in the Roncador Field off coast of Brazil in May 2000 and it conveniently processes 180,000 bpd and 7.2 million cubic metres of gas daily [58]. The Petrobras P-36 rig which had a production capacity of 84,000 barrels of oil and 1.3 million cubic metres of gas per day was devastated by two explosions and consequently the Petrobras P-36 Rig became submerge. On the 14th March day of 2001, an explosion happened at 10.21 pm and the cost implication of this incidence was US\$350 million (US\$495 million) and on 15 March 2001, an explosion took place in the starboard aft column, leading to mechanical rupturing of the starboard Emergency Drain Tank (EDT), thus the released gas-saturated water and oil into the aft starboard column resulted to the explosion at the platform at 0027 hours [58]. Furthermore, another huge gas explosion occurred killing 11 members, 137 people injured, and injuring seriously a member of the firefighting crew caused by two explosions that occurred on the drilling rig. Eventually, the Petrobras P-36 rig, sank on 20th March 2001. at about 0022 hours (12:22 am) (see Figures 2.3 (a) and (b) in Section 2.2.3) [58].

In the Petrobras P-36 Offshore oil Rig Accident, Brazil, an environment saturated with volatile hydrocarbons at such oil drilling rig which resulted to such disaster due to the kinetic nature and geometry, and this research work will attend to the explosion disaster. In preventing the possible occurrence of fire explosions in an offshore drilling rig of this nature with highly volatile hydrocarbons, the following steps are taken:

- 1) Ensure all personnel are adequately trained in relevant courses to offshore rig operations.
- 2) Safety rules to be consistently enforced, drillers to adhere to all offshore safety standards and regulations including rules that forbid use of drugs and alcohols.
- 3) Workers to be cycled regularly
- 4) All offshore workers to be supplied with necessary protective wears, e.g. hard hats, gloves, safety glasses and respirators.

- 5) Be consistent with proper housekeeping. Offshore drillers should ensure that all areas are clear of hazards that can cause injuries to workers or cause them to trip or fall.
- 6) Ensure that equipment is well maintained. To be in good working condition by implementing a mechanical integrity programme [58].

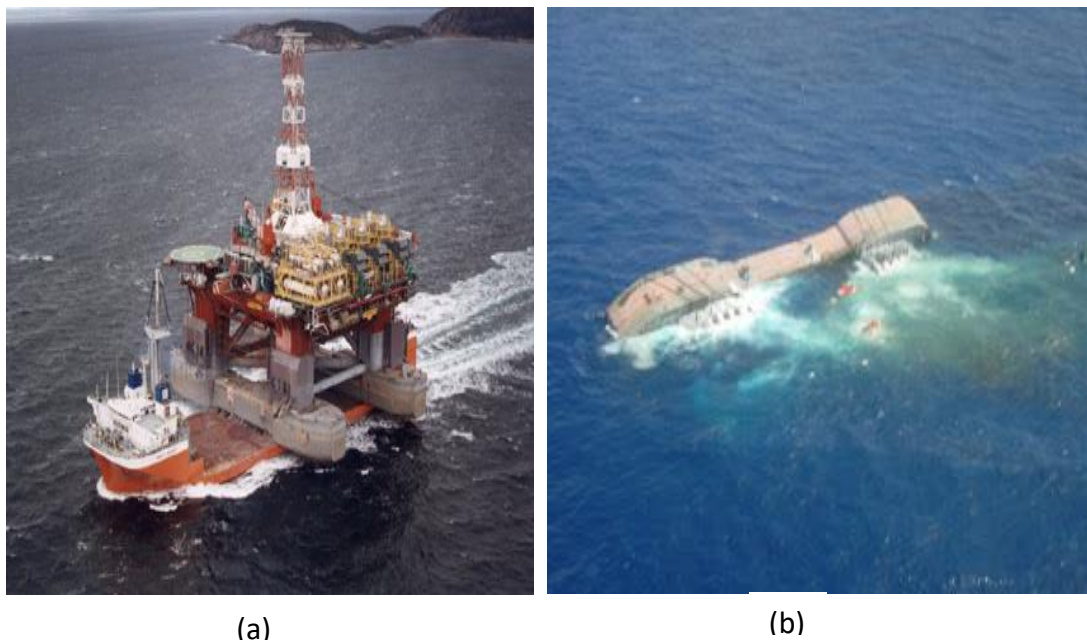


Figure 2.3 (a): Petrobras P-36 rig, Brazil prior to the incident; (b): Last minute of P-36 rig after the incident [58].

The actual reasons for the damage of the Petrobras P-36 rig were absolutely due to the alignment of the port EDT to the Production Header rather than to the Production Caisson, allowing hydrocarbons into the starboard EDT [58]. Moreover, another factor was the delay in the activation of the port EDT drainage pump, permitting the reverse flow of hydrocarbons for about one hour, and coupled with the failure of activators to close ventilation dampers, which made water to flood the starboard column and pontoon compartments. In addition, other causes for the incidence were the two sea water pumps which were under repair without measures in place in case of emergency. The additional probable cause was the inadequate contingency plans and inadequate training for handling emergency ballast and stability control situations [58]. Having considered explosion disasters in the oil and gas sector, we will therefore proceed to review the explosion blast waves in the next section.

2.3 Explosion blast waves

Blast wave in fluid dynamics is referred to as the increase in pressure and flow that result from a huge amount of energy deposited in a very small, localised volume. The flow field being equivalent to a shock wave that comes after a self-similar subsonic flow field. Furthermore, a blast wave as an area of pressure which expands supersonically outward from an explosive core is usually accompanied by a blast wind of negative pressure [59]. Consequently, blast wave is harmful whenever one is quite close to the centre and blast waves are generated through the detonation of high explosives. A mathematical investigation of the behaviour of the blast wave from an exploding spherical volume is propagated over the entire range of blast-wave. Moreover, the computational method uses analytical results for a similar problem for a point explosion with counter pressure and the theory of an asymptotically equivalent point explosion. The spatial distribution of the blast-front pressure is established for combustible gaseous systems and solid explosives, and the theoretical results obtained thus agreed quantitatively with available experimental measurements [59]. Moreover, blast wave usually generated by an explosion comprises a shock front in which the pressure rises almost immediately, accompanied by an expansion wave whereby the pressure goes back to its ambient value [43]. The pressure usually over expands below ambient pressure thereby having a negative phase as well as a positive phase from explosion centre on a long range.

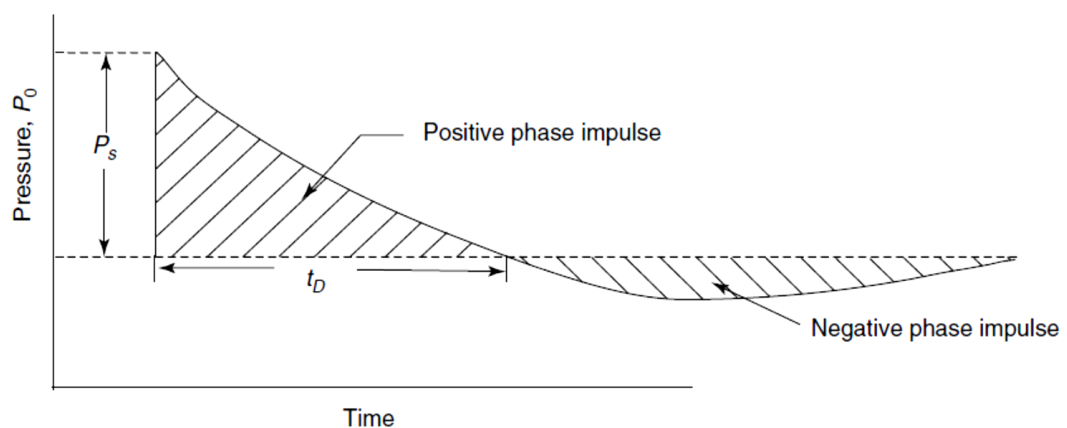


Figure 2.4: Blast wave generated by an explosion [60].

Figure 2.4 in Section 2.3 clearly describes the characteristic form of an ideal blast wave. In addition, the magnitudes of the pressure go up across the shock front, P_s , and the other blast wave parameters represented in Figure 2.4 depend absolutely on the explosion energy release characteristics and the distance from the effective explosion centre. Generally, the shock pressure P_s , increases, which decreases with distance from the centre of explosion. Consequently, the blast wave decays to an acoustic wave traveling at the speed of sound in air of about 330 m/s [60].

Furthermore, both the shock front pressure rise, P_s , and the impulse, I_s , determine the effect of a blast wave and this is the area under the positive phase of the pressure versus time curve. When both the impulse and the shock pressure P_s exceed damage threshold values, any specific object will suffer damage [60].

The Table 2.2 below explains the damage threshold pressures and impulses and their related impact on structural damage and injuries to persons coupled with consequential effects on Oil storage tank in operational production settings.

Table 2.2: Blast damage and personal injury pressures and impulses [60].

| Structure/object | | Pressure (psig) | Impulse (psi-msec) |
|---------------------------------|---|-----------------|--------------------|
| Plate Glass Windows: | 20 ft ² pane, 3/16" thick | 0.3-0.6 | - |
| | 10 ft ² pane, 3/16" thick | 0.6-1.0 | - |
| | 10 ft ² pane, 1/4" thick | 1.1-1.6 | - |
| | Wood Roof Joist, 13 ft span | 0.5 | - |
| | Brick wall – Minor damage | 0.7 | 16 |
| | Brick wall – Major damage | 2.0 | 43 |
| | Wood Stud wall, 7.5 ft high | 1.0 | 1 |
| | Sheet metal panel Buckling | 1.1 – 1.8 | - |
| | Wood siding Failure | 1.1 – 1.8 | - |
| | Cinder Block wall Failure | 1.8 – 2.9 | - |
| | Wood frame building collapse | 3.0 – 4.5 | 36 |
| | Oil storage Tank Rupture | 3.0 – 4.5 | - |
| | Structural steel building | 4.5 – 7.3 | - |
| | Reinforced concrete wall | 6.0 – 9.0 | - |
| | Total destruction of most buildings | 10 - 12 | - |
| Overturning of 10 ft high truck | 0.3 | 110 | |
| Personal Injury | Personnel knock down | 0.5-1,5 | - |
| | Eardrum rupture threshold | 5 | 7 |
| | 50 th percentile eardrum rupture | 15 | 22 |
| | Lung damage threshold | 10 | 340 |
| | 99% Lethal lung damage | 50 | 1940 |

(a) Ideal blast waves

Furthermore, an ideal blast wave is one in which the energy is released rapidly compared to the time required for the blast wave to propagate to a particular target. The explosive energy released can occur within a short distance compared to the distance to the target. In addition, the blast waves associated with condensed phase explosives such as explosive 2,4,6 -Trinitrotoluene (TNT), $C_7H_5N_3O_6$ are prominently ideal blast waves with a molar mass of 227.13g/mol [61].

Mathematically, both the blast wave pressure and impulse vary as distance divided by the one-third power of the blast wave energy for ideal blast waves. Also, the nondimensionalised distance of a target from the energy release centre can be represented by,

$$\bar{R} = R(p_0/E)^{1/3} \quad (2.1)$$

where R is the distance from energy source (m), \bar{R} is the nondimensional distance, p_0 is the ambient pressure (kPa), and E is the blast wave energy (kJ).

In addition, the blast wave energy is expressed in terms of the equivalent weight of TNT that can produce the same energy, and the relationship would be:

$$W_{TNT} = E/4200 \text{ kg} \quad (2.2)$$

where W_{TNT} stands for the equivalent weight of TNT (kg), E is the blast wave energy (kJ), and 4200 kJ/kg is the specific energy potential of TNT.

The blast wave energy, E , generated during the rupture of a pressure vessel containing a compressed gas is given by,

$$-E = V (P_1 - P_0)/(\gamma - I_r) \quad (2.3)$$

where I_r is the reflected shock wave, I_s is the positive phase impulse, and P_r/P_s is the ratio of reflected shock pressure to incident shock pressure

If the vessel contains a liquefied gas that may partially condense upon sudden expansion, the energy released in expansion is equal to the change in internal energy, i.e.

$$E = m(u_1 - u_2) \quad (2.4)$$

where u_1 and u_2 designate the fluid internal energy prior to and immediately after expansion to ambient pressure [61]. In the next section, this report will then peruse deflagration and detonation as well as Chapman-Jouguet waves.

2.4 Deflagration and detonation

2.4.1 Deflagration waves

Generally, a deflagration wave is a gas explosion in which the flame front propagates at a subsonic speed that is absolutely relative to the unburnt gas, just in front of the wave. During a gas explosion, the velocity of the gas propagation can cover more than three orders of magnitude, and the mechanism of flame propagation varies with different flow velocities. Besides, when a weak ignition source ignites the cloud, the resulting flame is a laminar flame [43]. Figure 2.5 below explains the structure of a laminar flame and a laminar flame propagates at a velocity of $3 - 4 \text{ ms}^{-1}$. The type of fuel and the fuel concentration are the determinant factors for the speed of the propagation of the laminar flame. Figure 2.6 in Section 2.4.1 indicates that the velocity of the flame front is relative to the unburnt mixture just ahead of the flame, and the laminar burning velocity for mixtures such as methane-air, ethylene-air and hydrogen-air has about 0.4 ms^{-1} as the maximum burning velocity. Typically, hydrocarbons have maximum laminar burning velocities of $0.4 - 0.5 \text{ ms}^{-1}$. Based on the fast chemical kinetics and high molecular diffusivity, ethylene, acetylene and hydrogen have higher burning velocities [62].

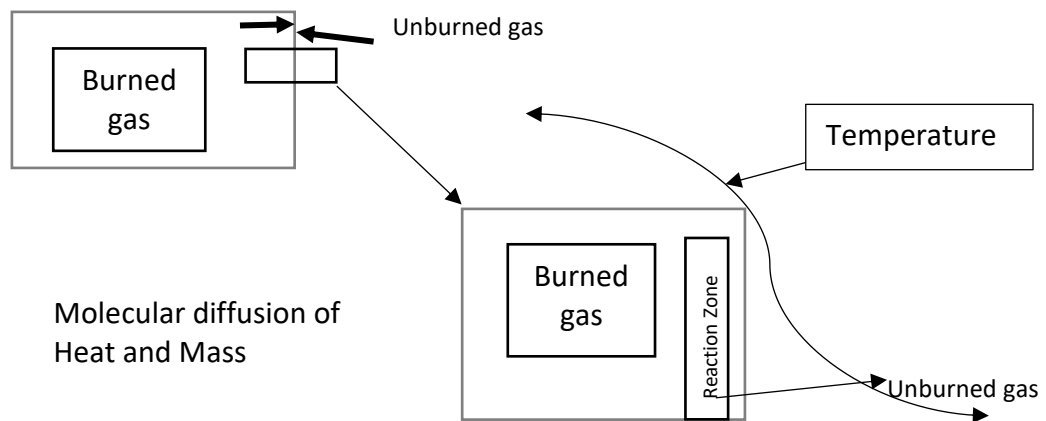


Figure 2.5: Illustration of the structure of a laminar flame front in a premixed gas [63].

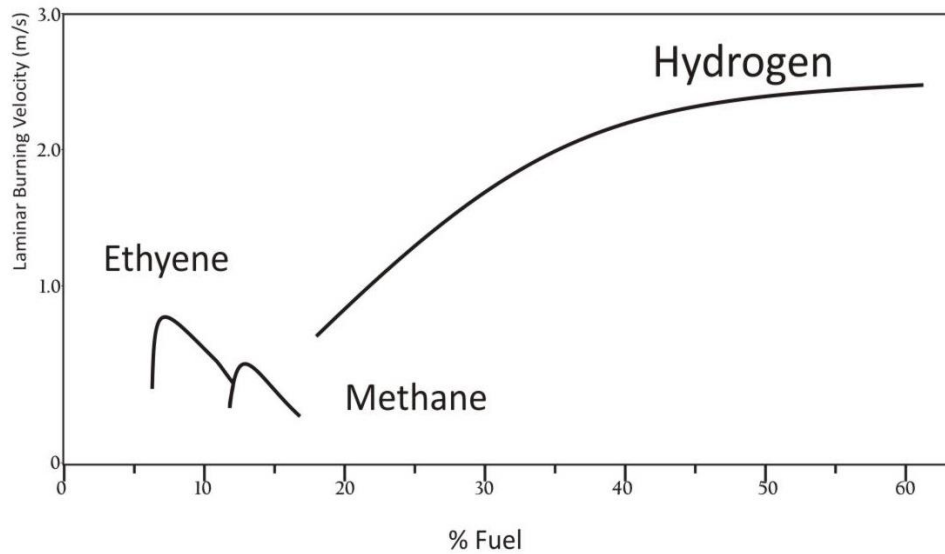


Figure 2.6: Laminar burning velocity for methane-, ethylene- and hydrogen-air [63].

Because the flow field ahead of the flame front becomes turbulent, the laminar flame accelerates and transits into a turbulent deflagration (turbulent flame) in several accidental explosions. The interaction of the flow field with process equipment, piping, structures to mention a few accounts for the turbulence [63]. Considering how turbulence influences the structure of the front which consequently increases the burning rate, and the increase in burning rate is caused by the wrinkling of the flame front due to large turbulent eddies. The increased flame surface area will make the burning rate to increase. Besides, this regime is identified by the turbulent integral length scale, l_t , which is typically larger than the thickness of the flame front, δ . However, when the turbulent integral length scale, l_t , is of the order of the thickness of the flame front δ or smaller, the flame will thus become a thick, turbulent flame brush. The turbulence accounts for increased diffusion of heat and mass and thus resulting in a high burning rate in this regime [63]. Two mechanisms that result in pressure build-up when a flame propagates through a premixed gas cloud are (i) fast flame propagation and (ii) burning in a confined volume. Usually, a combination of these two mechanisms is responsible for pressure build-up in several accidental explosions [61]. The drop in pressure at the flame front is needed so that the conservation equations across the flame front can be satisfied. Because the pressure behind the flame in the burnt gas will slowly decay away from the flame, the boundary conditions on the left end of the tube either open or closed tube and the flame velocity will determine the pressure decay. When a part of the vessel wall is opened and a relief

is provided, the pressure will consequently reduce. The speed at which the flame is burning in the vessel and the location and size of the vent area will determine the pressure reduction. An increase in the burning velocity (the difference between the flame speed and the mean flow velocity) will constitute a rise in explosion pressure. Figure 2.7 below describes the mechanism of flame acceleration resulting from repeated obstacles that produces a strong positive feedback loop [63].

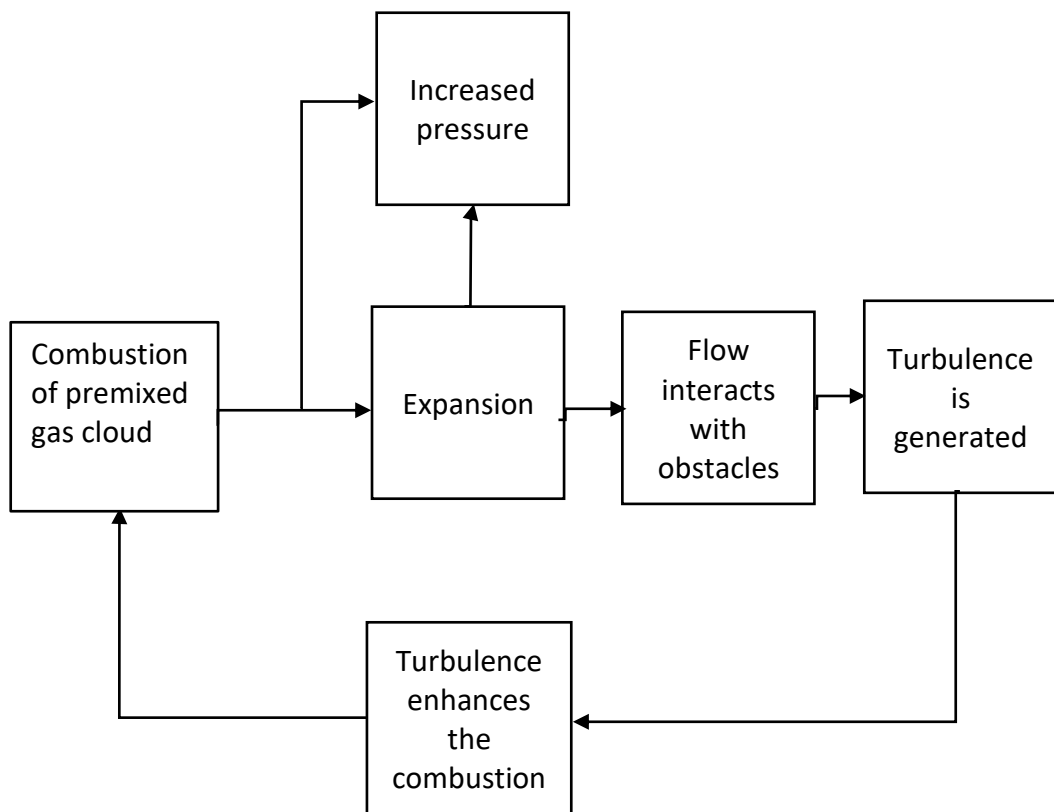


Figure 2.7: Positive feedback loop causing flame acceleration due to turbulence [63].

Deflagration waves are types of waves that usually travel in subsonic form with the signs $p_b < p_u$ and $v_b > v_u$, and this shows that crossing such a wave, there will be a decrease in both pressure and density, but with an increase in the velocity. Moreover, the likely reduction in pressure is bounded by the sign $0 \leq \hat{p} \leq 1$. However, the possible increase in specific volume is bounded by the signs;

$1 + \hat{q}_c(\gamma - 1)/\gamma \leq \hat{v} \leq 2\hat{q}_c + (\gamma + 1)/(\gamma - 1)$, which have the lower and upper limits respectively that relate to $\hat{p} = 1$ and $\hat{p} = 0$.

Furthermore, the solutions with higher and lower values of pressure decrease are known as strong and weak deflagrations respectively. However, there is also a maximum Rayleigh line beyond which no solution can exist. In addition, the point of tangency referred to as the lower CJ point, and the comparable wave is known as a CJ deflagration. Thus, it can be disputed that there is no occurrence of strong deflagrations. However, when the entropy decreases in crossing such a wave, it shows that strong deflagration will not take place, and consequent upon this situation, it can thus be contended that in the presence of the heat released (q_c) is greater than zero i.e. $q_c > 0$, there will be no existence/occurrence of strong deflagration [63]. Therefore, considering weak deflagrations where pressure is less than 1, that is $\hat{p} \lesssim 1$, this shows that the change in pressure across such wave would be very small. Hence the structure of such wave could be isobaric which implies that it is a thermodynamic process in which the pressure change is constant, that is $\Delta P = 0$ in this case. Also, applying the first law of thermodynamics, the heat transferred to the system works, but the internal energy of the system changes. This can be represented with equation (2.1):

$$Q = \Delta U + W \quad (2.5)$$

Where W is work, U is internal energy, and Q is heat

Also, when strong deflagrations have pressure less than 0, $\hat{p} < 0$, then only the weak deflagration intersection will occur, and this further cancels out its occurrence.

Deflagration waves travel subsonically which show that in crossing such deflagration waves, the pressure and density will decrease, but the velocity will increase. In addition, strong and weak deflagrations are determined by the solutions with higher and lower values of pressure reduction respectively. There also exists a maximum Rayleigh line beyond which no solution exists. The point of tangency is called the lower CJ point and the corresponding wave is the CJ deflagration. Consequently, in the presence of heat release, strong deflagration does not occur.

Moreover, for weak deflagrations where density, $\hat{p} \lesssim 1$, and this implies that the pressure change across the wave will be very small, whereas for strong deflagration, the pressure change will be $\hat{p} < 0$.

Deflagration: If the combustion wave is very slow, it is not explosion, but if the combustion wave is very fast, it is explosion, hence fast deflagration is explosion because the overpressure is double that of fire [63].

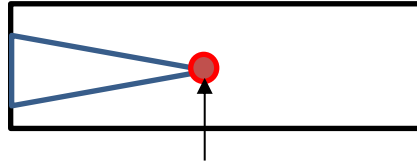
2.4.2 Detonation waves

The theory of detonation that explained the supersonic combustion wave propagating at a specific velocity was second to none to be presented by Chapman and Jouguet. In addition, the detonation wave as a discontinuity with infinite reaction rate was handled by the CJ (Chapman-Jouguet) theory [64]. The distinctive solution for the detonation velocity (CJ-velocity) and the state of combustion products just before the detonation wave was obtained by the conservation equations for mass, momentum, and energy across the one-dimensional wave. When the mixture of the gas is known, then the detonation velocity, detonation pressure etc. can be calculated [48].

Generally, these types of waves travel in supersonic form with the signs $p_b > p_u$ and $v_b < v_u$, and this shows that crossing such a wave, the pressure and the density will increase but the velocity will consequently decrease. The pressure that probably increases are limited by the signs $1 + (\gamma - 1)\hat{q}_c \leq \hat{p} \leq \infty$, which have the lower limit that relates to the sign $\hat{v} = 1$ as shown in equation (1). The specific volume that is likely reduced is limited by the sign $(\gamma - 1)/(\gamma + 1) \leq \hat{v} \leq$, which has a lower limit that relates to $p = \infty$ [31].

Furthermore, the results of higher and lower values of the pressure jump are identified independently as strong detonation and weak detonation. Usually, the minimum Rayleigh line is a tangent to the Hugoniot line showed that there is no solution beyond this point. This point of tangency is known as the upper Chapman–Jouguet (CJ) point and thus the relating wave is referred to as the Chapman–Jouguet detonation, and this is the point of “weakest” strong detonation possible. When $\hat{q}_c = 0$, this relates to the hydrodynamic shock wave, and thus the strong solution occurs. Moreover, weak detonations that have exothermic reactions hardly occur, and detonations do propagate at the Chapman–Jouguet wave speed under several experimental conditions [65].

Direct or indirect initiation can lead to the production of detonation wave, and a high amount of energy is speedily released into a certain volume of a mixture which can result in the formation of detonation wave (see Figure 2.8 below). Detonation is judged by pressure wave and combustion wave speed [63].



DDT and Detonation starts here

Figure 2.8: Detonation waves

2.4.3 Hugoniot conditions

Usually, the Hugoniot conditions equally known as Hugoniot jump conditions explain the relationship between the states on both sides of a combustion shock wave either for deflagration or detonation in a one-dimensional flow in fluids. The Hugoniot condition work was implemented by French engineer Pierre Henri Hugoniot.

Mathematically, the Hugoniot conditions can be expressed as:

$$\rho_1 u_1 = \rho_2 u_2 = m \quad \text{Conservation of mass} \quad (2.6)$$

$$\rho_1 u_1^2 + p_1 = \rho_2 u_2^2 + p_2 \quad \text{Conservation of momentum} \quad (2.7)$$

$$h_1 + u_1^2/2 = h_2 + u_2^2/2 \quad \text{Conservation of energy} \quad (2.8)$$

where m is the mass flow rate per unit area, ρ_1 and ρ_2 are the mass density of the fluid upstream and downstream of the wave, u_1 and u_2 are the fluid velocity upstream and downstream of the wave, p_1 and p_2 are the pressures in the two regions. Also, h_1 and h_2 are the specific enthalpies in the two regions.

Furthermore, if the flow is reactive, then the species conservation equations would be:

$$\omega_{i,1} = \omega_{i,2} = 0, \quad 1, 2, 3 \dots N, \quad \text{Conservation of species} \quad (2.9)$$

This is to eliminate the upstream and downstream fluid of the wave. From equation (2.9) above, ω is the mass production rate of the i th species of total N species that took part in the reaction.

A combination of equations (2.6) and (2.7) would give:

$$\frac{p_2 - p_1}{1/\rho_2 - 1/\rho_1} = m^2 \quad (2.10)$$

This describes a straight line often referred to as the Rayleigh line which has a negative slope because the m^2 is always positive in the $p - \rho^{-1}$ plane. From equation (2.10),

applying the Rankine-Hugoniot equations for the conservation of mass and momentum would remove u_1 and u_2 , thereby expressing the conservation of energy equation as the Hugoniot equation as shown in equation (2.11) below:

$$h_2 - h_1 = \frac{1}{2} \left(\frac{1}{\rho_2} + \frac{1}{\rho_1} \right) (p_2 - p_1) \quad (2.11)$$

Moreover, the specific volume can be expressed as an inverse of the density, $v = 1 / \rho$ and the relation between the upstream and downstream equation of state can be defined as:

$$f(p_1, \rho_1, T_1, Y_{i,1}) = f(p_2, \rho_2, T_2, Y_{i,2}) \quad (2.12)$$

where Y_i is the mass fraction of the species.

2.4.4 Rankine-Hugoniot relations

By the foregoing assumptions, the Rankine-Hugoniot equations are simplified, and the gas mixture is considered to obey the ideal gas law thereby writing the relation between the downstream and upstream equation of state as:

$$\frac{p_2}{\rho_2 T_2} = \frac{p_1}{\rho_1 T_1} = \frac{R}{\bar{W}} \quad (2.13)$$

where R is the universal gas constant, and \bar{W} is the mean molecular weight considered to be constant and it is dependent on the mass fraction of the whole species. Mathematically, the specific heat at constant pressure c_p is constant across the combustion reaction wave, and thus, the change in enthalpies can be written as:

$$h_2 - h_1 = -q + c_p(T_2 - T_1) \quad (2.14)$$

where the first term in equation (2.14) stands for the amount of heat released per unit mass of the upstream mixture by the wave and the second term means the sensible heating. However, by eliminating the temperature using the equation of state and also substituting equation (2.14) for enthalpies change into the Hugoniot equation, thereby obtaining a Hugoniot equation expressed particularly in relation to pressure and densities,

$$\left(\frac{\gamma}{\gamma-1} \right) \left(\frac{p_2}{\rho_2} - \frac{p_1}{\rho_1} \right) - \frac{1}{2} \left(\frac{1}{\rho_2} - \frac{1}{\rho_1} \right) (p_2 - p_1) = q \quad (2.15)$$

Where γ is the specific heat ratio,

Moreover, Hugoniot curve without heat release ($q = 0$) can be referred to as Shock Hugoniot. Also, combining with the Rayleigh line equation, the above equation (2.15) absolutely governs the state of the system. Furthermore, these two equations can be written clearly through the introduction of the following non-dimensional scales as,

$$\bar{p} = \frac{p_2}{p_1}, \quad \bar{v} = \frac{\rho_1}{\rho_2}, \quad \alpha = \frac{q\rho_1}{p_1}, \quad \mu = \frac{m^2}{p_1\rho_1}. \quad (2.16)$$

Then the Rayleigh line equation and the Hugoniot equation can be broken down to

$$\frac{\bar{p}-1}{\bar{v}-1} = \mu \quad (2.17)$$

$$(\gamma + 1)/(\gamma - 1) = \frac{[2\alpha + (\gamma + 1)/(\gamma - 1) - \bar{v}]}{[(\gamma + 1)/(\gamma - 1)]\bar{v} - 1}. \quad (2.18)$$

Considering the upstream conditions, the divergence of the above two equations (2.17) and (2.18) in the $\bar{p} - \bar{v}$ plane would establish the downstream conditions. Taking for instance, if there is no heat release, and for shock waves without chemical reaction, then $\alpha = 0$. Moreover, the Hugoniot curves asymptote to the lines;

$\bar{v} = (\gamma - 1)/(\gamma + 1)$ and $p = -(\gamma - 1)/(\gamma + 1)$, i.e., the pressure jump across the wave can take values between $0 \leq \bar{p} < \infty$. However, the specific volume ratio is limited to the interval $(\gamma - 1)/(\gamma + 1) \leq \bar{v} \leq 2\alpha + (\gamma + 1)/(\gamma - 1)$, and this is because the upper bound is obtained for the case $\bar{p} \rightarrow 0$, most especially, pressure has no negative values. Furthermore, the Chapman–Jouguet condition is the point Rayleigh line is tangent to the Hugoniot curve [66]. Additionally, if $\gamma = 1.4$ for a diatomic gas which has no vibrational mode excitation, the interval will be,

$1/6 \leq \bar{v} \leq 2\alpha + 6$. Furthermore, the shock wave can cause increase in density by a factor of 6, and for a monoatomic gas in which the $\gamma = 5/3$, thus, the density ratio is restricted by the interval $1/4 \leq \bar{v} \leq 2\alpha + 4$. Nevertheless, the vibrational mode excited of diatomic gases has $\gamma = 9/7$ which leads to the interval $1/8 \leq \bar{v} \leq 2\alpha + 8$. Because of molecular dissociation and ionisation, the specific heat ratio is not constant in the shock wave, although, the density ratio is limited to a factor of between 11 and 13 [63].

2.4.5 Chapman–Jouguet waves

Furthermore, the Chapman–Jouguet waves have certain unique properties that give an overview of the entire structure of detonation and deflagration waves. Generally, detonation or deflagration wave is not obtainable from the relationship of Rankine–Hugoniot, and the propagation velocities of the upper and lower Chapman–Jouguet waves are clearly defined for given values of (γ, \hat{q}_c) due to the additional tangency requirement [66]. In determining the properties of the CJ waves, the equations will be evaluated thereby giving equations (2.19) and (2.20):

$$\left(\frac{d\hat{p}}{d\hat{v}}\right)_{Rayleigh} = \frac{\hat{p}-1}{\hat{v}-1} \quad (2.19)$$

By differentiating equation (2.19), we obtain equation (2.20) below,

$$\left(\frac{d\hat{p}}{d\hat{v}}\right)_{Hugoniot} = -\frac{[(\gamma+1)/(\gamma-1)]\hat{p}+1}{[(\gamma+1)/(\gamma-1)]\hat{v}-1} \quad (2.20)$$

The relationship between equations (2.19) and (2.20) revealed that equation (2.21) is equivalent to equation (2.22).

$$\left(\frac{d\hat{p}}{d\hat{v}}\right)_{Hugoniot} \geq \left(\frac{d\hat{p}}{d\hat{v}}\right)_{Rayleigh} \quad (2.21)$$

$$\frac{(\hat{p}-1)\hat{v}}{\gamma(1-\hat{v})\hat{p}} \leq 1. \quad (2.22)$$

Mathematically, looking at equation (2.21), the left-hand side of equation (2.22) would be M_b^2 , and then equation (2.21) will be equal to equation (2.23)

$$M_b^2 \geq 1. \quad (2.23)$$

Equation (2.23) shows that the wave flow downstream can be sonic ($M_b = 1$) for the CJ wave, and for strong detonation and weak deflagration, the Hugoniot curve has a greater slope than that of Rayleigh line. However, the opposite denotes weak detonation and strong deflagration, hence, it can be wrapped up that $M_b < 1$ is for the first and $M_b > 1$ is for the second [67].

The radical term in equation (2.30) can be made to zero to establish the speed of the combustion of the CJ wave to give equation (2.24),

$$(M_{u,CJ})_{\pm}^2 = 1 + \frac{(\gamma^2-1)\hat{q}_c}{\gamma} \left\{ 1 \pm \left[1 + \frac{2\gamma}{(\gamma^2-1)\hat{q}_c} \right]^{1/2} \right\} \quad (2.24)$$

This reveals that $(M_{u,CJ})_+ > 1$ and $(M_{u,CJ})_- < 1$,

$$\hat{v}_{CJ,\pm} - 1 = \hat{q}_c \frac{(\gamma-1)}{\gamma} \left\{ 1 \mp \left[1 + \frac{2\gamma}{(\gamma^2-1)\hat{q}_c} \right]^{1/2} \right\} \quad (2.25)$$

$$\hat{p}_{CJ,\pm} - 1 = \hat{q}_c \frac{(\gamma-1)}{\gamma} \left\{ 1 \pm \left[1 + \frac{2\gamma}{(\gamma^2-1)\hat{q}_c} \right]^{1/2} \right\} \quad (2.26)$$

One should bear in mind that the upper and lower Chapman–Jouguet states are noted by the signs (\pm) in equations (2.24) to (2.26) [67].

The next proceeding section will carefully examine the unsteady deflagration-to-detonation transition and this section includes detonation and its origin; upper CJ and lower CJ point curves of detonation; Hugoniot curve; Rankine Hugoniot relations; and Hugoniot relations of detonation.

2.4.6 Upper CJ and Lower CJ Point curves of detonation

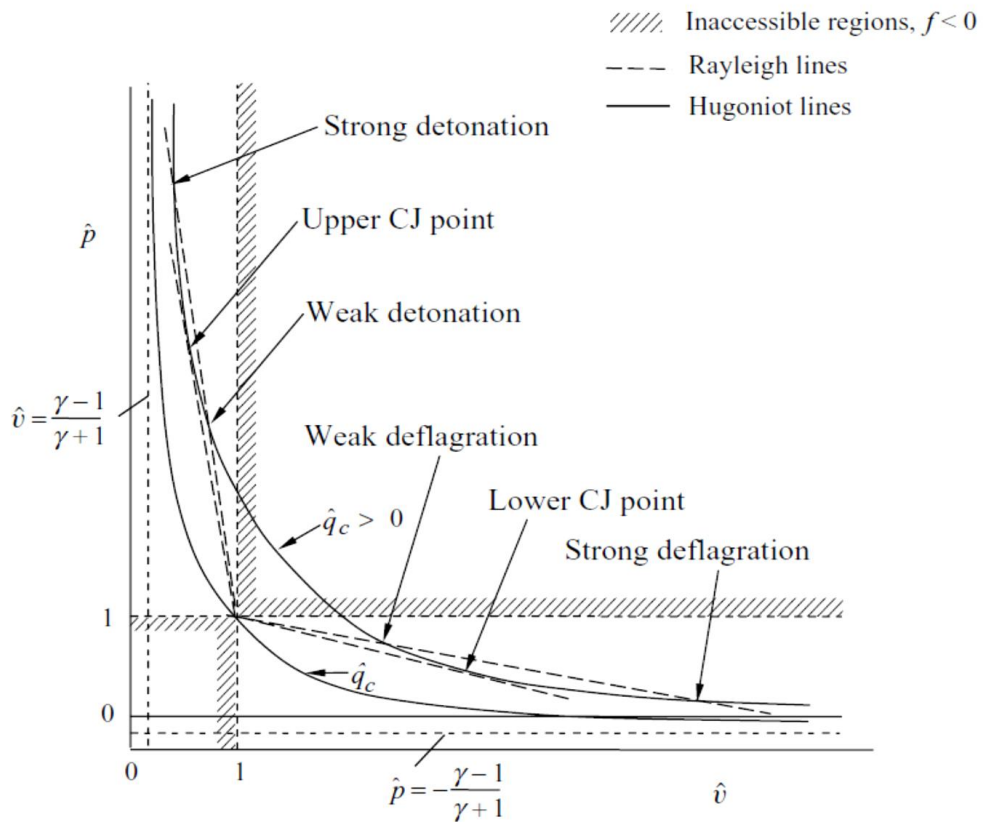


Figure 2.9: Schematic identifying the Rankine – Hugoniot solutions [68].

Furthermore, the two most important in Figure 2.9 in Section 2.4.6 are upper CJ point (detonation) and lower CJ point (deflagration) and there is no transition. However, for Hugoniot curves of combustion requires good explanation, but no theory has been able to explain this concept of Hugoniot curve of combustion. No transition takes place in the Hugoniot curves. It has been observed that as the pressure increases, the density equally increases thereby bringing about increase in explosion waves [63].

Note that q_c = amount of heat release per unit mass flux and constant c_p , we have,

$$h_b - h_u = -q_c + c_p(T_b - T_u). \quad (2.27)$$

Applying the equation of state for ideal gas with constant molecular weight,

$$p = \rho RT \quad (2.28)$$

2.5 Deflagration-to-detonation transition

Generally, a sudden transition from deflagration to detonation will eventually take place when a deflagration suddenly becomes strong enough. Several experiments of Deflagration to detonation transition (DDT) involving highly reactive mixtures which include near-stoichiometric acetylene-air, hydrogen-air or fuels do occur in oxygen-enriched atmospheres [43]. A few good examples of deflagration to detonation transition in fuel-air mixtures with average level of reactivity amongst others include:

- i) A transition from deflagration to detonation was observed when a 10m long wedge-shaped vessel was used with stoichiometric propane-air, 100% top confinement and circular obstructions in one CMR experiment. From the experiment, it reveals that a propane-air explosion that began with a weak ignition source even speed up to detonation in less than 10m, if enough confinement and obstructions are existing [43].
- ii) Jet flames can lead to the transition of deflagration to detonation as observed. The report found in one test that there is a transition from deflagration to detonation in a lean mixture of acetylene-air (5% C_2H_2) in a basically loosed situation [43].

- iii) The shooting of jet flames into the loosed cloud resulted to the transition of deflagration to detonation. The experiments showed that detonations can be induced in a loosed fuel-air cloud with mild reaction rates if the size of the cloud is broad [43].

- iv) In the experiments conducted by British Gas in a pipe rack geometry equally demonstrated transition of deflagration to detonation for propane-air mixtures, and the transition took place after 15m. Furthermore, the experiment exhibited that in relatively 'open' situations, such as a pipe bridge, the flame speed of deflagration to detonation transition is supported by the geometry [43].

Moreover, experiments reveal that the transition of deflagration to detonation can be achieved by flame acceleration caused by obstacles and confinement, or it can be obtained if a jet flame is shot out from an opening in a confined volume into a loosed cloud. However, the mechanism of deflagration to detonation transition is not yet completely understood, but for now, there is no theory which can predict conditions for deflagration to detonation transition [43].

Furthermore, Deflagration to detonation is a combustion phenomenon which results when ignitable mixtures of a flammable gas and air (oxygen) suddenly undergoes a transition from the process of deflagration form of combustion to detonation form of explosion. Deflagration is a chemical process in which a substance rapidly burns, and is faster than combustion, but it is slower than detonation. A simple example is adding water to burning oil leading to deflagration, and it instantaneously boils to form steam, thus, the oil droplets are forcefully discharged into the flame thereby adding fuel to the fire [48], [61]. Furthermore, a deflagration process is distinguished by a subsonic nature of flame propagation velocity of less than 100m/s or 220 mph, and an overpressure of below 0.5 bars (7.3 psi). Deflagration, in its mild form can be referred to as a flash fire. However, detonation is identified by a supersonic nature of flame propagation velocities of more than 1,000 m/s, but maximally 2,000 m/s, equivalent to 4,500 mph and a significant overpressure of up to 20 bars (290 psi). A dominant pressure wave is the key mechanism of combustion propagation that compact the unburnt gas ahead of the wave to a temperature higher than the auto-ignition temperature, termed the combustion reaction zone. It is a self-driven shock wave where

the reaction zone and the shock are simultaneous, and the chemical combustion reaction are caused by the shock wave. Consequently, this detonation process is likened to a diesel engine ignition, but it is much more unexpected and destructive. Considering certain geometrical conditions like partial confinement and several obstacles in the flame path responsible for turbulent flame eddy currents, a subsonic flame can accelerate to supersonic velocity thereby progressing from deflagration to detonation.

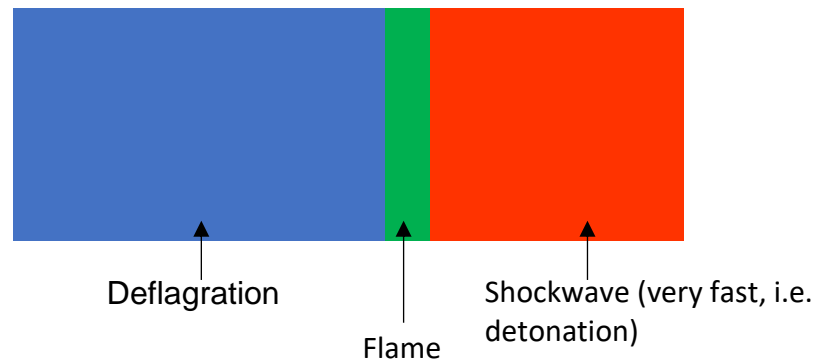


Figure 2.10: Position of deflagration and detonation in a combustion wave

In understanding the actual mechanisms of deflagration and detonation, the two concepts will be modelled to predict the transition phenomenon. Deflagration propagates by heat conduction, mass diffusion from the hot burnt products of the chemical combustion reaction and the cold explosive ahead as shown in Figure 2.10 above. Deflagration is an exothermic chemical reaction propagating from the burning gas to the unreacted material by conduction, convection, and radiation. This combustion process progresses at a rate less than the velocity of sound. Detonation is an exothermic chemical reaction characterised by shock wave in the material which maintains the reaction. In detonation, the combustion process accelerates at a velocity greater than the velocity of sound and it propagates through shock explosive compression [31].

Moreover, deflagration wave is in certain areas identical with that of detonation, but the overpressure is much less, and the dimensional extent of the shock front is significantly higher than that of detonation. The deflagration wave accelerates at subsonic speed and the chemical combustion reaction is accompanied by heat transfer and by overpressure of the shock. Ordinary fires are identified to be deflagration waves; and the flame front in a candle is a deflagration pushing through the burning

gases at subsonic speed. For instance, gunpowder experiences deflagration rather than detonation, because it can produce a prominent shock in air. The deflagration can generate explosions and thus can be extremely noising and damaging. In detonation, the shock has a very sharp and a very high-pressure wave that can pass through material with an explosive quality capable of undergoing an exothermic chemical combustion reaction based on its overpressure [66]. Besides, a detonation shock wave front in a material, travels much faster than that of sound, hence, its flow is supersonic because acoustic waves travel through the combustion reaction zone thereby maintaining the high overpressure. Thus, in combustion, deflagration differs from detonation due to over-pressure and speed. In deflagration, the combustion wave propagates at a subsonic velocity, but in detonation, the combustion wave spreads at supersonic velocity. However, a condition such as pre-ignition can be confused with detonation and it takes place immediately the combustion chamber gets so much hot that it becomes an ignition source thereby making the fuel to ignite before the spark plug fires, thus leading to a detonation case. Hence, in a situation where fuel would have ignited rightly to provide the crankshaft a smooth kick in the correct direction, rather, the fuel will ignite early thereby leading to short backlash due to the piston turning the crankshaft in the improper direction. When a hot engine is shut off, it will lead to pre-ignition. The following factors can lead to detonation, and they include: reducing ignition timing; the enrichment of air/fuel mixture ratio thus altering the chemical combustion reaction; the reduction of peak cylinder pressure. Other factors include the use of fuel with high octane rating thereby increasing the combustion temperature; the reduction on engine load; exhaust gas back pressure in the combustion chamber, This is not all, a reduction of the throttle opening decreasing the manifold pressure; an intercooler system lowering the efficiency of the engine; and the ambient heat running close to the detonation threshold which can be terrific [67].

Table 2.3: Relationship between deflagration and detonation [67]

| S/No. | Factors | Deflagration | Detonation |
|-------|-------------------|----------------------|------------------------|
| 1 | Mach number | $M < 1$ | $M > 1$ |
| 2 | Pressure | 2 bars | 20 bars |
| 3 | Speed | 200m/s | 1000m/s |
| 4 | Mach Number level | Subsonic ($M < 1$) | Supersonic ($M > 1$) |

Table 2.3 in Section 2.5 demonstrates the relationships between deflagration and detonation. In CFD simulation, when the Mach number is less than 1 ($M < 1$), it implies that the combustion wave is deflagration, but if the Mach number is greater than 1 ($M > 1$), it shows that the combustion wave is detonation. However, if the pressure and the speed of the combustion waves are 2 bars and 200 m/s respectively, it shows that it is deflagration and subsonic velocity, but when the pressure and the speed of the combustion waves are 20 bars and 1000 m/s, such combustion wave is said to be detonation and supersonic speed.

In the Hugoniot curves, there are different release heat at different points of the curves. For example, if the same piece of paper undergoes combustion, the chemical energy is the same and therefore, the release heat will be the same even if the paper undergoes combustion for durations of 100 seconds and 5 seconds respectively.

$$50\text{J} \longrightarrow 50\text{J}, \text{ Heat Energy} = 100 \text{ secs} \quad (2.29)$$

$$50\text{J} \longrightarrow 50\text{J}, \text{ Heat Energy} = 5 \text{ secs} \quad (2.30)$$

For equations (2.29) and (2.30), the release heat will be the same because the chemical energy is the same, but if the heat release rate (HRR) is large, the kinetics will be very large [68]. Besides, if the heat release rate (HRR) of one combustion is fast, and the heat release rate (HRR) of another is slow, this is due to the combustion reaction [63]. Moreover, the release heat for a particular material says a paper is the same even if the combustion or the reaction rate varies, but the heat release rate (HRR) depends on the reaction rates present [68]. Also release heat usually depends on the materials for combustion. In addition, different materials such as paper, textile or wood have different release heat, but same material as paper has the same release heat no matter the combustion reaction. Hence, different release heat will produce different combustion models. The heat release rate (HRR) is independent of the combustion wave. Also, another factor that affect combustion wave is compressibility influence [63], [68].

For weak deflagration where,

$$\frac{\Delta u}{u_1} = 1 - \frac{\rho_1}{\rho_2} = 1 - \frac{T_2}{T_1} < 0; T_2 = T_1 + \frac{q}{\gamma R/(\gamma-1)} \quad (2.31)$$

For turbulent flames, $u_1 = S_T$ (depends additionally on turbulence properties)

Where $P_2 > P_1$, then detonation occurs.

$$\frac{\Delta u}{u_1} = 1 - \frac{\rho_1}{\rho_2} > 0 \quad (2.32)$$

An illustration of Rankine Hugoniot relations curves shows the different locations of the combustion processes as follows as represented in Figure 2.11 below:

- i) Above D: strong detonations ($M_2 < 1$)
- ii) D – B: weak detonations ($M_2 > 1$) (point B: mass flow = ∞)
- iii) B – C: impossible (mass flow imaginary)
- iv) C – E: weak deflagration ($M_2 < 1$) (point C: mass flow = 0)
- v) Below E: strong deflagrations ($M_2 > 1$)

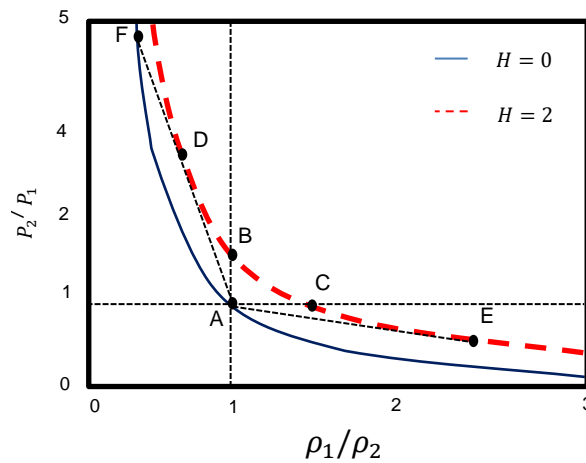


Figure 2.11: Compressible flows within more complex Geometries than Shock Tube [68].

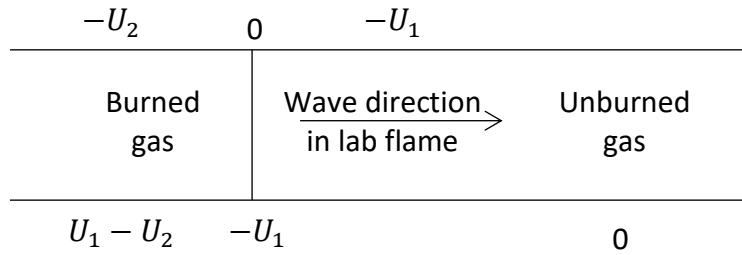


Figure 2.12: Velocities used in analysis of detonation problem [53]

In analysing the method of calculating the steady, planar, and one-dimensional gaseous detonation velocity, a system configuration similar to velocities with wave fixed in lab space has to be used as shown in Figure 2.12 above [53].

The integrated conservation and static equations for detonation velocities are written as follows:

$$\rho_1 u_1 = \rho_2 u_2 \quad (2.33)$$

$$P_1 + \rho_1 u_1^2 = P_2 + \rho_2 u_2^2 \quad (2.34)$$

$$c_p T_1 + \frac{1}{2} u_1^2 + q = c_p T_2 + \frac{1}{2} u_2^2 \quad (2.35)$$

$$P_1 = \rho_1 R T_1 \quad (2.36)$$

$$P_2 = \rho_2 R T_2 \quad (2.37)$$

In a process like this, all combustion events can collapse into a wave. Hence, the unknowns are u_1 , u_2 , ρ_2 , T_2 , and P_2 [69]. Empirically, it is observed that for a given mixture, the detonation velocity is distinctly constant. The rate of reaction must be known in identifying all the unknowns, or a detonation velocity case must be determined [53], [69].

Chapter 3 Basic Equations and Numerical Schemes

3.1 Introduction

This chapter will clearly explain the reactive Navier-Stokes equations (governing equations/basic equations), the numerical methods and the adaptive mesh refinement in object-oriented C++ (AMROC). The chemical explosions in gaseous chemical mixtures involve four processes: - the flows, heat-transfer, mass transfer and chemical reactions. The flow and heat and mass transfer processes are controlled by three conservation principles, i.e. the laws for mass, momentum, and energy conservations, while the chemical reactions are described by the laws of chemical kinetics [70]. These laws are expressed in mathematical equations, and they will form the basic equations for this thesis, which will be addressed in the first half of this chapter. In the second half of this chapter, the numerical solutions for the basic equations will be presented and verified [1], [71].

3.2 Reactive Navier – Stokes equations

The reactive Navier-Stokes equations are the basic equations of this project which are based on the three conservation laws of mass, momentum, energy, and chemical reaction kinetics [72]. When these laws are applied, the reactive Navier – Stokes equations are obtained.

3.2.1 Continuity equations

The first basic equation is the continuity equation. It reflects that the mass of the gaseous mixture is conserved during all the processes as shown below:

$$\frac{\partial \rho}{\partial t} + \frac{\partial}{\partial x_j}(\rho u_j) = 0 \quad (3.1)$$

Or

$$\frac{\partial \rho}{\partial t} + \sum_{n=1}^d u_n \frac{\partial \rho}{\partial x_n} + \rho \sum_{n=1}^d \frac{\partial u_n}{\partial x_n} = 0, \quad (3.2)$$

where $x_j (j = x, y, z)$ stands for the coordinates, u_j or (u_x, u_y, u_z) represents the components of the velocity vector \vec{u} (m/s), t denotes the time in seconds for the coordinate and ρ stands for the density of the mixture [72].

3.2.2 Equation of momentum

The law of momentum conservation is actually the same as Newton's second law of motion which states that the change rate of momentum is equal to all the forces acting on the mixture.

When it is applied to a flow particle, we will have mathematical equations as follows:

$$\frac{\partial(\rho u_i)}{\partial t} + \frac{\partial}{\partial x_i}(\rho u_i u_j) = -\frac{\partial}{\partial x_i} p + \frac{\partial}{\partial x_i}(\tau_{ij}) + \rho g_i \quad (3.3)$$

where p represents the static pressure, τ_{ij} stands for the viscous stress tensor and ρg_i denotes the gravitational body force [72]. In modelling chemical reactions, the body force can be ignored. In addition, the viscous stress tensor can be explained in terms of molecular viscosity, μ , and local velocity gradient as

$$\tau_{ij} = \mu \left(\frac{\partial}{\partial x_i} u_j + \frac{\partial}{\partial x_j} u_i - \frac{2}{3} \frac{\partial}{\partial x_k} u_k \delta_{ij} \right) \quad (3.4)$$

where $\delta_{i,j}$ stands for the kronecker delta i.e., ($\delta_{i,j} = 1$ if $i = j$ and $\delta_{i,j} = 0$ otherwise).

3.2.3 Equation for energy

The mathematical derivation of the energy equation is obtained from the first law of thermodynamics for the fluid that is, the change rate of total energy in a control volume is equal to the heat gained and the work done by the fluid [72]. It involves the static temperature, static enthalpy, and internal energy represented as follows:

$$\frac{\partial}{\partial t}(\rho e) + \frac{\partial u_j}{\partial x_i}(\rho e + p) = -\frac{\partial}{\partial x_i} q_j + Q_r \quad (3.5)$$

where, q_j stands for the heat flux, and Q_r represents the internal production rate for thermal energy, and e is the specific inner energy.

The energy equation can be written as another form,

$$\frac{\partial}{\partial t}(\rho h) + \frac{\partial u_j}{\partial x_i}(\rho h) = \frac{\partial p}{\partial t} - \frac{\partial}{\partial x_i} q_j + Q_r \quad (3.6)$$

$$h = e + \frac{p}{\rho} \quad (3.7)$$

where h represents the enthalpy of the mixture. then equation (3.5) will be as follows:

By its definition in terms of species enthalpy, the enthalpy in equation (3.6) is written as,

$$h = \sum_i^{N_g} Y_i h_i \quad (3.8)$$

where h_i denotes the absolute internal enthalpy for species i and the enthalpy is a major function of temperature for an ideal gas [72]. At a given temperature, the enthalpy is approximately obtained by

$$h_i(T) = h_i^0 + \int_{T_0}^T C_{p,i}(T) dT \quad (3.9)$$

where h_i^0 stands for the heat of formation of species i at a given temperature T_0 (298.15 K) and $c_{p,i}(T)$ is the specific heat at constant pressure of species i .

$$C_{p,i} = \left(\frac{\partial h}{\partial T} \right)_p \quad (3.10)$$

At constant pressure, the specific heat for the mixture c_p would be,

$$c_p = \sum_i^{N_g} Y_j c_{p,j} \quad (3.11)$$

The energy flux q_j is divided into three different parts [73]

$$q_j = q_j^c + q_j^d + q_j^D \quad (3.12)$$

From equation (3.12), q_j^c stands for energy flux owing to conduction of species j , and q_j^d stands for energy flux due to diffusion of species j and q_j^D represents energy flux

caused by concentration gradients. Normally, the latter, q_j^D is much smaller than the other two components q_j^c and q_j^d [73] and this will not be treated in this work.

Fourier's law expressed energy flux due to conduction as follows:

$$q_j^c = -\lambda \frac{\partial T}{\partial x_j} \quad (3.13)$$

Where λ is the thermal conductivity of the mixture.

However, considering enthalpy as a function, by combining equations (3.8), (3.9) and (3.10) the energy flux due to conduction would be written as

$$q_j^c = \frac{\lambda}{c_p} \left(\sum_i^{N_g} h_i \frac{\partial Y_i}{\partial x_j} - \frac{\partial h}{\partial x_j} \right) \quad (3.14)$$

Therefore, based on the name, the diffusion resulting from the energy flux due to diffusion is caused by the diffusion of species having different enthalpy and is illustrated by

$$q_j^d = \sum_i^{N_g} h_i J_{1,j} \quad (3.15)$$

Similar to the introduction of Schmidt number in mass flux, the non-dimensional

$$q_j^d = -\frac{\mu}{Sc} \sum_i^{N_g} h_i \frac{\partial Y_i}{\partial x_j} \quad (3.16)$$

Hence, the energy flux can be written as

$$q_j = -\lambda \frac{\partial T}{\partial x_j} - \frac{\mu}{Sc} \sum_i^{N_g} h_i \frac{\partial Y_i}{\partial x_j} \quad (3.17)$$

In simplifying the description of energy flux, the non-dimensional Prandtl number (Pr) would be introduced and this is comparable to Schmidt number in mass flux.

$$Pr = \frac{\mu c_p}{\lambda} \quad (3.18)$$

However, the ratio of Schmidt and Prandtl numbers gives the Lewis number

$$Le = \frac{Sc}{Pr} \quad (3.19)$$

Therefore, the total energy flux would be,

$$q_j = \frac{\mu}{Pr} \left[-\frac{\partial h}{\partial x_j} + \left(1 - \frac{1}{Le}\right) \sum_i^{N_g} h_i \frac{\partial Y_i}{\partial x_j} \right] \quad (3.20)$$

According to K. K. Kuo (2011), the Lewis number for most gases is close to unity [74], and assuming that $Le = 1$, equation (3.20) will be simplified further. Thus, equation (3.6) is more simplified by assuming that $Le = 1$ to the following equation:

$$\frac{\partial}{\partial t}(\rho h) + \frac{\partial u_j}{\partial x_j}(\rho h) = \frac{\partial p}{\partial t} - \frac{\partial}{\partial x_i} \frac{\mu}{Pr} \left(-\frac{\partial h}{\partial x_i} \right) + Q_r \quad (3.21)$$

where Q_r represents the internal production rate

3.2.4 Equation for species mass concentrations

The species concentrations are often expressed by their fractions. So, the equations for fractions of the species concentrations are given as follows:

$$\frac{\partial}{\partial t}(\rho Y_i) + \frac{\partial}{\partial x_i}(\rho u_i Y_i) = \frac{\partial}{\partial x_i}(J_{ij}) + R_i^{hom} \quad i = 1, \dots, N \quad (3.22)$$

Mathematically, the two terms on left hand side of equation (3.22) stands for the rate of change of mass of species i and the change rate of mass of species i resulting from convection respectively. In addition, the two terms on right hand side of equation (3.22) are the rate of change of mass of species i caused by diffusion and the net rate of increase of mass of species i resulting from source [74].

Considering equation (3.22) above, Y_i denotes mass fraction of species i in the mixture, N_g stands for the number of species in the gas phase, R_i^{hom} ($\text{kg}/\text{m}^3 \cdot \text{s}$) represents the net rate of production of species i caused by homogeneous chemical reactions and $J_{i,j}$ ($\text{kg}/\text{m}^2 \cdot \text{s}$) is the molecular mass flux of species i . Usually, the equation has three components which include mass diffusion, pressure diffusion and thermal diffusion.

However, according to Warnatz et al (2001), pressure diffusion and thermal diffusion can be ignored for majority of the combustion processes [73]. In explaining mass flux, it again simplified through the introduction of non-dimensional Schmidt number.

$$Sc = -\frac{\mu}{\rho D_i} \quad (3.23)$$

Where Sc stands for Schmidt number

Then,

$$J_{ij} = -\frac{\mu}{Sc} \frac{\partial F_i}{\partial x_i} \quad (3.24)$$

Where D_i (m^2/s) represents the diffusion coefficient for species i and it is different for different species, but in this work, it is done in a way that all species have the same diffusion coefficient [74].

Alternatively, the equations of species fractions can be written as (3.25) as well

$$\frac{\partial Y_i}{\partial t} + \sum_{n=1}^d u_n \frac{\partial Y_i}{\partial x_n} = \frac{W_i \dot{\omega}_i}{\rho}, \quad i = 1, \dots, K - 1. \quad (3.25)$$

Where ρ stands for density; u denotes velocity; $\dot{\omega}$ represents reaction rate; p is pressure; T is temperature [75].

3.2.5 Thermodynamical properties of the mixture

The thermodynamical properties of the mixture are calculated in the equations below.

(a) Thermodynamical state of the mixture

Mixture is not simple for reactions involving hydrogen and oxygen as well as that of hydrocarbons precisely propane, but this research work is all about more complex mixtures [74], [76]. This is especially how to calculate absolute temperature T , specific heat, density and the gas constant, and the pressure p is obtained by (3.26).

$$p = \rho R_u T \sum_1^{N_g} \frac{Y_i}{M_{w,i}} \quad (3.26)$$

Where p represents pressure

Alternately, the state equation for the mixture can be written as (3.27)

$$p = \rho R_u \frac{T}{\sum_i^{Ng} X_i M_{w,i}} \quad (3.27)$$

Where $M_{w,i}$ and X_i are the molecular weight and mole fraction of species i , respectively, and T stands for the temperature of the mixture in (K), while R_u represents the universal gas constant ($R_u = 8.1314 \text{ KJ/kmol} \cdot \text{K}$) [76].

$$p_i = \rho_i \frac{R}{W} T = \rho_i R_i T \quad (3.28)$$

$$p = \sum_{i=1}^K p_i \quad (3.29)$$

(b) Mass and mole fractions

The mass fractions are the ratio of the partial densities in relation to the density of the mixture, and the mole fractions are the concentrations of the chemical product rates and this is to allow for the computation of all mixture properties [76].

$$Y_i := \frac{\rho_i}{\rho} \quad (3.30)$$

$$C_i = \frac{\rho_i}{W_i} = \rho \frac{Y_i}{W_i} \quad (3.31)$$

$$X_i := \frac{C_i}{\sum_{j=1}^K C_j} \quad (3.32)$$

$$W = \sum_{i=1}^K X_i W_i \quad (3.33)$$

$$W = (\sum_{i=1}^K Y_i W_i)^{-1} \quad (3.34)$$

$$X_i = Y_i \frac{W}{W_i} \quad (3.35)$$

(c) Enthalpy and internal energy

Generally, every gaseous species is a perfect gas that is thermally active, and for this work, the specific heats at constant pressure and volume,

$C_p = C_p(T)$ and $C_v = C_v(T)$ are therefore specifically functions of temperature [76].

$$h_i(T) = h_i^0 + \int_{T^0}^T c_{pi}(s) ds \quad (3.36)$$

$$e_i(T) = h_i^0 + \int_{T^0}^T c_{vi}(s) ds \quad (3.37)$$

$$c_{pi}(T) = \frac{\mathcal{R}}{W_i} + \left(\begin{array}{c} a_{1i} + a_{2i}T \\ + a_{3i}T^2 + a_{4i}T^3 + a_{5i}T^4 \end{array} \right) \quad (3.38)$$

$$h(Y_1, \dots, Y_K, T) = \sum_{i=1}^K Y_i h_i(T) \quad (3.39)$$

$$e(Y_1, \dots, Y_K, T) = \sum_{i=1}^K Y_i e_i(T) \quad (3.40)$$

$$c_p(Y_1, Y_K, T) = \frac{\partial h}{\partial T} = \sum_{i=1}^K Y_i c_{pi}(T), \quad (3.41)$$

$$c_v(Y_1, Y_K, T) = \frac{\partial e}{\partial T} = \sum_{i=1}^K Y_i c_{vi}(T). \quad (3.42)$$

(d) Specific gas constant and adiabatic exponent

The ideal gas relations of the specific heats for the mixture would be applied to the specific gas constant R_i and the adiabatic exponent $\gamma_i(T)$ of a single species which can be carried over directly to the corresponding properties for the mixture [76].

$$R_i = \frac{\mathcal{R}}{W_i} = c_{pi}(T) - c_{vi}(T), \quad (3.43)$$

$$\gamma_i(T) = \frac{c_{pi}(T)}{c_{vi}(T)} \quad (3.44)$$

$$R(Y_1, \dots, Y_K) = \frac{\mathcal{R}}{W(Y_1, \dots, Y_K)} \quad (3.45)$$

$$\gamma(Y_1, \dots, Y_K, T) = c_p(Y_1, \dots, Y_K, T) - c_v(Y_1, \dots, Y_K, T) \quad (3.46)$$

$$\gamma(Y_1, \dots, Y_K, T) = \frac{c_p(Y_1, \dots, Y_K, T)}{c_v(Y_1, \dots, Y_K, T)} \quad (3.47)$$

$$\gamma - 1 = \left(\sum_{i=1}^K \frac{x_i}{\gamma_i - 1} \right)^{-1} \quad (3.48)$$

3.2.6 Boundary and initial conditions

The complete mathematical models require not only the reactive Navier – Stokes equations mentioned above, but also boundary and initial conditions. The boundary conditions are the solutions on the boundaries $\partial\Omega$ of domain $\Omega \in \mathbb{R}^d$ [76]. The boundary conditions which are of four kinds are applied in this work. Boundary conditions are about the computing quantities on boundaries, such as inlet, outlet, openings and wall. (a) Inlet boundary condition is completely giving the computing quantities on an inlet boundary; (b) Outlet boundary condition is generally gradient of the computing quantities on outlet is zero; (c) Opening boundary condition is similar to outlet boundary condition, but pressure on opening boundary is equal to atmospheric pressure; and (d) Wall boundary condition is flow velocity on walls which is zero.

The initial conditions are the initial state of the flow and varies with different case studies. Furthermore, the initial conditions are about the computing quantities, such as flow velocity, temperature, pressure and mixture concentrations, at time $t = 0$. We use initial conditions to setup ignition source. Therefore, it will be explained in the concrete case studies in chapters 5 and 6.

(i) Symmetry planes or impermeable walls

When fluid flow issues are symmetric in relation to one or more planes, on the plane of symmetry [76], the component of the velocity vector is of normal to the boundary and the gradients of the other variables [77].

(ii) Inlet and outlet

Inlet boundary conditions are the Dirichlet boundary conditions, that is, the values of the variables on inlets are given [76]. The outflow boundaries in this work are specified as follows:

$$\frac{\partial q}{\partial n} = 0 \quad (3.49)$$

This is not all, the next section shall focus on numerical methods which shall constitute the bedrock of this research work and finite volume method shall be employed for purposes of obtaining accurate and robust results.

3.3 Numerical methods

There are two ways to solve the equations in section 3.2 - analytical solution method and numerical solution [76]. Analytical solutions are not available to the problems in this work, the numerical solutions are used. There are three possible numerical methods for the numerical solutions which include finite difference, finite volume, and finite element, but for this research work, we will use finite volume method [76].

3.3.1 Finite volume methods

The finite volume method is to solve the equation (3.2) with the form of integration. To start with, the computational domain is meshed and the finite volumes over the domain are built up. Then, the basic equations with the form of integration are discretised in each control volume [76]. Finally, the discrete equations are solved and calculated to obtain the numerical solutions of the problems. The meshes employed in this work are the structured mesh of square element or cell, that is, a square is one finite volume. As is well known, the resolution of mesh is critical for accurate numerical simulations [77]. Therefore, technique of adaptive mesh refinement (AMR) is applied to generate the reasonably fine meshes and distribute the dense elements into the necessary areas of the domain. One of the structured mesh's disadvantages is that it cannot mesh geometry-complex domain, however, its advantage is that it is able to produce very accurate numerical results [76]. Fortunately, the computational domains in this work are not complex, so the structured mesh is one of the best options to the problems of this work [77].

Adaptive mesh refinement is a complicated procedure which will be addressed in coming section in detail.

Having the meshes of computational domain, the next step is to calculate all the quantities of the variables in the finite volumes and on its surfaces, which are detailed below.

3.3.2 Calculations of various fluxes on the surfaces of control volumes

Generally, the finite volume method entails a splitting of $f(q)$ into two components $f^+(q)$ and $f^-(q)$, to obtain equation (3.52),

$$f(q) = f^+(q) + f^-(q) \quad (3.50)$$

This is satisfied under the restriction that the eigenvalues $\bar{\lambda}_m^+$ and $\bar{\lambda}_m^-$ of the split Jacobian matrices and this is to meet the conditions $\bar{\lambda}_m^+ \geq 0$ and $\bar{\lambda}_m^- \leq 0$ for all $m = 1, \dots, M$ as shown in equations (3.53) and (3.54) below and the splitting is needed to reproduce regular upwinding i.e.

$$\hat{A}^+(q) = \frac{\partial f^+(q)}{\partial q} \quad (3.51)$$

$$\hat{A}^-(q) = \frac{\partial f^-(q)}{\partial q} \quad (3.52)$$

Also, the finite volume method will then lead an unknown flux $F(q_L, q_R)$ by

$$F(q_L, q_R) = f^+(q_L) + f^-(q_R). \quad (3.53)$$

This is the nonlinear equation

$$\frac{\partial \bar{q}}{\partial t} + \frac{\partial \bar{f}(\bar{q})}{\partial x} = 0 \quad (3.54)$$

$$\int_0^{S_R \Delta t} q(x, \Delta t) dx - S_R \Delta t q_R + \Delta t [f(q_R) - F(q_L, q_R)] = 0 \quad (3.55)$$

and for equation (3.56)

$$\int_0^{S_R \Delta t} \bar{q}(x, \Delta t) dx - S_R \Delta t q_R + \Delta t [\bar{f}(q_R) - \bar{F}(q_L, q_R)] = 0 \quad (3.56)$$

As the integrals in (3.55) and (3.56) must be equal, we immediately find the correct expression for the flux approximation for a scheme that internally utilises a modified conservation law:

$$F(q_L, q_R) = \bar{F}(q_L, q_R) - \bar{f}(q_R) + f(q_R) \quad (3.57)$$

An analogous calculation for the smallest eigenvalue S_L and integration gives $[S_L \Delta t, 0] \times [0, \Delta t]$ gives,

$$F(q_L, q_R) = \bar{F}(q_L, q_R) - \bar{f}(q_L) + f(q_L) \quad (3.58)$$

We insert for $\bar{F}(q_L, q_R)$ and $\bar{f}(q_{L/R})$ the expressions from equation (3.57) and (3.58) and derive,

$$F(q_L, q_R) = f(q_L) + \sum_{\hat{\lambda}_m < 0} a_m \hat{\lambda}_m \hat{r}_m = f(q_R) - \sum_{\hat{\lambda}_m \geq 0} a_m \hat{\lambda}_m \hat{r}_m \quad (3.59)$$

$$F(q_L, q_R) = f(q_L) + \hat{A}^- \Delta q = f(q_R) - \hat{A}^+ \Delta q \quad (3.60)$$

Using the finite volume method, equation (3.63) will be obtained

$$Q_j^{l+1} = Q_j^l - \frac{\Delta t}{\Delta x} \left(\begin{array}{l} \hat{A}^-(Q_j^l, Q_{j+1}^l) \Delta Q_{j+\frac{1}{2}}^l \\ + \hat{A}^+(Q_{j-1}^l, Q_j^l) \Delta Q_{j-\frac{1}{2}}^l \end{array} \right) \quad (3.61)$$

$$\hat{A}^-(q_L, q_R) \Delta q = \sum_{\hat{\lambda}_m < 0} a_m \hat{\lambda}_m \hat{r}_m \quad (3.62)$$

$$\hat{A}^+(q_L, q_R) \Delta q = \sum_{\hat{\lambda}_m \geq 0} a_m \hat{\lambda}_m \hat{r}_m \quad (3.63)$$

Considering the notations $\mathcal{A}^\pm \Delta := \hat{A}^\pm(q_L, q_R) \Delta q$ and by applying the waves, $\mathcal{W}_m := a_m \hat{r}_m$ the fluctuations (3.64) can thus be written

$$\mathcal{A}^- \Delta = \sum_{\hat{\lambda}_m < 0} \hat{\lambda}_m \mathcal{W}_m \quad (3.64)$$

$$\mathcal{A}^+ \Delta = \sum_{\hat{\lambda}_m \geq 0} \hat{\lambda}_m \mathcal{W}_m \quad (3.65)$$

3.3.3 Calculations of the sources

In discretising directly, the system of partial differential equations (PDEs), the finite difference discretisations are obtained through the process of replacement of the derivatives [77]. Finite volume (FV) approach as another ideal is based on the discretisation of the integral form and this can result in numerical schemes that are conservative for $s \equiv 0$. According to the theorem postulated by Lax and Wendroff which shows that the limit $q(x, t)$ of a converging conservative scheme is constantly

a weak solution. A rectangular computational cell C_{jk} which surrounds each mesh point (x_1^j, x_2^k) can be defined, and the domain of cell C_{jk} can be interpreted as,

$$I_{jk} = [x_1^{j-\frac{1}{2}}, x_1^{j+\frac{1}{2}}] \times [x_2^{k-\frac{1}{2}}, x_2^{k+\frac{1}{2}}] \quad (3.66)$$

The I_{jk} and the discrete time interval $[t_l, t_{l+1}[$ as integration domain are used in the integral form and equation (3.67) is obtained,

$$\int_{I_{jk}} + \sum_{t_l}^{t_{l+1}} \int_{\partial I_{jk}} f_n(q(o, t)) \sigma_n(o) \delta o \delta t = \int_{t_l}^{t_{l+1}} \int_{I_{jk}} s(q(x, t)) \delta x \delta t \quad (3.67)$$

The value $Q_{jk}(t)$ is an approximation within each computational cell C_{jk} are the exact cell average value,

$$Q_{jk}(t) = \frac{1}{|I_{jk}|} \int_{I_{jk}} q(x, t) \delta x \quad (3.68)$$

By employing the approximated values $Q_{jk}(t)$ instead of $q(x, t)$ as argument for $s(q(x, t))$ a natural approximation to the cell average of the source term function is found immediately:

$$s(Q_{jk}(t)) = \frac{1}{|I_{jk}|} \int_{I_{jk}} s(x, t) \delta x \quad (3.69)$$

Furthermore, we define numerical flux functions F^n at the sides of C_{jk} by

$$F_{jk}^{1,+1/2}(Q(t)) = \frac{1}{\Delta x_2} \int_{x_2^{k-1/2}}^{x_2^{k+1/2}} f_1(q(x_1^{j+1/2}, x_2, t)) \delta x_2 \quad (3.70)$$

$$F_{jk}^{2,+1/2}(Q(t)) = \frac{1}{\Delta x_1} \int_{x_1^{j-1/2}}^{x_1^{j+1/2}} f_2(q(x_1, x_2^{k+1/2}, t)) \delta x_1 \quad (3.71)$$

When equation (3.68) is approximated and divided by $|I_{jk}|$, equation (3.69) is obtained,

$$Q_{jk}(t_{l+1}) = Q_{jk}(t_l) - \sum_{n=1}^d \frac{1}{\Delta x_n} \int_{t_l}^{t_{l+1}} (F_{jk}^{n,+1/2}(Q(t)) - F_{jk}^{n,-1/2}(Q(t))) \delta t \quad (3.72)$$

3.3.4 Explicit schemes

This is the simplest method of evaluating all fluxes and sources of known values at t_n . The time explicit scheme will be obtained when the Euler method is employed to estimate all time integrals of equation (3.74) [77].

$$Q_{jk}^{l+1} = Q_{jk}^l - \sum_{n=1}^d \frac{\Delta t}{\Delta x_n} \left(F_{jk}^{n,+1/2}(Q^l) - F_{jk}^{n,-1/2}(Q^l) \right) + \Delta t s(Q_{jk}^l) \quad (3.73)$$

Where t stands for time in seconds

3.3.5 Explicit-implicit schemes

In this method, stability is of great requirement because the analysis of the methods for ordinary differential equations (ODEs) would need the use of backward or implicit Euler method. Also, in this method, all the fluxes and sources will be evaluated using unknown variable values at the new level. However, when all fluxes disappear, $f_n \equiv 0$, then equation (3.1) above becomes ordinary differential equation (ODE) [77].

$$\frac{\partial q}{\partial t} = s(q(t)) \quad (3.74)$$

$$Q_{jk}^{l+1} = \int_{t_l}^{t_{l+1}} s(Q_{jk}(t)) dt \quad (3.75)$$

$$Q_{jk}^{l+1} = Q_{jk}^l - \sum_{n=1}^d \frac{\Delta t}{\Delta x_n} \left(F_{jk}^{n,+1/2}(Q^l) - F_{jk}^{n,-1/2}(Q^l) \right) \quad (3.76)$$

$$Q_{jk}^{l+1} = Q_{jk}^l - \sum_{n=1}^d \frac{\Delta t}{\Delta x_n} \left(F_{jk}^{n,+1/2}(Q^l) - F_{jk}^{n,-1/2}(Q^l) \right) \quad (3.77)$$

3.3.6 Method of fractional steps

The time-operator splitting that is applied determines the method of fractional steps. The initial conditions resulting from the preceding step would be employed in solving the homogenous partial differential equation and the ordinary differential equation [77].

$$\frac{\partial q}{\partial t} + \sum_{n=1}^d \frac{\partial}{\partial x_n} f_n(q) = 0 . IC: Q^l \xrightarrow{\Delta t} \tilde{Q}^{l+1} \quad (3.78)$$

$$\frac{\partial q}{\partial t} = s(q), \quad IC: \bar{Q}^{l+1} \xrightarrow{\Delta t} Q^{l+1} \quad (3.79)$$

$$Q^{l+1} = S^{(\Delta t)} \mathcal{H}^{(\Delta t)}(Q^l) \quad (3.80)$$

$$Q^{l+1} = S^{(\frac{1}{2}\Delta t)} \mathcal{H}^{(\Delta t)} S^{(\frac{1}{2}\Delta t)}(Q^l) \quad (3.81)$$

$$Q^{l+1} = \chi_2^{(\Delta t)} \chi_1^{(\Delta t)}(Q^l) \quad (3.82)$$

$$Q^{l+1} = \chi_1^{(\frac{1}{2}\Delta t)} \chi_2^{(\Delta t)} \chi_1^{(\frac{1}{2}\Delta t)}(Q^l) \quad (3.83)$$

$$\begin{aligned} F(q_L, q_R) &= Aq_L + A^- \Delta_q \\ &= Aq_R - A^+ \Delta_q = A^+ q_L + A^- q_R. \end{aligned} \quad (3.84)$$

$$F(q_L, q_R) = \frac{1}{2} (Aq_L + Aq_R - |A| \Delta_q). \quad (3.85)$$

$$Q_j^{l+1} = Q_j^l - \frac{\Delta t}{\Delta x} (F(Q_j^l, Q_{j+1}^l) - F(Q_{j-1}^l, Q_j^l)) \quad (3.86)$$

$$= Q_j^l - \frac{\Delta t}{\Delta x} (A^- Q_{j+1/2}^l + A^+ Q_{j+1/2}^l) \quad (3.87)$$

3.3.7 Courant-Friedrichs Lewy (CFL) Condition

In CFD simulation, the CFL number describes how fluid is flowing through the computational cells. This implies that if the Courant number is ≤ 1 , then the fluid particles are flowing from one computational cell to another within one-time step, but if the Courant number is > 1 , it shows that the fluid particles are running through two or more computational cells at each time step. Therefore, it is a good way of controlling the time step using CFL Numbers [77].

$$\frac{|\lambda_m| \Delta t}{\Delta x} \leq 1, \quad \text{for all } m = 1, \dots, M. \quad (3.88)$$

where u is the magnitude of the velocity (whose dimension is length/time); Δt is the time step (whose dimension is time); Δx is the length interval (whose dimension is length). The following next section will be centred on adaptive mesh refinement in object-oriented C++ (AMROC) which is very central in this research work.

3.4 Adaptive Mesh Refinement

AMROC software [78] provides an object-oriented implementation in C++ of the block structured adaptive mesh refinement algorithm by Anshu Dubey et al in 2021 [79] and Oda Marit Olmheim in 2021 [80]. With the AMR tools, the flow solvers are implemented, which calculate the equations in section 3.3 and solve for the basic equations in section 3.2. The calculated results are stored in the Hierarchical Data Structures, i.e., HDF4 format [79].

3.4.1 Adaptive mesh refinement strategies

Generally, a broad range of different scales is involved in detonation simulations and non-reactive inviscid fluid flow computations [77], [80]. In obtaining a high resolution of the physical relevant phenomena, a viable implementation of the finite volume shock utilises non-uniform grids [81].

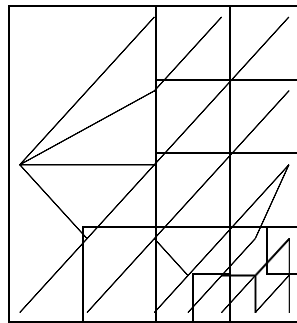


Figure 3.1: Unstructured refinement strategy [76], [81].

There are two techniques of adaptive mesh refinement (AMR) which include (1) unstructured approach and (2) structured approach adaptive mesh refinement.

(1) Unstructured approach

The cells that need refinement are purely substituted by finer cells and in addition, the numerical solution is updated on the entire grid at the same time. Also, superior

geometrical flexibility accounts for unstructured triangulations [77], [80]. The vertices and their coordinates are kept explicitly, and the basic discretisation is virtually non-uniform as shown in Figure 3.1 above. In recombining the fine cells, a coarsening step would be needful. The CFL condition for the smallest cell would need a time step thereby making time-explicit finite volume schemes incapable [81].

(2) Structured approach

One of the advantages of structured approach over that of the unstructured is that the structured mesh has the capability of accepting optimisation which can regulate the technical disadvantages of the techniques of unstructured refinement. Moreover, a typical refinement block of cells is a substitute for a single coarse cell in a structured refinement strategy [81]. For instance, using a general data tree, refinement blocks achievable can be effectively obtained as represented in Figure 3.2 below. Also, the data tree can skip explicit storage of parent- or child-relations and the application of integer coordinate system which permits the easy check of neighbourhood relationships.

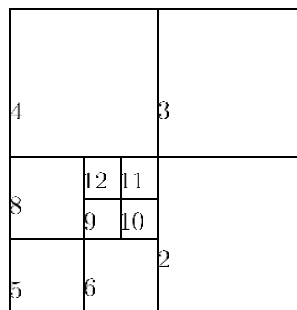


Figure 3.2: Mesh and local quadtree-tree of a structured mesh refinement strategy [76] [81].

However, considering the time-explicit finite volume schemes, the time-space constructed include interior boundary conditions that can be handled with average expense thereby permitting a successive time step refinement with refinement factor r [81]. The hanging of nodes along the coarse fine interfaces which is certain is the associated disadvantage. The structured approach which operates with accessible computer memory is better than the unstructured technique, consecutive memory blocks of cells, consecutive memory blocks of r^d cells [81]. In addition, a boundary size of at least two ghost cells and the memory demand for the boundaries only can

suddenly exceed that of the mere refinement regions which accounts for high resolution schemes [81]. However, if refinement blocks of random size are examined, unwanted overlapping refinement boundaries can thus be absolutely removed. A real systematic strategy that entails a remarkably greater algorithmic complexity and a broad software infra-structure is applied in a block structured approach.

Grid hierarchy

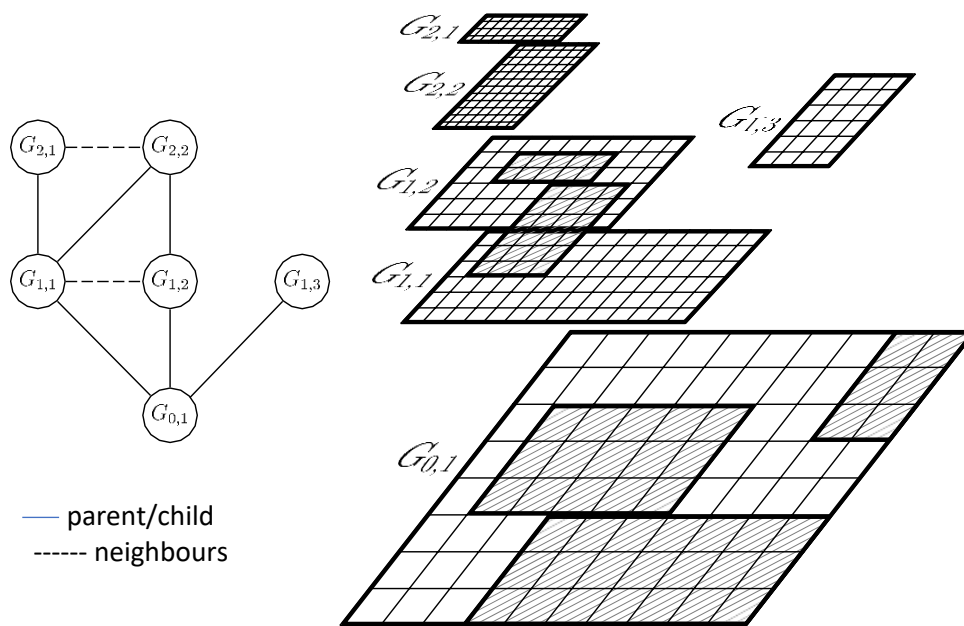


Figure 3.3: The block structured refinement grids of the AMR method create a hierarchy of rectangular sub grids [76], [81].

3.4.2 Block structured adaptive mesh refinement

Berger and Olinger were the first to initiate the study of block structured adaptive mesh refinement technique (AMR or SAMR) for hyperbolic partial differential equations, but the initial method employed considered rotated refinement grids that required complex conservative interpolation operations. Presently, Adaptive Mesh Refinement (AMR) is the clarified variant of the work of Berger and Colella that only permits refinement patches in conformity with the coarse grid mesh [82]. A pathway refinement strategy is stuck to rather than replacing single cells with finer ones of the AMR method. There is the need of the geometrical description of the refinement regions and sub grids using the same refinement factor in all space-directions and in time. A separate refinement factor r_i can be employed considering the hierarchical

level such as the structured approach which required just the implementation of the numerical scheme on a single rectangular grid [82]. Refined grids are obtained from coarser cells and the grid patches are perfectly embedded as shown in Figure 3.3 in section 3.4.2.

(1) Conditions for Adaptive Mesh refinement

Certain conditions are employed in the selection of scalar quantities such as vector of state and assessed derived quantities for example, the hydrodynamic pressure [82]. The conditions for the selection include the following:

(a) Scaled Gradients

Evaluating gradients multiplied by the step size (scaled gradients) in all directions are obtainable through an adaptation along discontinuities [82]. If the scalar quantity w , obtained from the vector of state $Q_i(t)$ are achieved, then the cells j, k as represented in equation (3.92) below are good to go for refinement.

$$|w(Q_{j+1,k}) - w(Q_{jk})| > w, \quad (3.89)$$

$$|w(Q_{j,k+1}) - w(Q_{jk})| > w, \quad (3.90)$$

$$|w(Q_{j+1,k+1}) - w(Q_{jk})| > w \quad (3.91)$$

Where w stands for the scalar quantity

(b) Heuristic error estimation

Richardson extrapolation showed that the heuristic estimation of the local truncation error indicates a simple adaptation criterion for regions of smooth solutions [82]. However, the local truncation error of a difference scheme of order meets this equation:

$$q(x, t + \Delta t) - H(\Delta t)(q(:, t)) = C\Delta t^{o+1} + O(\Delta t^{o+2}) \quad (3.92)$$

3.4.3 Object-oriented implementation

The detailed description of the Adaptive Mesh Refinement (AMR) method constitutes the basis of the Adaptive Mesh Refinement in Object-oriented C++ (AMROC).

(i) Three-level design

There are three levels pinpoint in the Adaptive Mesh Refinement (AMR). Numerical scheme and functions are crucial to set the initial and physical boundary conditions. During implementation, these functions are in Fortran-77 and mimic the syntax of the popular non-adaptive code Clawpack. Moreover, the Interface objects in C++ supply a generic approach to these functions to the Adaptive Mesh Refinement (AMR) level below [76]. The middle level comprises (i) the parallel AMR algorithm and its components for error estimation, (ii) grid generation and (iii) flux correction and this is completely in C++. The central class of the Adaptive Mesh Refinement AMR-Solver (AMR-Solver) consists of Algorithms 2 and 3. An object of this type coordinates the whole computation and cells methods of the component classes Flagging, Clustering and Fix up according to the Algorithms 2 and 3 [76]. The middle level operates mainly on grid-based hierarchical data structure that are supplied by the base level.

(ii) The Hierarchical data structures

Several grid-based data and the hierarchy constitute the base level, and it provides standard operations which require topological information for example ghost cell synchronization, interpolation or averaging to the middle level [76]. The mesh widths $\Delta x_{n,i}, i = 0, \dots, i_{max}$ can be replaced by increasing integers, i.e.

$$\Delta x_{n,i} = \prod_{k=i+1}^{i_{max}} r_k \quad \text{for all } n = 1, \dots, d. \quad (3.93)$$

The Framework of AMROC

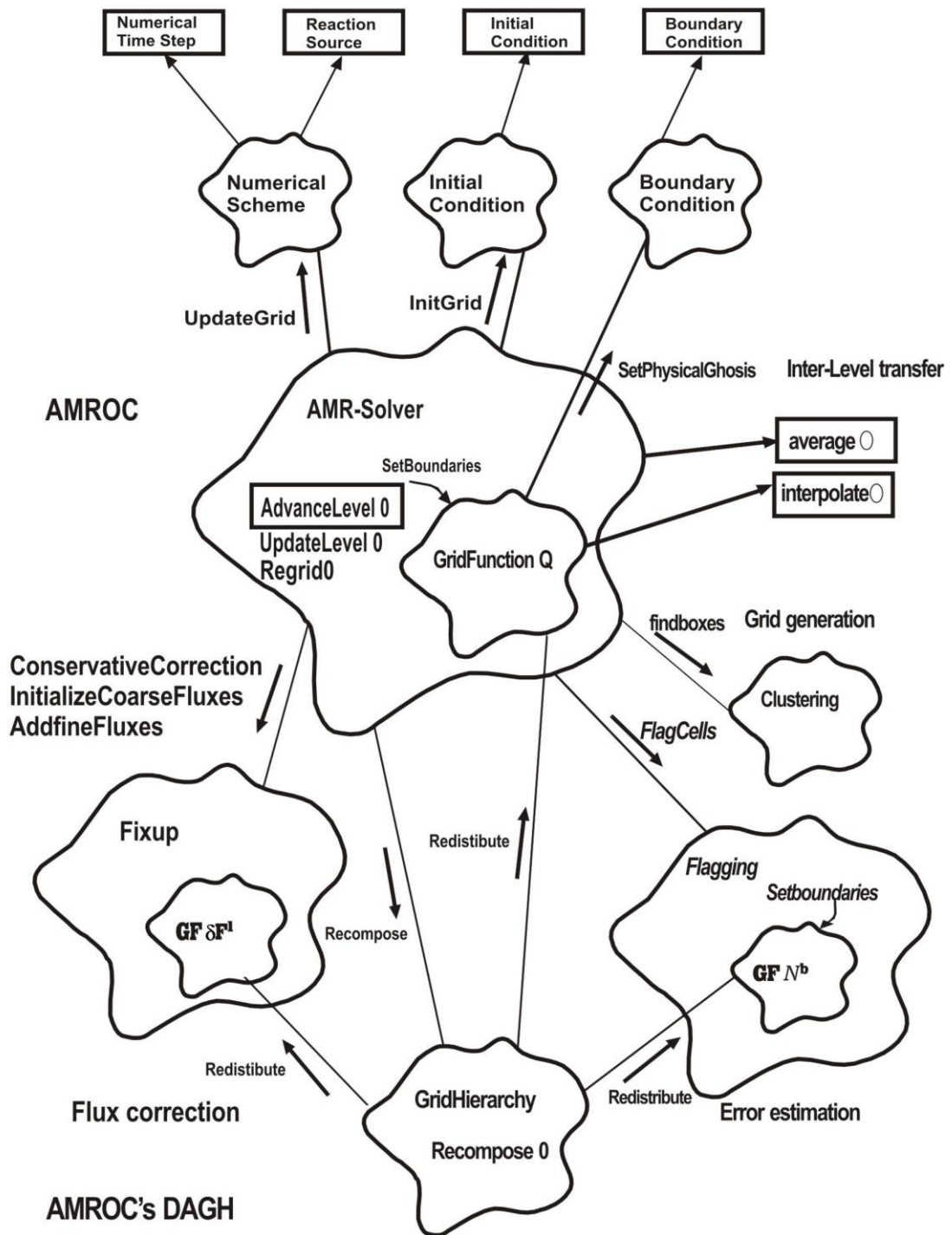


Figure 3.4: Object-oriented design of the AMROC framework [76].

The middle level also centred on the object diagram of the entire design as shown in Figure 3.4, and each arrow in Figure 3.4 above represents a straightforward message to the object to which it points, and GF stands for Grid-Function.

3.4.4 AMROC's DAGH

According to Parashar and Browne [83], the base level is an extension of the DAGH (Distributive Adaptive Grid Hierarchies) package in implementation, and it is complete in Adaptive Mesh Refinement in Object-oriented C++ (AMROC). AMROC's version of DAGH implements Grid Function- and Grid Hierarchy-classes that are much more general and allow a more efficient adaptation than those of the original DAGH package [83]. The Grid Function-class of the original DAGH package is limited to grids that are aligned to the base mesh that coarsened by a factor of 2. Thus, the original DAGH usually refines more cells than may be needed.

Table 3.1: Refinement after the last time step of a typical test problem for four computations with an increasing number of refinement levels with AMROC's DAGH and the original DAGH [76].

| | i_{max} | Level 0 | Level 1 | Level 2 | Level 3 | Level 4 |
|-------------|-----------|-----------|-----------|------------|------------|-------------|
| AMROC's | 1 | 43/22500 | 145/38696 | | | |
| DIAGH | 2 | 42/22500 | 110/48708 | 283/83688 | | |
| grids/cells | 3 | 36/22500 | 78/54796 | 245/109476 | 582/165784 | |
| | 4 | 41/22500 | 88/56404 | 233/123756 | 476/220540 | 1017/294828 |
| Original | 1 | 238/22500 | 125/41312 | | | |
| DIAGH | 2 | 494/22500 | 435/48832 | 190/105216 | | |
| grids/cells | 3 | 695/22500 | 650/55088 | 462/133696 | 185/297984 | |
| | 4 | 875/22500 | 822/57296 | 677/149952 | 428/349184 | 196/897024 |

The simplifying assumption that two grids on neighbouring levels only can be connected by a 1:1 relation is limited in Distributive Adaptive Grid Hierarchies (DAGH). AMROC's DAGH is a important improvement over the original package. The maximal number of grids on all levels is equal and this reduces the recompositing overhead on higher levels but leads to an increasing waste in advancing the numerical solution, and the coarser level grids will split [83].

Table.3.1 represents the number of grids and cells for a uniform refinement factor of 2. Hilbert's space-filling curve on 7 computing nodes is applied for computing all solutions. However, if only one or two refinement levels are applied, the simplification in Distributive Adaptive Grid Hierarchies (DAGH) will not be considered, but if a higher number of levels is required, then permitting arbitrary AMR will be paramount to have a drastic improvement [83]. In AMROC's DAGH, level-dependent refinement

factors such as multiple periodic boundary conditions, a restart option from memory for automatic time step algorithms and a restart feature for a variable number of computing nodes would be needed as supplementary new features [76].

3.4.5 Capabilities of AMROC over other CFD software

The advantages of AMROC include:

- (1) There are several CFD software used for CFD simulations, but AMROC is unique for simulating detailed chemical combustion reactions, although Fluent may be used [82], [83].
- (2) Because in CFD simulations, AMROC has an adaptive refinement and mesh refinement quality. This enables us to do direct numerical simulation (DNS) for combustion simulation [84].

3.4.6 Limitation of AMROC

The major limitation of AMROC is its mesh. As it uses block structured meshes, the simulated domain configuration must be quite regular, but cannot be complex. Thus, it is limited to study the mechanisms of explosions in simple geometries [84].

3.5 Validation and verification of this research work

Validation of this research work is on different pages of this research report:

Experimental methods are very difficult, and thus measuring fast combustions at 300K looks absolutely impossible.

However,

- Comparison of induction time of numerical simulation and that of experiment as presented on page 108 of this Thesis report shows consistency.
- Also, from Liberman's result, it showed that reaction zones and flow patterns were consistent as showed on page 109 of this Thesis report.
- In addition, Kuznetsov's results showed that the results obtained were consistent as shown on page 109 of this Thesis report.
- Comparing this research work result with already published work.

To this end, it showed that the results were accurate and correct.

Chapter 4 Chemical Kinetics

4.1 Introduction

In this chapter, the following concepts will be treated such as the basic concepts of reaction rates, the chain reaction theory, the mechanisms for combustion reactions of hydrocarbon fuels, the oxidation mechanisms of hydrogen and carbon monoxide as well as the oxidation of hydrocarbons. Chemical kinetics is a theory on chemical reaction rates that is an essential part in the basic equations in chapter 3. This theory stemmed from the pioneering researches of Guldberg and Waage between 1864 and 1879, and they published the following papers which include (1) The Henderson approximation and the mass action law of Guldberg and Waage (2002) [85]; (2) Guldberg and Waage and the law of mass action (2021) [86]; (3) Cato Guldberg and Peter Waage, the history of the Law of mass action, and its relevance to clinical pharmacology (2021) [87]. Others include (4) Deviations of H-bonded aggregates in liquids from the Guldberg and Waage equilibrium expression (2019) [88]; (5) MAGE: A semantics retaining K-anonymization method for mixed data (2014) [89]; and (6) Note on an Extension of the Theoretical Applicability of Guldberg and Waage's mass Law (2021) [90], [91]. Their study established the law of mass action and the concept of chemical equilibrium which laid a foundation for chemical kinetics [92]. Afterwards, many researchers proposed various concepts and mechanisms on chemical reactions and contributed to the completeness of the theory of chemical kinetics [93]. In this chapter, the chemical kinetics relevant to hydrocarbon combustion reactions is reviewed and discussed.

4.2 Basic concepts on reaction rates

4.2.1 Law of mass action

The law of mass action is a basic law for chemical reaction rates [94]. To discuss this law, let us present a forward chemical reaction as follows:



The rate of change in the molar concentration c_i (moles per unit volume) of species i , is the reaction rate for this species and is calculated by:

$$\hat{\omega}_i = \frac{dc_i}{dt} \quad (4.2)$$

One can see that equation (4.2) is distinctively related to $\hat{\omega}_i$ of species j by

$$\frac{\hat{\omega}_i}{v_i - v'_i} = \frac{\hat{\omega}_j}{v_j - v'_j} = \omega \quad (4.3)$$

Where ω represents the reaction rate

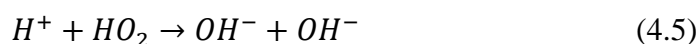
The law of mass action states that the reaction rate, ω , is proportional to the product of the concentrations of the reactants as represented in equation (4.4) below

$$\omega = k_f(T) \prod_{i=1}^N c_i^{v'_i} \quad (4.4)$$

Where ω stands the reaction rate

where the proportionality factor $k_f(T)$, to be specified later, is called the specific reaction rate constant and is primarily a function of temperature.

For instance, an elementary reaction involving:



It can undergo oxidation of hydrogen and hydroperoxyl and this can be represented as

$$\omega = -\frac{d[H^+]}{dt} = -\frac{d[HO_2]}{dt} = \frac{1}{2} \frac{d[OH^-]}{dt} \quad (4.6)$$

and the reaction rate based on the law of mass action would be given by

$$\omega = k_f[H^+][HO_2] \quad (4.7)$$

4.2.2 Reversible and multistep reactions

(a) Reversible reactions

The forward reaction of the law of mass action, equation (4.8) below is a match for backward reaction,



$$\sum_{i=1}^N v_i'' M_i \xrightarrow{k_b} \sum_{i=1}^N v_i' M_i \quad (4.9)$$

A combination of the reaction rate of the forward and backward reactions of,

$\widehat{\omega}_i = \widehat{\omega}_{i,f} + \widehat{\omega}_{i,b} = (v_i'' - v_i')(\omega_f - \omega_b) = (v_i'' - v_i')\omega$, with ω would give,

$$\omega = k_f \prod_{i=1}^N c_i^{v_i'} - k_b \prod_{i=1}^N c_i^{v_i''} \quad (4.10)$$

When the reactions are at equilibrium, $\omega \equiv 0$, k_f and k_b are obtained since the forward reaction rate is balanced by the backward reaction rate, equation (4.10) resulting in

$$\frac{k_f}{k_b} = \prod_{i=1}^N c_i^{(v_i'' - v_i')} \quad (4.11)$$

Thus, the equilibrium constant, K_c is obtained from equation (4.11) above yielding,

$$\frac{k_f}{k_b} = K_c \quad (4.12)$$

A substitution of equation (4.12) into equation (4.10) will give equation (4.13)

$$\omega = k_f \left(\prod_{i=1}^N c_i^{v_i'} - K_c^{-1} \prod_{i=1}^N c_i^{v_i''} \right) \quad (4.13)$$

The backward reaction and its progress can be grossly affected if the reaction is endothermic or has a high energy barrier, and this is referred to as an irreversible reaction.

$$\omega \cong k_f \prod_{i=1}^N c_i^{v_i'} \quad (4.14)$$

(b) Multistep reactions

In certain reactions, the original reactants react with each other in a single step as shown in equation (4.14) above, the stoichiometric methane oxidation is represented as,



In addition, the products comprise many more species than only CO₂ and H₂O, as do others. Therefore, if there are K such intermediate reactions involved,

$$\sum_{i=1}^N v'_{i,k} M_i \rightleftharpoons \sum_{i=1}^N v''_{i,k} M_i, \quad k = 1, 2, \dots, K, \quad (4.16)$$

then the generalised law of mass action is

$$\omega_k = k_{k,f} \prod_{i=1}^N c_i^{v'_{i,k}} - k_{k,b} \prod_{i=1}^N c_i^{v''_{i,k}}, \quad k = 1, 2, \dots, K, \quad (4.17)$$

Thus,

$$\hat{\omega}_i = \sum_{k=1}^K (v''_{i,k} - v'_{i,k}) \omega_k \quad (4.18)$$

It may be noted that in the above the subscript for $\hat{\omega}$ is for species i , whereas that for ω is for reaction k .

4.2.3 Reaction equilibrium

(1) Steady-state approximation

A complex chemical reaction scheme that usually results in the formation of products from reactants often produce reaction intermediate. Hence, if i is such an intermediate [93], then the reaction rate is expressed as,

$$\hat{\omega}_i = \frac{dc_i}{dt} = \hat{\omega}_i^+ - \hat{\omega}_i^- \quad (4.19)$$

where $\hat{\omega}_i^+$ and $\hat{\omega}_i^-$ represent the rates of generation and consumption reactions respectively, then the steady-state approximation would be,

$$\left| \frac{dc_i}{dt} \right| \ll (\hat{\omega}_i^+, \hat{\omega}_i^-) \quad (4.20)$$

Therefore,

$$\hat{\omega}_i^+ = \hat{\omega}_i^- \quad (4.21)$$

(2) Partial equilibrium approximation

Partial equilibrium approximation accepts that the forward and backward rates of a reaction k will be much larger than the net reaction ω_k and thus, $\omega_k \approx 0$ [93] as represented in equation (4.22), showing that

$$\frac{\hat{\omega}_i}{v_i'' - v_i'} = \frac{\omega_j}{v_j'' - v_j'} = \omega, \quad (4.22)$$

Thus,

$$k_{k,f} \prod_{i=1}^N c_i^{v_{i,k}'} = k_{k,b} \prod_{i=1}^N c_i^{v_{i,k}''}. \quad (4.23)$$

When ω_k is considered in relationship with the forward and backward reactions in equation (4.17) above, it would be small, but it would not actually be small when compared to $\hat{\omega}_i$ in equation (4.18).

$$\hat{\omega}_i = \frac{dc_i}{dt} = (v_{i,1}'' - v_{i,1}')\omega_1 + \sum_{k=2}^K \hat{\omega}_{i,k}, \quad i = 1, 2, \dots, N, \quad (4.24)$$

But when $i=1$, it would become,

$$\omega_1 = \frac{dc_1}{dt} = (v_{1,1}'' - v_{1,1}')\omega_1 + \sum_{k=2}^K \hat{\omega}_{1,k}. \quad (4.25)$$

By method of elimination, removing ω_1 would give,

$$\frac{dc_i}{dt} = \sum_{k=2}^K \hat{\omega}_{i,k} + \left(\frac{v_{i,1}'' - v_{i,1}'}{v_{1,1}'' - v_{1,1}'} \right) \left[\frac{dc_1}{dt} - \sum_{k=2}^K \hat{\omega}_{1,k} \right], \quad i = 2, \dots, N. \quad (4.26)$$

4.2.4 Arrhenius law: theories of reaction rates

Basically, the specific reaction rate constant $k(T)$ is temperature dependent, and the Arrhenius law states that,

$$\frac{d \ln k(T)}{dT} = \frac{E_a}{R^0 T^2}, \quad (4.27)$$

where E_a is the activation energy of the reaction (cal/mole or joule/mole).

By integrating equation (4.27) when E_a is a constant in relation to temperature will give,

$$k(T) = Ae^{-E_a/R^0T}, \quad (4.28)$$

where A = the frequency factor or the preexponential factor, and R^0 is a constant.

$$T_a = \frac{E_a}{R^0}, \quad (4.29)$$

For constant values of A and E_a , a plot of $\ln k(T)$ versus $1/T$ exhibits a linear relationship, with A and E_a respectively obtained from the intercept and slope of such a plot as shown in Figure 4.1 below [95], [96], [97], [98]. Moreover, a modified Arrhenius equation can thus, be introduced by expressing

$$A = A(T) = BT^\alpha \quad (4.30)$$

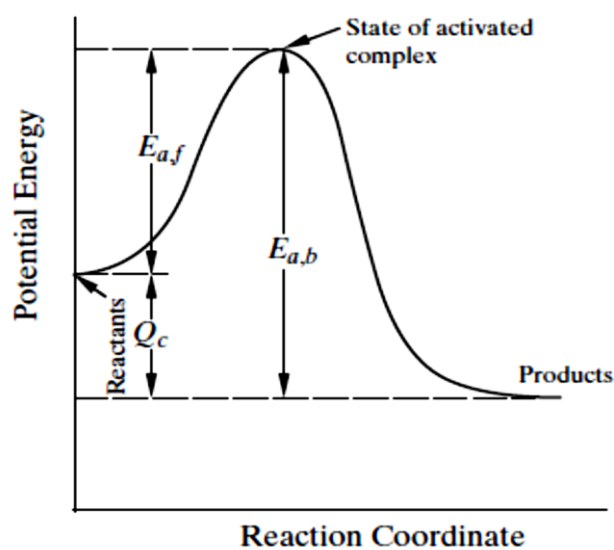


Figure 4.1: Potential energy diagram showing the concept of reaction activation [95].

$$k(T) = BT^\alpha e^{-E_a/R^0T}, \quad (4.31)$$

where B stands for a constant, and α is temperature exponent.

$$\prod_{i=1}^N p_i^{(v_i'' - v_i')} = K_p(T), \quad (4.32)$$

$$K_p(T) = \exp\left\{-\left[\sum_{i=1}^N (v_i'' - v_i')\right]/(R^0T)\right\} \quad (4.33)$$

$$\sum_{i=1}^N v_i' M_i \rightleftharpoons \sum_{i=1}^N v_i'' M_i, \quad (4.34)$$

$$\frac{dN_i}{v_i'' - v_i'} = \frac{dN_j}{v_j'' - v_j'} = d\lambda, \quad (4.35)$$

$$dN_i = (v_i'' - v_i') d\lambda, \quad (4.36)$$

4.2.5 Rates of reactions and their temperature dependence

Generally, chemical reactions like hydrolysis, or combustion type occur at a definite rate and are determined by the conditions of the system [95]. Thus, the reaction rate could be expressed as the rate of decrease of a reactant concentration or that of increase of a reaction product [93]. Experimentally, the law of mass action states that the rate of disappearance of a chemical species i , defined as RR_i is proportional to the product of the concentrations of the reacting chemical species, wherein each concentration is raised to a power equal to the corresponding stoichiometric coefficient; (see equation (4.36) below) [95].

$$RR_i \sim \prod_{j=1}^n (M_j)^{v_j'}, \quad RR_i = k \prod_{j=1}^n (M_j)^{v_j'} \quad (4.37)$$

Where k is the proportionality constant termed the specific reaction rate coefficient, $\sum v_j'$ and it is symbolised as n , which is referred to as the overall order of the reaction; v_j' itself and would be the order of the reaction in relation to species j [94]. The rate of change of the concentration of a given species i in a reacting system is represented by

$$\frac{d(M_i)}{dt} = [v_i'' - v_i'] RR = [v_i'' - v_i'] k \prod_{j=1}^n (M_j)^{v_j'} \quad (4.38)$$

since v_j'' moles of M_i are formed for every v_j' moles of M_i consumed. In many systems M_j cannot only be formed from a single-step reaction as represented in equation (4.37) but can equally be formed from many different steps. In evaluating experimental data, a pseudo-first-order condition can occur when one of the reactants, generally the oxidizer in a combustion system is in large excess [96].

4.3 Chain reaction theory

Chain reactions play fundamental roles in combustion reaction mechanisms. They are comprised of three basic steps, i.e. chain initiating step, chain carrying or propagating step and chain terminating step. The most important chain reactions to combustion processes are two in them: - straight-chain and branched-chain reactions, and they shall be treated in detail individually [95]. In the section below, we will treat hydrogen-oxygen reactions as examples and explain the two chain reactions.

4.3.1. Straight-chain reactions: the Hydrogen–Halogen system

Hydrogen–halogen system has a direct reaction path and it is used in this context to explain straight-chain reactions as shown below:

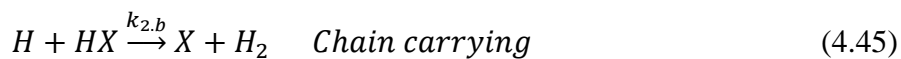
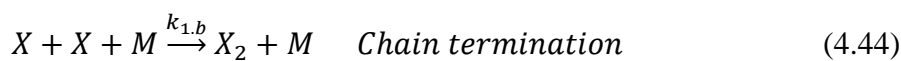
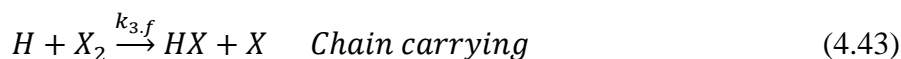
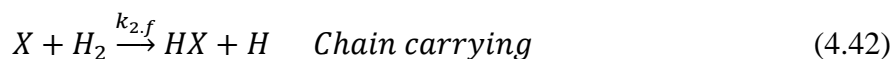
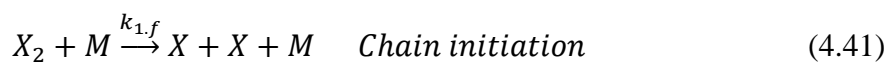


And the rate of product formation of HX is given by

$$\frac{d[\text{HX}]}{dt} = 2k_0[\text{H}_2][\text{X}_2] \quad (4.40)$$

where X_2 stands for halogen molecule F_2 , Cl_2 , Br_2 , or I_2 .

Nevertheless, it is worthy to note that the reaction between H_2 and X_2 to produce HX often takes a more complex scheme comprising these consecutive five major steps [76] which are as follows:



In distinguishing the reactant, the reaction number of a reaction mechanism is used by the symbol. For instance, H is used for reactions involving hydrogen oxidation, M for methane oxidation, C_2 for the C_2 hydrocarbon species, to mention a few [76]. Considering the halogen–hydrogen mechanism above, the reaction (4.41) is the chain initiation step in which a halogen molecule is broken down into two halogen atoms [97]. Also, immediately a halogen atom X is produced through reaction (4.41), then the production of hydrogen halogen, HX will be affected by reactions (4.42) and (4.43)

above by the reaction intermediates which are known as chain carriers, H and X [76]. Hence, these reactions (4.42) and (4.43) are the chain-carrying steps and this is based on the fact that in each of them the breakage of one chain carrier will eventually result in the formation of a new chain carrier thereby making the number of chain carriers in each step constant. Thus, a closed sequence of reactions (4.42) and (4.43) will be formed in that at the end of the reaction sequence (4.43), a new halogen atom, X , will be formed capable of starting the process all over again from reaction (4.42) [76]. The net result of reactions (4.42) and (4.43) will be exactly equal to that of the direct path of above reaction (4.42) [97]. Also, reactions of (4.41) and (4.42) are the forward reactions of reactions (4.44) and (4.45) respectively; but reaction (4.44) is a chain-termination step in which two halogen atoms, X will recombine by colliding with the third body M and reaction (4.45) is the chain-carrying step [93]. However, this hinders the rate of the net production of hydrogen-halogen, HX . Reaction (4.43) is greatly endothermic, hence not vital for reaction [95].

The reaction rates of the concentration variation of the five components are presented as follows:

$$\frac{d[H_2]}{dt} = -k_{2.f}[X][H_2] + k_{2.b}[H][HX] \quad (4.46)$$

$$\frac{d[X_2]}{dt} = -k_{1.f}[X_2][M] - k_{3.b}[H][X_2] + k_{1.b}[X]^2[M] \quad (4.47)$$

$$\frac{d[H]}{dt} = k_{2.f}[X][H_2] - k_{3.f}[H][X_2] - k_{2.b}[H][HX] \quad (4.48)$$

$$\begin{aligned} \frac{d[X]}{dt} = & 2k_{1.f}[X_2][M] - k_{2.f}[X][H_2] + k_{3.f}[X][H_2] + \\ & k_{2.b}[H][HX] - 2k_{1.b}[X]^2[M] \end{aligned} \quad (4.49)$$

$$\frac{d[HX]}{dt} = k_{2.f}[X][H_2] + k_{3.f}[H][X_2] - k_{2.b}[H][HX] \quad (4.50)$$

Considering the steady-state assumption by the equation below,

$$\frac{d[H]}{dt} = 0 \text{ and } \frac{d[X]}{dt} = 0 \quad (4.51)$$

In solving equations (4.48) and (4.49) for the concentrations of hydrogen $[H]$ and halogen $[X]$ respectively and making a substitution of equations (4.47) and (4.48) into (4.50) will give equation (4.52) below,

$$\frac{d[H]}{dt} = \frac{2k_{2,f}(k_{1,f}/k_{1,b})^{1/2}[H_2][X_2]^{1/2}}{1+(k_{2,b}/k_{3,f})[HX]/[X_2]} \quad (4.52)$$

Table 4.1: Heats of reaction steps for the halogen–hydrogen systems at 300 K in kcal/mole [97]

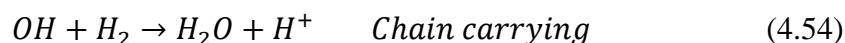
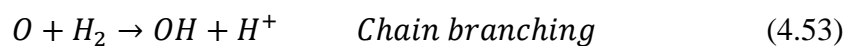
| Reaction | Equation | F | Cl | Br | I |
|---------------------------------|----------|--------|-------|-------|-------|
| $H_2 + X_2 \rightarrow 2HX$ | (4.39) | -129.7 | -44.0 | -17.4 | -2.8 |
| $X_2 + M \rightarrow X + X + M$ | (4.40) | 37.8 | 57.8 | 53.6 | 36.4 |
| $X + H_2 \rightarrow HX + H$ | (4.41) | -31.6 | 1.2 | 16.7 | 32.5 |
| $H + X_2 \rightarrow HX + X$ | (4.42) | -98.1 | -45.2 | -34.1 | -35.3 |

A comparison of equation (4.52) with equation (4.45) for the direct path of the reaction (4.39) shows that the two reaction rate expressions are not absolutely the same. The chain mechanism accurately shows that the increasing concentration of the product has an inhibitive effect on its own production rate, such that $d[HX]/dt$ varies inversely with $[HX]$ [93]. Table 4.1 in section 4.3 explains the influence of the heats of reaction of the individual steps of the reactions on their relative efficiencies in the chain process coupled with the behaviour of the various halogens [97]. Furthermore, Table 4.1 reveals that the net change of all the halogens in equations (4.39) and (4.42) are exothermic and the initiation reactions for all the halogens in equation (4.40) are endothermic, but, for equation (4.41), the net change of all the halogens in equations (4.41) is endothermic except for fluorine which was exothermic [76]. To this background, the hydrogen-halogen reactions are not spontaneous and thus, an ignition stimulus would be required. It is observed that the basic chain reactions carrying $F - H_2$ and $H - F_2$ steps of the $F_2 - H_2$ system of the reaction will be extremely exothermic which shows that the general reaction would progress rapidly though its initiation reaction is endothermic by 37.8 kcal/mole [97]. The moderate endothermicity of the $Br - H_2$ reaction would weaken the intensity of the general

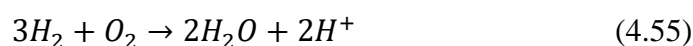
chain mechanism of the $Br - H_2$ reaction, and for the $I - H_2$ reaction steps, the endothermicity is definitely high [95].

4.3.2 Branched-chain reactions

In branched chain reactions, there is the net formation of chain carriers, and this can result to a very fast rate of the general reaction which will eventually lead to an explosion [76]. A very good illustration is the chain cycle involving hydrogen–oxygen reaction scheme.



In the above chain reactions, the O and H atoms and the OH^- radical are the chain carriers, and it shows that in each of reactions (4.52) and (4.53), two chain carriers can result when one chain carrier is present as a reactant, hence they are thus known as chain-branching steps [76]. Besides, the net reaction of the chain cycle of reaction (4.52) to reaction (4.54) indicates that two H ions are produced per chain cycle.

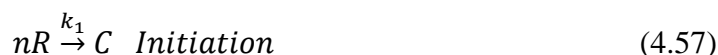


The chemical reactivities of different chain carriers are not the same, but the chain-carrying reaction can be reduced or empowered.

For instance, a good illustration of such reaction is:



From reaction (4.59), when a very active carrier H is consumed, then a very inactive carrier HO_2 will be formed. In the reaction $CH_4 + H \rightarrow CH_3 + H_2$, the reactive H atom will be interchanged for the less reactive radical CH_3 . Thus, pressure and temperature are determinant factors of the common behaviour of an explosive mixture, and this can be demonstrated by the following process [95]:



It can be stated that in the above reactions that C is the chain carrier where $a > 1$ is the multiplication factor in the chain branching cycle, and P the stable products obtained. Also, the gas termination reaction has a three-body process, but surface termination has one-body process.

In obtaining C , its production rate can be written as:

$$\frac{d[C]}{dt} = k_1[R]^n + (a - 1)k_2[R][C] - k_g[R]^2[C] - k_w[C] \quad (4.61)$$

Also, it can be better written as:

$$\frac{d[C]}{dt} = k_1[R]^n + k_2[R](a - a_c)[C] \quad (4.62)$$

where

$$a_c = 1 + \frac{k_g[R]^2 + k_w}{k_2[R]} \quad (4.63)$$

The concentration of the chain carrier, $[C]$ in equation (4.62) varies with time, for $(a - a_c) > 0$ and the situation of $a \geq a_c$ leads to the condition for the occurrence of branched-chain explosion, and the term a_c is the critical multiplication factor at which the mixture becomes very explosive [95].

Explosion is quite feasible for small a_c that relates to situations of fast chain-branching reactions (large k_2) and/or slow chain-termination reactions (small k_g and k_w) as noticed in equations (4.62) and (4.63). Thus, since $[R]$ is proportional to the system pressure p , equation (4.64) will be obtained,

$$\begin{aligned} a_c &\rightarrow 1 + \frac{k_w}{k_2[R]} \rightarrow \infty, \text{ as } p \rightarrow 0, \\ a_c &\rightarrow 1 + \frac{k_g[R]}{k_2} \rightarrow \infty, \text{ as } p \rightarrow \infty, \end{aligned} \quad (4.64)$$

This reveals that explosion will not be practicable for conditions of very low or very high pressures [99]. Furthermore, as the gas density decreases with $p \rightarrow 0$, the chain cycle will be less efficient since it involves the collision between two molecules [98]. Nevertheless, the wall termination reaction is determined by only the concentration of

the chain carrier thus becoming more efficient and consequently the resulting effect will retard explosion [76]. In like manner, as $p \rightarrow \infty$, the increase in density will make the three-body gas termination reaction to occur when related to two-body chain-branching reaction, and this further retard explosion [98]. Conversely, the gas and wall termination reactions are not temperature sensitive, thereby making k_g and k_w to be very close constants, and thus, the activation energies found to be exactly zero [98]. However, as the temperature is increasing, the critical multiplication, a_c consequently decreases and the gas will become more explosive [76]. Based on the release of energy from the activated radicals, the termination reactions will become highly exothermic. Figure 4.2 clearly explains the above behaviour which is illustrated with a C-shaped explosion limit curve. Usually, increasing the pressure ceaselessly of an initially nonexplosive gas at a given temperature will make it to become first explosive and again become nonexplosive, this continuously increasing temperature will broaden the explosivity range [95], [98].

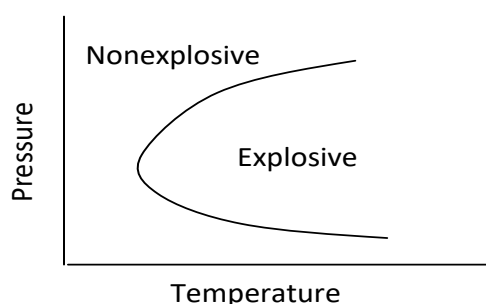


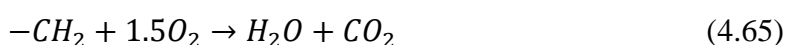
Figure 4.2: C-shaped pressure–temperature explosion limits due to chain mechanisms and wall termination [95].

A specific mass of the reactive mixture has to be heated to an adequately high temperature; the rate of chemical heat generation would be higher than that of heat loss through various transport mechanisms during a thermal ignition mechanism [98]. Thus, the chain and thermal mechanisms are however connected that the creation of chain carriers through the endothermic chain branching reactions would need energy as well as the presence of heating. Hence, a sudden rise in the concentration of the radical would result in the initiation of several extremely exothermic, chain-terminating reactions [95].

4.4 Combustion mechanisms of hydrocarbon fuels

The reaction mechanisms of hydrocarbon combustions are extremely complex and not well understood in detailed so far [100]. According to the kinetics as understood, the combustion reactions can be basically divided into two classes of reactions: pyrolysis reactions to H_2 and partial oxidation reactions to CO [101]. Then the chain reaction mechanisms for $H_2 + O_2$ and $CO + O_2$ are applied to complete the kinetics of general hydrocarbon fuel combustions [100].

This section will extensively treat the oxidation mechanisms of certain fuel systems which entail hydrogen, carbon monoxide, and different hydrocarbons as well as the production of pollutants in the environment. Quantitatively, fuel consumption, the formation and destruction of intermediate species, and the formation of final product are caused by the reaction pathways [102]. In the formation of products from reactants, several elementary chemical reactions take place and these reactions usually do not play the same roles in different combustion environments. that for a given fuel. Also, the oxidation of hydrocarbons shows the involvement of chemical kinetics in combustion through the difficult paths. Furthermore, it would be explained that a limited number of reactions can exercise an important effect in the combustion process thereby showing the reaction mechanisms of fuel oxidation coupled with the oxidation mechanisms of hydrogen and carbon monoxide [76]. This section will equally study the high-temperature oxidation mechanisms of methane as hydrocarbons, higher aliphatic hydrocarbons, and that of aromatic hydrocarbon oxidation at low to intermediate temperatures and the chemistry of pollutant formation. Besides, the physical states under normal conditions are used for the categorisation of fuels and such gaseous fuels include hydrogen (H_2), carbon monoxide (CO), and the light hydrocarbons (HC). Generally, liquid fuels are heavier hydrocarbons and alcohols, and solid fuels include carbon, coal, wood, metals, solid propellants, to mention but a few. Hydrocarbons constitute majority of the fuel supply among all materials since great amount of heat is released when hydrocarbons under complete oxidation. The stoichiometric oxidation of one $-CH_2-$ group in a typical aliphatic fuel molecule would release about 156 kcal amount of heat per mole of CH_2 consumed [95],



During combustion process of hydrocarbon, the mechanism of the oxidation of hydrocarbon is designed to introduce the nomenclature and the molecular structures of major hydrocarbon fuels and the intermediates [76].

Two grounds are needful for the oxidation of hydrogen and carbon monoxide. To start with, hydrogen and carbon monoxide are the main sources of fuels, and secondly, the oxidation mechanisms of hydrogen and carbon monoxide are the subunits of the oxidation mechanisms of the ones of hydrocarbons which consist of hydrogen and carbon. Thus, the oxidation mechanisms of hydrogen and carbon monoxide and that of hydrocarbons will be individually treated. Table 4.2 below explains the complete reaction mechanism for the oxidation of hydrogen and carbon monoxide, their reaction numbers, and their reaction rate constants. Also, a negative sign in the reaction number would mean a reverse reaction [95].

4.5 Oxidation mechanisms of hydrogen and carbon monoxide reactions

Usually, the reactions involving hydrogen and oxygen produces water vapour, and the pressure that is produced increases the reaction except it is slowed down by the water vapour. However, the vapour pressure of the water can be checked by temperature variation of the walls of the vessel. Also, it was found that the pressures of the reactions of hydrogen and of oxygen showed that the rate of the chemical reaction was affected by pressure variation [102].

The chemical reaction kinetics gives information concerning the rates and product distributions of elementary chemical reactions and the thermochemistry of unstable free radicals

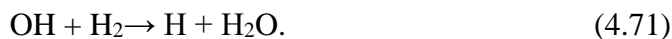
In the chemical runaway of a homogeneous mixture when subjected to wall deactivation, the chain mechanism of the hydrogen–oxygen system will show a Z-shaped pressure–temperature explosion-limit boundary conditions as illustrated in Figure 4.3 below, and this Figure below clearly explains the oxidation process which was carried out in a heated and pressurised chamber [95]. At high temperatures, explosion is always feasible and when the pressure increase is stable [103], [104].

When there is high temperatures during processes of hydrogen-oxygen mixtures, explosion is regularly practicable, but when there is moderate temperature with a consistent pressure increase, there will initially be non-explosive mixture and consequently the non-explosive mixture will suddenly become explosive [76]. The

situation of this kind which has been noticed both experimentally and computationally for hydrogen–oxygen mixtures in other systems for instance the ignition temperature of a uniform flow for a given pressure and residence time will entail the Z-shaped response [76]. However, there will be three feasible initiation reactions for the present H₂–O₂ system which include the dissociation of H₂, the dissociation of O₂, and the reaction between H₂ and O₂ because the starting reactions contain only the reactant species which are as follows:



Furthermore, the endothermicities of these three reactions which relate to the increase in enthalpy are 104, 118, and 55 kcal/mole respectively, because the activation energy of a dissociation reaction is approximately equal to its endothermicity reaction (4.68) and this is the most important initiation reaction under absolute all conditions [93]. Reaction (4.66) may also contribute to initiation, but only at high temperatures [76]. Reaction (4.67) is usually not preferred because oxygen has a larger dissociation energy than hydrogen because of the presence of double bond. Considering the production of H from either (4.66) or (4.68), the following chain reaction is initiated:



In this work, Table 4.2 below describes the kinetics of the hydrogen–oxygen reactions and its dissociation/recombination as well as the formation of H₂O₂ and HO₂ free radicals coupled with the oxidation of carbon monoxide [95].

Table 4.2: Oxidation of H₂---CO mixtures [8]

| No. | Reaction | B [cm, mol, s] | α | Ea (kcal/mol) |
|---|--|--|----------|-----------------|
| H ₂ ---O ₂ Chain Reactions | | | | |
| 1 | H + O ₂ ⇌ O + OH | 1.9 X 10 ¹⁴ | 0 | 16.44 |
| 2 | O + H ₂ ⇌ H + OH | 5.1 X 10 ⁰⁴ | 2.67 | 6.29 |
| 3 | OH + H ₂ ⇌ H + H ₂ O | 2.1 X 10 ⁰⁸ | 1.51 | 3.43 |
| 4 | O + H ₂ O ⇌ OH + OH | 3.0 X 10 ⁰⁶ | 2.02 | 13.40 |
| H ₂ - O ₂ Dissociation/ Recombination | | | | |
| 5 | H ₂ + M ⇌ H + H + M | 4.6 X 10 ¹⁹ | -1.40 | 104.38 |
| 6 | O + O + M ⇌ O ₂ + M | 6.2 X 10 ¹⁵ | -0.50 | 0 |
| 7 | O + H + M ⇌ OH + M | 4.7 X 10 ¹⁸ | -1.0 | 0 |
| 8 | H + OH + M ⇌ H ₂ O + M | 2.2 X 10 ²² | -2.0 | 0 |
| Formation and Consumption of HO ₂ | | | | |
| 9 | H + O ₂ + M ⇌ HO ₂ + M | 6.2 X 10 ¹⁹ | -1.42 | 0 |
| 10 | HO ₂ + H ⇌ H ₂ + O ₂ | 6.6 X 10 ¹³ | 0 | 2.13 |
| 11 | HO ₂ + H ⇌ OH + OH | 1.7 X 10 ¹⁴ | 0 | 0.87 |
| 12 | HO ₂ + O ⇌ OH + O ₂ | 1.7 X 10 ¹³ | 0 | -0.40 |
| 13 | HO ₂ + OH ⇌ H ₂ O + O ₂ | 1.9 X 10 ¹⁶ | -1.00 | 0 |
| Formation and Consumption of H ₂ O ₂ | | | | |
| 14 | HO ₂ + HO ₂ ⇌ H ₂ O ₂ + O ₂ | 4.2 X 10 ¹⁴ 1.3 X 10 ¹¹ | 0 | 11.98 -1.629 |
| Oxidation of H ₂ ---CO mixtures contd. | | | | |
| 15 | H ₂ O ₂ + M ⇌ OH + OH + M | 1.2 X 10 ¹⁷ | 0 | 45.50 |
| 16 | H ₂ O ₂ + H ⇌ H ₂ O + OH | 1.0 X 10 ¹³ | 0 | 3.59 |
| 17 | H ₂ O ₂ + H ⇌ H ₂ + HO ₂ | 4.8 X 10 ¹³ | 0 | 7.95 |
| 18 | H ₂ O ₂ + O ⇌ OH + HO ₂ | 9.5 X 10 ⁰⁶ | 2.0 | 3.97 |
| 19 | H ₂ O ₂ + OH ⇌ H ₂ O + HO ₂ | 1.0 X 10 ¹² 5.8 X 10 ¹⁴ | 0 | 0 9.56 |
| Oxidation of CO (Carbon monoxide) | | | | |
| 1 | CO + O + M ⇌ CO ₂ + M | 2.5 X 10 ¹³ | 0 | -4.54 |
| 2 | CO + O ₂ + M ⇌ CO ₂ + O | 2.5 X 10 ¹² | 0 | 47.69 |
| 3 | CO + OH + M ⇌ CO ₂ + H | 1.5 X 10 ⁰⁷ | 1.3 | -0.765 |
| 4 | CO + HO ₂ + M ⇌ CO ₂ + OH | 2.5 X 10 ¹³ | 0 | 22.95 |

4.5.1 Hydrogen and carbon monoxide oxidation reaction

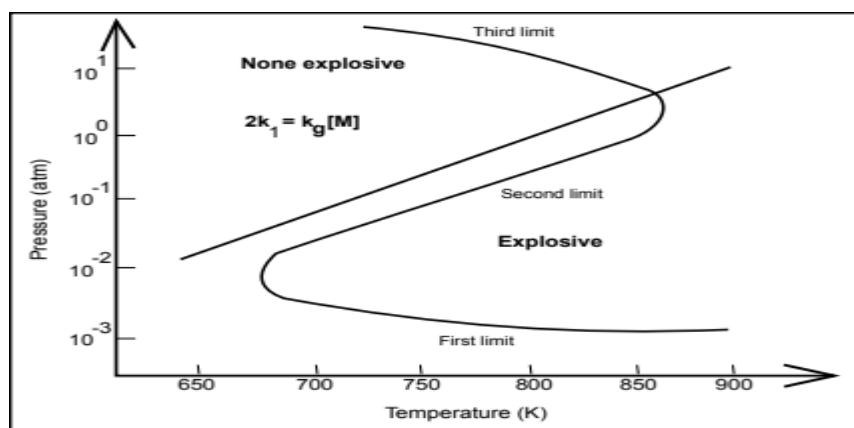


Figure 4.3: Explosion Limits of a Stoichiometric H₂---O₂ Mixture [95]

Because reactions (4.72) and (4.73) entail the collisions between two radical species whose concentrations are very low, the reverse reactions for the two reactions are not significant.

Based on the low concentration of the product species, H₂O, during the initiation stage of explosion, the reverse reaction of reaction (4.74) is equally not crucial. Moreover, explosion would not be visible even with the addition of some H or OH radicals for adequately low temperatures and pressures owing to the fact that the main chain-branching step reaction (4.72) is endothermic by 17 kcal/mole and thus would not be proper at low temperatures [76]. Also, these active species will rapidly diffuse to the chamber wall where they are destroyed at low pressures.

H, O, OH → chamber wall destruction

Collision will become more frequent and thus reactions are enhanced due to increase in pressure,

On crossing the first explosion limit, the rate of branching will become massively fast relative to either the rate of removal at the wall or the finite residence time, and consequently explosion will take place [93]. In addition, the three-body reaction occurs as pressure again increases owing to the dominant reaction between H and O₂.



Thus, as the chain sequence of reactions (4.69) – (4.71) becomes broken, reaction (4.72) will become an effective termination step of the radical chain process [93]. The competition between the growth of reactions (4.69) – (4.71) and destruction of reaction (4.72) of the H atom will determine the second explosion limit. In determining the p-T dependence of this limit, the rate equations for the H, O, and OH radicals will be written as

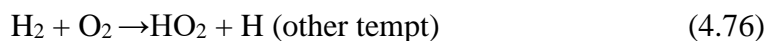
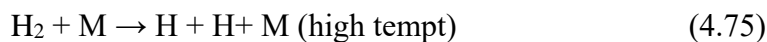
$$\frac{d[\text{H}]}{dt} = -k_1[\text{H}][\text{O}_2] + k_2[\text{O}][\text{H}_2] + k_3[\text{OH}][\text{H}_2] - k_9[\text{H}][\text{O}_2][\text{M}] \quad (4.73)$$

$$\frac{d[\text{O}]}{dt} = k_1[\text{H}][\text{O}_2] - k_2[\text{O}][\text{H}_2] \quad (4.74)$$

4.5.2 Detailed reaction mechanisms for $\text{H}_2 + \text{O}_2$ reaction

Chain
initiating

The initiation reactions are:



The chain reaction steps involving O, H and OH radicals are:

Chain
Branching



The chain terminating steps involving O, H, and OH radicals are the three body recombination reactions [93].

Chain
Terminating



$\text{A}^* \rightarrow \text{Products}$

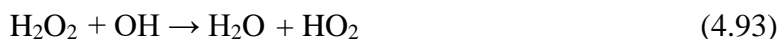
M = third body = any molecules

In completing the detailed reaction mechanism, the following chemical reactions involving hydroperoxyl radical (HO_2), and hydrogen peroxide (H_2O_2) will take place [93]:



Then, the HO_2 will eventually turns active, and the following reactions occur:





For example, in heterogenous reaction involving hydrogen and oxygen molecules, when the pressure is dominant/very high, explosion will certainly take place owing to free radicals of molecules/atoms with unpaired electrons [93].

This can further be explained from the chemical processes below:

- (i) heterogeneous reaction:



- (ii) chain initiating



- (iii) chain branching and propagating



- (iv) chain terminating



- (v) chain branching



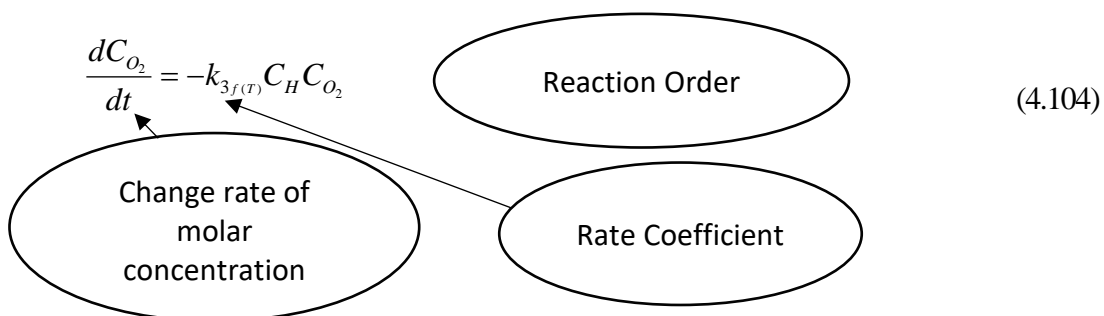
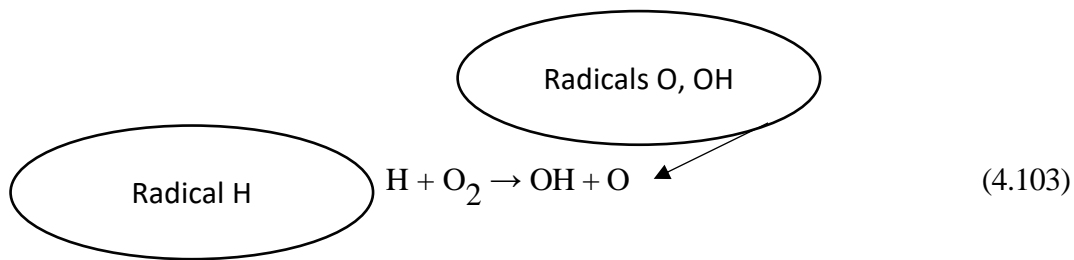
4.5.3 Calculations of reaction rates

$$\frac{dC}{dt} \propto kC^n \quad (4.102)$$

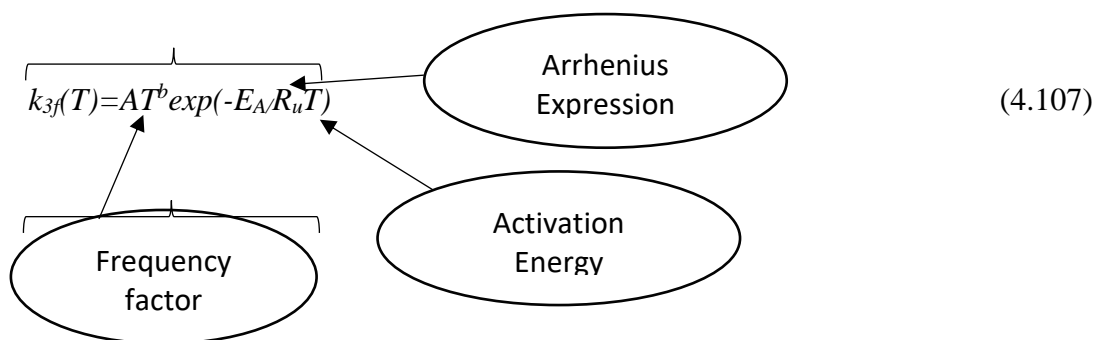
All units in mole/m³

(a) Reaction rates for unimolecular reactions

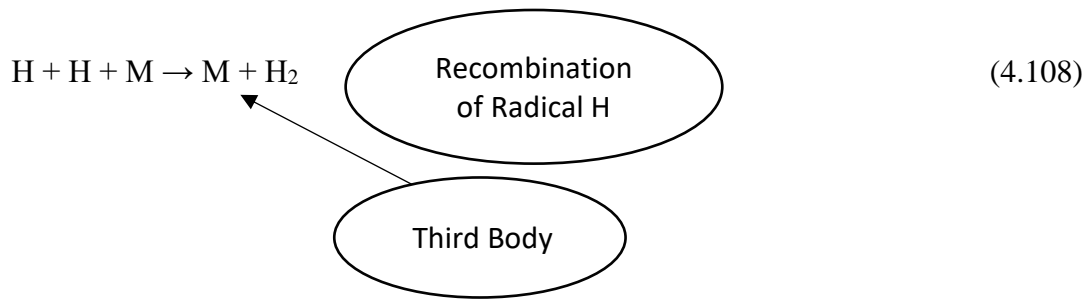
Law of Mass Action



(b) Reaction rates for bimolecular reactions



(c) Termolecular reactions



$$\frac{dC_{\text{H}}}{dt} = -k_{\text{ter(T)}} C_{\text{M}} C_{\text{H}}^2 \quad (4.109)$$

M is a third body representing any molecules carrying away produced energy.

Besides, termolecular reactions are more unique than bimolecular reactions and unimolecular reactions at high pressures [93]. Reaction mechanisms in chemical kinetics can be subdivided into two: (a) thermochemical data for chemical species which are grouped into a systematic form which explains the combustion of the fuel, and (b) the coefficients of species' reaction-rate for the chemical reactions [103]. The factors affecting the rates of chemical reactions include concentrations of reactants, temperature at which reaction occurs, presence of a catalyst, and the surface area of solid or liquid reactants. The Arrhenius reaction rate, k , is modified thus:

$$k = AT^n \exp(-E_a/RT) \quad (4.110)$$

where, coefficients A , n , and E_a are individual reaction mechanisms; T represents temperature of the burning system, and R for universal gas constant. However, researchers have developed detailed chemical kinetic reaction mechanisms for sensitive reaction rates of hydrocarbon combustion with smallest molecules such as H_2 , O_2 , CO , and CO_2 [103]. Consequently, an increase in the molecular size of fuels in a kinetic model will increase the numbers of chemical species and elementary reactions. Also, reaction mechanisms produced for fuels showed that gasoline, diesel and biofuels had 16 to 18 carbon atoms comprising primary reference fuels, n -alkane, and methyl stearate [104]. Also, a model for the oxidation of hydrogen would contain 10 chemical species and 30 elementary reactions: and for methane, 30 species and 300 reactions, whereas, for n -cetane, 1,200 species and 7,000 chemical reactions [103].

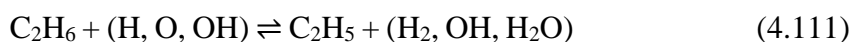
4.6 Oxidation of hydrocarbons

The relationship between the oxidation of hydrocarbons and this research topic is that the oxidation of hydrocarbon is a chemical reaction in which a hydrocarbon reacts with oxygen to produce carbon dioxide, water and heat during a combustion reaction. The combustion of propane is explained by a detailed chemical kinetic reaction mechanism, and the mechanism comprises 15 chemical reacting species and 24 chemical reactions [93]. The ignition and combustion results obtained from the study using shock tube are necessary in evaluating the reaction mechanism. However, the chemical kinetic behaviour showed by the mechanism for stoichiometric mixtures using numerical simulation of the shock tube experiments is in order with the experimental results obtained for the whole investigated temperature range. Studies conducted showed that the reaction mechanism of hydrocarbon reactions which are involved in the formation of the HO₂ radical and the H₂O₂ molecule are so vital in the chemical reaction mechanism. Also, the nonlinear behaviour of ignition delay time noticed with the decreasing temperature can be explained in terms of the increased importance of the HO₂ and H₂O₂ reactions at the lower temperatures [93].

Petroleum gases (hydrocarbons) are obtained as petroleum products during fluid catalytic cracking and thermal heating processing of crude oil and natural gas. Petroleum gases can undergo some specific chemical reactions such as combustion reactions and halogenation. Among these hydrocarbons, propane is highly detected in the air and the possible pathway through which the general populace inhale propane is unprotected against it and it is emitted from natural gas, barbeque grills and automobile emissions [93]. Propane is one of the lightest hydrocarbons in nature and that makes it one of the cleanest burning fossil fuels and it is non-toxic. Its molecular formula is C₃H₈. Besides, it is one of the hydrocarbon components of raw natural gas, a fossil fuel and it is removed from natural gas before it is sold to consumers as fuel.

The oxidation mechanisms of the hydrocarbons, such as ethane (C₂H₆), ethylene (C₂H₄), and acetylene (C₂H₂) will be explained in this chapter. During the combustion of methane, ethane is formed as a main intermediate, and it is also second main hydrocarbon of the natural gas. Other fuels include ethylene and acetylene, and they are the important intermediates of the oxidation of ethane and higher hydrocarbons. Therefore, the oxidation mechanisms of the first three hydrocarbons in high temperature flames will be explained [93]. Ethyl radical is produced by the oxidation

of ethane in flames through the removal of hydrogen from ethane, C_2H_6 by hydrogen (H), oxygen (O), and hydroxyl radical (OH), [103].



The free radical, ethyl radical C_2H_5 is very unstable, and it produces ethylene and a hydrogen atom, H when it reacts quickly with hydrogen (H) and oxygen, (O_2).



or the free radical, ethyl radical C_2H_5 will react with oxygen forming acetaldehyde (CH_3CHO),



Furthermore, acetaldehyde will thus react with hydrogen (H), oxygen (O), and hydroxyl radical (OH) thereby producing the ethanoyl free radical (CH_3CO), followed by its unimolecular decomposition which will eventually form methyl radical (CH_3) and carbon monoxide (CO) [103].



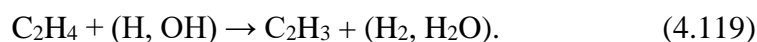
Also, the ethyl radical can react with the oxygen atom, O to produce methyl (CH_3) and methanal (CH_2O).



Besides, the oxidation mechanisms of ethylene and alkanes are not the same because the oxidation mechanism of ethylene does not need the removal of hydrogen in the reaction before it can undergo oxidation [93]. Usually, the double bond in ethylene can easily be attacked directly by oxygen atom and hydroxyl radical, hence, when ethylene reacts with the oxygen atom (O), it will form methyl radical (CH_3) and methanoyl radical (HCO) because of the easy breakage of the double bond.



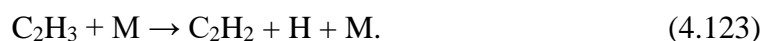
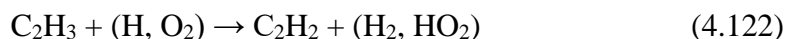
Also, the reaction (4.118) will yield a secondary chain-branching step that can greatly increase the oxidation process based on the free radicals formed as products in the above reaction. In addition, the vinyl radical (C_2H_3) is formed when H and OH are the main source of ethylene consumption through the removal of H atom during fuel rich mixtures [103].



The vinyl radical (C_2H_3) is very reactive just as that of ethyl radical, and it simply reacts with oxygen (O_2) thereby forming CH_2O and HCO , and CH_2CHO and O .



In addition, the vinyl radicals can undergo these reactions which can produce acetylene,



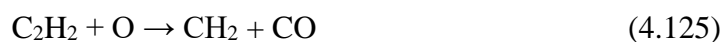
During the fuel-rich combustion of methane, acetylene is a main intermediate and also, it is an important product of incomplete, fuel-rich combustion which is the thermodynamics of a fuel molecule to be converted to acetylene [103]. An acetylene can be converted from a $\text{---CH}_2\text{---}$ grouping in an aliphatic hydrocarbon through,



Typically, the process is purely endothermic by about 32 kcal/mol at 1,600 K and the acetylene is made easy by the change in entropy of the process, and the hydrogen released will produce a substantial amount of entropy which at the same temperature evolves 30.8 cal/mol-K [103]. Acetylene, with an enthalpy of formation of 54 kcal/mol

at the standard state is a highly energetic and dangerous fuel, and in the absence of oxygen will undergo spontaneous polymerisation [93].

When acetylene is being used as a fuel, it stands for a compound with the greatest energy density among the readily available fuels with an adiabatic flame temperature which is basically higher than those of other fuels at the same stoichiometry [93]. Furthermore, the reaction between acetylene and oxygen atom, O is very fast, and acetylene will not involve the removal of hydrogen, H to start the process of oxidation



The methylene radical is easily formed when the ketenyl radical, HCCO is very active, thus reacting easily with the hydrogen, H.



In fuel-rich mixtures, acetylene may also combine with the H atom to produce the vinyl radical. The vinyl radical can be oxidised very speedily through reactions (4.120) and (4.121), if oxygen is available [104]. Moreover, the reaction for ethane, ethylene and acetylene combustion has gone to the stage that all the species such as CH₃, CH₂S, CH₂O, HCO, and CO can take part in the oxidation mechanism of methane, and thus CH₄---O₂ chemistry can explain it [103].

Chapter 5 Chemical Reaction Mechanisms of Explosions

5.1 Introduction

This chapter will explore the influences and effects of chemical reaction mechanisms to generations, propagations, and transitions of explosion waves. To this end, two premixed combustible mixtures: - hydrogen-oxygen and propane-oxygen are selected and filled into two-dimensional tube domains, then the mixtures are ignited. The detailed chemical and physical processes are numerically and accurately simulated. The results are presented and investigated in this chapter. However, this chapter will carefully examine the effects of kinetics on the combustion reactions of hydrogen-oxygen and propane filled in a tube. The layout of this chapter is structured analytically to cover the sections: Section 1 entails the effects of kinetics on H₂-O₂ combustion reactions for case studies 2, 3, 4, and 5; section 2 contains the effects of kinetics on H₂-O₂ combustion reactions for case studies a, b, c, d, and e; and section 3 covers the effects of kinetics on propane-oxygen combustion reactions for case studies 20, 21, 30, 31, and 40. Moreover, section 1 comprises 4 case studies; section 2 consists of 5 case studies; and section 3 is made of 5 case studies, thereby having a total of 14 case studies, but this chapter shall discuss each section separately. This chapter will critically treat the influences and effects of kinetics on explosion of hydrogen-oxygen and propane -oxygen reactions using numerical simulation method while also looking at other diverse factors. Besides, the different factors that will be considered are greatly useful for designing process safety programmes and fire investigation not only to protect the assets of an organisation, but to ensure the safe evacuation of all the personnel present.

5.2 Setup of simulations

Configuration of the case studies and computational setup are detailed below in this section 1. The explosions to be simulated take place in a domain of tube. Premixed mixture of fuel and oxidant is filled into tube. A hot gas with very small area is located at an end or inside of tube as ignition source. Using external energy, the source initialises the reactions of the combustible mixture which will drive various chemical reaction waves within the tube.

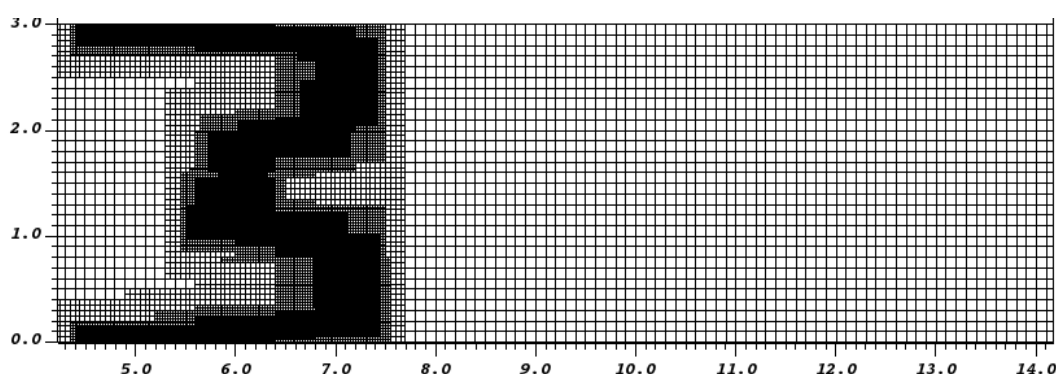
Some similar phenomena can be observed in a so-called shock tube. The shock tube can be rectangular or circular in cross-section, usually constructed of metal, in which

a gas at low pressure and a gas at high pressure are separated using some form of diaphragm. Shock tube ranges in diameter from 0.6m to 2m and in length from 3m to 15m. It has peak dynamic pressures of 7MPa to 200MPa and has durations of a few hundred microseconds to several milliseconds. A diaphragm consists of aluminium foil lying between shock tube pipe segments. In prearranged conditions, the diaphragm can suddenly burst open thereby producing a wave propagating through the low-pressure section. Eventually, the formed shock wave can cause an increase in temperature and pressure of the test gas which leads to a fluid flow in the direction of the shock wave. Moreover, the low-pressure gas called the driven gas, is governed by the shock wave, and the high-pressure gas is referred to as the driver gas. Generally, for safety purposes, the driver gas has a low molecular weight e.g. helium or hydrogen and high speed of sound but may be slightly diluted to ‘tailor’ interface conditions across the shock [39]. The fundamental difference between the shock tube and chemical reaction tube is in the driven force: shock tube is driven by the high pressure gas while chemical reaction tube by the combustion reactions.

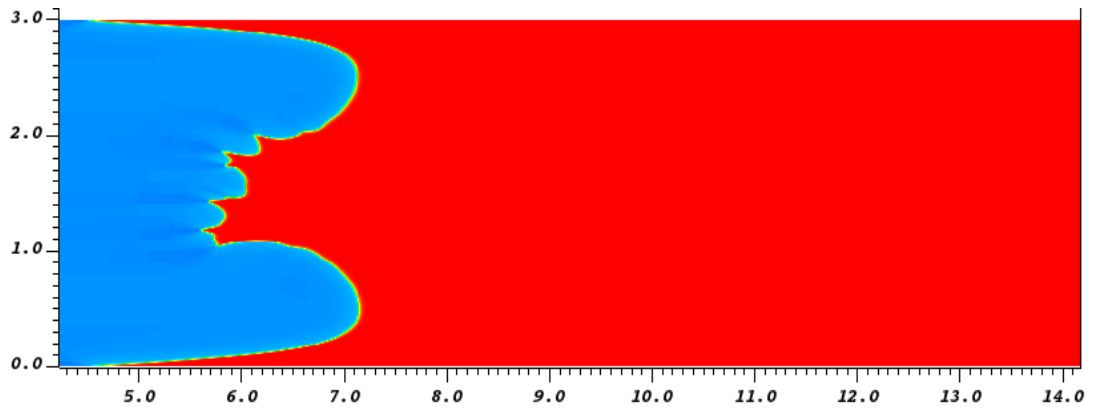
5.2.1 Domain mesh

The initial mesh consists of uniformly squared elements of 1mm in length. The initial elements will be adaptively refined up to 32 times smaller as the solution needs. For illustration, Figures below show an example of computational mesh that is 16 times refined and coarsens and refines varying in the computational domain with the requirement by solution.

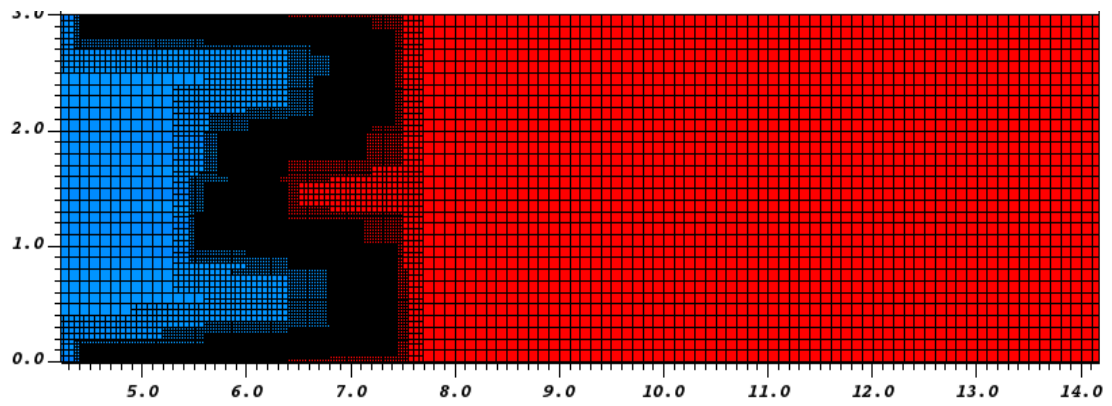
For Figures 5.1, 5.2 and 5.3 below, the length unit on the vertical and horizontal of each Figure is in centimetre (cm).



(a) Computational mesh at time t_0

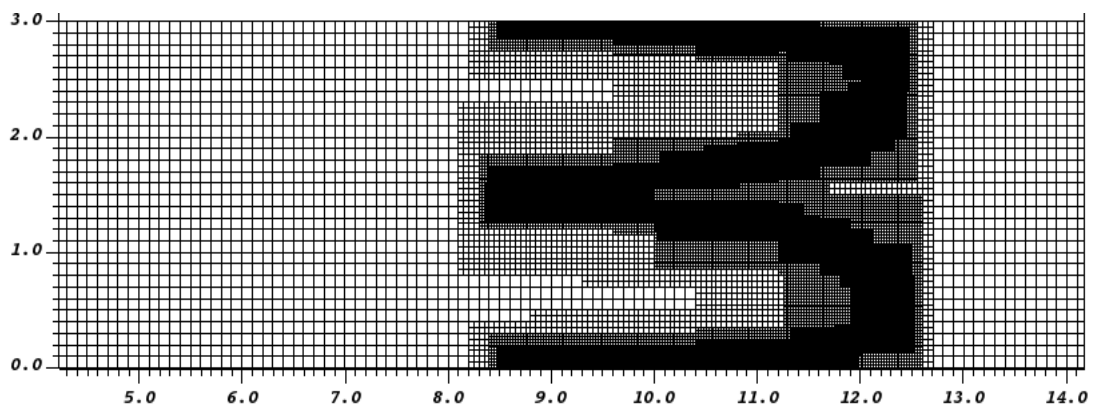


(b) Density of mixture at time t_0

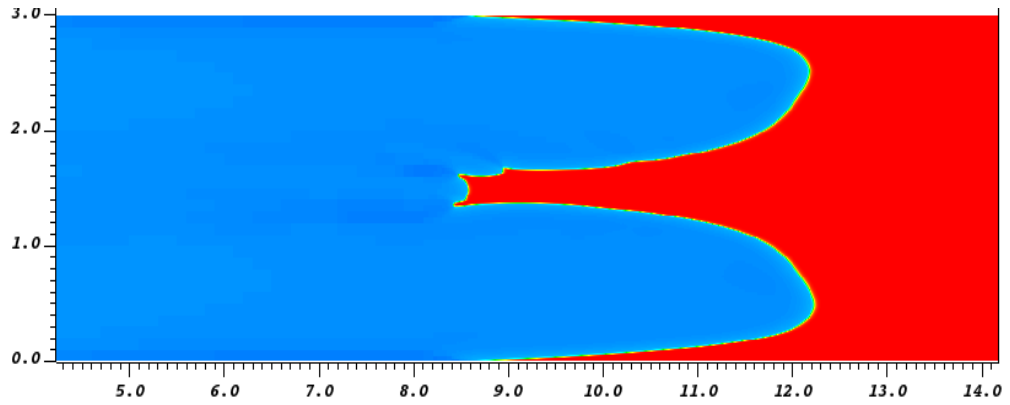


(c) Coupled mesh and its simulated results at time t_0

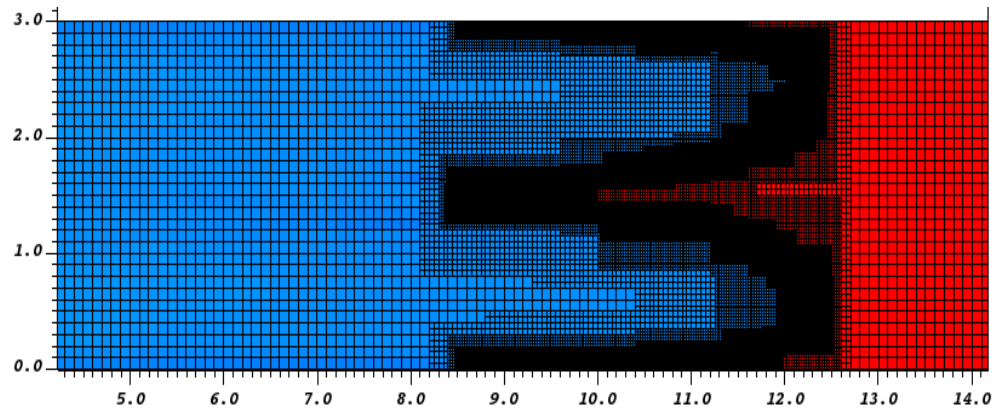
Figure 5.1 Computational mesh and its simulated results at a time instant.



(a) Computational mesh at time $t_0 + \Delta t$



(b) Density of mixture at time $t_0 + \Delta t$



(c) Coupled mesh and its simulated results at time $t_0 + \Delta t$

Figure 5.2 Computational mesh and its simulated results at another time instant.

Figure 5.3 is an enlarged part of the mesh showed in Figure 5.2 (a). One can see that there are 4 layer refinements, which makes the cell size from 1mm to 0.0625mm. From the definition of CFL number in chapter 3, the finer the mesh, the smaller the time step, and so the more the computational time. As we employ mesh adaptive technology, the very fine mesh is always limited to a small area and very necessary to ensure the high accuracy of the computations. As a result, the computational time significantly reduces that enable us to do direct numerical simulation of the combustions.

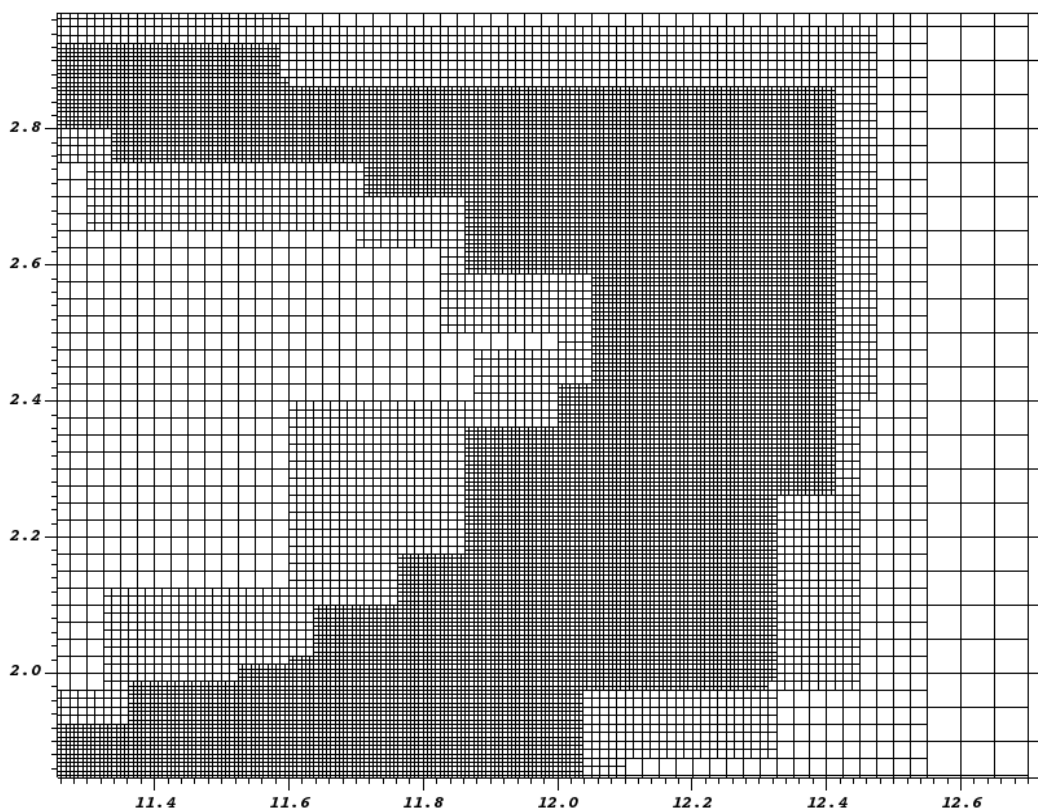


Figure 5.3 Visualisation of a part mesh enlarged and refined in Figure 5.2

5.2.2 Initial conditions and ignition sources

Nine cases for hydrogen–oxygen mixtures and five cases for propane–oxygen mixtures respectively were studied. The initial conditions reflect situations of the ignitions for each case and are shown in Tables 5.1, 5.2, and 5.3, and other considerations for this simulation work include the initial state of the elements, the reacting species and the reactions shown in Tables 5.4, 5.5 and 5.6 respectively.

Table 5.1: Initial conditions of kinetics for 4 case studies of H₂-O₂ combustion

| Case Studies | Temperature (K) | | Concentration (%) | | | | Pressure (Pa) | |
|--------------|-----------------|--------------|-------------------|----------------|----------------|----------------|---------------------|---------------------|
| | Left (Hot) | Right (Cool) | Left (Hot) | | Right (Cool) | | Left | Right |
| | | | H ₂ | O ₂ | H ₂ | O ₂ | | |
| 2 | 3,000 | 300 | 0.0 | 0.0 | 0.15 | 0.20 | 2 x 10 ⁶ | 1 x 10 ⁵ |
| 3 | 3,000 | 300 | 0.0 | 0.0 | 0.15 | 0.20 | 1 x 10 ⁶ | 1 x 10 ⁵ |
| 4 | 3,000 | 300 | 0.0 | 0.0 | 0.15 | 0.20 | 9 x 10 ⁵ | 1 x 10 ⁵ |
| 5 | 2,800 | 300 | 0.0 | 0.0 | 0.68 | 0.17 | 1 x 10 ⁶ | 1 x 10 ⁵ |

Table 5.2: Initial conditions of kinetics for 5 case studies of H₂-O₂ combustion

| Case Studies | Temperature (K) | | Concentration (%) | | | | Pressure (Pa) | |
|--------------|-----------------|--------------|-------------------|----------------|----------------|----------------|---------------------|---------------------|
| | Left (Hot) | Right (Cool) | Left (Hot) | | Right (Cool) | | Left | Right |
| | | | H ₂ | O ₂ | H ₂ | O ₂ | | |
| a | 3,000 | 300 | 0.0 | 0.0 | 0.15 | 0.20 | 1 x 10 ⁴ | 1 x 10 ⁵ |
| b | 3,000 | 300 | 0.0 | 0.0 | 0.15 | 0.20 | 3 x 10 ⁴ | 1 x 10 ⁵ |
| c | 3,000 | 300 | 0.0 | 0.0 | 0.15 | 0.20 | 5 x 10 ⁴ | 1 x 10 ⁵ |
| d | 2,800 | 300 | 0.0 | 0.0 | 0.68 | 0.17 | 7 x 10 ⁴ | 1 x 10 ⁵ |
| e | 2,800 | 300 | 0.0 | 0.0 | 0.68 | 0.17 | 9 x 10 ⁴ | 1 x 10 ⁵ |

Table 5.3: Initial conditions of kinetics for 5 case studies of propane combustion

| Case Studies | Temperature (K) | | Concentration (%) | | | | Pressure (Pa) | |
|--------------|-----------------|--------------|-------------------|----------------|----------------|----------------|---------------------|---------------------|
| | Left (Hot) | Right (Cool) | Left (Hot) | | Right (Cool) | | Left | Right |
| | | | H ₂ | O ₂ | H ₂ | O ₂ | | |
| 20 | 3,000 | 300 | 0.0 | 0.0 | 0.15 | 0.20 | 1 x 10 ⁵ | 1 x 10 ⁵ |
| 21 | 3,000 | 300 | 0.0 | 0.0 | 0.15 | 0.20 | 1 x 10 ⁵ | 1 x 10 ⁵ |
| 30 | 3,000 | 300 | 0.0 | 0.0 | 0.15 | 0.20 | 2 x 10 ⁵ | 1 x 10 ⁵ |
| 31 | 2,800 | 300 | 0.0 | 0.0 | 0.68 | 0.17 | 2 x 10 ⁵ | 1 x 10 ⁵ |
| 40 | 2,800 | 300 | 0.0 | 0.0 | 0.68 | 0.17 | 3 x 10 ⁵ | 1 x 10 ⁵ |

On Tables 5.1, 5.2, 5.3 above the hot side (left side) is of very high temperature and pressure which is the ignition source while the cool side (right side) contains the premixed combustion gas mixtures of hydrogen-oxygen and propane-oxygen for Tables 5.1, 5.2 and 5.3 respectively. The cool side keeps constant the temperature and pressure, but the concentrations of chemical species comprising the combustible gas mixture are varied with different case studies. Additionally, on the left side (hot side), the temperature is very high, and the concentrations of H₂ and O₂ are not actually zero, therefore, no fuel (H₂), no oxygen (O₂) and on the left side, no combustion mixture, but the right side has premixed combustion mixture. The results were visualised using VISIT. The programme is a general data processing programme and can be executed in parallel and therefore particularly suitable to deal with a large database.

Table 5.4: Elements Considered for simulation

| Elements Considered | Symbol |
|---------------------|--------|
| Hydrogen | H |
| Oxygen | O |
| Nitrogen | N |
| Carbon | C |
| Argon | Ar |
| Helium | He |

Table 5.4 in section 5.2.2 showed that in the first stage of this work, hydrogen, and oxygen as well as nitrogen and argon were simulated, but in the second stage, carbon, hydrogen and helium (a noble gas) will be added which will constitute the petroleum gas.

Table 5.5: Reacting species considered

| S/No. | Reacting Species | Temperature | | Elements Count | | | | | |
|-------|-------------------------------|-------------|------|----------------|---|---|---|----|----|
| | | Low | High | H | O | N | C | Ar | He |
| 1 | H ₂ | 300 | 5000 | 2 | 0 | 0 | 0 | 0 | 0 |
| 2 | O ₂ | 300 | 5000 | 0 | 2 | 0 | 0 | 0 | 0 |
| 3 | H ₂ O | 300 | 5000 | 2 | 1 | 0 | 0 | 0 | 0 |
| 4 | H | 300 | 5000 | 1 | 0 | 0 | 0 | 0 | 0 |
| 5 | O | 300 | 5000 | 0 | 1 | 0 | 0 | 0 | 0 |
| 6 | OH | 200 | 6000 | 1 | 1 | 0 | 0 | 0 | 0 |
| 7 | HO ₂ | 200 | 3500 | 1 | 2 | 0 | 0 | 0 | 0 |
| 8 | H ₂ O ₂ | 300 | 5000 | 2 | 2 | 0 | 0 | 0 | 0 |
| 9 | Ar | 300 | 5000 | 0 | 0 | 0 | 0 | 1 | 0 |
| 10 | N ₂ | 300 | 5000 | 0 | 0 | 2 | 0 | 0 | 0 |
| 11 | He | 300 | 5000 | 0 | 0 | 0 | 0 | 0 | 1 |
| 12 | CO | 300 | 5000 | 0 | 1 | 0 | 1 | 0 | 0 |
| 13 | CO ₂ | 300 | 5000 | 0 | 2 | 0 | 1 | 0 | 0 |

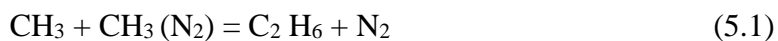
On Table 5.5, the hot element will ignite the cool element during chemical reaction, the left side which is the hot side with high temperature is the ignition source and it is to ignite the right side which is the cool side that has a lower temperature.

Table 5.6: Reactions considered ($K = AT^b e^{-(E_a/RT)}$)

| S/No | Reactions | E _a (J/mol) | A | b |
|------|--|------------------------|-------------------------|-------|
| 1 | H + O ₂ = O + OH | 16,599 | 3.55 x 10 ¹⁵ | - 0.4 |
| 2 | O + H ₂ = H + OH | 6,290 | 5.08 x 10 ⁴ | 2.7 |
| 3 | H ₂ + OH = H ₂ O + H | 3,430 | 2.16 x 10 ⁸ | 1.5 |
| 4 | O + H ₂ O = OH + OH | 13,400 | 2.97 x 10 ⁶ | 2.0 |
| 5 | H ₂ + M = H + H + M | 104,380 | 4.58 x 10 ¹⁹ | - 1.4 |
| | H ₂ | Enhanced | 2.500 | |
| | H ₂ O | Enhanced | 1.200 x 10 ¹ | |
| | CO | Enhanced | 1.900 | |
| | CO ₂ | Enhanced | 3.800 | |
| | Ar | Enhanced | 0.00 | |
| | He | Enhanced | 0.00 | |
| 6 | H ₂ + Ar = H + H + Ar | 104,380 | 5.84 x 10 ¹⁸ | - 1.1 |
| 7 | H ₂ + He = H + H + He | 104,380 | 5.84 x 10 ¹⁸ | - 1.1 |
| 8 | O + O + M = O ₂ + M | 0.0 | 6.16 X 10 ¹⁵ | - 0.5 |
| | H ₂ | Enhanced | 2.500 | |
| | H ₂ O | Enhanced | 1.200 x 10 ¹ | |
| | Ar | Enhanced | 0.000 | |
| | He | Enhanced | 0.000 | |
| | CO | Enhanced | 1.900 | |
| | CO ₂ | Enhanced | 3.800 | |
| 9 | O + O + Ar = O ₂ + Ar | 1,788 | 1.89 x 10 ¹³ | 0.0 |
| 10 | O + O + He = O ₂ + He | 1,788 | 1.89 x 10 ¹³ | 0.0 |
| 11 | O + H + M = OH + M | 0.0 | 4.71 x 10 ¹⁸ | - 1.0 |

| Table 5.6: Reactions considered contd. | | | | |
|--|--|----------|--------------------------|-------|
| | H ₂ | Enhanced | 2,500 | |
| | H ₂ O | Enhanced | 1,200 x 10 ¹ | |
| | Ar | Enhanced | 7,5000 x 10 ¹ | |
| | He | Enhanced | 7,5000 x 10 ¹ | |
| | CO | Enhanced | 1,900 | |
| | CO ₂ | Enhanced | 3,800 | |
| 12 | H + OH + M = H ₂ O + M | 0.0 | 3,800 x 10 ²² | - 2.0 |
| | | Enhanced | 2,500 | |
| | | Enhanced | 1,200 x 10 ¹ | |
| | | Enhanced | 3,800 x 10 ¹ | |
| | | Enhanced | 3,800 x 10 ¹ | |
| | | Enhanced | 1,900 | |
| | | Enhanced | 3,800 | |
| 13 | H + O ₂ (+ M) = HO ₂ (+M) | 0.0 | 1.48 x 10 ¹² | 0.6 |
| | H ₂ | Enhanced | 2,000 | |
| | H ₂ O | Enhanced | 1,100 x 10 ¹ | |
| | O ₂ | Enhanced | 7.80 x 10 ⁻¹ | |
| | CO | Enhanced | 1,900 | |
| | CO ₂ | Enhanced | 3,800 | |
| | | Enhanced | | |
| 14 | HO ₂ + H = H ₂ + O ₂ | 823.0 | 1.66 x 10 ¹³ | 0.0 |
| 15 | HO ₂ + H = OH + OH | 295.0 | 7.08 x 10 ¹³ | 0.0 |
| 16 | HO ₂ + O = O ₂ + OH | 0.0 | 3.25 x 10 ¹³ | 0.0 |
| 17 | HO ₂ + OH = H ₂ O + O ₂ | 497.0 | 2.89 x 10 ¹³ | 0.0 |
| 18 | HO ₂ + HO ₂ = H ₂ O ₂ + O ₂ | 11,982 | 4.20 x 10 ¹⁴ | 0.0 |
| 19 | HO ₂ + HO ₂ = H ₂ O ₂ + O ₂ | 1,629.3 | 1.30 x 10 ¹¹ | 0.0 |
| 20 | H ₂ O ₂ + (+M) = OH + OH (+M) | 48,430 | 2.95 x 10 ¹⁴ | 0.0 |
| | H ₂ | Enhanced | 2,500 | |
| | H ₂ O | Enhanced | 1,20 x 10 ¹ | |
| | CO | Enhanced | 1,900 | |
| | CO ₂ | Enhanced | 3,800 | |
| | Ar | Enhanced | 6.40 x 10 ⁻¹ | |
| | He | Enhanced | 6.40 x 10 ⁻¹ | |
| 21 | H ₂ O ₂ + H = H ₂ O + OH | 3,970 | 2.41 x 10 ¹³ | 0.0 |
| 22 | H ₂ O ₂ + H + HO ₂ + H ₂ | 7,950 | 4.82 x 10 ¹³ | 0.0 |
| 23 | H ₂ O ₂ + O = OH + HO ₂ | 3,970 | 9.55 x 10 ⁶ | 0.0 |
| 24 | H ₂ O ₂ + OH + HO ₂ + H ₂ O | 0.0 | 1.00 x 10 ²² | 0.0 |
| 25 | H ₂ O ₂ + OH = HO ₂ + H ₂ O | 9,557 | 5.80 x 10 ¹⁴ | 0.0 |

Generally, a chemical reaction has 1 or 2 species as reactant and produces 1 or 2 products. When reactions are in fall-off regions, however, the pressure effect in the kinetics is necessarily considered and third-party species are involved which attack other molecules, not participating in the reaction and only exchanging the momentum. The third party species can be all the species in the mixture. While the reaction is enhanced, the third party species are not all the species, but particularly specified, e.g. noble gases like He and Ar.



Only N₂ is the enhanced concentration.

5.3 Comparison of numerical simulation with experimental results

In this section, we compared the numerical results and experimental observations and measurements. Typical numerical simulations involve in ignition, flame development and deflagration-to-detonation transition. Therefore, we compare the results from three aspects.

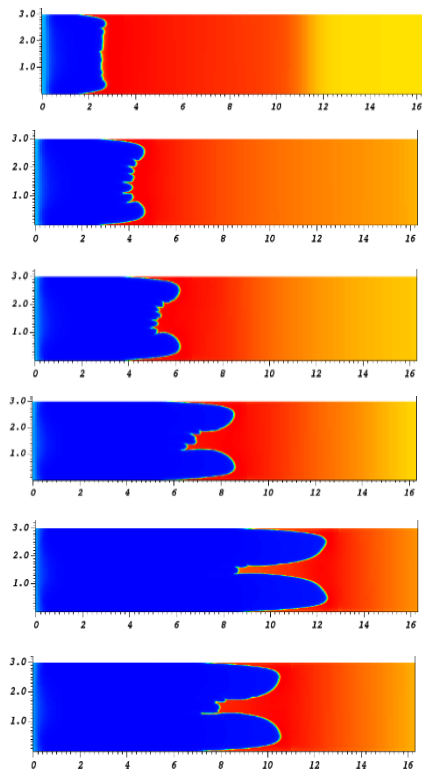
The induction time is a characteristic time scale for ignition of a flame. It reflects the nature of chemical reaction kinetics. Through the comparison, the kinetics used in this project would be verified. First of all, therefore, let us compare the induction time of numerical simulation and experimental measurement, which is showed in Table 5.7.

Table 5.7: Comparison of induction time for numerical simulations and Experimental studies [39].

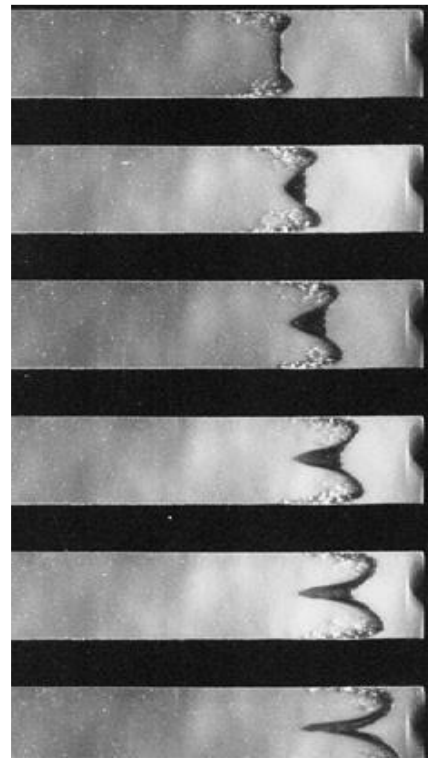
| Case Studies | Factors | Numerical (second) | Experimental (second) |
|--------------|--|--------------------|-----------------------|
| 1 | 20% CH ₄ $p = 0.975\text{Mpa}$ | 0.0020 | 0.0030 |
| 2 | 100% H ₂ $p = 0.975\text{Mpa}$ | 0.0037 | 0.0042 |
| 3 | 60% CH ₄ $p = 0.99\text{Mpa}$ | 0.0023 | 0.0030 |
| 4 | 40% CH ₄ $p = 0.99\text{Mpa}$ | 0.0025 | 0.0030 |

The ignition temperature in Table 5.7 is same and 300K. From the comparison, one sees that the induction time produced by numerical simulations is a little bit shorter over the experimental. It may be because the numerical errors exist and make both results different, however, such difference is minor

After ignition, the flame will develop and accelerate generally. Liberman et al [39] experimentally investigated such flame developments. Therefore, we compare the numerical results with their experimental observations. Figure 5.4 below illustrates the visualisation of simulated mixture density and pictures from the experiments. It is found that the numerical results produce the reaction zones and flow patterns consistent with those observed in the experiments



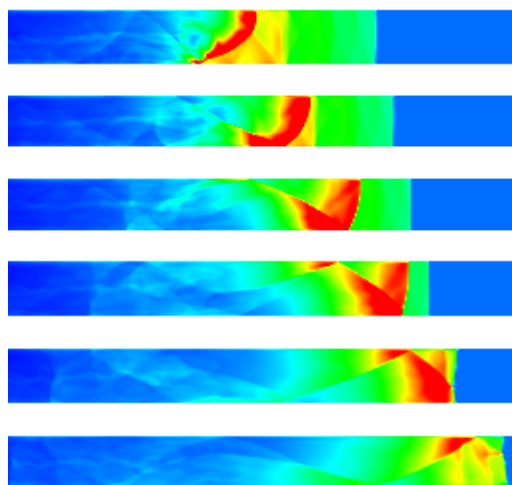
(a) Numerical results of this work



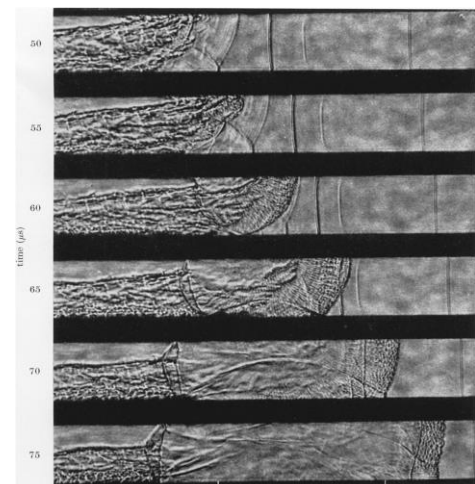
(b) Experimental results from Liberman et al

Figure 5.4 Comparison of the numerical results with the experiments done by Liberman et al [39].

The famous experiments of Liberman and Kuznetsov recorded deflagration-to-detonation transitions with their pictures. This provides possibility for comparison of experimental observations and numerical investigations. A set of comparisons of numerical and experimental results are showed in Figure 5.5 below. One can see that both are consistent in structures.



(a) Computational results of this work



(b) Experimental results from Kuznetsov et al [40].

Figure 5.5 Comparison of numerical solutions and experiments of Kuznetsov et al [40].

5.4 Effects of kinetics of H₂-O₂ combustion reactions

(a) Summary of Results of 4 case studies by kinetics on H₂-O₂ combustion

Table 5.8: Effects and influences of kinetics on H₂-O₂ combustion processes (see Appendix 1)

| Case Studies | Time range (sec) x 10 ⁻⁴ | Temperature range (K) | Fuel Conc, range (%) x 10 ⁴ | Flame Speed (m/s) | | | |
|--------------|-------------------------------------|-----------------------|--|-------------------|----|-----|------|
| | | | | LF | FD | DDT | DD |
| Reactions: 2 | 0.00 – 0.5026 | 2800 – 3454 | 0.00 – 101.4 | 0 | - | - | 2850 |
| 3 | 0.00 – 0.7716 | 2800 – 3502 | 0.00 – 106.8 | 0 | - | - | 2860 |
| 4 | 0.00 – 0.67 | 2800 – 2700 | 0.00 – 123.8 | 0 | - | - | 1350 |
| 5 | 0.00 – 0.81 | 2800 – 3752 | 0.00 – 103.0 | 0 | - | - | 2880 |

From Table 5.8 above, the influences and effects of kinetics on explosion due to H₂-O₂ combustion reaction processes were studied and it was observed that as the concentration of the chemical species increases, the temperature also increases, and this will cause an increase to the flame velocity and detonation results which will consequently lead to explosion. However, no DDT and FD were formed for case studies 2, 3, 4, and 5 and this was because it is an open-end tube and there is no limited gas expansion, and no artificial obstacle, and therefore, deflagration-to-detonation transition (DDT) and fast deflagration (FD) were not formed, but the ignition process moves straight to detonation, thus forming a single explosion.

(b) Effects and influences of kinetics on H₂-O₂ combustion processes

1) Case study R2

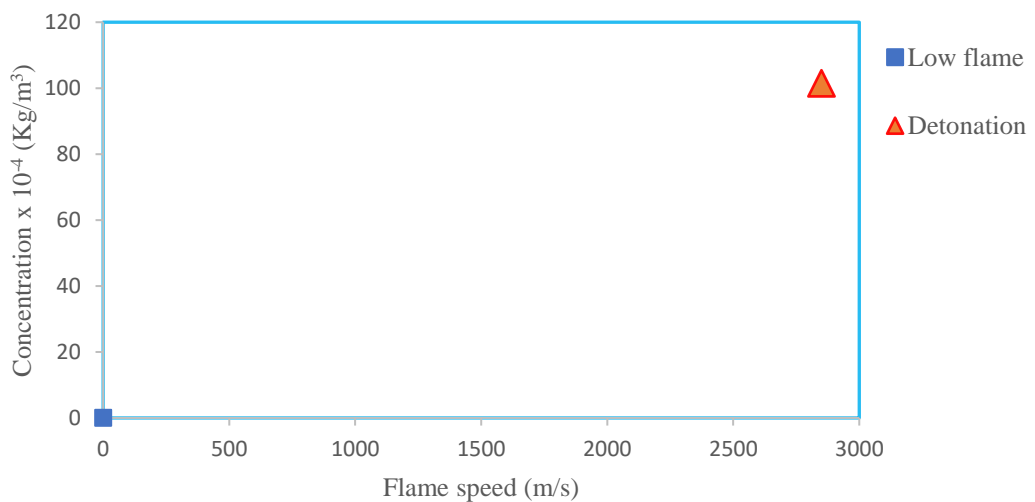


Figure 5.6: Concentration (kg/m³) against flame speed (m/s) for case study R2

2) Case study R3

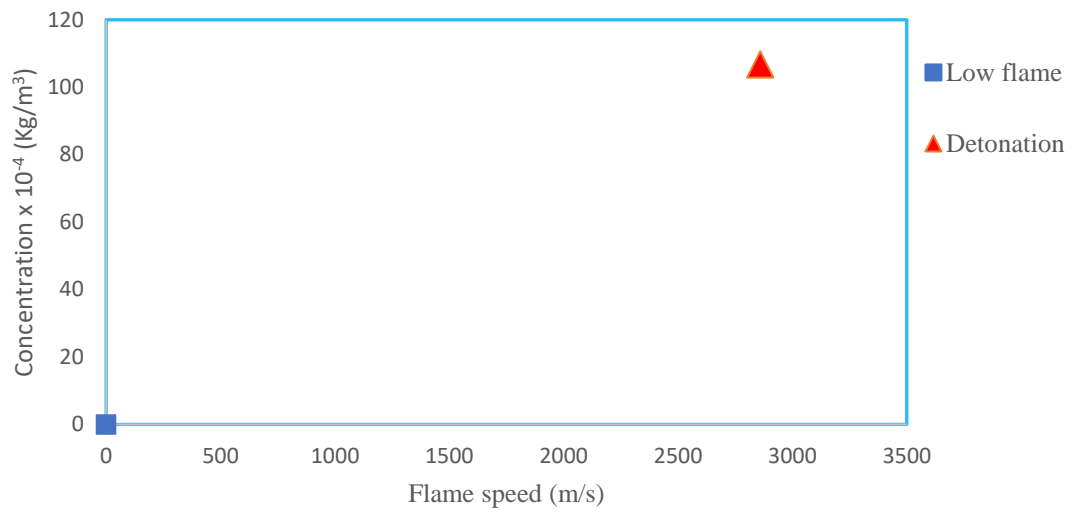


Figure 5.7: Concentration (kg/m³) against flame speed (m/s) for case study R3

3) Case study R4

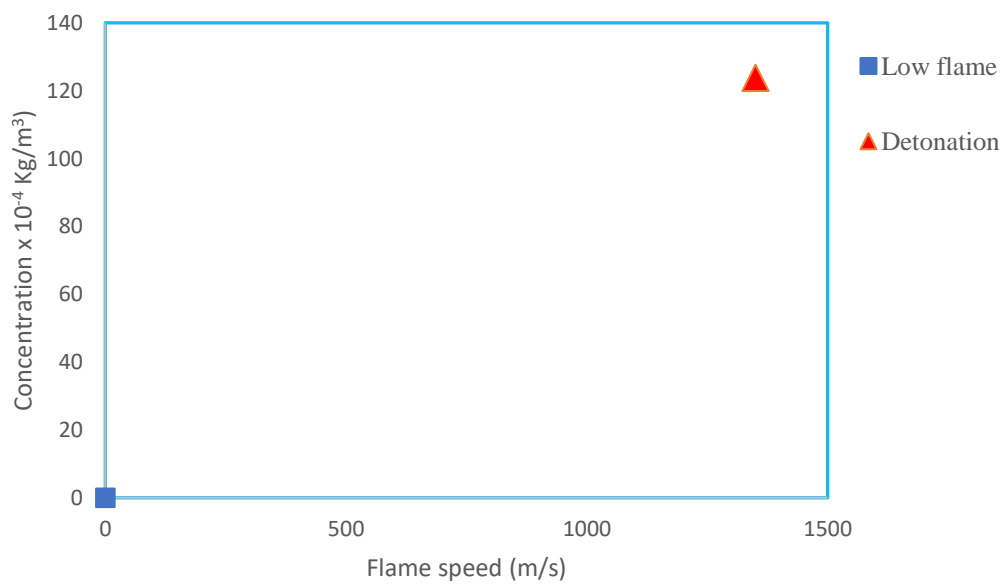


Figure 5.8: Concentration (kg/m³) against flame speed (m/s) for case study R4

4) Case study R5

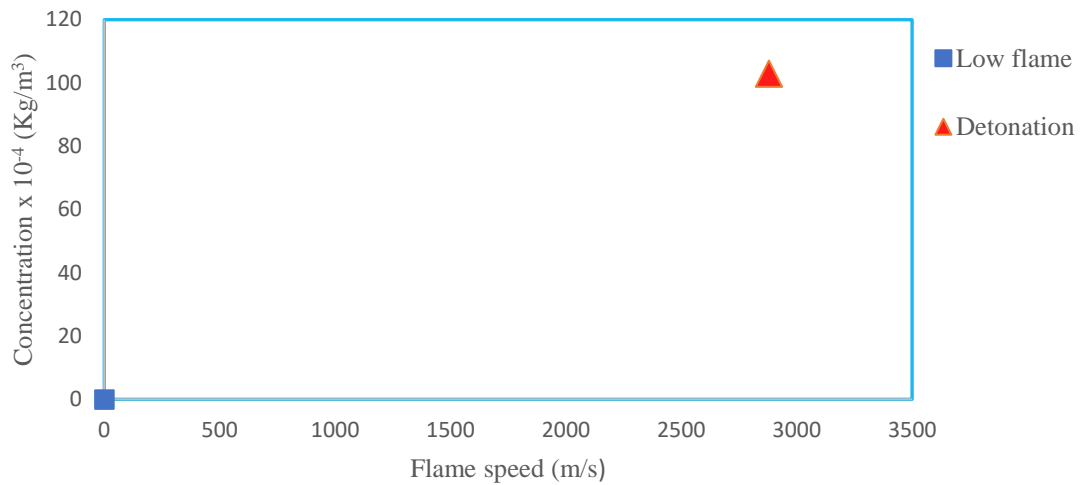
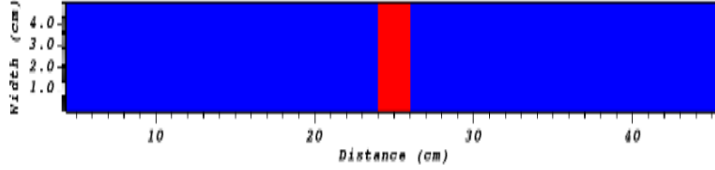
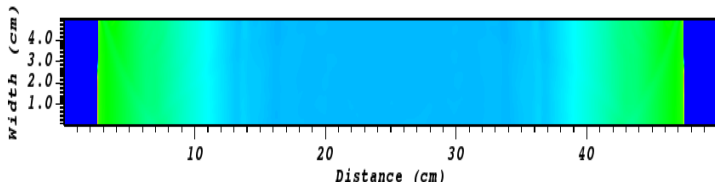
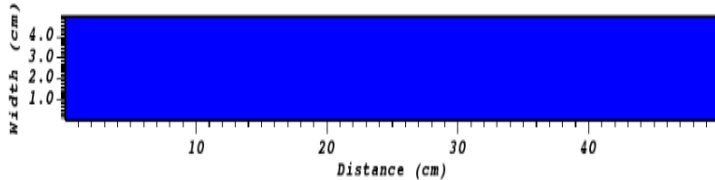
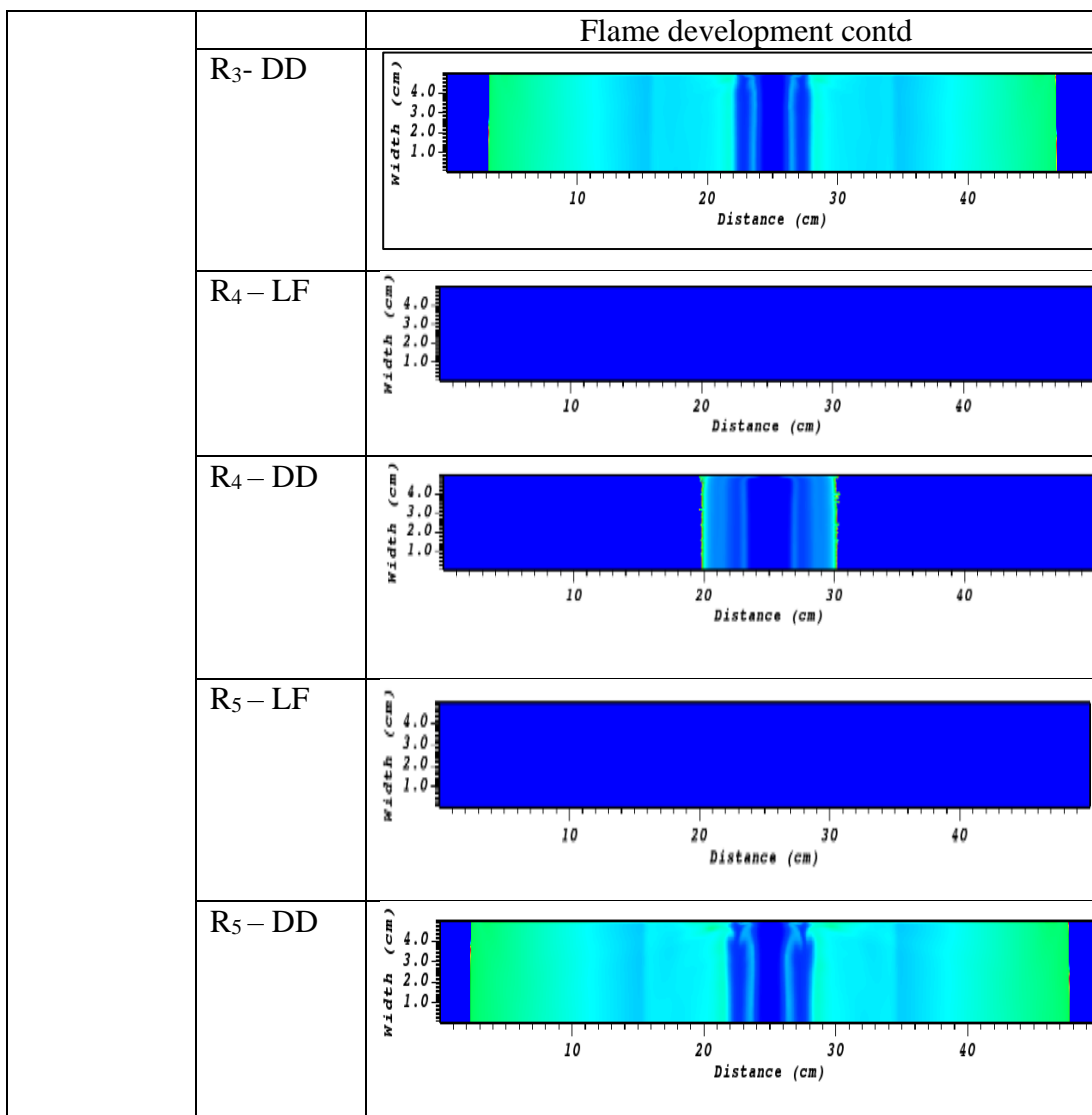


Figure 5.9: Concentration (kg/m³) against flame speed (m/s) for case study R5

Figures 5.6, 5.7, 5.8 and 5.9 above of the graphical illustration for case studies 2, 3, 4 and 5 showed a clearer position of the quantum jump from laminar (low flame) straight to detonation and this is because when the ignition occurs forming laminar flames and the ignition process moves straight to detonation, this is a single explosion, and it is direct initiation, and then explosion will occur.

Table 5.9: Effects of kinetics on H₂-O₂ combustion reactions of case studies 2, 3, 4 and 5

| Case studies | Reactions | Flame development |
|-----------------|---------------------|--|
| Reactions: R | R ₂ – LF |  |
| | R ₂ - DD |  |
| | R ₃ - LF |  |



For Tables 5.9 above, a summary of the AMROC simulation result pictures for this work is an evidence to support the above explanation of the graphical presentation that flame propagation takes place at various locations because of varied chemical kinetics. Moreover, the simulation picture colours on Table 5.6 in section 5.4 for case studies 2, 3, 4, and 5 of H₂-O₂ indicate that the blue locations represent zero concentration (unreacted mixture); and the light green shows maximum or largest volume of concentration. This is just for the operation of VISIT programme. In addition, the flame fronts of the pictures of the different combustion forms formed showed that for detonation, the flame front is flat/sharp because it is a very fast detonation and boundary layer effect is very small and flame front move along, but for laminar flame, it is very tenacious.

(c) Summary Results of 5 case studies by kinetics on H₂-O₂ combustion

Table 5.10: Effects and influences of kinetics on H₂-O₂ combustion reaction processes(see Appendix 2)

| Case Studies | Time range (sec) x 10 ⁻⁴ | Temperature range (K) | Fuel Conc, range (%) x 10 ⁴ | Flame Speed (m/s) | | | |
|--------------|-------------------------------------|-----------------------|--|-------------------|-----|-----|------|
| | | | | LF | FD | DDT | DD |
| Reactions: a | 0.00 – 34.5 | 1500 – 2805 | 0.00 – 118.5 | 0 | 280 | 440 | - |
| b | 0.00 – 17.0 | 1500 – 2956 | 0.00 – 96.07 | 0 | 220 | 404 | - |
| c | 0.00 – 13.5 | 1500 – 3023 | 0.00 – 82.90 | 0 | 140 | 480 | - |
| d | 0.00 – 11.0 | 1500 – 3146 | 0.00 – 71.49 | 0 | 210 | 470 | - |
| e | 0.00 – 10.5 | 1500 – 3912 | 0.00 – 70.54 | 0 | 280 | 400 | 1200 |

Table 5.10 above clearly showed the influences and effects of kinetics on explosion due to H₂-O₂ combustion reaction processes studied, and in this study, it was revealed that as the concentration of the chemical species increases of each case study increases, the temperature also increases, and this will cause an increase to the flame velocity and then FD and DDT were formed for case studies a, b, c, and d, but no detonation was formed. However, comparing the different case studies of reactions of H₂-O₂ mixture studied: a, b, c, d, and e that were simulated, it was only case study e that formed detonation as well as FD and DDT and consequently explosion occurred, and that was because case study e had the highest temperature, slight reduction in fuel concentration and a very high pressure.

(d) Effects and influences of kinetics on H₂-O₂ combustion reaction processes

5) Case study Ra

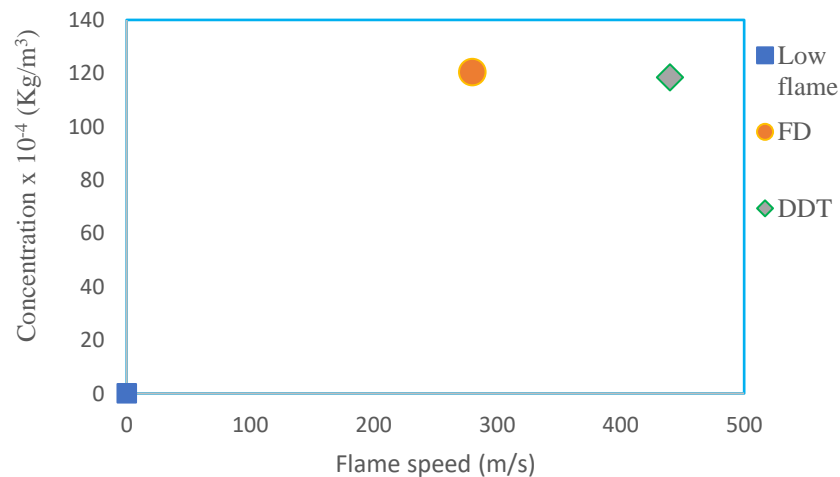


Figure 5.10: Concentration (kg/m³) against flame speed (m/s) for case study Ra

6) Case study Rb

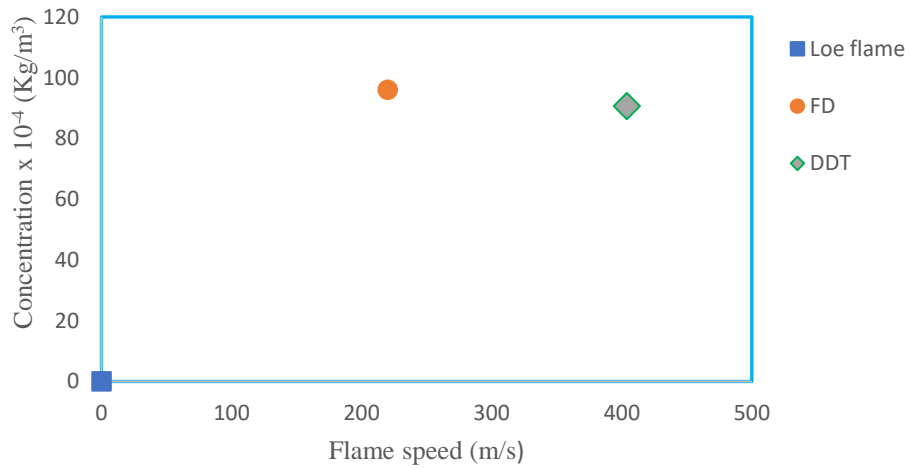


Figure 5.11: Concentration (kg/m³) against flame speed (m/s) for case study Rb

7) Case study Rc

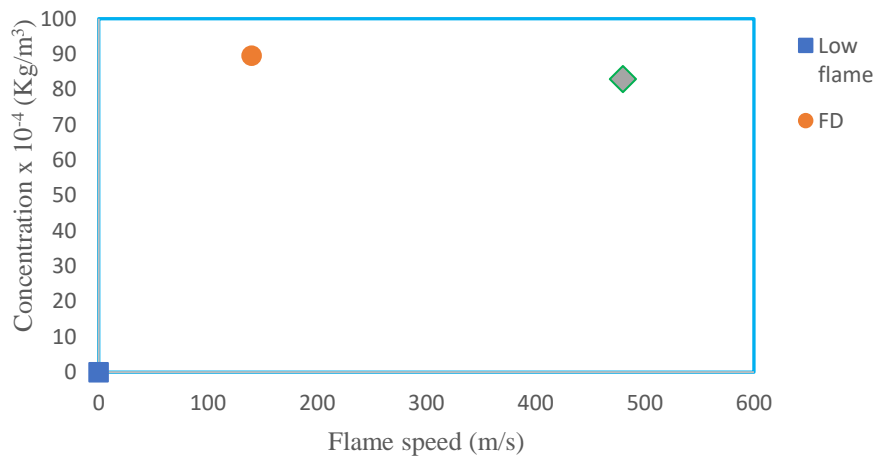


Figure 5.12: Concentration (kg/m³) against flame speed (m/s) for case study Rc

8) Case study Rd

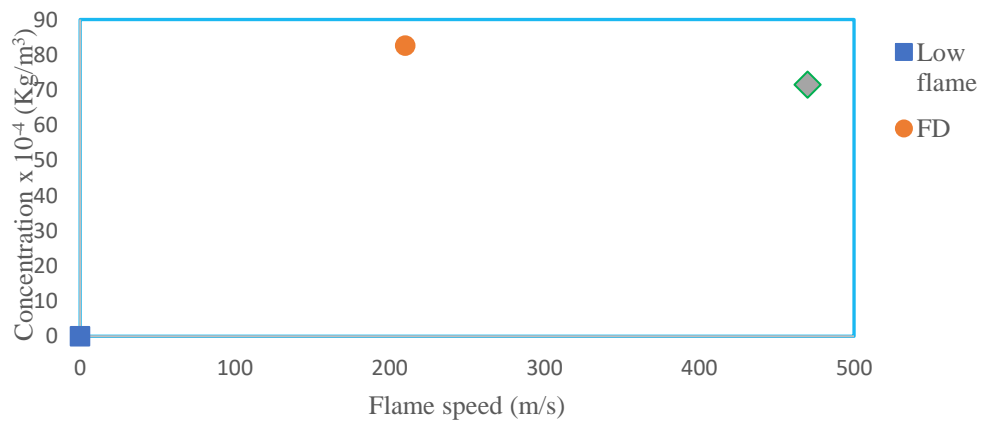


Figure 5.13: Concentration (kg/m³) against flame speed (m/s) for case study Rd

9) Case study R_e

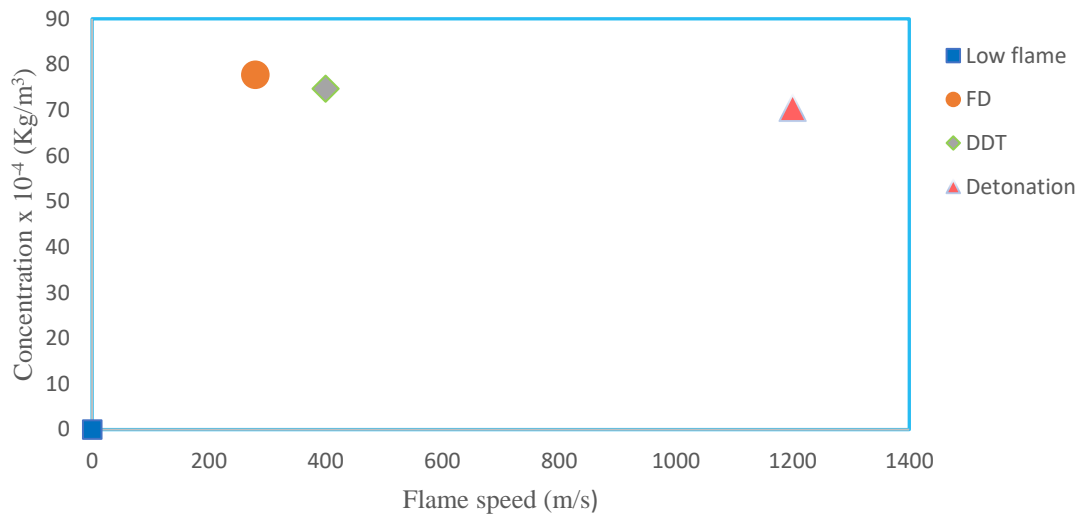
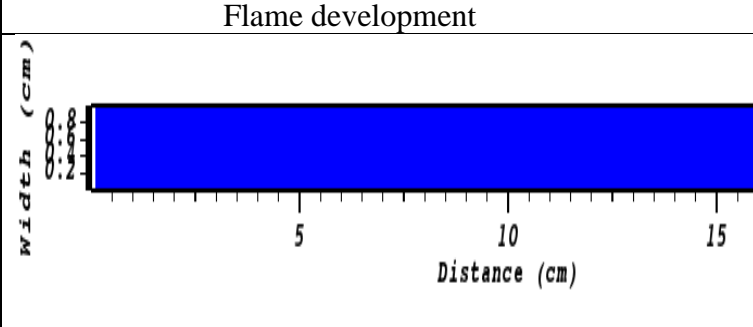
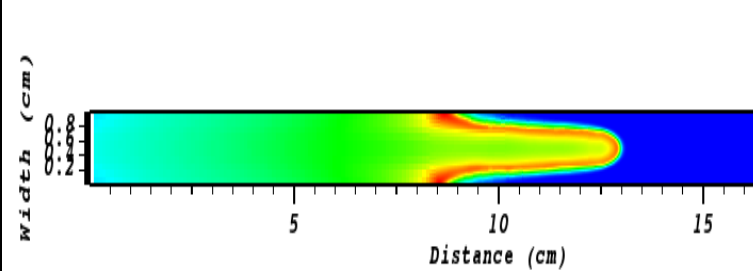
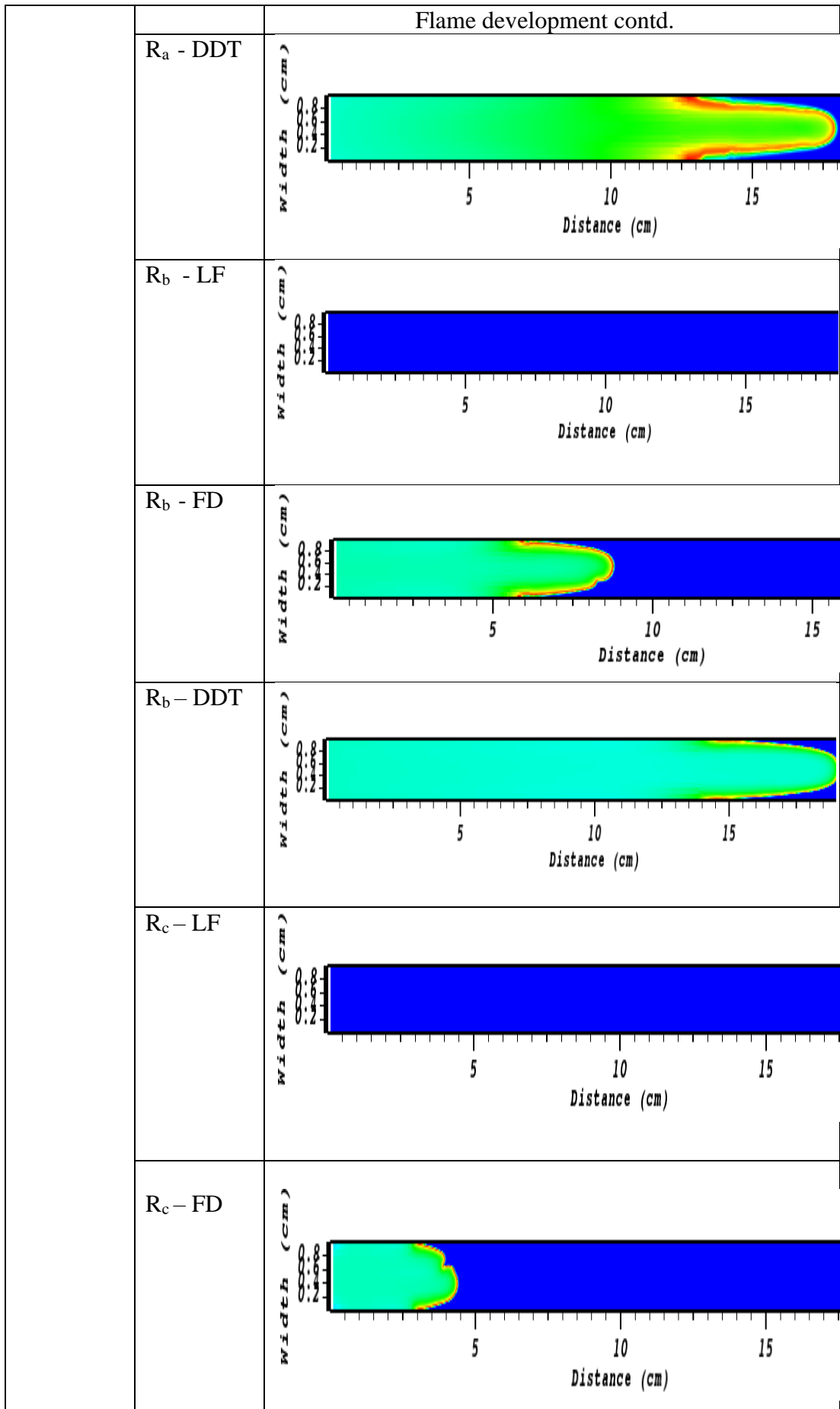


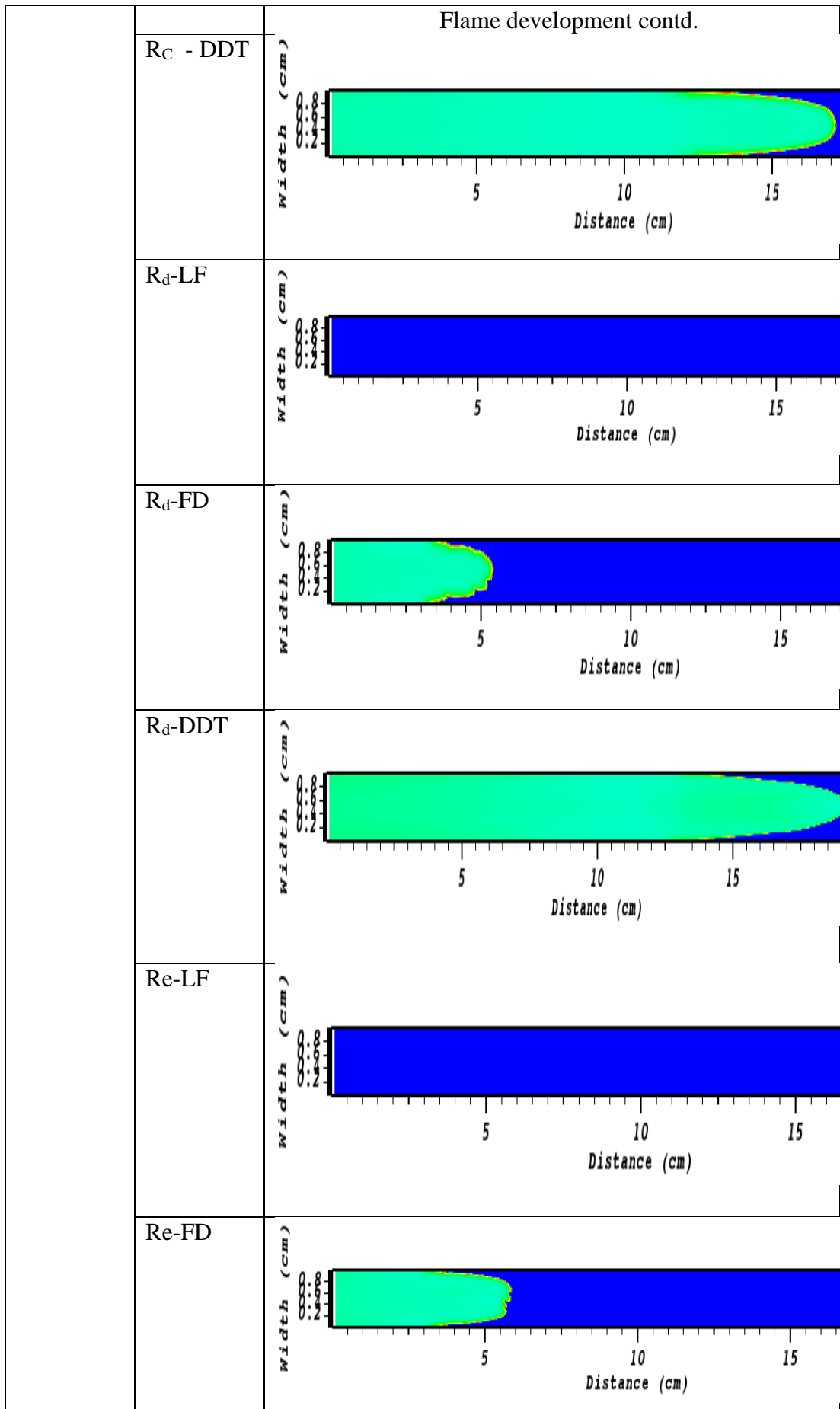
Figure 5.14: Concentration (kg/m^3) against flame speed (m/s) for case study R_e

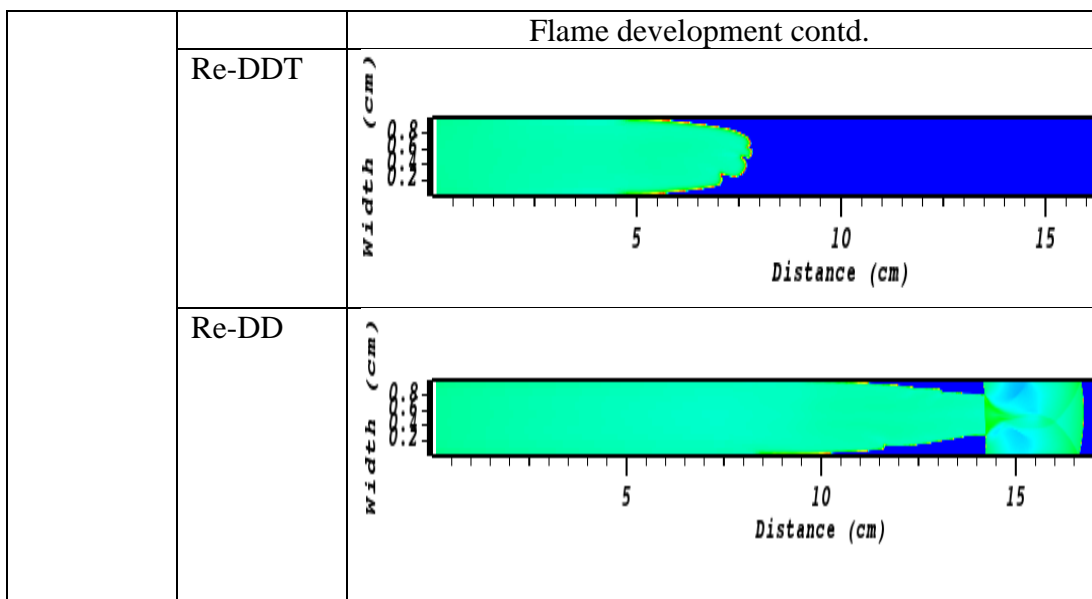
From the graphical illustration of the simulation results displayed on Figures 5.10, 5.11, 5.12, 5.13 and 5.14 above, the results displayed a clearer position of the simulation work which showed a slight reduction in fuel concentration and this indicates that the processor becomes relatively stable and thus FD, DDT were observed for case studies a, b, c, and d, but for case study e, as the processor also becomes relatively stable, FD, DDT and detonation were formed and thus explosion will eventually take place.

Table 5.11: Effects of kinetics on $\text{H}_2\text{-O}_2$ combustion reactions of case studies a, b, c, d and e

| Case studies | Reactions | Flame development |
|-------------------|--|--|
| | $R_a - \text{LF}$ |  |
| $R_a - \text{FD}$ |  | |







For Tables 5.11 above, a summary of the AMROC simulation result pictures for this work is an evidence to support the above explanation of the graphical presentation that flame propagation takes place at various locations because of varied chemical kinetics. Furthermore, the simulation picture colours on Table 5.8 in section 5.4 for case studies a, b, c, d, and e of H₂-O₂ revealed that the blue locations represent zero concentration (unreacted mixture); and the light green shows maximum volume of concentration. This is just for the operation of VISIT programme. In addition, the flame fronts of the pictures of the different combustion forms formed showed that for detonation, the flame front is sharp because it is a very fast detonation, and boundary layer effect is very small and flame front move along, but for DDT, its flame front is pointed due to its instability, boundary layer effect and numerical error due to computer capability; and for laminar flame, it is very viscous.

(e) Summary Simulation Results of 5 case studies by kinetics on propane combustion

Table 5.12: Effects of kinetics on propane combustion reaction processes (see Appendix 3)

| Case Studies | Time range (sec) x 10 ⁻⁴ | Temperature range (K) | Fuel Conc, range (%) x 10 ⁴ | Flame Speed (m/s) | | | |
|---------------|-------------------------------------|-----------------------|--|-------------------|-----|-----|------|
| | | | | LF | FD | DDT | DD |
| Reactions: 20 | 0.00 – 8.0 | 2500 – 3213 | 0.00 – 30.41 | 0 | 200 | 480 | - |
| 21 | 0.00 – 11.5 | 2500 – 3350 | 0.00 – 30.88 | 0 | 240 | 480 | 1300 |
| 30 | 0.00 – 4.95 | 3000 – 4260 | 0.00 – 42.16 | 0 | 130 | 440 | 2530 |
| 31 | 0.00 – 9.55 | 2500 – 4140 | 0.00 – 35.01 | 0 | 120 | 430 | 2800 |
| 40 | 0.00 – 2.85 | 3000 – 4500 | 0.00 – 47.44 | 0 | 200 | 470 | 2560 |

A close look at Table 5.12 in section 5.4 showed that the influences and effects of kinetics on explosion due to propane combustion reaction processes were evident, and it was observed that the simulation results revealed that as the concentration of the chemical species of each of the case studies 20, 21, 30, 31 and 40 increases, the temperature also increases. However, in comparing the case studies of reactions of propane studied, it showed that it was only case study 20 which formed FD and DDT, but no detonation was observed. Moreover, FD, DDT and detonation flame forms were observed for the remaining case studies 21, 30, 31 and 40, and this is because case studies 21, 30, 31 and 40 had high fuel concentration and high temperatures, and thus explosion will result.

(f) Effects and influences of kinetics on propane combustion reaction processes

10) Case study R₂₀

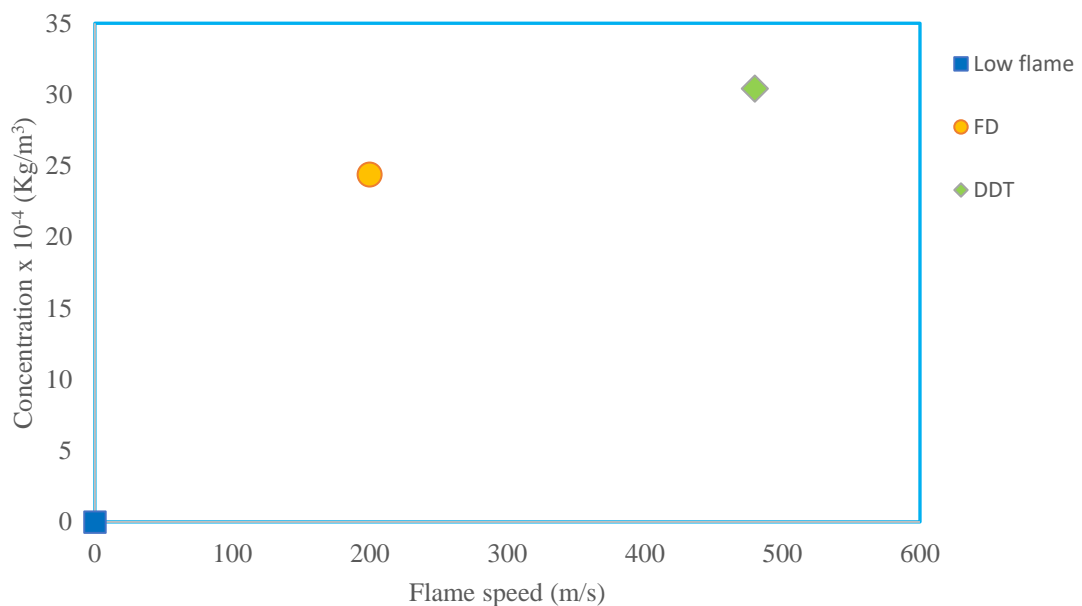


Figure 5.15: Concentration (kg/m³) against flame speed (m/s) for case study R₂₀

11) Case study R₂₁

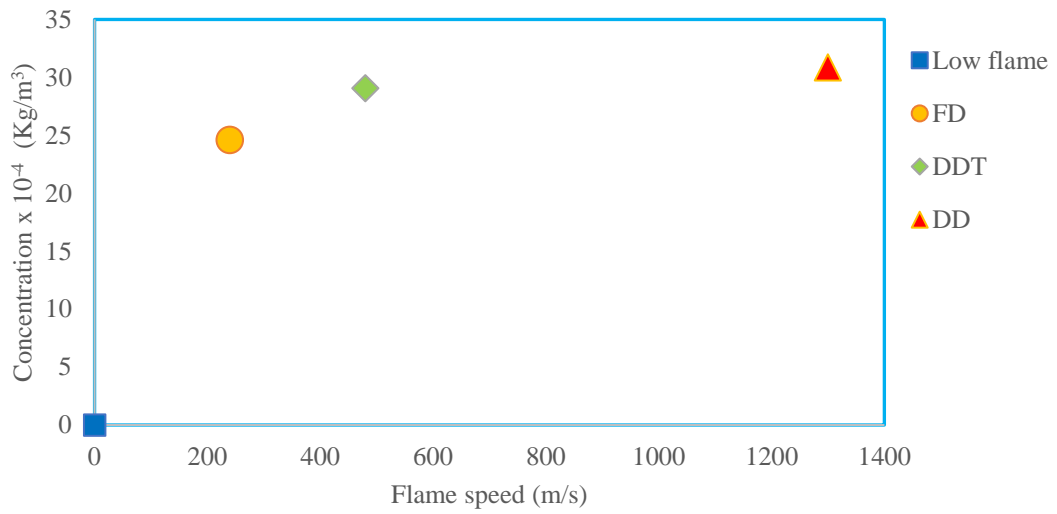


Figure 5.16: Concentration (kg/m³) against flame speed (m/s) for case study R₂₁

12) Case study R₃₀

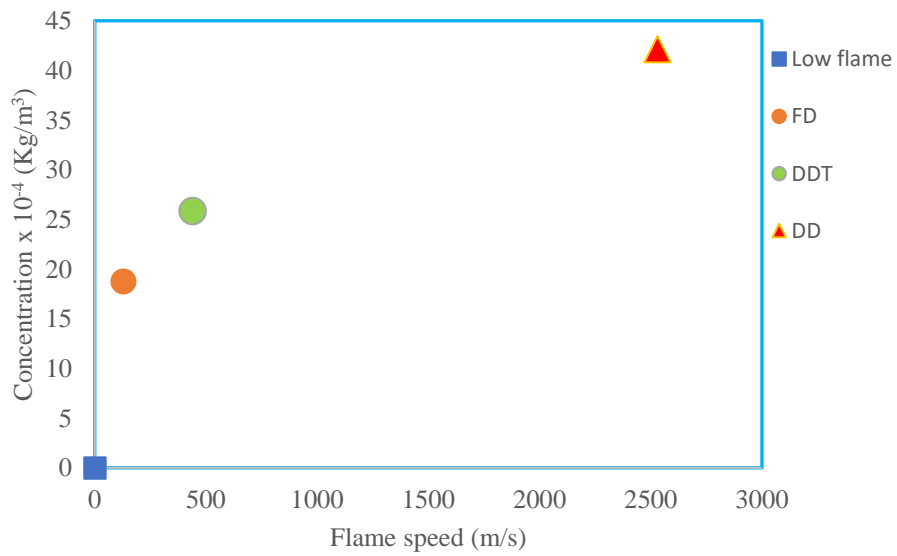


Figure 5.17: Concentration (kg/m³) against flame speed (m/s) for case study R₃₀

13) Case study R₃₁

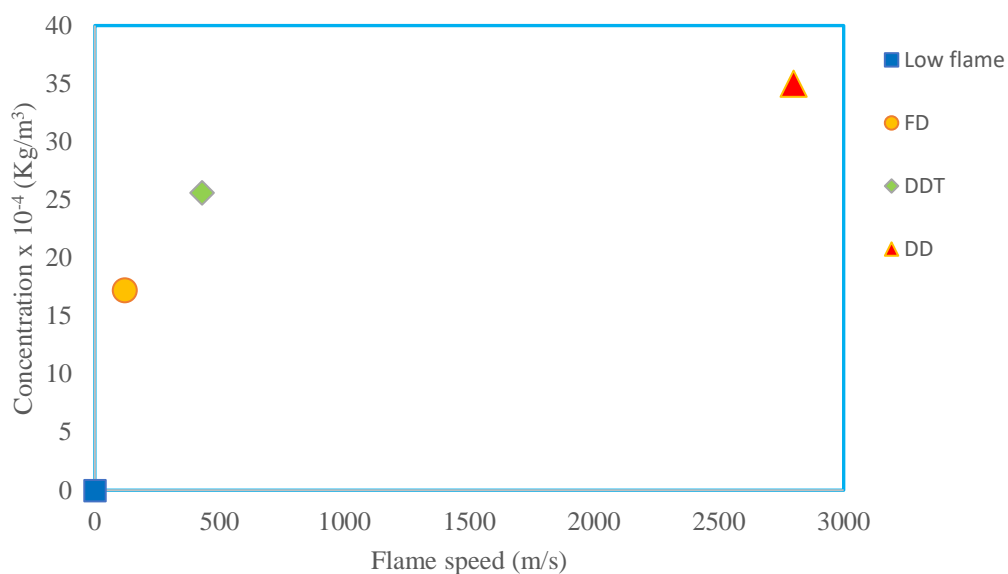


Figure 5.18: Concentration (kg/m³) against flame speed (m/s) for case study R₃₁

14) Case study R₄₀

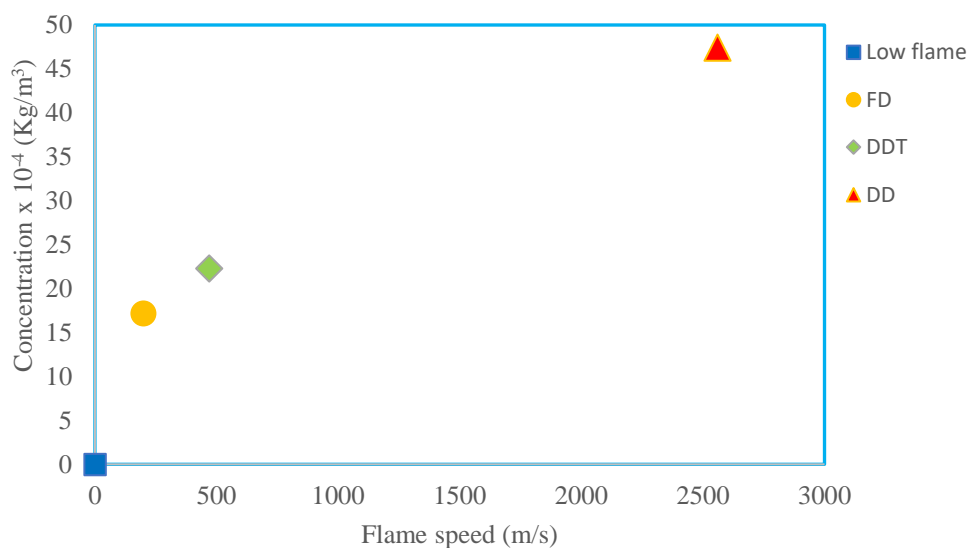
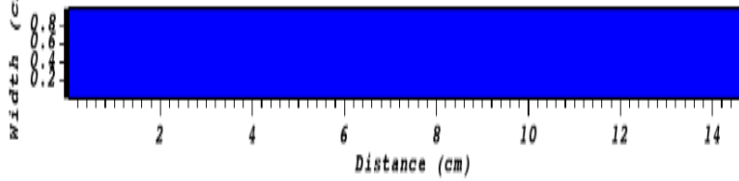
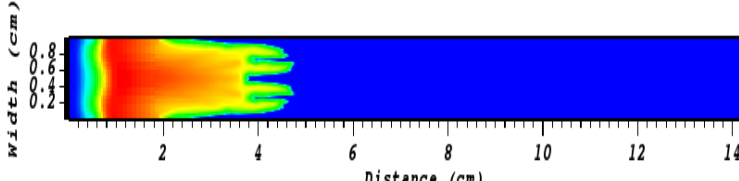
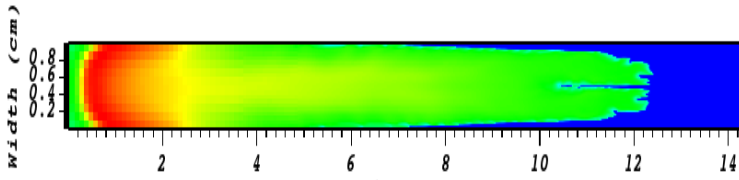
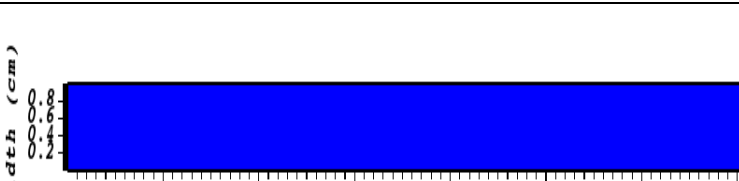
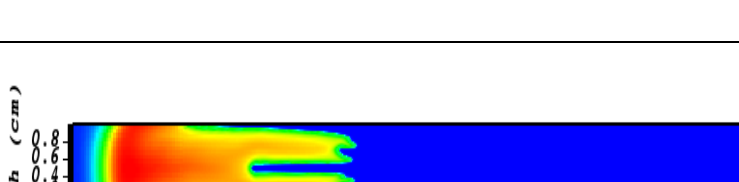


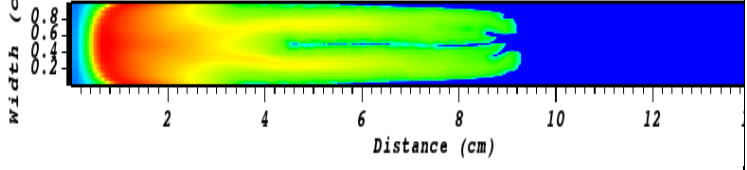
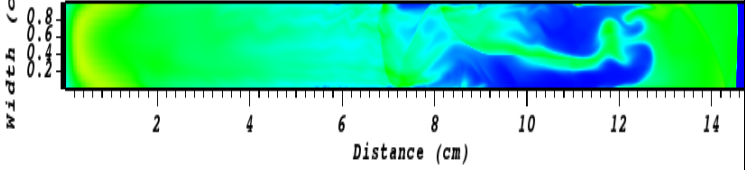
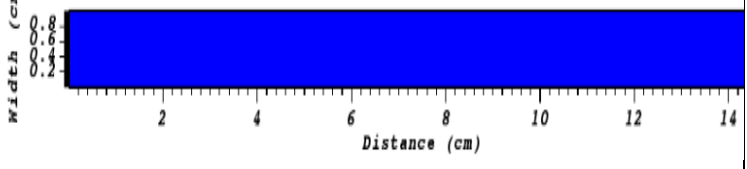
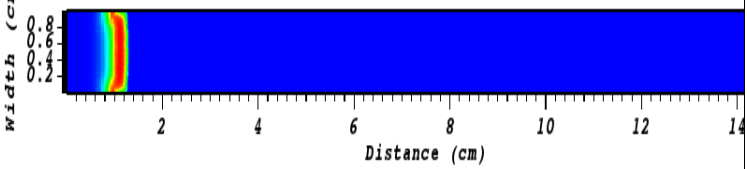
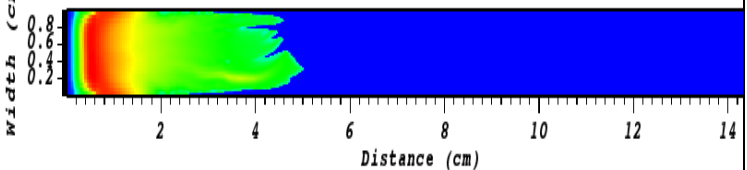
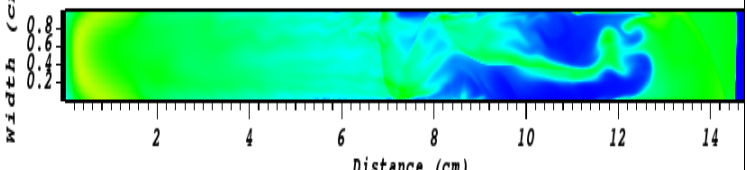
Figure 5.19: Concentration (kg/m³) against flame speed (m/s) for case study R₄₀

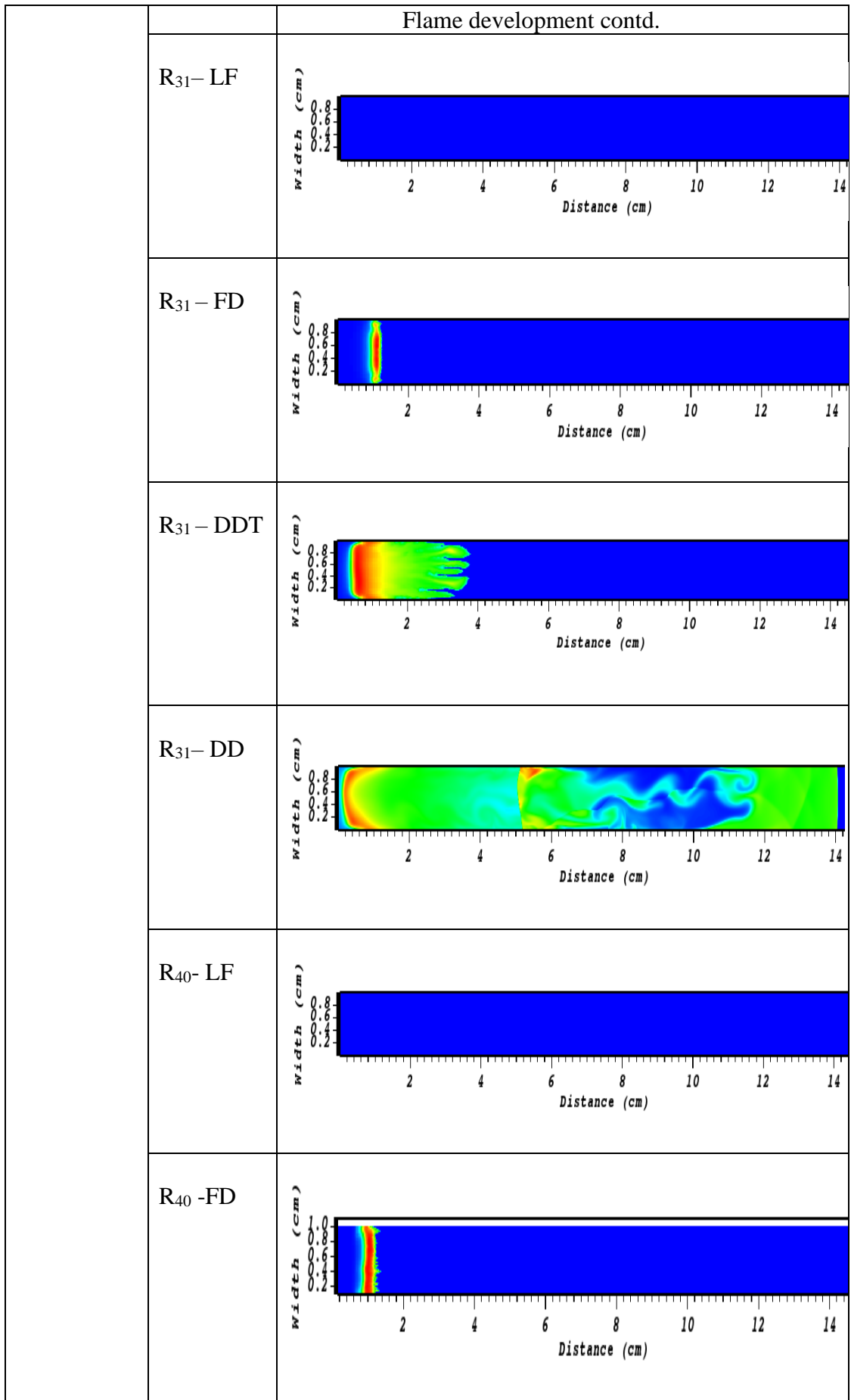
The simulation results displayed by the graphical illustration in Section 5.4 of Figures 5.15, 5.16, 5.17, 5.18 and 5.19 showed a more beautiful position of the results that there was a sharp increase in concentration of the chemical reacting species which

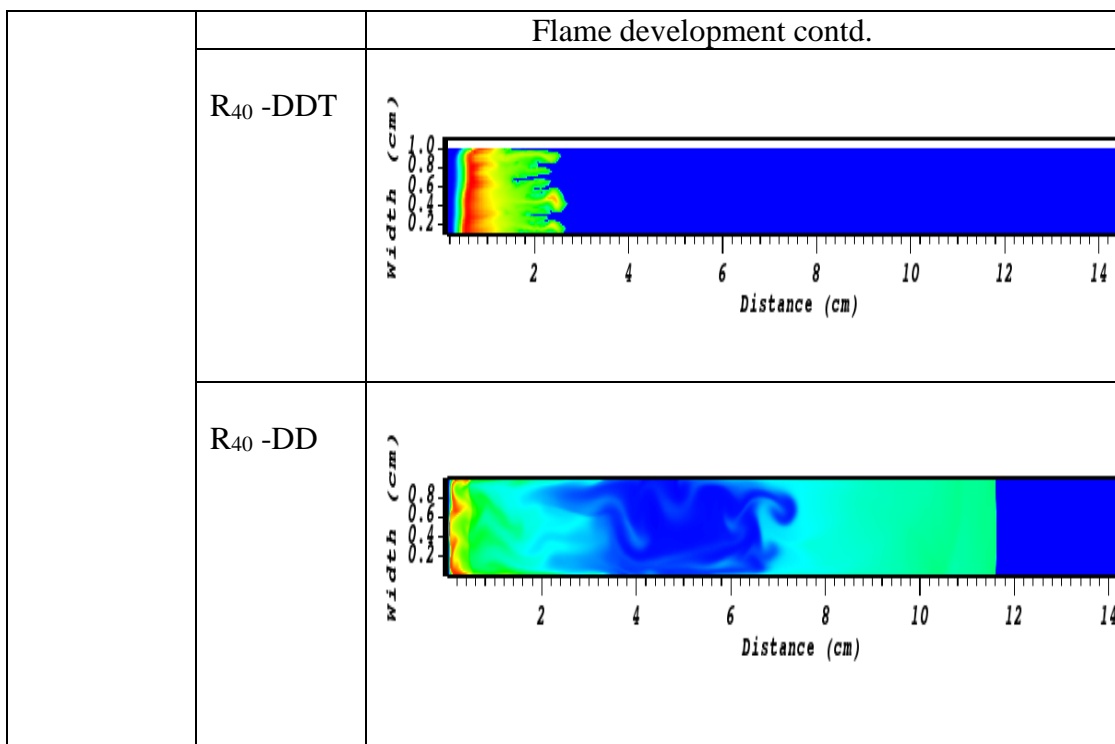
indicates that more heat will be produced and thus FD and DDT were observed for case studies 20, but comparatively FD, DDT and detonation were formed for case studies 21, 30, 31, and 40, and this is attributable to their high fuel concentration and high temperatures, and consequently explosion would take place.

Table 5.13: Effects of kinetics on Propane combustion of case studies 20, 21, 30, 31, and 40

| Case studies | Reactions | Flame development |
|--------------|----------------------|--|
| | R ₂₀ – LF |  |
| | R ₂₀ – FD |  |
| | R ₂₀ -DDT |  |
| | R ₂₁ -LF |  |
| | R ₂₁ -FD |  |

| | | Flame development contd. |
|--|-----------------------|--|
| | R ₂₁ – DDT |  |
| | R ₂₁ – DD |  |
| | R ₃₀ - LF |  |
| | R ₃₀ – FD |  |
| | R ₃₀ – DDT |  |
| | R ₃₀ – DD |  |





A good observation of the summary of the AMROC simulation result pictures on Table 5.13 in Section 5.4 for case studies 20, 21, 30, 31, and 40 showed a very vivid explanation with the graphical presentation that flame propagation takes place at various locations because of varied chemical kinetics. Moreover, the simulation picture colours on Table 5.13 above for case studies 20, 21, 30, 31, and 40 of propane revealed that the blue locations represent minimum concentration (unreacted mixture), and the light green shows largest volume of concentration. This is just for the operation of VISIT programme. In addition, the flame fronts of the pictures of the different combustion forms observed showed that for detonation, the flame front is flat/sharp because it is a very fast detonation and boundary layer effect is very small and flame front move along, but for DDT, its flame front is pointed due to its instability, boundary layer effect and numerical error due to computer capability; and for laminar flame, it is very slimy.

5.5 Brief Summary

Chapter 5 examined the influences and effects of chemical reaction mechanisms to generations, propagations, and transitions of explosion waves. To this background, two premixed gaseous combustibles: - hydrogen-oxygen and propane-oxygen were selected and filled into two-dimensional tube domains, then the mixtures are ignited.

Furthermore, this chapter has carefully studied the effects and the influences of chemical kinetics on explosion due to the combustion reactions of hydrogen-oxygen and propane-oxygen reactions. The layout of this chapter is structured analytically to cover the sections: (1) the effects of kinetics on H₂-O₂ combustion reactions for case studies 2, 3, 4, and 5; (2) the effects of kinetics on H₂-O₂ combustion reactions for case studies a, b, c, d, and e and (3) the effects of kinetics on propane-oxygen combustion reactions for case studies 20, 21, 30, 31 and 40. The results obtained showed that chemical kinetics have effects and influences on the explosion based on the case studies investigated. However, no DDT and FD were formed for case studies 2, 3, 4, and 5 and this was because it was an open-end tube and there is no limited gas expansion, and no artificial obstacle, and therefore, deflagration-to-detonation transition (DDT) and fast deflagration (FD) were not formed, but the ignition process moves straight to detonation, thus forming a single explosion. Comparing the different case studies of H₂-O₂ studied: a, b, c, d, and e showed that it was only case study e that formed detonation, DDT, and FD, and consequently explosion occurred, and that was because case study e had very high temperature. In addition, in comparing the case studies of the reactions of propane investigated, it showed that it was only case study 20 did not form detonation. However, the rest case studies 21, 30, 31 and 40 formed FD, DDT and detonation flame forms, and this is because case studies 21, 30, 31 and 40 had high fuel concentration and high temperatures, and hence explosion occurred.

Chapter 6 Effects of Complex Geometric Configurations

6.1 Introduction

This chapter will investigate the influences and effects of geometric configurations on explosion waves. Therefore, the computational domain is not tube-shaped like one in the last chapter. In this chapter, two premixed combustible mixtures: - hydrogen-oxygen and propane-oxygen are chosen and investigated. This chapter will logically examine the influences and effects of geometric configurations of effectobstacle, vent and oneBlock on explosion involving the combustion reaction processes of H₂-O₂ and propane combustible mixtures respectively. However, the layout of this chapter is systematically structured to cover the sections, and section 1 envelopes the effects and influences of geometric configurations on H₂-O₂ combustion reactions for case studies block, step, and wall; section 2 embraces the effects and influences of geometric configurations on H₂-O₂ combustion reactions for case studies A, B, and C; and section 3 covers the effects and influences of geometric configurations on propane-oxygen combustion reactions for case studies 20, 21, 30, 30x 31, and 31x. In addition, section 1 comprises 3 case studies; section 2 consists of 3 case studies; and section 3 consists of 6 case studies, thus amounting to a total of 12 case studies, but this chapter shall explain each section individually. This chapter will clearly address the influences and effects of geometric configurations on explosion of hydrogen-oxygen and propane - oxygen reactions using numerical simulation method while also considering other factors. Also, several factors will be examined that are greatly important for achieving desired safety and fire scene investigation programmes to mention but a few, not absolutely to guard against destruction of company assets due to ravaging fires and explosions, thus saving lives. This chapter 6 will thoroughly consider the influences and effects of geometrical configuration on explosion in petroleum tank farm operation thereby obtaining good safety management suitable for the daily operations.

6.2 Setup of simulations

When geometric configuration is changed, the nature of combustion waves will change.

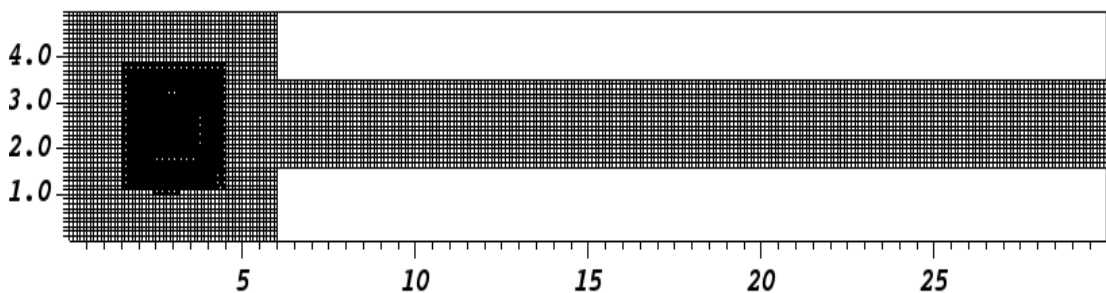
The simulated scenarios in this chapter were mainly to investigate such changes and variations. To that end, this chapter will explore the concentration of chemical species and pressure and the flame propagation during combustion processes. The reaction

rates are dominant for processes of different combustion nodes – slow flame (SF), fast flame (FF), deflagration-to-detonation transition (DDT) and detonation. To simulate the reaction processes accurately, an integration time step is in the order of 10^{-8} second.

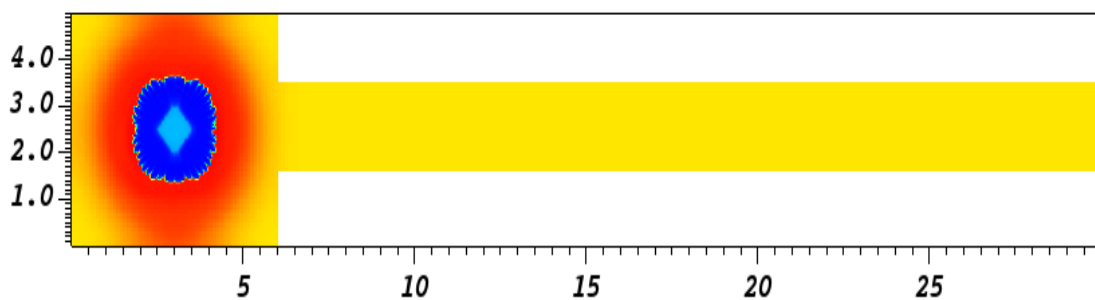
6.2.1 Domain mesh

AMROC tool amongst others has strong advantage for detailed kinetics of chemical reactions and can do parallel computations with mesh – adaptive refinement. The finest mesh resolution is at 0.03125mm and it means that there are about 35 nodes in the flame. The domains are meshed by square elements and the initial element is 1mm long and 1mm wide. This initial mesh will be adaptively refined until the finest mesh resolution is obtained. To demonstrate the mesh refinements, an example case study in section 6.3 is showed as follows. Figures 6.1, 6.2, 6.3 and 6.4 show the mesh variation and simulated results responding to the meshes, at 4 times instants. The four instants represent typical stages during the development of combustion waves, i.e. ignition: slow flame, fast flame, DDT and detonation.

For Figures 6.1, 6.2, 6.3, 6.4 and 6.5 in Section 6.2.1, the length unit on the vertical and horizontal of each Figure is in centimetre (cm).

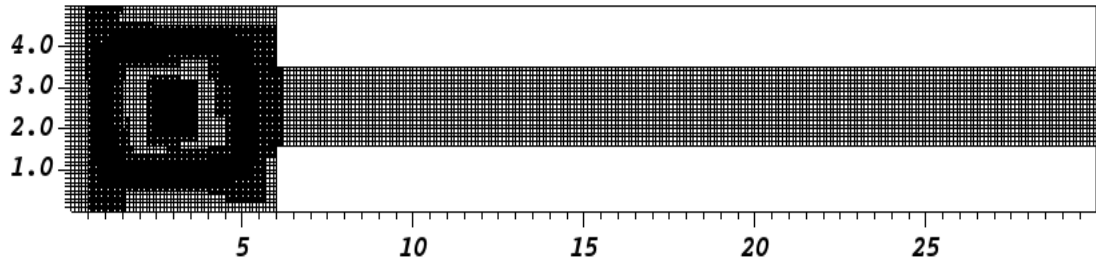


(a) Mesh

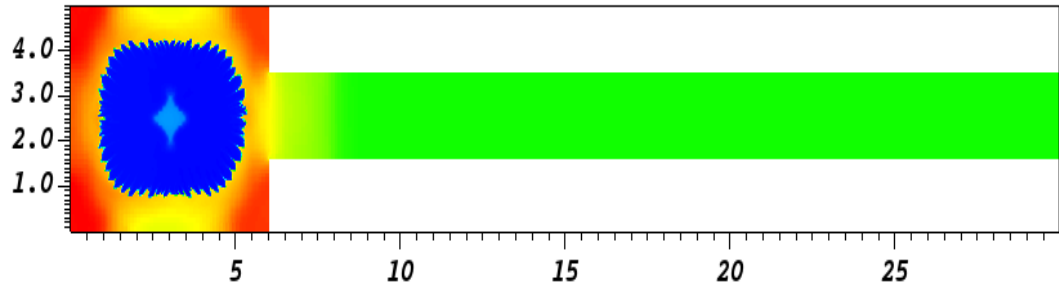


(b) Density

Figure 6.1 Time is at 0.0001 second from ignition, ignition state.

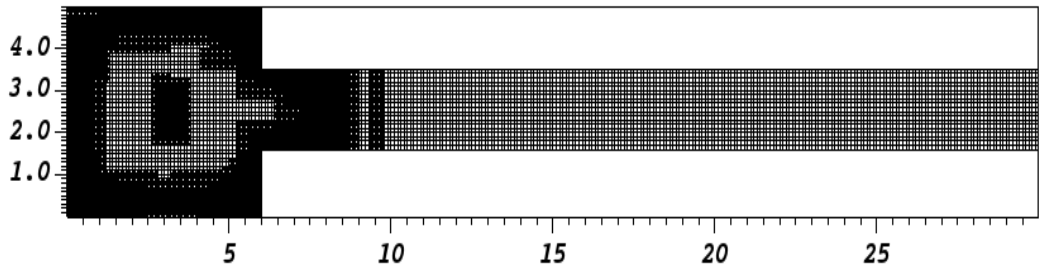


(a) Mesh

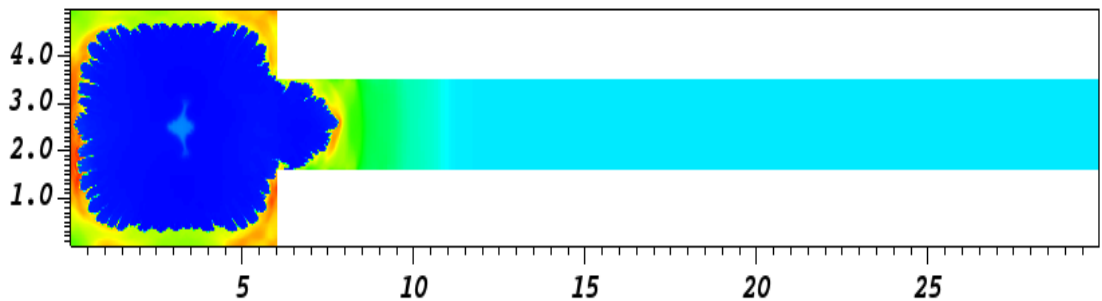


(b) Density

Figure 6.2 Time is at 0.000145 second, slow flame mode of combustion waves.

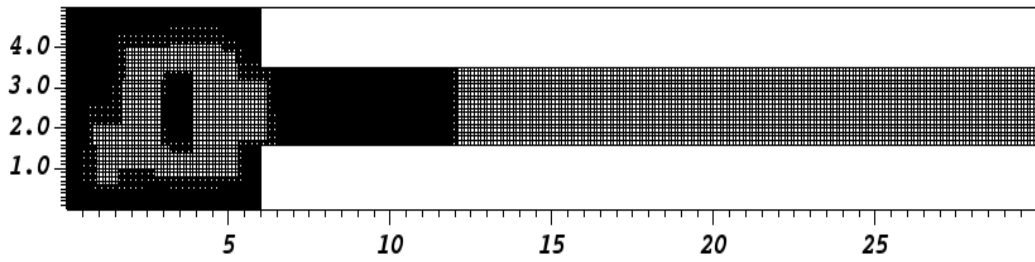


(a) Mesh

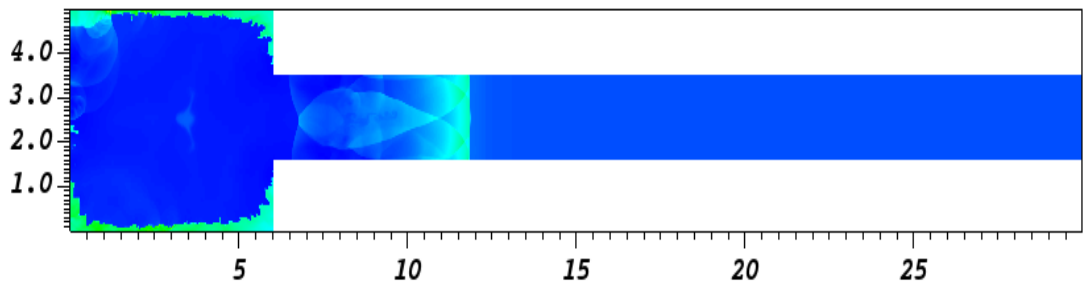


(b) Density

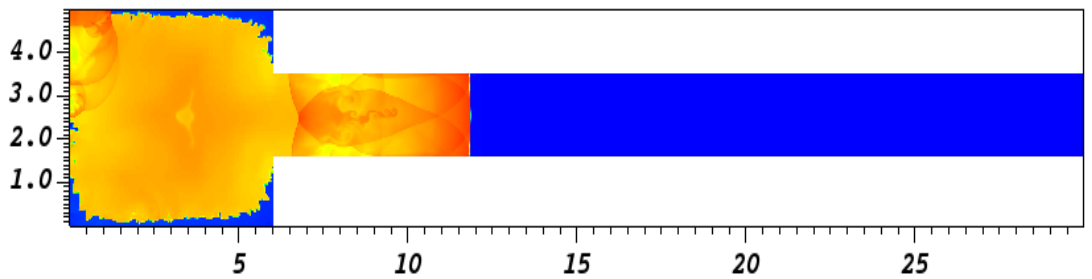
Figure 6.3 Time is at 0.000195 second, fast flame mode of combustion waves.



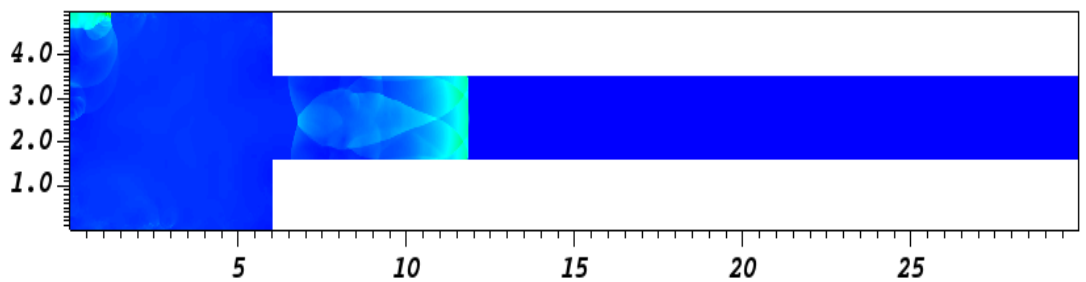
(a) Mesh



(b) Density



(c) Temperature



(d) Pressure

Figure 6.4 Time is at 0.00022 second at which the detonation is initialised

Figure 6.5 below shows the details of the mesh structure at detonation. One can see in the areas where the flow changes sharply the mesh is the finest while the others have coarse mesh.

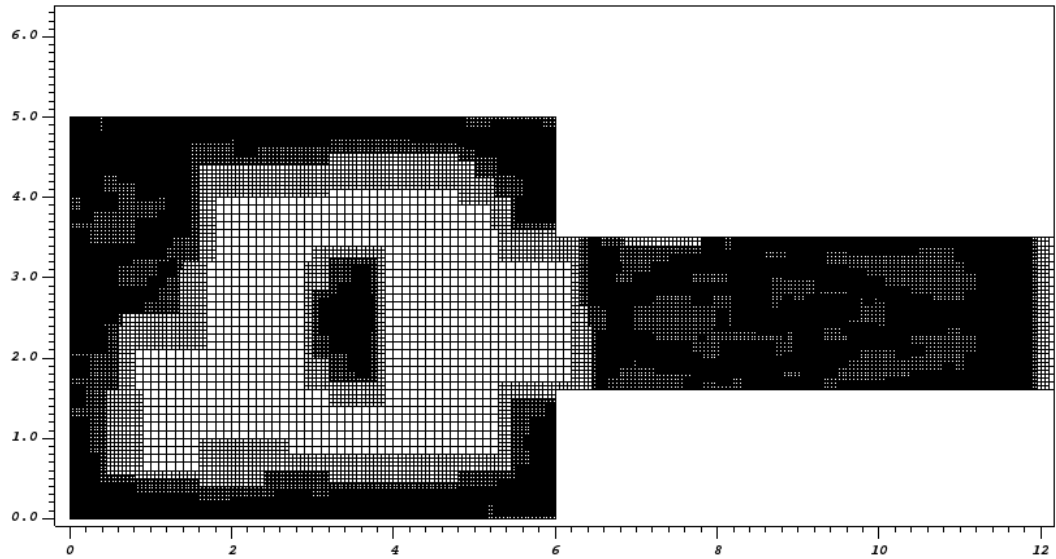


Figure 6.5 Detailed mesh structure for the detonation

6.2.2 Initial Conditions and ignition sources

Three, three, and six case studies respectively were studied, and their initial conditions are shown in Tables 6.1, 6.2, and 6.3 in Section 6.2.2, and other considerations for this simulation work include the initial state of the elements, the reacting species and the reactions shown in Tables 6.4, 6.5 and 6.6 in Section 6.2.3 respectively.

Table 6.1: Initial conditions of complex geometry for 3 case studies of H₂-O₂ combustion reaction

| Case Studies – species | Temperature (K) | | Concentration (%) | | | | Pressure (Pa) | |
|------------------------|-----------------|--------------|-------------------|----------------|----------------|----------------|---------------------|---------------------|
| | Left (Hot) | Right (Cool) | Left (Hot) | | Right (Cool) | | Left | Right |
| | | | H ₂ | O ₂ | H ₂ | O ₂ | | |
| Block | 3,000 | 300 | 0.0 | 0.0 | 0.15 | 0.20 | 1 x 10 ⁵ | 1 x 10 ⁵ |
| Step | 3,000 | 300 | 0.0 | 0.0 | 0.15 | 0.20 | 1 x 10 ⁵ | 1 x 10 ⁵ |
| Wall | 3,000 | 300 | 0.0 | 0.0 | 0.15 | 0.20 | 1 x 10 ⁵ | 1 x 10 ⁵ |

Table 6.2: Initial conditions of complex geometry for 3 case studies of H₂-O₂ combustion reactions

| Case Studies | Temperature (K) | | Concentration (%) | | | | Pressure (Pa) | |
|--------------|-----------------|--------------|-------------------|----------------|----------------|----------------|---------------------|---------------------|
| | Left (Hot) | Right (Cool) | Left (Hot) | | Right (Cool) | | Left | Right |
| | | | H ₂ | O ₂ | H ₂ | O ₂ | | |
| A | 3,000 | 300 | 0.0 | 0.0 | 0.15 | 0.20 | 1 x 10 ⁵ | 1 x 10 ⁵ |
| B | 3,000 | 300 | 0.0 | 0.0 | 0.15 | 0.20 | 1 x 10 ⁵ | 1 x 10 ⁵ |
| C | 3,000 | 300 | 0.0 | 0.0 | 0.15 | 0.20 | 1 x 10 ⁶ | 1 x 10 ⁵ |

Table 6.3: Initial conditions of complex geometry for 6 case studies of propane combustion

| Case Studies | Temperature (K) | | Concentration (%) | | | | Pressure (Pa) | |
|--------------|-----------------|--------------|-------------------|----------------|----------------|----------------|---------------------|---------------------|
| | Left (Hot) | Right (Cool) | Left (Hot) | | Right (Cool) | | Left | Right |
| | | | H ₂ | O ₂ | H ₂ | O ₂ | | |
| 20 | 3,000 | 300 | 0.0 | 0.0 | 0.15 | 0.20 | 1 x 10 ⁵ | 1 x 10 ⁵ |
| 21 | 3,000 | 300 | 0.0 | 0.0 | 0.15 | 0.20 | 1 x 10 ⁵ | 1 x 10 ⁵ |
| 30 | 3,000 | 300 | 0.0 | 0.0 | 0.15 | 0.20 | 2 x 10 ⁶ | 1 x 10 ⁵ |
| 30x | 2,800 | 300 | 0.0 | 0.0 | 0.68 | 0.17 | 2 x 10 ⁵ | 1 x 10 ⁵ |
| 31 | 2,800 | 300 | 0.0 | 0.0 | 0.68 | 0.17 | 2 x 10 ⁵ | 1 x 10 ⁵ |
| 31x | 2,800 | 300 | 0.0 | 0.0 | 0.68 | 0.17 | 2 x 10 ⁶ | 1 x 10 ⁵ |

On Tables 6.1, 6.2 and 6.3 above, the hot side (left side) is of very high temperature and pressure which is the ignition source while the cool side (right side) contains the premixed combustion gas mixtures of hydrogen-oxygen and propane-oxygen for Tables 6.1, 6.2 and 6.3 respectively. The cool side keeps constant the temperature and pressure, but the concentrations of chemical species comprising the combustible gas mixture are varied with different case studies. Additionally, on the left side (hot side), the temperature is very high, and the concentrations of H₂ and O₂ are not actually zero, therefore, no fuel (H₂), no oxygen (O₂) and on the left side, no combustion mixture, but the right side has premixed combustion mixture. The results were visualised using VISIT. The programme is a general data processing programme and can be executed in parallel and therefore particularly suitable to deal with a large database.

6.2.3 Chemical kinetics

Table 6.4 below showed that in the first stage of this work, hydrogen and oxygen as well as nitrogen and argon were simulated, but in the second stage, carbon, hydrogen and helium (a noble gas) are added which will thus constitute the petroleum (hydrocarbon) gas.

Table 6.4: Elements Considered for hydrocarbon simulation

| Elements Considered | Symbol |
|---------------------|--------|
| Hydrogen | H |
| Oxygen | O |
| Nitrogen | N |
| Carbon | C |
| Argon | Ar |
| Helium | He |

On Table 6.5 below, the hot element will ignite the cool element during chemical reaction, the left side is the hot side with high temperature is the ignition source and it is to ignite the right side which is the cool side with a lower temperature.

Table 6.5: Reacting Species considered

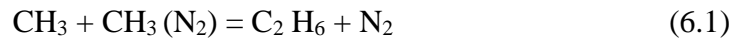
| S/No. | Reacting Species | Temperature | | Elements Count | | | | | |
|-------|-------------------------------|-------------|------|----------------|---|---|---|----|----|
| | | Low | High | H | C | O | N | Ar | He |
| 1 | C ₃ H ₈ | 300 | 5000 | 8 | 3 | 0 | 0 | 0 | 0 |
| 2 | O ₂ | 300 | 5000 | 0 | 0 | 2 | 0 | 0 | 0 |
| 3 | N ₂ | 300 | 5000 | 0 | 0 | 0 | 2 | 0 | 0 |
| 4 | H | 300 | 5000 | 1 | 0 | 0 | 0 | 0 | 0 |
| 5 | H ₂ | 300 | 5000 | 2 | 0 | 0 | 0 | 0 | 0 |
| 6 | O | 200 | 6000 | 0 | 0 | 1 | 0 | 0 | 0 |
| 7 | OH | 200 | 3500 | 1 | 0 | 1 | 0 | 0 | 0 |
| 8 | H ₂ O | 300 | 5000 | 2 | 0 | 1 | 0 | 0 | 0 |
| 9 | CO | 300 | 5000 | 0 | 1 | 1 | 0 | 0 | 0 |
| 10 | HCO | 300 | 5000 | 1 | 1 | 1 | 0 | 0 | 0 |
| 11 | CO ₂ | 300 | 5000 | 0 | 1 | 2 | 0 | 0 | 0 |
| 12 | CH ₃ | 300 | 5000 | 3 | 1 | 0 | 0 | 0 | 0 |
| 13 | CH ₂ O | 300 | 5000 | 2 | 1 | 1 | 0 | 0 | 0 |
| 14 | C ₂ H ₄ | 300 | 5000 | 4 | 2 | 0 | 0 | 0 | 0 |
| 15 | C ₂ H ₅ | 300 | 5000 | 5 | 2 | 0 | 0 | 0 | 0 |

Table 6.6: Reactions considered ($K = AT^b e^{-(E_a/RT)}$)

| S/No | Reactions | E (J/mol) | A (mole-cm-sec-k) | b |
|------|---|-----------|-------------------------|------|
| 1 | HCO + OH = CO + H ₂ O | 0.0 | 1.00 x 10 ¹⁴ | 0.0 |
| 2 | OH + CO = H + CO ₂ | -765.0 | 1.50 x 10 ⁷ | 1.3 |
| | Reverse Arrhenius Coefficients: | 21,580.0 | 1.68 x 10 ⁹ | 1.3 |
| 3 | H + O ₂ = O + OH | 16,790.0 | 1.86 x 10 ¹⁴ | 0.0 |
| | Reverse Arrhenius Coefficients: | 677.0 | 1.48 x 10 ¹³ | 0.0 |
| 4 | H ₂ + O = H + OH | 8,900.0 | 1.80 x 10 ¹⁰ | 1.0 |
| | Reverse Arrhenius Coefficients: | 6,950.0 | 1.83 x 10 ⁹ | 1.0 |
| 5 | O + H ₂ O = OH + OH | 18,350.0 | 6.80 x 10 ¹³ | 0.0 |
| | Reverse Arrhenius Coefficients: | 1,100.0 | 6.30 x 10 ¹² | 0.0 |
| 6 | H + H ₂ O = OH + H ₂ | 20,300.0 | 9.50 x 10 ¹³ | 0.0 |
| | Reverse Arrhenius Coefficients: | 5,146.0 | 2.20 x 10 ¹³ | 0.0 |
| 7 | HCO + M = H + CO + M | 19,000.0 | 1.45 x 10 ¹⁴ | 0.0 |
| | Reverse Arrhenius Coefficients: | 1,553.0 | 5.05 x 10 ¹¹ | 1.0 |
| 8 | C ₂ H ₄ + O = CH ₃ + HCO | 1,130.0 | 3.30 X 10 ¹² | 0.0 |
| 9 | C ₂ H ₅ + M = C ₂ H ₄ + H + M | 30,000.0 | 2.00 X 10 ¹⁵ | 0.0 |
| 10 | H ₂ O + M = H + OH + M | 105,000.0 | 2.20 x 10 ¹⁶ | 0.0 |
| | Reverse Arrhenius Coefficients: | 0.0 | 1.40 x 10 ²³ | -2.0 |
| 11 | CO ₂ + M = CO + O + M | 131,800.0 | 5.50 x 10 ²¹ | -1.0 |
| | Reverse Arrhenius Coefficients: | 4,100.0 | 5.90 x 10 ¹⁵ | 0.0 |
| 12 | CO ₂ + O = CO + O ₂ | 43,830.0 | 2.78 x 10 ¹² | 0.0 |
| | Reverse Arrhenius Coefficients: | 37,600.0 | 3.14 x 10 ¹¹ | 0.0 |
| 13 | HCO + H = CO + H ₂ | 0.0 | 2.00 x 10 ¹⁴ | 0.0 |
| | Reverse Arrhenius Coefficients: | 90,000.0 | 1.31 x 10 ¹⁵ | 0.0 |
| 14 | O + HCO = CO + OH | 0.0 | 1.00 x 10 ¹⁴ | 0.0 |
| 15 | CH ₂ O + M = HCO + H + M | 81,000.0 | 3.30 x 10 ¹⁶ | 0.0 |
| 16 | CH ₂ O + OH = HCO + H ₂ O | 170 | 7.50 x 10 ¹² | 0.0 |
| 17 | CH ₂ O + H = HCO + H ₂ | 10,500.0 | 3.30 x 10 ¹⁴ | 0.0 |
| | Reverse Arrhenius Coefficients: | 25,170.0 | 2.64 x 10 ¹³ | 0.0 |
| 18 | CH ₂ O + O = HCO + OH | 4,600.0 | 5.00 x 10 ¹³ | 0.0 |
| 19 | CH ₃ + OH = CH ₂ O + H ₂ | 0.0 | 4.00 x 10 ¹² | 0.0 |
| 20 | CH ₃ + O = CH ₂ O + H | 2,000.0 | 1.30 x 10 ¹⁴ | 0.0 |
| 21 | OH + M = O + H + M | 103,700.0 | 8.00 x 10 ¹⁹ | -1.0 |
| | Reverse Arrhenius Coefficients: | 0.0 | 1.00 x 10 ¹⁶ | 0.0 |
| 22 | H + H + M = H ₂ + M | 0.0 | 3.00 x 10 ¹⁵ | 0.0 |

| Reactions considered contd. | | | | |
|-----------------------------|-------------------------------|----------|-----------------------|------|
| 23 | $C_2H_4 + OH = CH_3 + CH_2O$ | 956.0 | 2.00×10^{12} | 0.0 |
| 24 | $C_2H_5 + M = C_2H_4 + H + M$ | 0.0 | 4.9×10^{19} | -2.0 |
| | H ₂ | Enhanced | 2.000 | |
| | H ₂ O | Enhanced | 6.000 | |
| | CO | Enhanced | 1.500 | |
| | CO ₂ | Enhanced | 2.000 | |

Generally, a chemical reaction has 1 or 2 species as reactants and produces 1 or 2 products. When reactions are in fall-off regions, however, the pressure effect in the kinetics is necessarily considered and third-party species are involved which attack other molecules, not participating in the reaction and only exchanging the momentum. The third-party species can be all the species in the mixture. While the reaction is enhanced, the third-party species are not all the species, but particularly specified. E.g., noble gases like He and Ar.



Only N₂ is the enhanced concentration.

6.3 Effects of Geometric configurations of H₂-O₂ combustion reactions

(a) Summary of Results of 3 cases by geometric configurations on H₂-O₂ combustion

Table 6.7: Effects of geometric configuration on H₂-O₂ combustion (see Appendix 4)

| Case Studies | Time range (sec) x 10 ⁻⁴ | Temperature Range (K) | Fuel concentration range (%) x 10 ⁻⁴ | Flame Speed (m/s) | | | |
|--------------|-------------------------------------|-----------------------|---|-------------------|-----|-----|------|
| | | | | SF | FD | DDT | DD |
| Block | 0.00-0.68 | 300 – 3839 | 0.00 – 83.29 | 0 | 250 | 450 | 2690 |
| Step | 0.00-0.06 | 300 – 3789 | 0.00 – 82.79 | 0 | - | - | 2750 |
| Wall | 0.00-0.02 | 300 – 3600 | 0.00 – 51.59 | 0 | - | - | 3000 |

From Table 6.7 above, the influences and effects of geometric configuration on explosion due to H₂-O₂ combustion reaction processes were investigated and it was observed that as the concentration of the chemical species increases, the temperature also increases, and this will cause an increase to the flame velocity and detonation will result which will consequently lead to explosion. Moreover, for closed end tube such as that of case study Block reaction studied in this work, the block constitutes an artificial obstacle, hence, FD, DDT, and detonation were formed. However, no DDT and no FD were formed for case studies step and wall, the wall has influence because

the wall and the step as artificial obstacles will block the gas and thus the gas will become hot and expand, hence the ignition process will move straight to detonation, this is a single explosion, and it is direct initiation. Therefore, no FD and no DDT were formed for case studies step, and wall.

(b) Effects and influences of geometrical configuration on H₂-O₂ combustion reaction

1) Case study Block

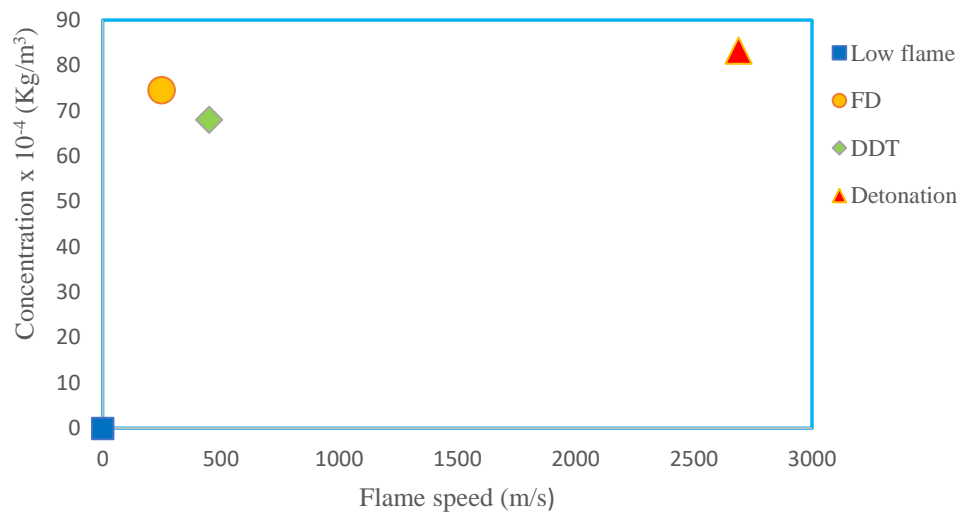


Figure 6.6: Concentration (kg/m³) against flame speed (m/s) for case study Block

2) Case study Step

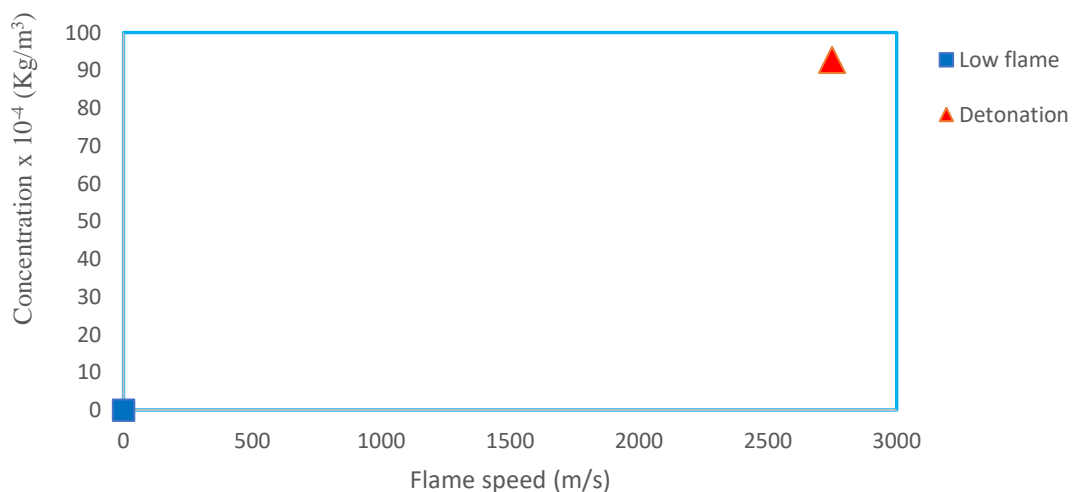


Figure 6.7: Concentration (kg/m³) against flame speed (m/s) for case study Step

3) Case study Wall

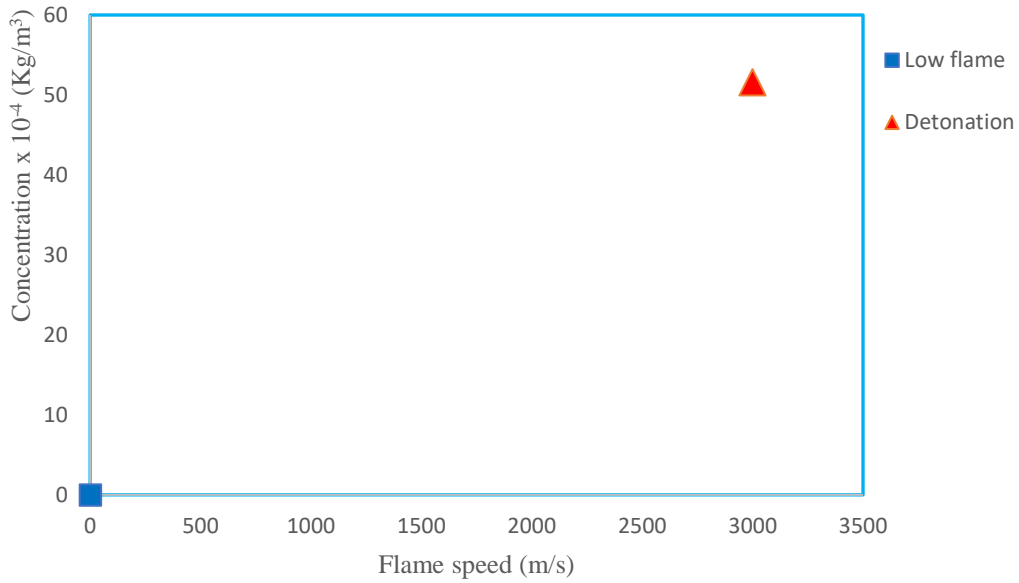
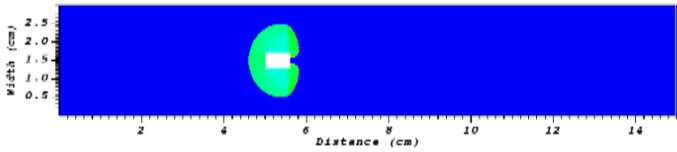
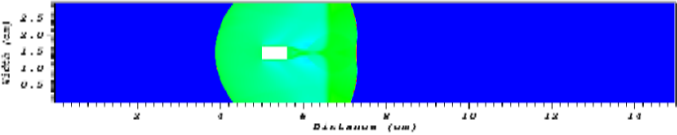
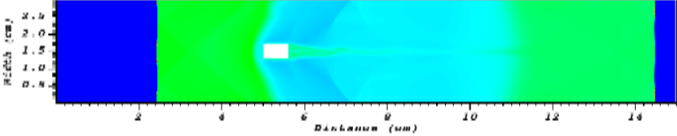
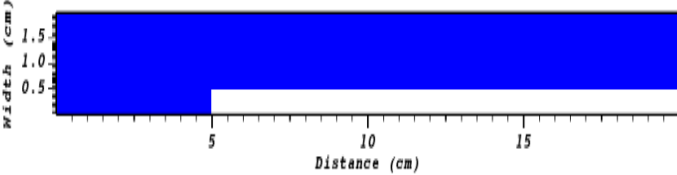
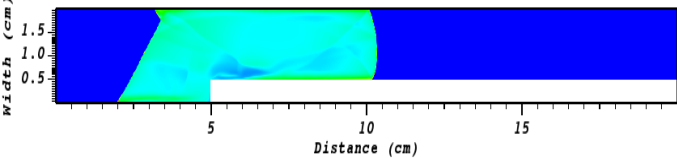
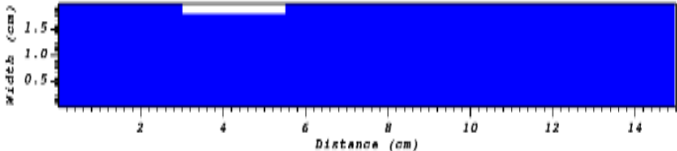
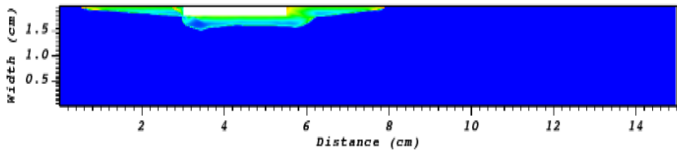


Figure 6.8: Concentration (kg/m³) against flame speed (m/s) for case study Wall

A close look at the influences and effects of geometric configuration on H₂-O₂ combustion reactions on case studies Block, Step, and Wall on Figures 6.6, 6.7, and 6.8 showed that a high delay of induction time was observed. It was found that the geometrical configuration has influence and effects on the combustion reactions of hydrogen oxygen reactions. It was also observed that even at the initial stage of the reaction, owing to different artificial obstacle in position of the tube, the geometrical effects on H₂-O₂ reaction process were quite different. For example, for case study Block, FD and DDT as well detonation was formed, however for case studies Step and Wall, no FD and DDT were formed, but the ignition process moves straight to detonation thereby forming single explosion.

Table 6.8: Effects of geometric configuration on H₂-O₂ reaction of case studies Block, step and wall

| Case Studies | Reactions | Flame development |
|--------------|-----------|-------------------|
| Block | LF | |

| | | Flame development contd. |
|------|-----|---|
| | FD |  <p>A 2D plot showing the initial flame development. The y-axis is labeled 'Width (cm)' with values 0.5, 1.0, 1.5, 2.0, 2.5. The x-axis is labeled 'Distance (cm)' with values 2, 4, 6, 8, 10, 12, 14. A small, bright, circular flame kernel is visible at approximately 5 cm distance and 1.5 cm width.</p> |
| | DDT |  <p>A 2D plot showing the flame development at the Deflagration-to-Detonation Transition (DDT). The axes are the same as in the FD plot. The flame kernel has significantly increased in size and is now elongated, with a bright core and a surrounding luminous region.</p> |
| | DD |  <p>A 2D plot showing the flame development at the Detonation stage (DD). The axes are the same. The flame has become a long, narrow, high-speed detonation wave traveling through the channel, with a very bright, narrow core.</p> |
| Step | LF |  <p>A 2D plot showing the flame development for a Step geometry. The y-axis is labeled 'Width (cm)' with values 0.5, 1.0, 1.5. The x-axis is labeled 'Distance (cm)' with values 5, 10, 15. A flame kernel is visible at approximately 5 cm distance, showing a step-like profile.</p> |
| | DD |  <p>A 2D plot showing the flame development for a Step geometry at the Detonation stage. The axes are the same as in the LF plot. The flame has become a long, narrow, high-speed detonation wave traveling through the channel, with a very bright, narrow core.</p> |
| Wall | LF |  <p>A 2D plot showing the flame development for a Wall geometry. The y-axis is labeled 'Width (cm)' with values 0.5, 1.0, 1.5. The x-axis is labeled 'Distance (cm)' with values 2, 4, 6, 8, 10, 12, 14. A flame kernel is visible at approximately 5 cm distance, showing a wall-like profile.</p> |
| | DD |  <p>A 2D plot showing the flame development for a Wall geometry at the Detonation stage. The axes are the same as in the LF plot. The flame has become a long, narrow, high-speed detonation wave traveling through the channel, with a very bright, narrow core.</p> |

Carefully considering the summary of the AMROC simulation result pictures on Table 6.8 for case studies Block, step, and wall presented a beautiful explanation with the graphical presentation that flame propagation takes place at various locations because of different geometric configurations. Moreover, the simulation picture colours on Table 6.8 in Section 6.3 for case studies Block, step, and wall of H₂-O₂ chemical reactions reveal that the blue locations stand for minimum concentration; and the light green represent maximum volume of concentration. This is just for the operation of VISIT programme. In addition, the flame fronts of the pictures of the different combustion forms obtained showed that for detonation, the flame front is sharp because it is a very fast detonation and boundary layer effect is very small and flame front move along, but for DDT, its flame front is pointed due to its instability, boundary layer effect and numerical error due to computer capability; and for laminar flame, it is very viscous. However, the effects of the geometric configuration of step and wall on explosion were also obvious.

(c) Summary Results of 3 case studies by geometric configurations on H₂-O₂ combustion reactions

Table 6.9: Effects of geometric configuration with vent on H₂-O₂ combustion process(see Appendix5)

| Case Studies - Reactions | Time range (sec) x 10 ⁻⁴ | Temperature Range (K) | Fuel concentration range (%) x 10 ⁻⁴ | Flame Speed (m/s) | | | |
|--------------------------|-------------------------------------|-----------------------|---|-------------------|-----|-----|------|
| | | | | SF | FD | DDT | DD |
| A | 0.00 – 2.20 | 2250 – 4011 | 0.00 – 89.7 | 0 | 170 | 470 | 2800 |
| B | 0.00 – 2.65 | 2250 – 3735 | 0.00 – 87.05 | 0 | 250 | 450 | 2710 |
| C | 0.00 – 6.65 | 2000 – 3689 | 0.00 – 72.91 | 0 | 280 | 480 | 2650 |

Table 6.9 above showed that the influences and effects of geometric configuration on explosion due to H₂-O₂ combustion reaction processes were obvious, and it was observed for each case study of the case studies A, B, and C, the concentration of the chemical reacting species increases with increase in temperature and therefore, DDT and detonation will be formed, and more heat release rate is produced. In this research, vent is created in the tube, and if there is no vent, there will be no explosion, and this is because the burnt wave is deflagration and not detonation. Hence, when vent is created in the tube, DDT will occur and consequently detonation is achieved, and vent explosion will take place. The simulated results agreed with the principles of the effects of complex geometry on explosion.

(d) Effects and influences of Geometric configurations on H₂-O₂ combustion reactions

4) Case study A

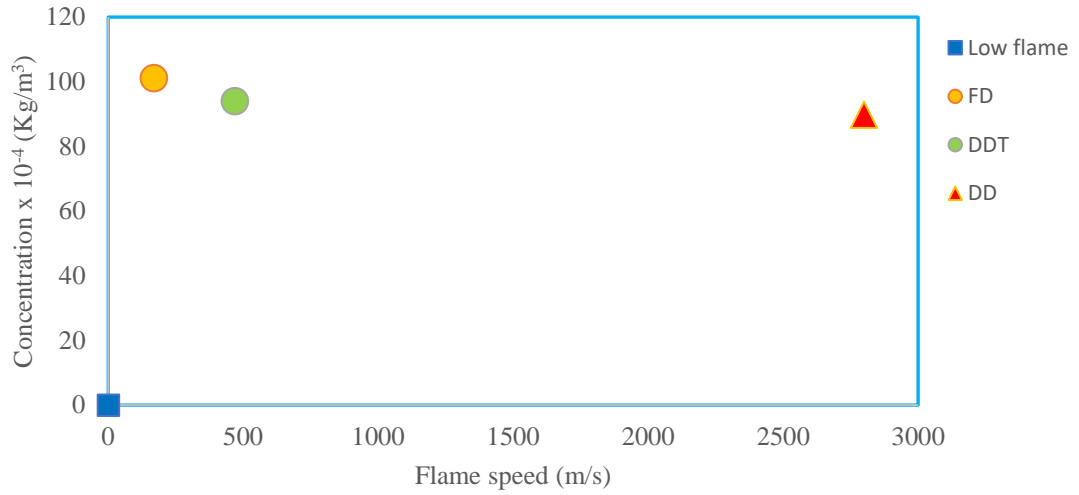


Figure 6.9: Concentration (kg/m³) against flame speed (m/s) for case study A

5) Case study B

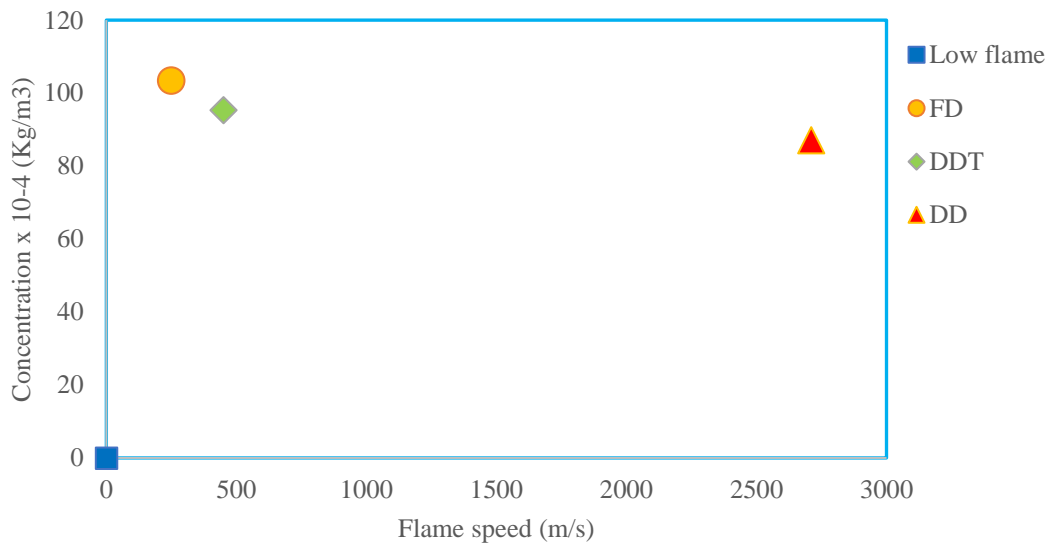


Figure 6.10: Concentration (kg/m³) against flame speed (m/s) for case study B

6) Case study C

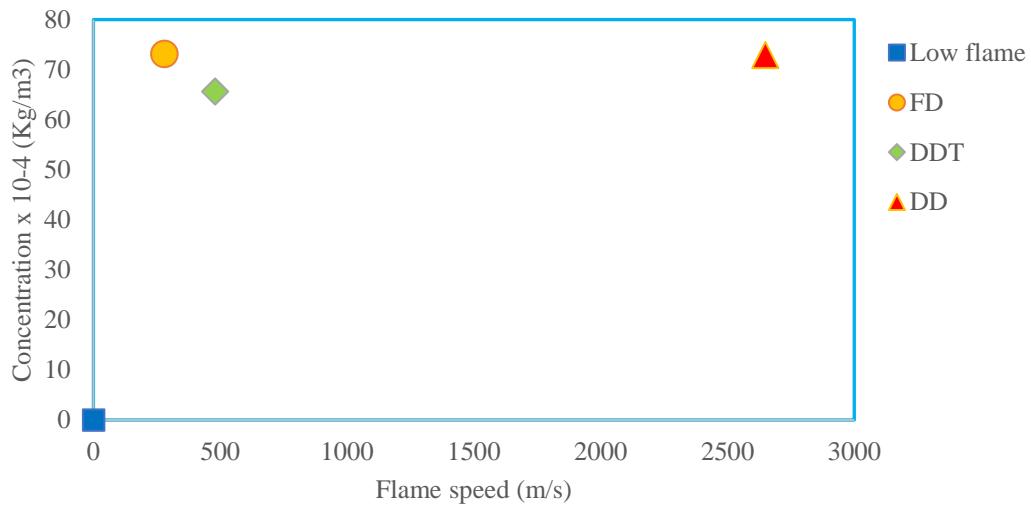


Figure 6.11: Concentration (kg/m³) against flame speed (m/s) for case study C

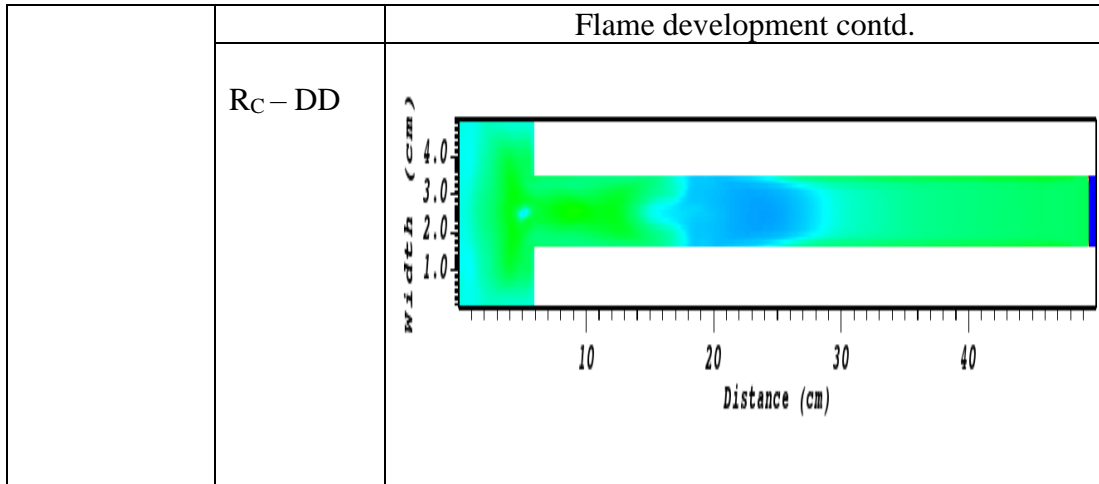
A close examination of the influences and effects of geometric configuration on H₂-O₂ combustion reactions on case studies A, B, and C on Figures 6.9, 6.10, and 6.11 showed that a sudden increase in concentration of the chemical reacting species which indicates that more heat will be produced and thus DDT and detonation were observed for case studies A, B, and C.

Table 6.10: Effects of geometric configuration on combustion of case studies A, B, and C.

| Case studies | Reactions | Flame development |
|--------------|---------------------|-------------------|
| | R _A – LF | |
| | R _A – FD | |

| | | Flame development contd. |
|--|-------------|--------------------------|
| | $R_A - DDT$ | |
| | $R_A - DD$ | |
| | $R_B - LF$ | |
| | $R_B - FD$ | |
| | $R_B - DDT$ | |

| | | Flame development contd. |
|--|-------------|--------------------------|
| | $R_B - DD$ | |
| | $R_C - LF$ | |
| | $R_C - FD$ | |
| | $R_C - DDT$ | |



A close look at Table 6.10 above showed that the influences and effects of geometric configuration on explosion due to H₂-O₂ combustion reaction processes were evident. From Table 6.10 above, the AMROC simulation result pictures for this work is unique for supporting the explanation presented by the graphical presentation that flame propagation takes place at various locations because of the vent created. Moreover, the simulation picture colours on Table 6.8 in Section 6.3 for case studies A, B, and C of H₂-O₂ reaction indicate that the blue locations represent zero concentration; and the light green shows largest volume of concentration. This is just for the operation of VISIT programme. In addition, the flame fronts of the pictures of the different combustion forms formed showed that for detonation, the flame front is flat/sharp because it is a very fast detonation and boundary layer effect is very small and flame front move along, but for laminar flame, it is very tenacious.

(e) Summary Results of 6 case studies by geometric effects during propane combustion

Table 6.11: Effects of geometric configuration with oneblock on propane combustion (see Appendix 6)

| Case Studies | Time range (sec) x 10 ⁻⁴ | Temperature range (K) | Fuel Conc, range (%) x 10 ⁴ | Flame Speed (m/s) | | | |
|---------------|-------------------------------------|-----------------------|--|-------------------|-----|-----|------|
| | | | | LF | FD | DDT | DD |
| Reactions: 20 | 0.00 – 8.0 | 3000 – 3619 | 0.00 – 31.04 | 0 | 300 | 420 | - |
| 21 | 0.00 – 11.5 | 2500 – 3351 | 0.00 – 30.62 | 0 | 240 | 410 | - |
| 30 | 0.00 – 4.9 | 3000 – 4364 | 0.00 – 53.89 | 0 | 230 | 440 | 2670 |
| 30x | 0.00 – 4.9 | 3000 – 4364 | 0.00 – 53.89 | 0 | 300 | 480 | 1200 |
| 31 | 0.00 – 9.55 | 2500 – 4334 | 0.00 – 54.99 | 0 | 300 | 480 | 2970 |
| 31x | 0.00 – 9.55 | 2500 – 4208 | 0.00 – 47.12 | 0 | 280 | 450 | 2580 |

Table 6.11 in Section 6.3 showed the effects and influences of geometric configuration on propane combustion concentration of the chemical species were evident, and it was observed that as concentration increases, the temperature also increases, and this will cause an increase to the flame velocity and detonation will result which will consequently lead to explosion. Moreover, for closed end tube such as that of case study with oneBlock, the block would constitute an artificial obstacle, hence, FD, DDT, and detonation were formed. When shock tube is without block(s), DDT might occur at 60cm, whereas when oneblock is in shock tube, DDT could occur at 27cm, and this is because the block stands as an obstacle. Therefore, this implies that the more the number of blocks in the tube, the more the effect of the blocks on the position of the DDT and Detonation, and consequently the explosion.

(f) Effects and influences of geometrical configuration on propane combustion reactions

7) Case study R₂₀

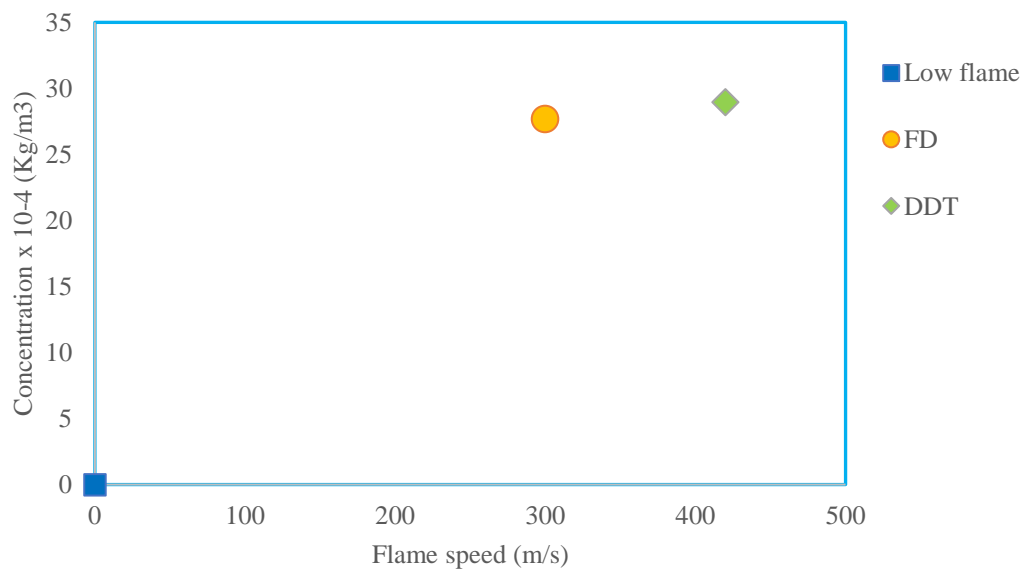


Figure 6.12: Concentration (kg/m³) of propane against flame speed (m/s) for case study R₂₀

8) Case study R₂₁

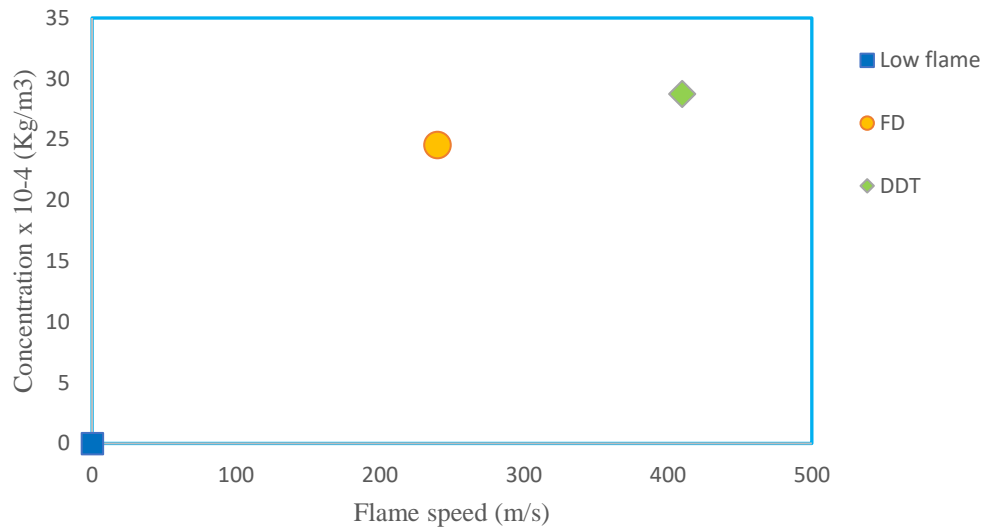


Figure 6.13: Concentration (kg/m³) of propane against flame speed (m/s) for case study R₂₁

9) Case study R₃₀

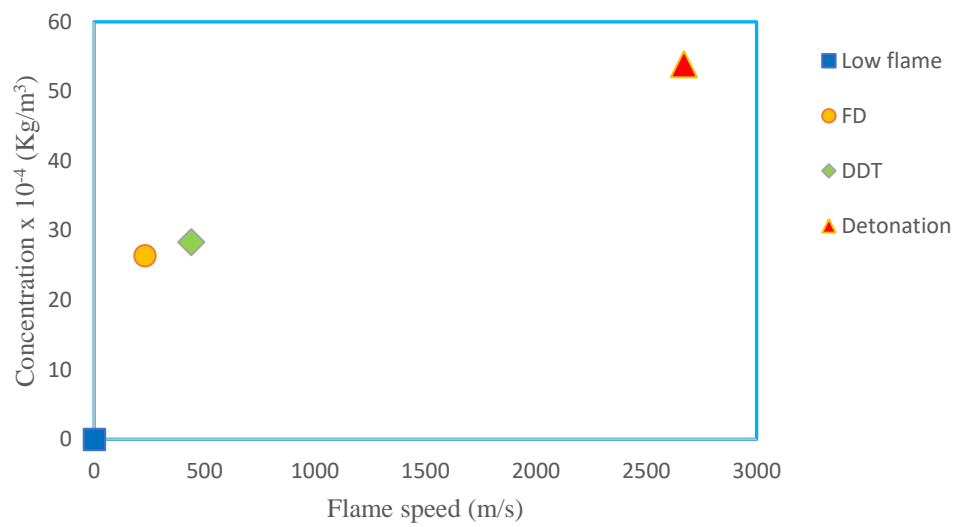


Figure 6.14: Concentration (kg/m³) of propane against flame speed (m/s) for case study R₃₀

10) Case study R_{30x}

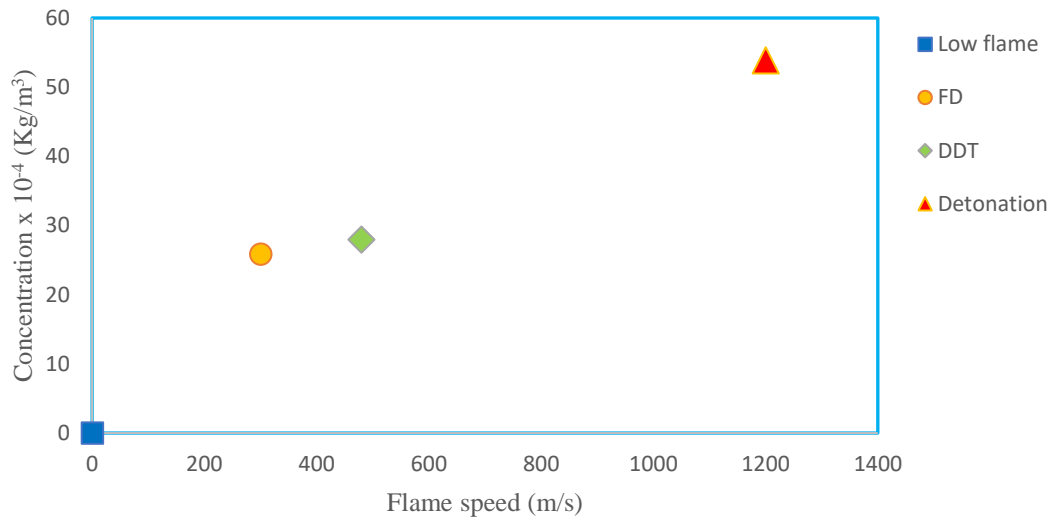


Figure 6.15: Concentration (kg/m³) of propane against flame speed (m/s) for case study R_{30x}

11) Case study R₃₁

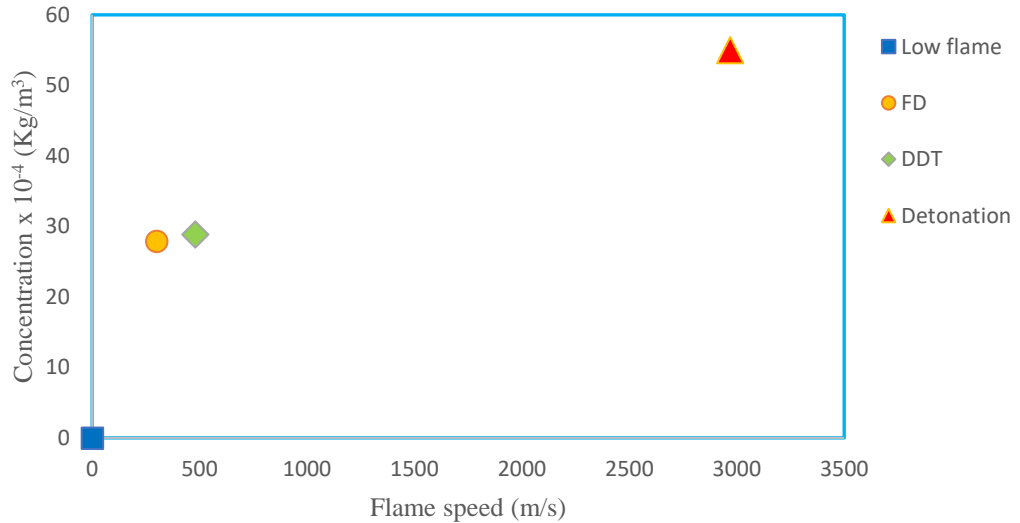


Figure 6.16: Concentration (kg/m³) of propane against flame speed (m/s) for case study R₃₁

12) Case study R_{31X}

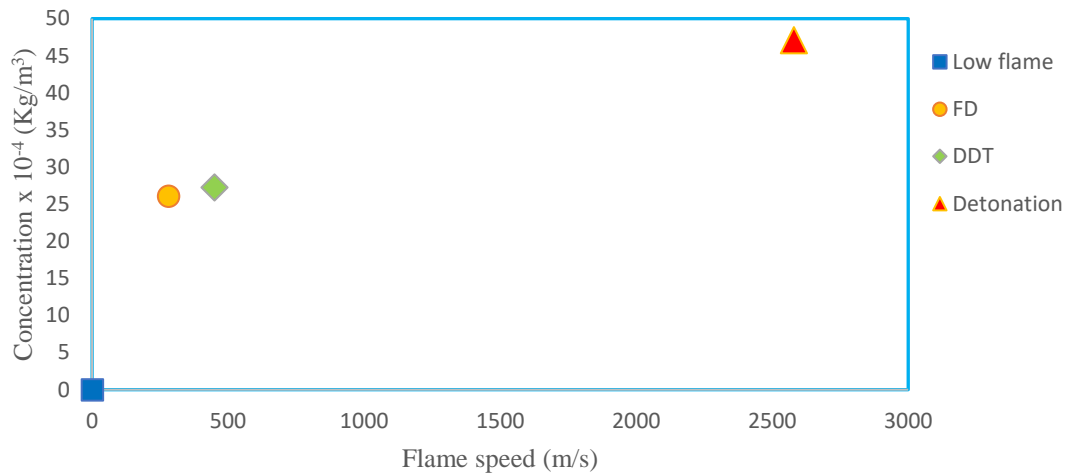
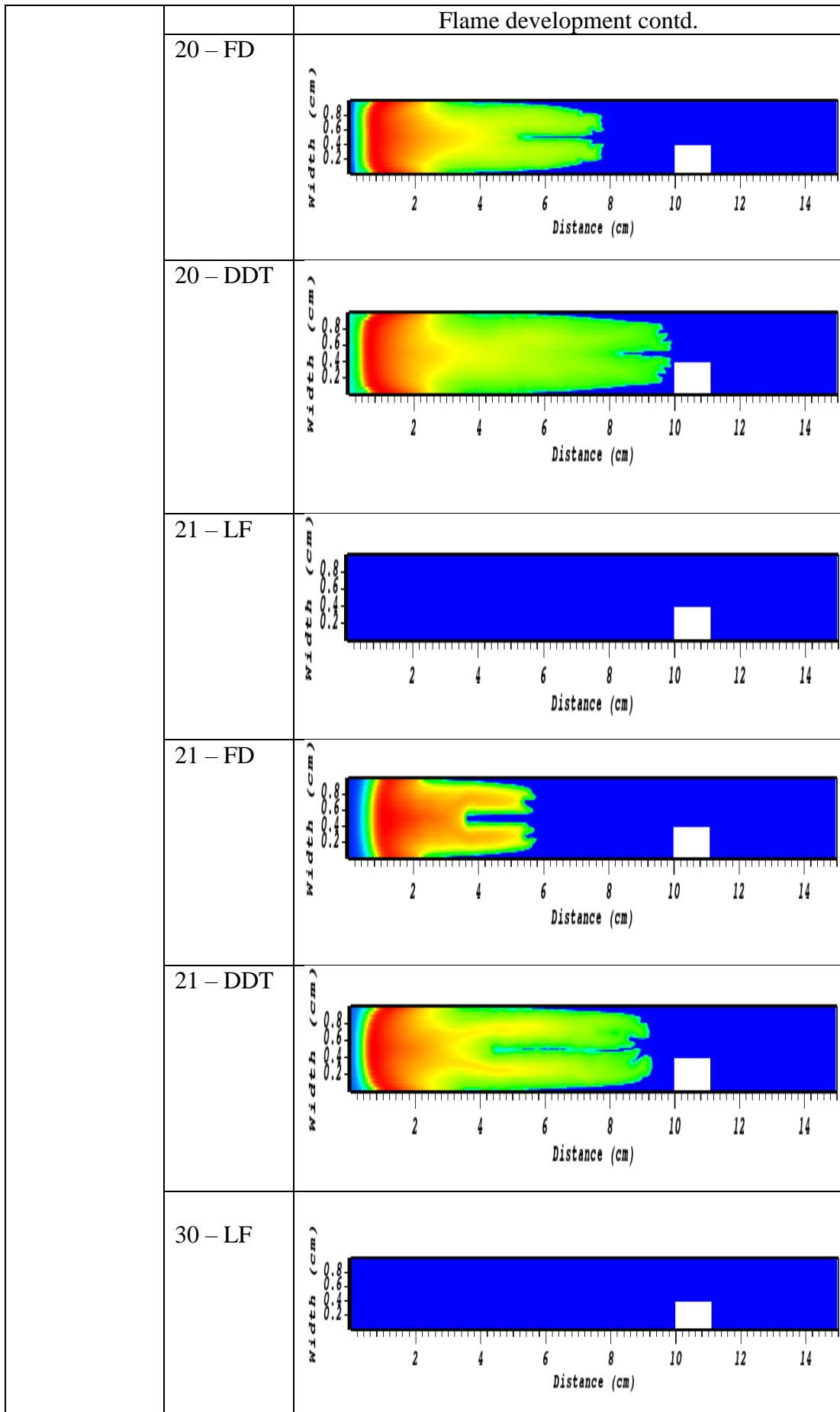


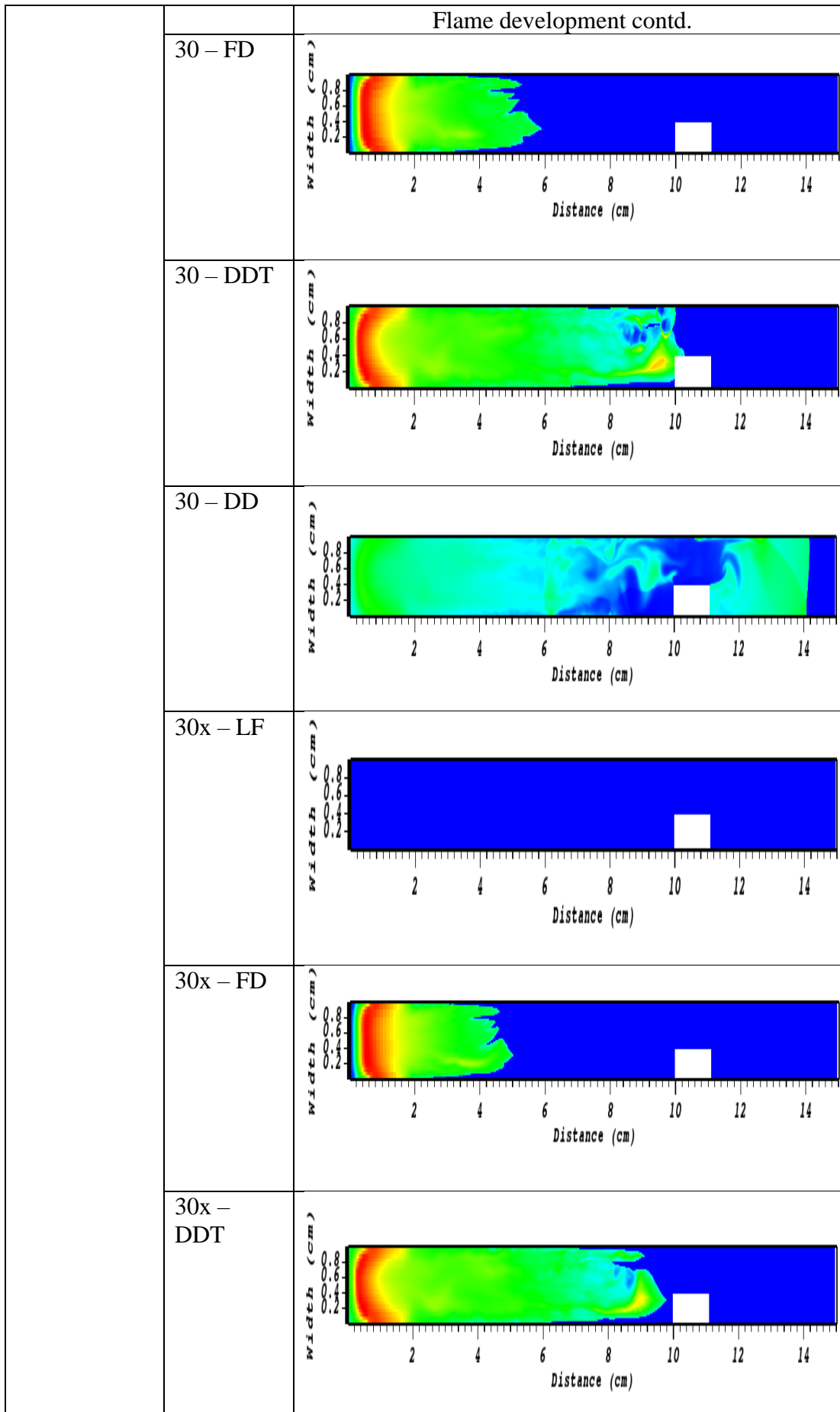
Figure 6.17: Concentration (kg/m³) of propane against flame speed (m/s) for case study R_{31X}

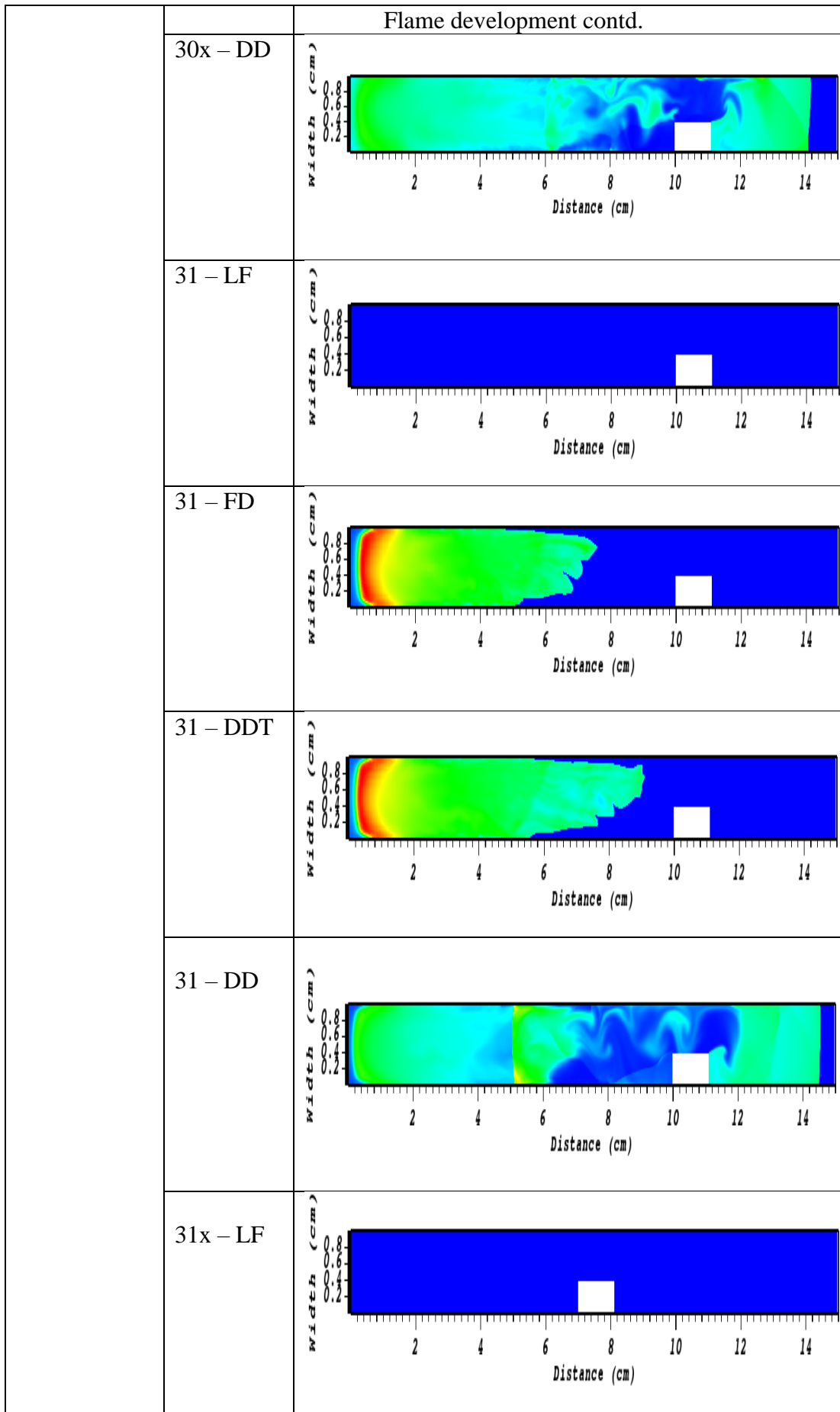
From Figures 6.12, 6.13, 6.14, 6.15, 6.16 and 6.17 above, it showed that the effects and influences of geometric configuration on explosion due to oneblock were evident and it showed that in each case study, as the concentration increases, the flame velocity increases. Moreover, the simulation results for case studies 20, 21, 30, 30X, 31 and 31X showed that the ignition occurs forming FD, DDT, and Detonation for case studies 30, 30X, 31 and 31X except for case studies 20, and 21 that formed FD and DDT only. A good comparison of the effects and influences of simulation results of case studies 20, and 21 showed that there was no Detonation formed, but concerning that of case studies 30, 30X, 31 and 31X, there was quantum jump from DDT to Detonation, hence, fast detonation occurred, and explosion suddenly resulted.

Table 6.12: Effects of geometric configuration on propane of case studies 20, 21, 30, 30x, 31, 31x

| Case Studies | Reactions | Flame development |
|--------------|-----------|-------------------|
| Propane | 20 – LF | |







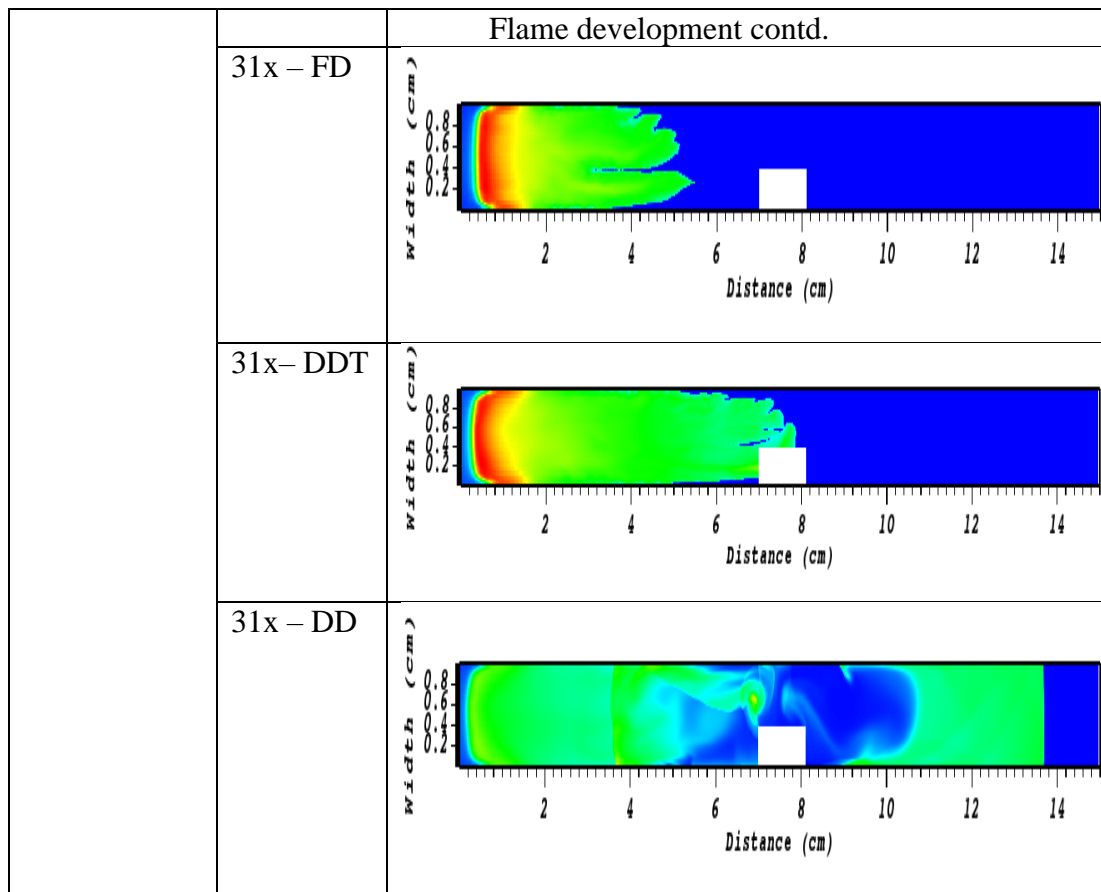


Table 6.12 above showed that the influences and effects of geometric configuration on explosion due to propane combustion reaction processes were observed. From Table 6.12 above, the AMROC simulation result pictures for case studies 20, 21, 30, 30x, 31, and 31x showed a very brilliant explanation with the graphical presentation that flame propagation takes place at various locations because of varied geometric configuration. Moreover, the simulation picture colours on Table 6.12 above for case studies 20, 21, 30, 30x, 31, and 31x of propane reveal that the blue locations represent zero concentration: and the light green shows maximum greatest concentration. This is just for the operation of VISIT programme. In addition, the flame fronts of the pictures of the different combustion forms obtained showed that for detonation, the flame front is sharp because it is a very fast detonation and boundary layer effect is very small and flame front move along, but for DDT, its flame front is pointed due to its instability, boundary layer effect and numerical error due to computer capability; and for laminar flame, it is very viscous.

6.4 Brief Summary

Chapter 6 investigated the influences and effects of complex geometric configuration on explosions. To this background, two premixed gaseous combustibles: - hydrogen-oxygen and propane-oxygen were selected and filled into two-dimensional tube domains, then the mixtures are ignited. Furthermore, this chapter has carefully determined the effects and the influences of complex geometric configuration on explosion due to the combustion reactions of hydrogen-oxygen and propane-oxygen reactions. The layout of this chapter is logically arranged to cover the sections: (1) the effects of complex geometric configuration on H₂-O₂ combustion reactions for case studies block, step, and wall; (2) the effects of complex geometric configuration on H₂-O₂ combustion reactions for case studies A, B, and C using vent; and (3) the effects of complex geometric configuration on propane-oxygen combustion reactions for case studies 20, 21, 30, 30x, 31, and 31x using oneBlock. The results obtained showed that complex geometric configuration has influences and effects on hydrogen-oxygen and propane oxygen reactions based on the case studies investigated. It was also observed that even at the initial stage of the reaction, owing to different artificial obstacle in position of the tube, the geometrical effects on H₂-O₂ reaction process were quite different. For example, for case study Block, FD, DDT and detonation were formed, however for case studies Step and Wall, no FD and no DDT were formed, but the ignition process moves straight to detonation thereby forming a single explosion. Also, for case studies block, step and wall species, it was observed that as the concentration of the chemical species increases, the temperature also increases, and this will cause an increase to the flame velocity and detonation will result which will consequently lead to explosion. Moreover, for closed end tube such as that of case study Block species studied in this work, the block constitutes an artificial obstacle, hence, FD, DDT, and detonation were formed. In addition, for case studies step and wall, the wall has influence because the wall and the step as artificial obstacles will block the gas and thus the gas will become hot and expand, hence the ignition process will move straight to detonation, this is a single explosion, and it is direct initiation. Therefore, no FD and no DDT were formed for case studies step, and wall species. Furthermore, for case studies A, B, and C, the concentration of the chemical reacting species increases with increase in temperature and therefore, DDT and detonation will be formed, and more heat release rate is produced. In this research, vent is created in the

tube, and if there is no vent, there will be no explosion, and this is because the burnt wave is deflagration and not detonation. Hence, when vent is created in the tube, DDT will occur and consequently detonation is achieved, and vent explosion will take place. The simulated results agreed with the principles of the effects of complex geometry on explosion. For case studies 20, 21, 30, 30x, 31, and 31x of propane using oneblock, it was noted that as the concentration of the chemical species increases, the temperature also increases, and this will cause an increase to the flame velocity and detonation will result which will consequently lead to explosion. Moreover, for closed end tube such as that of case study with one Block, the block would constitute an artificial obstacle, hence, FD, DDT, and detonation were formed. When shock tube is without block(s), DDT might occur at 60cm, whereas when one block is in shock tube, DDT could occur at 27cm, and this is because the block stands as an obstacle. Therefore, this implies that the more the number of blocks in the tube, the more the effect of the blocks on the position of the DDT and Detonation.

Chapter 7 Conclusions/Limitations/Recommendations

7.1 Conclusions

Computational Fluid Dynamics (CFD) is a tool able to predict and simulate complex physical and chemical courses, e.g., chemical explosions, movements of smoke and spreads of fires. They comprise numerous complicated physical and chemical interactions that include fluid dynamics, thermodynamics, combustion, radiation, or even multi-phase effects. CFD can produce more detailed results than experimental methods. It is particularly true to study chemical explosions because certain experimental conditions are more difficult to carry out at very fast combustions experimentally, but with numerical simulations, it is very possible. Using CFD approach, therefore, this work investigates the explosions produced by gas combustions.

Furthermore, this numerical simulation intends to attend to the problems posed by combustion waves in the petroleum tank farms through: (i) the initiation of combustion waves, (ii) the propagation of combustion waves, (iii) the transition of different forms of combustion waves, and (iv) the consequences of the combustion. The numerical simulation work showed that there are two parts, and they are: (a) the ignition stage of combustion waves, and (b) the flame development of the explosion waves. How can the above situation be achieved? In achieving the above, the combustion mixture is ignited by the application of an external energy input in the form of heat for substances like solids and liquids thereby breaking down the molecules in the fuel to form chemically reactive species called free radicals which then combine with the oxidizer. The research findings of my numerical simulation work proved that complex configurations have effects and influences on explosion of combustible reacting mixtures of hydrogen and propane studied in this research. This research work also revealed that chemical kinetics have influences and effects on explosion of reacting mixtures of hydrogen and propane. From the research results of this work obtained in line with the contributing effects and influences of kinetics and geometric configuration, the problems of explosions associated with tank farm operations can be prevented and thus make petroleum tank farm operations safe. Furthermore, the flame velocities in the open-tubes are usually not very high as those of the closed-end tubes, remarkably the maximum flame velocity. Moreover, the open-end tube supports flame retardation, but the closed end tube encourages flame acceleration. In the open-end

tube, there is no limited gas expansion, and the speed up is weak and thus no DDT is formed. In the closed-end tube, there is limited gas expansion, and the speed up is strong and hence DDT is achieved. Also, if there is no vent, there will be no explosion and this is because the burnt wave is deflagration and not detonation, but when there is vent created in the tube mode, DDT will occur and eventually detonation will take place and consequently explosion follows. During DDT, the flame is not uniform, hence, explosion will likely be formed.

The results obtained showed that chemical kinetics have effects and influences on the explosion based on the case studies investigated. However, no DDT and no FD were formed for case studies 2, 3, 4, and 5 and this was because it is an open-end tube and there is no limited gas expansion, and no artificial obstacle, and therefore, deflagration-to-detonation transition (DDT) and fast deflagration (FD) were not formed, but the ignition process moves straight to detonation, thus forming a single explosion. Comparing the different case studies of H_2-O_2 studied: a, b, c, d, and e showed that it was only case study e that formed detonation, DDT, and FD, and consequently explosion occurred, and that was because case study e had very high temperature. In addition, in comparing the case studies of the reactions of propane investigated, it showed that it was only case study 20 did not form detonation. However, the rest case studies 21, 30, 31 and 40 formed FD, DDT, and detonation flame forms, and this is because case studies 21, 30, 31 and 40 had high fuel concentration and high temperatures, and hence explosion occurred.

The results obtained showed that complex geometric configuration has influences and effects on hydrogen-oxygen and propane oxygen reactions based on the case studies investigated. It was also observed that even at the initial stage of the reaction, owing to different artificial obstacle in position of the tube, the geometrical effects on H_2-O_2 reaction process were quite different. For example, for case study Block, FD, DDT and detonation were formed, however for case studies Step and Wall, no FD and DDT were formed, but the ignition process moves straight to detonation thereby forming a single explosion. Also, for case studies block, step and wall species, it was observed that as the concentration of the chemical species increases, the temperature also increases, and this will cause an increase to the flame velocity and detonation will result which will consequently lead to explosion. Moreover, for closed end tube such as that of case study Block species studied in this work, the block constitutes an artificial obstacle, hence, FD, DDT, and detonation were formed. However, for case

studies step and wall, the wall has influence because the wall and the step as artificial obstacles will block the gas and thus the gas will become hot and expand, hence the ignition process will move straight to detonation, this is a single explosion, and it is direct initiation. Therefore, no FD and no DDT were formed for case studies step, and wall species. Furthermore, for case studies A, B, and C, the concentration of the chemical reacting species increases with increase in temperature and therefore, DDT and detonation will be formed, and more heat release rate is produced. In this research, vent is created in the tube, and if there is no vent, there will be no explosion, and this is because the burnt wave is deflagration and not detonation. Hence, when vent is created in the tube, DDT will occur and consequently detonation is achieved, and vent explosion will take place. The simulated results agreed with the principles of the effects of complex geometry on explosion [39]. For case studies 20, 21, 30, 30x, 31, and 31x of propane using oneblock, it was noted that as the concentration of the chemical species increases, the temperature also increases, and this will cause an increase to the flame velocity and detonation will result which will consequently lead to explosion. Moreover, for closed end tube such as that of case study with one Block, the block would constitute an artificial obstacle, hence, FD, DDT, and detonation were formed. When shock tube is without block(s), DDT might occur at 60cm, whereas when one block is in shock tube, DDT could occur at 27cm, and this is because the block stands as an obstacle. Therefore, this implies that the more the number of blocks in the tube, the more the effect of the blocks on the position of the DDT and Detonation

7.2 Limitations of this research work

- 1) This research work will investigate absolutely the mechanisms and consequences of explosions in Petroleum Storage tank farms by detailed chemical kinetics using CFD Simulations.
- 2) According to the previous works of NUREG-1824, there has been no petroleum gas chemical kinetics programme in AMROC, and thus a new programme involving petroleum gas kinetics in AMROC was generated in this work.
- 3) Certainly, this dissertation research work was not able to cover all the available methods of simulating the kinetics of petroleum gas in petroleum storage tank farm operations.

- 4) On this background, the utilisation of the research findings obtained from the design of this study and or the methods used to establish internal and external validity is not certain.
- 5) In addition, there are no similar experimental data to judge the dissertation results of the AMROC simulation against for purpose of comparison.

7.3 Recommendations for the future researches

A general overview of an investigation into mechanism and consequences of explosions in Petroleum Storage Tank Farm Operations in the Oil and Gas Industries showed that there are many virgin areas yet to explore to making tank farm operations adequately safe. Moreover, AMROC software tool was employed in studying the numerical simulation of the chemical kinetics of hydrogen-oxygen and hydrocarbon gases detailing on the deflagration to detonation transitions as major factors contributing to tank farm incidents in order to attain viable, reliable and dependable results useful for good analysis should of necessity be considered. Other CFD software useful for simulating the kinetics of such gases include:

- (i) ANSYS CFX Software
- (ii) ANSYS Fluent Software
- (iii) Salome Software

Also, other variables that can equally be studied include:

- (a) Smoke visibility
- (b) Flame height
- (c) Natural factors like earthquake, tornado, hurricane etc.
- (d) Simulating tank diameters greater than 10 metres and above.
- (e) Simulating varied tank heights
- (f) A mesh size of 8,000,000 cells and above
- (g) Other variables of fire spread such as conduction, convection etc.

In addition, other researchers to use 3D for simulation.

References

- [1] M. H. Abbasi, E. Benhela and Arshad Ahmadi, "Designing an Optimal Safe Layout for a Fuel Storage Tanks Farm: Case study of Jaipur Oil Depot," *International Journal of Chemical, Molecular, Nuclear Materials and Metallurgical Engineering*, vol. 8, no. 2, pp. 147-155, 2014.
- [2] Society of Fire Protection Engineering, SFPE Handbook of Fire Protection Engineering, 18th edition ed., New York: Springer Publishers, 2016.
- [3] L. H. Ferguson and C. A. Janicak, Fundamentals of Fire Protection for the Safety Professional, First edition ed., USA: Government Institutes: An imprint of The Scarecrow Press Inc, 2005.
- [4] I. Glassman, R. A. Yetter and N. G. Glumac, Combustion, London: Elsevier Inc., 2015.
- [5] P. E. Ross, "Fire Prevention: A guide to protecting employees and property," *Journal of professional safety*, vol. 56, no. 10, pp. 62-69, 2011.
- [6] H. Ji, F.-S. Lien and E. Yee, "A new adaptive mesh refinement data structure with an application to detonation," *Journal of computational physics*, vol. 229, pp. 8981-8993, 2010.
- [7] W. Liu and G. Makhviladze, "An implicit finite element solution of thermal flows at low Mach number," *Journal of computational physics*, vol. 227, pp. 2743-2757, 2008.
- [8] L. Cai and H. Pitsch, "Optimized chemical mechanism for combustion of gasoline surrogate fuels," *Journal of combustion and flame*, vol. 162, pp. 1623-1637, 2015.
- [9] W. Atherton and J. W. Ash, "Review of failure, causes and consequences in the bulk storage industry," HSE Research Report 333, UK, 2005.

- [10] Nairametrics, ""Nigeria's explosions timeline from 21st March 2019 to 11th October 2022," 11 October 2020. [Online]. Available: <https://nairametrics.com >2020/10/10> nigerias-explosions-timeline-from-2019>. [Accessed 15 June 2022].
- [11] Buncefield Investigation, "http://www.buncefieldinvestigation.gov.uk/reports/," 2005. [Online]. Available: <http://www.buncefieldinvestigation.gov.uk/reports/index.htm>. [Accessed 23 July 2014].
- [12] API 2610, "Design, Construction, Operation, Maintenance and Inspection of Terminal and Tank Facilities," API Publishers, USA, 2000.
- [13] J. I. Chang and C.-C. Lin, "A Study of storage tank accidents," *Journal of Loss Prevention in the Process Industries*, vol. XIX, pp. 51-59, 2006.
- [14] D. Baraldi, A. G. Venetsanos, E. Papanikolaou and V. Dallas, "Numerical analysis of Release, Dispersion and Combustion of liquid hydrogen in a mock-up hydrogen refuelling stations," *Journal of Loss Prevention in the Process Industries*, vol. XXII, pp. 303-315, 2009.
- [15] G. Fu, J. Wang and M. Yan, "Analysis of Tianjin Port fire and explosion: Process and causes," *Journal of process safety progress*, vol. 35, no. 3, pp. 216-220, 2016.
- [16] C.-h. Chen, Yeong-Nain and H.-Y. Wang, "Case analysis of catastrophic underground pipeline gas explosion in Taiwan," *Journal of Engineering Failure Analysis*, vol. 65, pp. 39-47, 2016.
- [17] A. Bhusari, A. Goh, H. Ai, S. Sathanapally, M. Jalal and R. A. Mentzer, "Process safety incidents across 14 industries," *Journal of Process safety progress*, vol. 40, no. 1, 2021.
- [18] M. D. Kohler, A. Massari, T. H. Heaton, H. Kanamori, E. Hauksson, R. Gug, R. W. Clayton, J. Burn and K. M. Chandy, "Downtown Los Angeles 52-Story High-Rise and free-Field Response to Oil Refinery Explosion," *Journal of Earthquake Spectra*, vol. 32, no. 3, pp. 1793-1820, 2016.

- [19] M.-S. Sandulescu, "Sustainability reporting and impression management: A case study in the Oil and Gas Industry," *Journal of Accounting and Management Information Systems*, vol. 26, no. 2, pp. 264-289, 2021.
- [20] US Chemical Safety and Hazard Investigation Board, "Monthly incident news reports," Report No. 2001-05-1-DE, Washington DC, USA, 2002.
- [21] S. O. Clark, D. M. Deaves, I. G. Lines and L. C. Henson, "Effects of secondary containment on source Term Modeling," HSE 324/2001, USA, 2001.
- [22] E. O. Omodanisi, A. O. Eludoyin and A. T. Salami, "Ecological effects and perceptions of victims of pipeline explosion in a developing country," *International Journal of Environmental Science and Technology*, vol. 12, pp. 1635-1646, 2014.
- [23] G. M. Anderson and R. L. Lorber, SAFETY 24/7-Building an incident-free culture, 1st edition ed., Texas, USA: Design, art direction and production, 2006.
- [24] R. Klinoff, Introduction to Fire Protection and Emergency Services, USA: Jones and Bartlett Learning Press, 2019.
- [25] T. Skjold, V. Wingerden and Klees, "The investigation of an expansion in a gasoline purification plant," *Process Safety Progress*, vol. 32, no. 3, pp. 268-276, 2013.
- [26] C. D. Argyropoulos, M. N. Christolis, Z. Nivolianitou and N. C. Markatos, "A hazard assessment methodology for large liquid hydrocarbon fuel tanks," *Journal of Loss Prevention in the Process Industries*, vol. 25, pp. 329-335, 2012.
- [27] H. Persson and A. Lonnermark, "SP Report 2004: Tank fires," SP Swedish National Testing and Research Institute, Boras Sweden, 2004.
- [28] C. C. Lin, "A Safety study of Oil tank farms, M. S. thesis," National Kaohsiung first University of Science and Technology, Taiwan, 2003.

- [29] J. O. Adoghe, *Issues in Oil/Gas and Transportation Safety*, Lagos Nigeria: Omo-ojo Print & Publishers Nig. Coy, 2012.
- [30] J. A. Marc and K. E. Kakosimos, *Fires, Explosions, and Toxic Gas Dispersions: Effects Calculation and Risk Analysis*, London: CRC Press, 2010.
- [31] American Institute of Chemical Engineers, *Guidelines for Vapour cloud Explosion, Pressure vessel Burnst, BLEVE and Flash Fire Hazards*, New Jersey: A John Wiley & Sons Inc, 2010.
- [32] S. Mannan, *Lee's Loss Prevention in the Process Industries: Hazard identification, Assessment, and Control- Volume 1*, 3rd ed., USA: Elsier Inc, 2006.
- [33] A. Johnson, "Aspects of Shell's Approach to Storage Tank Fire Protection for the PearlGTL Project," Royal Dutch Shell Plc, Institute of Risk Management, Doha, 2010.
- [34] J. O. Adoghe, *Fire Protection in the Oil and Gas Industry*, Warri Nigeria: Jonokase Nig Co, 2014.
- [35] Z. Ruming, N. Baisheg, H. Xueqiu, W. Chao, Z. Caihong, D. Linchao, L. Qian, L. Xinna and L. Hailong, "Different gas explosion mechanisms and explosion suppression techniques," *Journal of Procedia Engineering*, vol. XVI, pp. 1467-1472, 2011.
- [36] M. Zhang, Z. Dou, L. Liu, J. Jiang, A. Mebarki and L. Ni, "Study of optimal layout based on integrated probabilistic framework (IPF): Case of a crude oil tank farm," *Journal of Loss Prevention in the Process Industries*, vol. 48, pp. 305-311, 2017.
- [37] L. Cai and H. Pitsch, "Mechanism optimization based on reaction rate rules," *Journal of Combustion and flame*, vol. 161, pp. 405-415, 2014.

- [38] USEPA, "Chemical Safety Alert: Catastrophic failure of storage tanks," United States Environmental Protection Agency(EPA 550-F-2021-002b), USA, 2021.
- [39] M. A. Liberman, M. Kuznetsov, A. Ivanov and I. Matsukov, "Formation of the preheated zone ahead of a propagating flame and the mechanism underlying the deflagration-to-detonation transition," *Journal of Physics Letters A*, vol. 773, pp. 501-510, 2009.
- [40] M. Kuznetsov, M. Liberman and I. Matsukov, "Experimental study of the preheated zone formation and deflagration-to-detonation transition," *Journal of Combustion Science and Technology*, vol. 182, pp. 1628-1644, 2010.
- [41] J. O. Adoghe, "Investigation into fire spread in petroleum storage tank farm Operations using CFD Simulations," M.Sc. Dissertation, UCLan, Preston, UK, 2014.
- [42] E. Ufuah and C. G. Bailey, "Flame radiation characteristics of open hydrocarbon pool fires," in *Proceedings of the World congress on Engineering*, London, UK, 2011.
- [43] W. Liu, "Numerical Investigation into deflagration and its transition to detonation in smooth tube," in *Proceedings of the European Combustion meeting, Centre for Research in fire and hazard science, University of Central Lancashire*, Preston, UK, 2015.
- [44] P. Middha, O. R. Hansen, J. Grune and A. Kotchourko, "CFD Calculations of gas leak dispersion and subsequent gas explosion: Validation against ignited impinging hydrogen jet experiments," *Journal of Hazardous Materials*, vol. 179, pp. 84-94, 2010.
- [45] G. H. Yeoh and K. K. Yeun, *Computational Fluid Dynamics in Fire Engineering-Theory, Modeling and Practice*, 2nd edition ed., London: Elsevier Academic Press, 2010.

- [46] Q. Zhang, L. Pang and H. M. Liang, "Effect of scale on the explosion of methane in and its shockwave," *Journal of Loss Prevention in the Process Industries*, vol. 24, pp. 43-48, 2011.
- [47] R. G. Gann and R. Friedman, *Principles of Fire behaviour and Combustion*, USA: NFPA Printing press, 2013.
- [48] W. Liu, "Mechanism of direct initiation of detonation," *Journal of Combustion and flamme*, vol. 159, pp. 1997-2007, 2012.
- [49] E. S.Oran and V. N. Gamezo, "Origins of the deflagration-to-detonation transitions in gas-phase combustion," *Journal of Combustion and Flame*, vol. 148, pp. 4-47, 2007.
- [50] B. E. Gelfand, M. V. Silnikov, S. P. Medvedev and S. V. Kkomik, *Thermo-Gas dynamic of hydrogen combustion and explosion*, vol. 17, New York: Springer-Verlag, 2012.
- [51] A. D. Kiverin, I. S. Yakovenko and M. F. Ivanov, "On the mechanisms and criteria of deflagration-to-detonation transition in gases," *Journal of Physics*, vol. 754, pp. 1-6, 2016.
- [52] W. Liu, "On self-sustained detonation," *Journal of Cogent Engineering*, vol. 6, pp. 1-13, 2019.
- [53] H. Chin, *Compressibility Mechanisms of Turbulent Flames and Detonations*, USA: University of Central Florida Press, 2021.
- [54] R. C. Schroll, *Industrial Fire Protection Handbook*, New York: CRC Press, 2016.
- [55] D. Razus, C. Movileanu, V. Brinzea and D. Oancea, "Explosion pressures of hydrocarbon-air mixtures in closed vessels," *Journal of Hazardous Materials*, vol. B135, pp. 58-65, 2006.

- [56] M. Reid, "The Piper Alpha Disaster: A personal perspective with Transferable Lessons on the Long-Term Moral Impact of Safety Failures," *Journal of ACS Chemical Health and Safety*, vol. 27, no. 2, pp. 73-132, 2020.
- [57] US Chemical Safety Board, "Deepwater Horizon Drilling Rig Explosion and Fire at the Macondo Well," US Chemical Safety and Hazard investigation Board, USA, 2010.
- [58] S. Whelan, "Petrobras P-36 Production Rig Explosion, Brazil," Memorial University of Newfoundland,, Canada, 2013.
- [59] S. K. Aslanov, "In the theory of blast waves," *Journal of Combustion, Explosion and shock waves*, vol. 42, pp. 450-455, 2006.
- [60] R. Dobashi, S. Kawamura, K. Kuwana and Y. Nakayama, "Consequence Analysis of blast wave from accidental gas explosions," *Proceedings of the Combustion Institute*, vol. 33, no. 2, pp. 2295-2301, 2011.
- [61] W. E. Baker, P. A. Cox, P. S. Westine, J. J. Kulesz and R. A. Strehlow, *Explosion Hazards and Evaluation*, New York: Elseir Press, 2012.
- [62] D. P. Nolan, *Handbook of fire and explosion protection Engineering principles for Oil, Gas, chemical and related facilities*, vol. 52, USA: Elsevier Publishers, 2014, pp. 1-150.
- [63] T. Tomizuka, K. Kuwana, T. Mogi, R. Dobashi and M. Koshi, "A study of numerical hazard prediction method of gas explosion," *International Journal of Hydrogen Energy*, vol. 38, no. 12, pp. 5176-5180, 2013.
- [64] Y. Zhang, J. Gong and T. Wang, "Numerical study on initiation of oblique detonations in hydrogen-air mixtures with various equivalence ratios," *Journal of Aerospace Science and Technology*, vol. 49, pp. 130-134, 2016.
- [65] S. B. Dorofeev, "Flame acceleration and explosion safety applications," *Proceedings of the Combustion Institute*, vol. 33, pp. 2161-2175, 2011.
- [66] E. V. Schwartz, *Fire and Explosion Risks: A Hand dealing with the detection, investigation and prevention of dangers arising from Fires and Explosions of*

Chemico-Technical substances and Establishments, USA: General Books LLC, 2012.

- [67] H. Ji, F.-S. Lien and E. Yee, "A new adaptive mesh refinement data structure with an application to detonation," *Journal of Computational Physics*, vol. 229, pp. 8981-8993, 2010.
- [68] C. K. Law, *Combustion Physics*, New York: University Press, 2006.
- [69] P. Clavin and B. Denet, "Decay of plane detonation waves to the self propagating Chapman-Jouguet regime," *Journal of Fluid Mechanics*, vol. 845, pp. 170-202, 2018.
- [70] G. H. Yeoh and K. K. Yuen, *Computational Fluid Dynamics in Fire Engineering: Theory, Modelling and Practice*, Second edition ed., USA: Butterworth-Heinemann, an imprint of Elsevier, 2010.
- [71] K. McGrattan, S. Hostikka, J. Floyd, H. Baum, R. Rehm, W. Mell and R. McDermott, "Fire Dynamics Simulator (Version 5) Technical Reference Guide Volume 1: Mathematical Model," NIST Special Publication 1018-5, USA, 2010.
- [72] B. S. A. Alganash, "Numerical investigation of the combustion process of various combustion regimes," University of Glasgow, UK, 2015.
- [73] J. Warnatz, U. Maas and R. W. Dibble, *Combustion: Physical and Chemical Fundamentals, Modeling and Simulations, Experiments, Pollutant Formation*, Berlin Heidelberg: Springer-Verlag, 3rd Edition, 2001.
- [74] K. K. Kuo, *Principles of Combustion*, New York: John Wiley & Sons, 2011.
- [75] W. Liu, "An Investigation into Influences of Chemical Reaction Kinetics on Self-Sustained Detonation Propagations using Direct Numerical Simulations," in *Proceedings of Centre for Research in fire and hazard science, University of Central Lancashire*, Preston, UK, 2016.

- [76] R. Deiterding, "Parallel Adaptive Simulation of multi-dimensional detonation structures," Brandenburgischen Technischen University Press, Germany, 2003.
- [77] X. Fend, Y. He and P. Huang, "A Stabilized implicit fractional θ -step method for the time-dependent Navier-Stokes equations using equal order pairs," *Journal of Mathematical Analysis and Applications*, vol. 392, pp. 209-224, 2012.
- [78] R. Deiterding, "Block-structured Adaptive mesh refinement- Theory, implementation and applications," *Journal of ESAM Proceedings*, vol. 7, pp. 1-10, 2011.
- [79] A. Dubey, M. Berzins, C. Burstedde, M. L. Norman, D. Unat and M. Wahib, "Structured Adaptive Mesh Refinement Adaptations to Retain Performance portability with increasing heterogeneity," *Journal of Computing in Science and Engineering*, vol. 23, no. 5, pp. 62-66, 2021.
- [80] O. M. Olmheim, "Analysis of AMR and other Mesh-refinement techniques for inviscid fluid problems," University of Bergen Press, Norway, 2021.
- [81] R. Deiterding, "Block-structured Adaptive mesh refinement - Theory, implementation and applications," *Journal of ESAM Proceedings*, vol. 7, pp. 1-10, 2011.
- [82] F. Loffler, Z. Cao, S. R. Brandt and Z. Du, "A new parallelization scheme for adaptive mesh refinement," *Journal of Computational Science*, vol. 16, pp. 79-88, 2016.
- [83] M. Parashar and J. C. Browne, "Systems Engineering for High Performance Computing software: The HDDA/DAGH Infrastructure for implementation of parallel structured Adaptive mesh," in *Structured Adaptive Mesh Refinement (SAMR) Grid Methods*, USA, 2000.
- [84] H. J. F.-S. Lien and E. Yee, "A new adaptive mesh refinement data structure with an application to detonation," *Journal of computational physics*, vol. 229, no. 23, pp. 8981-8993, 2010.

- [85] R. d. Levie, "The Henderson Approximation and the Mass Action Law of Guldberg and Waage," *Journal of the Chemical Educator*, vol. 7, pp. 132-135, 2002.
- [86] J. Quilez, "On the early thermodynamic and kinetic deductions of the equilibrium constant equation," *Journal of Foundation of Chemistry*, vol. 23, pp. 85-103, 2021.
- [87] R. E. Ferner and J. K. Aronson, "Cato Guldberg and Peter Waage, the history of the Law of Mass Action, and its relevance to Clinical Pharmacology," *British Journal of Clinical Pharmacology*, vol. 81, no. 1, pp. 52-55, 2016.
- [88] D. L. Reese and R. P. Steele, "Nuclear Motion in the Intramolecular Dihydrogen-Bound Regime of an Aminoborane Complex," *Journal of Physical Chemistry*, vol. 123, no. 30, pp. 6547-6563, 2019.
- [89] J. Han, J. Yu, Y. Mo, L. Jianfeng and H. Liu, "MAGE: A semantics retaining K-anonymization method for mixed data," *Journal of Knowledge-Based systems*, vol. 55, pp. 75-86, 2014.
- [90] T. B. Robertson, "Note on an Extension of the Theoretical Applicability of Guldberg and Waage's mass Law," *Journal of Physical Chemistry*, pp. 521-523, 2002.
- [91] R. Pisano, E. M. Pellegrino, A. Anakkar and M. Nagels, "Conceptual polymorphism of entropy into the history: extensions of the second law of thermodynamics towards statistical physics and chemistry during nineteenth-twentieth centuries," *Journal of Foundations of Chemistry*, vol. 23, pp. 337-378, 2021.
- [92] Keith J. Laidler, *Chemical Kinetics*, Ontario: Encyclopaedia Britannica, 2020.
- [93] J. M. Simmie, "Detailed chemical kinetic models for the combustion of hydrocarbon fuels," *Progress in Energy and Combustion Science*, vol. 29, pp. 599 - 634, 2003.

- [94] S. K. Upadhyay, *Chemical kinetics and Reaction dynamics*, India: Springer & Anamaya Publishers, 2006.
- [95] C. K. Law, *Combustion Physics*, Cambridge: Cambridge University Press, UK, 2006.
- [96] Z. Ruming, B. Nie, H. Xueqiu, W. Chao, Z. Caihong, D. Linchao, L. Qian, L. Xinna and L. Hailong, "Different gas explosion mechanisms and explosion suppression techniques," *Journal of Procedia Engineering*, vol. XVI, pp. 1467-1472, 2011.
- [97] J. Hicks, *Comprehensive Chemistry*, New York: Bright Sun Printing Press Co Ltd, 2002.
- [98] D. R. B. Jr., V. I. Babushok and J. A. Manion, "A Chemical kinetic mechanism for combustion and flame propagation of CH₂F₂/O₂/N₂ mixtures," *International Journal of Chemical Kinetics*, vol. 54, no. 3, pp. 154-187, 2022.
- [99] L. Arnaut, *Chemical Kinetics: From molecular structure to chemical reactivity*, UK: Elsevier Science, 2021.
- [100] P. Sabia and M. d. Joannon, "Critical issues of Chemical Kinetics in MILD Combustion," *Journal of frontiers in Mechanical Engineering*, vol. 6, no. 7, pp. 1-10, 2020.
- [101] A. Ushakova, V. Zatselin, M. Varfolomeev and D. Emelyanov, "Study of the radical chain mechanism of hydrocarbon oxidation for in situ combustion process," *Journal of Combustion*, vol. 2017, pp. 1-11, 2017.
- [102] A. H. Roshiko, D. F. Davidson and R. K. Hanson, "An improved H₂/O₂ mechanism based on the recent shock tube /Laser absorption measurements," *Journal of Combustion and flame*, vol. 158, no. 4, pp. 633-644, 2011.
- [103] K. C. Westbrook, W. J. Pitz, O. Herbinet, H. I. Curren and E. J. Silke, "A Comprehensive detailed chemical kinetic mechanism for combustion of n-alkane hydrocarbons from n-octane to n-hexadecane," *Journal of combustion and flame*, vol. 156, no. 1, pp. 181-190, 2009.

- [104] P. Atkins and J. d. Paula, *Physical Chemistry: Thermodynamics, Structure and Change*, UK: Oxford University Press, 2014.

Appendices

APPENDIX 1: Calculations of flame speed of H₂-O₂ of by kinetics for case studies 2, 3, 4, 5

| Case Studies | Flames | Simulation results | Calculated flame speed of H ₂ -O ₂ of by kinetics for case studies 2, 3, 4, 5 |
|----------------|--------|--|--|
| R ₂ | LF | $l_1 = 0 \text{ cm}$ $t_1 = 0 \times 10^{-4} \text{ sec}$ $c_1 = 0.000 \text{ kg/m}^3$ $=T_1 = 2800K$ | $v = \frac{l_2 - l_1}{t_2 - t_1} = \frac{0}{(0) \times 10^{-4}}$ $= 0 \text{ m/sec}$ |
| | DD | $l_1 = 32.7 \text{ cm}$ $t_1 = 0.246 \times 10^{-4} \text{ sec}$ $c_1 = 0.1021 \text{ kg/m}^3$ $T_1 = 3452K$ $l_2 = 40 \text{ cm}$ $t_2 = 0.5026 \times 10^{-4} \text{ sec}$ $c_2 = 0.01014 \text{ kg/m}^3$ $=T_2 = 3454K$ | $v = \frac{l_2 - l_1}{t_2 - t_1}$ $= \frac{40 - 32.7}{(0.5026 - 0.246) \times 10^{-4}}$ $= \frac{7.3}{0.2566 \times 10^{-4}} \text{ cm/sec}$ $= 28.4489 \times 10^4 \times 10^{-2} \text{ m/s}$ $= 28.45 \times 10^2 \text{ m/sec}$ $= 2850 = 2,850 \text{ m/sec}$ |
| R ₃ | LF | $l_1 = 0 \text{ cm}$ $t_1 = 0 \times 10^{-4} \text{ sec}$ $c_1 = 0.000 \text{ kg/m}^3$ $=T_1 = 2800K$ | $v = \frac{l_2 - l_1}{t_2 - t_1} = \frac{0}{(0) \times 10^{-4}}$ $= 0 \text{ m/sec}$ |
| | DD | $l_1 = 31.9 \text{ cm}$ $t_1 = 0.24671 \times 10^{-4} \text{ sec}$ $c_1 = 0.01019 \text{ kg/m}^3$ $T_1 = 3534K$ $l_2 = 46.9 \text{ cm}$ $t_2 = 0.771664 \times 10^{-4} \text{ sec}$ $c_2 = 0.01068 \text{ kg/m}^3$ $=T_2 = 3502K$ | $v = \frac{l_2 - l_1}{t_2 - t_1}$ $= \frac{46.9 - 31.9}{(0.771664 - 0.24671) \times 10^{-4}}$ $= \frac{15}{0.525 \times 10^{-4}} \text{ cm/s}$ $= 28.57 \times 10^4 \times 10^{-2} \text{ m/s}$ $= 28.60 \times 10^2 \text{ m/sec}$ $= 2,860 \text{ m/sec}$ |
| R ₄ | LF | $l_1 = 0 \text{ cm}$ $t_1 = 0 \times 10^{-4} \text{ sec}$ $c_1 = 0.000 \text{ kg/m}^3$ $=T_1 = 2800K$ | $v = \frac{l_2 - l_1}{t_2 - t_1} = \frac{0}{(0) \times 10^{-4}}$ $= 0 \text{ m/sec}$ |

| | | | |
|----------------|----|--|--|
| | | Calculated flame speed of H ₂ -O ₂ of by kinetics for case studies 2, 3, 4, 5 contd. | |
| | DD | $l_1 = 25\text{cm}$ $t_1 = 0.3 \times 10^{-4}\text{ sec}$ $c_1 = 0.01098\text{ kg/m}^3$ $T_1 = 2803\text{K}$ $l_2 = 30\text{ cm}$ $t_2 = 0.67 \times 10^{-4}\text{ sec}$ $c_2 = 0.01238\text{ kg/m}^3$ $=T_2 = 2700\text{ K}$ | $v = \frac{l_2 - l_1}{t_2 - t_1}$ $= \frac{30 - 25}{(0.67 - 0.3) \times 10^{-4}}$ $= \frac{5}{0.37 \times 10^{-4}}\text{ cm/s}$ $= 13.51 \times 10^4 \times 10^{-2}\text{m/s}$ $= 13.51 \times 10^2\text{ m/sec}$ $= 1351 = 1,350\text{ m/sec}$ |
| R ₅ | LF | $l_1 = 0\text{ cm}$ $t_1 = 0 \times 10^{-4}\text{ sec}$ $c_1 = 0.000\text{ kg/m}^3$ $=T_1 = 2800\text{K}$ | $v = \frac{l_2 - l_1}{t_2 - t_1} =$ $\frac{0}{(0) \times 10^{-4}}$ $= 0\text{ m/sec}$ |
| | DD | $l_1 = 29.9\text{ cm}$ $t_1 = 0.188 \times 10^{-4}\text{ sec}$ $c_1 = 0.01138\text{ kg/m}^3$ $T_1 = 3749\text{ K}$ $l_2 = 47.8\text{cm}$ $t_2 = 0.81 \times 10^{-4}\text{ sec}$ $c_2 = 0.0103\text{ kg/m}^3$ $=T_2 = 3752\text{ K}$ | $v = \frac{l_2 - l_1}{t_2 - t_1}$ $= \frac{47.8 - 29.9}{(0.81 - 0.188) \times 10^{-4}}\text{ cm/s}$ $= \frac{17.9}{(0.622) \times 10^{-4}}\text{ cm/s}$ $= 0.622 \times 10^4\text{ cm/s}$ $= 28.778 \times 10^4 \times 10^{-2}\text{m/s}$ $= 28.8 \times 10^2\text{ m/sec}$ $= 2,880\text{ m/sec}$ |

APPENDIX 2: Calculations of flame speed of H₂-O₂ of by kinetics for case studies a, b, c, d, e.

| Case Studies | Flame forms | Simulation results | Calculated flame speed of H ₂ -O ₂ of by kinetics for case studies a, b, c, d, e |
|----------------|-------------|--|--|
| R _a | LF | $l_1 = 0\text{ cm}$ $t_1 = 0 \times 10^{-4}\text{ sec}$ $c_1 = 0.000\text{ kg/m}^3$ $=T_1 = 1500\text{K}$ | $v = \frac{l_2 - l_1}{t_2 - t_1} =$ $\frac{0}{(0) \times 10^{-4}}$ $= 0\text{ m/sec}$ |

| Calculated flame speed of H ₂ -O ₂ by kinetics for case studies a, b, c, d, e contd. | | | |
|--|-----|---|--|
| | FD | $l_1 = 11.6 \text{ cm}$ $t_1 = 32.5 \times 10^{-4} \text{ sec}$ $c_1 = 0.01203 \text{ kg/m}^3$ $T_1 = 2682 \text{ K}$ $l_2 = 13 \text{ cm}$ $t_2 = 33.0 \times 10^{-4} \text{ sec}$ $c_2 = 0.01204 \text{ kg/m}^3$ $=T_2 = 2722 \text{ K}$ | $v = \frac{l_2 - l_1}{t_2 - t_1}$ $= \frac{13 - 11.6}{(33 - 32.5) \times 10^{-4}} \text{ cm/s}$ $= \frac{1.4}{(0.5) \times 10^{-4}} \text{ cm/s}$ $= 2.8 \times 10^4 \text{ cm/s}$ $= 2.8 \times 10^4 \times 10^{-2} \text{ m/s}$ $= 2.8 \times 10^2 \text{ m/sec} = 280 \text{ m/sec}$ |
| | DDT | $l_1 = 15.8 \text{ cm}$ $t_1 = 34 \times 10^{-4} \text{ sec}$ $c_1 = 0.01184 \text{ kg/m}^3$ $T_1 = 2784 \text{ K}$ $l_2 = 18 \text{ cm}$ $t_2 = 34.5 \times 10^{-4} \text{ sec}$ $c_2 = 0.01185 \text{ kg/m}^3$ $=T_2 = 2805 \text{ K}$ | $v = \frac{l_2 - l_1}{t_2 - t_1}$ $= \frac{18 - 15.8}{(34.5 - 34) \times 10^{-4}} \text{ cm/s}$ $= \frac{2.2}{(0.5) \times 10^{-4}} \text{ cm/s}$ $= 4.4 \times 10^4 \text{ cm/s}$ $= 4.4 \times 10^4 \times 10^{-2} \text{ m/s}$ $= 4.4 \times 10^2 \text{ m/sec} = 440 \text{ m/sec}$ |
| R _b | LF | $l_1 = 0 \text{ cm}$ $t_1 = 0 \times 10^{-4} \text{ sec}$ $c_1 = 0.000 \text{ kg/m}^3$ $=T_1 = 1500 \text{ K}$ | $v = \frac{l_2 - l_1}{t_2 - t_1} =$ $= \frac{0}{(0) \times 10^{-4}} \text{ cm/sec}$ $= 0 \text{ m/sec}$ |
| | FD | $l_1 = 7.5 \text{ cm}$ $t_1 = 13.5 \times 10^{-4} \text{ sec}$ $c_1 = 0.009693 \text{ kg/m}^3$ $T_1 = 2897 \text{ K}$ $l_2 = 8.6 \text{ cm}$ $t_2 = 14 \times 10^{-4} \text{ sec}$ $c_2 = 0.009607 \text{ kg/m}^3$ $=T_2 = 2901 \text{ K}$ | $v = \frac{l_2 - l_1}{t_2 - t_1}$ $= \frac{8.6 - 7.5}{(14 - 13.5) \times 10^{-4}} \text{ cm/s}$ $= \frac{1.1}{(0.5) \times 10^{-4}} \text{ cm/s}$ $= 2.2 \times 10^4 \text{ cm/s}$ $= 2.2 \times 10^4 \times 10^{-2} \text{ m/s}$ $= 2.2 \times 10^2 \text{ m/sec}$ $= 220 \text{ m/sec}$ |
| | DDT | $l_1 = 9.2 \text{ cm}$ $t_1 = 14.5 \times 10^{-4} \text{ sec}$ $c_1 = 0.01033 \text{ kg/m}^3$ $T_1 = 2905 \text{ K}$ $l_2 = 19.3 \text{ cm}$ $t_2 = 17 \times 10^{-4} \text{ sec}$ $c_2 = 0.00907 \text{ kg/m}^3$ $=T_2 = 2956 \text{ K}$ | $v = \frac{l_2 - l_1}{t_2 - t_1}$ $= \frac{19.3 - 9.2}{(17 - 14.5) \times 10^{-4}} \text{ cm/s}$ $= \frac{10.1}{(2.5) \times 10^{-4}} \text{ cm/s}$ $= 4.04 \times 10^4 \text{ cm/s}$ $= 4.04 \times 10^4 \times 10^{-2} \text{ m/s}$ $= 4.04 \times 10^2 \text{ m/sec} = 404 \text{ m/sec}$ |

| Calculated flame speed of H ₂ -O ₂ by kinetics for case studies a, b, c, d, e contd. | | | |
|--|-----|---|--|
| R _c | LF | $l_1 = 0 \text{ cm}$ $t_1 = 0 \times 10^{-4} \text{ sec}$ $c_1 = 0.000 \text{ kg/m}^3$ $=T_1 = 1500K$ | $v = \frac{l_2 - l_1}{t_2 - t_1} =$ $= \frac{0}{(0) \times 10^{-4}} \text{ cm/sec}$ $= 0 \text{ m/sec}$ |
| | FD | $l_1 = 2.3 \text{ cm}$ $t_1 = 7.5 \times 10^{-4} \text{ sec}$ $c_1 = 0.008751 \text{ kg/m}^3$ $T_1 = 2910 \text{ K}$ $l_2 = 4.4 \text{ cm}$ $t_2 = 9 \times 10^{-4} \text{ sec}$ $c_2 = 0.008954 \text{ kg/m}^3$ $=T_2 = 2928 \text{ K}$ | $v = \frac{l_2 - l_1}{t_2 - t_1}$ $= \frac{4.4 - 2.3}{(9 - 7.5) \times 10^{-4}} \text{ cm/s}$ $= \frac{2.1}{(1.5) \times 10^{-4}} \text{ cm/s}$ $= 1.4 \times 10^4 \text{ cm/s}$ $= 1.4 \times 10^4 \times 10^{-2} \text{ m/s}$ $= 1.4 \times 10^2 \text{ m/sec}$ $= 140 \text{ m/sec}$ |
| | DDT | $l_1 = 14.8 \text{ cm}$ $t_1 = 13 \times 10^{-4} \text{ sec}$ $c_1 = 0.008566 \text{ kg/m}^3$ $T_1 = 3001 \text{ K}$ $l_2 = 17.2 \text{ cm}$ $t_2 = 13.5 \times 10^{-4} \text{ sec}$ $c_2 = 0.008290 \text{ kg/m}^3$ $=T_2 = 3023 \text{ K}$ | $v = \frac{l_2 - l_1}{t_2 - t_1}$ $= \frac{17.2 - 14.8}{(13.5 - 13) \times 10^{-4}}$ $= \frac{2.4}{(0.5) \times 10^{-4}} \text{ cm/s}$ $= 4.8 \times 10^4 \times 10^{-2} \text{ m/s}$ $= 480 = 480 \text{ m/sec}$ |
| R _d | LF | $l_1 = 0 \text{ cm}$ $t_1 = 0 \times 10^{-4} \text{ sec}$ $c_1 = 0.000 \text{ kg/m}^3$ $=T_1 = 1500K$ | $v = \frac{l_2 - l_1}{t_2 - t_1} =$ $= \frac{0}{(0) \times 10^{-4}} \text{ cm/sec}$ $= 0 \text{ m/sec.}$ |
| | FD | $l_1 = 3.4 \text{ cm}$ $t_1 = 7 \times 10^{-4} \text{ sec}$ $c_1 = 0.008329 \text{ kg/m}^3$ $T_1 = 2968 \text{ K}$ $l_2 = 5.5 \text{ cm}$ $t_2 = 8 \times 10^{-4} \text{ sec}$ $c_2 = 0.008256 \text{ kg/m}^3$ $=T_2 = 2979 \text{ K}$ | $v = \frac{l_2 - l_1}{t_2 - t_1}$ $= \frac{5.5 - 3.4}{(8 - 7) \times 10^{-4}} \text{ cm/s}$ $= \frac{2.1}{(1) \times 10^{-4}} \text{ cm/s}$ $= 2.1 \times 10^4 \text{ cm/s}$ $= 2.1 \times 10^4 \times 10^{-2} \text{ m/s}$ $= 2.1 \times 10^2 \text{ m/sec}$ $= 210$ $= 210 \text{ m/sec}$ |

| Calculated flame speed of H ₂ -O ₂ by kinetics for case studies a, b, c, d, e contd. | | | |
|--|-----|---|---|
| | DDT | $l_1 = 5.5 \text{ cm}$ $t_1 = 8 \times 10^{-4} \text{ sec}$ $c_1 = 0.008256 \text{ kg/m}^3$ $T_1 = 2979 \text{ K}$ $l_2 = 19.5 \text{ cm}$ $t_2 = 11 \times 10^{-4} \text{ sec}$ $c_2 = 0.007149 \text{ kg/m}^3$ $=T_2 = 3146 \text{ K}$ | $v = \frac{l_2 - l_1}{t_2 - t_1}$ $= \frac{19.5 - 5.5}{(11 - 8) \times 10^{-4}} \text{ cm/s}$ $= \frac{14}{(3) \times 10^{-4}} \text{ cm/s}$ $= 4.67 \times 10^4 \times 10^{-2} \text{ m/s}$ $= 4.70 \times 10^2 \text{ m/sec}$ $v = 470 = 470 \text{ m/sec}$ |
| Re | LF | $l_1 = 0 \text{ cm}$ $t_1 = 0 \times 10^{-4} \text{ sec}$ $c_1 = 0.000 \text{ kg/m}^3$ $=T_1 = 1500 \text{ K}$ | $v = \frac{l_2 - l_1}{t_2 - t_1} =$ $= \frac{0}{(0) \times 10^{-4}} \text{ cm/sec}$ $= 0 \text{ m/sec.}$ |
| | FD | $l_1 = 4.4 \text{ cm}$ $t_1 = 8.5 \times 10^{-4} \text{ sec}$ $c_1 = 0.007912 \text{ kg/m}^3$ $T_1 = 3015 \text{ K}$ $l_2 = 5.8 \text{ cm}$ $t_2 = 9 \times 10^{-4} \text{ sec}$ $c_2 = 0.008256 \text{ kg/m}^3$ $=T_2 = 3031 \text{ K}$ | $v = \frac{l_2 - l_1}{t_2 - t_1}$ $= \frac{5.8 - 4.4}{(9 - 8.5) \times 10^{-4}} \text{ cm/s}$ $= \frac{1.4}{(0.5) \times 10^{-4}} \text{ cm/s}$ $= 2.8 \times 10^4 \text{ cm/s}$ $= 2.8 \times 10^4 \times 10^{-2} \text{ m/sec}$ $= 2.8 \times 10^2 \text{ m/sec} = 280 \text{ m/sec}$ |
| | DDT | $l_1 = 5.8 \text{ cm}$ $t_1 = 9 \times 10^{-4} \text{ sec}$ $c_1 = 0.007777 \text{ kg/m}^3$ $T_1 = 3031 \text{ K}$ $l_2 = 7.8 \text{ cm}$ $t_2 = 9.5 \times 10^{-4} \text{ sec}$ $c_2 = 0.007474 \text{ kg/m}^3$ $=T_2 = 3065 \text{ K}$ | $v = \frac{l_2 - l_1}{t_2 - t_1}$ $= \frac{7.8 - 5.8}{(9.5 - 9) \times 10^{-4}} \text{ cm/s}$ $= \frac{2.0}{(0.5) \times 10^{-4}} \text{ cm/s}$ $= 4.0 \times 10^4 \times 10^{-2} \text{ m/s}$ $= 4.0 \times 10^2 \text{ m/sec}$ $= 400 \text{ m/sec}$ |
| | DD | $l_1 = 10.8 \text{ cm}$ $t_1 = 10 \times 10^{-4} \text{ sec}$ $c_1 = 0.007147 \text{ kg/m}^3$ $T_1 = 3105 \text{ K}$ $l_2 = 16.8 \text{ cm}$ $t_2 = 10.5 \times 10^{-4} \text{ sec}$ $c_2 = 0.007054 \text{ kg/m}^3$ $=T_2 = 3912 \text{ K}$ | $v = \frac{l_2 - l_1}{t_2 - t_1}$ $= \frac{16.8 - 10.8}{(10.5 - 10) \times 10^{-4}} \text{ cm/s}$ $= \frac{6.0}{(0.5) \times 10^{-4}} \text{ cm/s}$ $= 12 \times 10^4 \times 10^{-2} \text{ m/s}$ $= 12.0 \times 10^2 \text{ m/sec}$ $= 1,200 \text{ m/sec.}$ |

APPENDIX 3: Calculations of flame speed of propane by kinetics for case studies 20, 21, 30, 31,40

| Case Studies | Flames | Propane Simulation results | Calculated flame speed of propane by kinetics for case studies 20, 21, 30, 31,40 |
|-----------------|--------|---|--|
| R ₂₀ | LF | $l_1 = 0 \text{ cm}$ $t_1 = 0 \times 10^{-4} \text{ sec}$ $c_1 = 0.000 \text{ kg/m}^3$ $=T_1 = 2500K$ | $v = \frac{l_2 - l_1}{t_2 - t_1} =$ $= \frac{0}{(0) \times 10^{-4}} \text{ cm/sec}$ $= 0 \text{ m/sec.}$ |
| | FD | $l_1 = 3.7 \text{ cm}$ $t_1 = 5.5 \times 10^{-4} \text{ sec}$ $c_1 = 0.002389 \text{ kg/m}^3$ $T_1 = 3377 \text{ K}$ $l_2 = 4.7 \text{ cm}$ $t_2 = 6.0 \times 10^{-4} \text{ sec}$ $c_2 = 0.002438 \text{ kg/m}^3$ $=T_2 = 3496 \text{ K}$ | $v = \frac{l_2 - l_1}{t_2 - t_1}$ $= \frac{4.7 - 3.7}{(6 - 5.5) \times 10^{-4}}$ $= \frac{1}{(0.5) \times 10^{-4}} \text{ cm/sec}$ $= 2 \times 10^4 \times 10^{-2} \text{ m/s}$ $= 2 \times 10^2 \text{ m/sec}$ $= 200 = 200 \text{ m/sec}$ |
| | DDT | $l_1 = 10 \text{ cm}$ $t_1 = 7.0 \times 10^{-4} \text{ sec}$ $c_1 = 0.0029 \text{ kg/m}^3$ $T_1 = 3105 \text{ K}$ $l_2 = 12.4 \text{ cm}$ $t_2 = 7.5 \times 10^{-4} \text{ sec}$ $c_2 = 0.002890 \text{ kg/m}^3$ $=T_2 = 3213 \text{ K}$ | $v = \frac{l_2 - l_1}{t_2 - t_1}$ $= \frac{12.4 - 10.0}{(8 - 7.5) \times 10^{-4}}$ $= \frac{2.4}{(0.5) \times 10^{-4}} \text{ cm/sec}$ $= 4.8 \times 10^4 \times 10^{-2} \text{ m/s}$ $= 4.8 \times 10^2 \text{ m/sec}$ $= 480 = 480 \text{ m/sec}$ |
| R ₂₁ | LF | $l_1 = 0 \text{ cm}$ $t_1 = 0 \times 10^{-4} \text{ sec}$ $c_1 = 0.000 \text{ kg/m}^3$ $; T_1 = 2500K$ | $v = \frac{l_2 - l_1}{t_2 - t_1} =$ $= \frac{0}{(0) \times 10^{-4}} \text{ cm/sec} = 0 \text{ m/sec.}$ |
| | FD | $l_1 = 4.5 \text{ cm}$ $t_1 = 9.5 \times 10^{-4} \text{ sec}$ $c_1 = 0.002318 \text{ kg/m}^3$ $T_1 = 3215 \text{ K}$ $l_2 = 5.7 \text{ cm}$ $t_2 = 10 \times 10^{-4} \text{ sec}$ $c_2 = 0.002461 \text{ kg/m}^3$ $=T_1 = 3221 \text{ K}$ | $v = \frac{l_2 - l_1}{t_2 - t_1}$ $= \frac{5.7 - 4.5}{(10 - 9.5) \times 10^{-4}}$ $= \frac{1.2}{(0.5) \times 10^{-4}} \text{ cm/sec}$ $= 2.4 \times 10^4 \times 10^{-2} \text{ m/s}$ $= 2.4 \times 10^2 \text{ m/sec}$ $= 240 = 240 \text{ m/sec}$ |

| Calculated flame speed of propane by kinetics for cases 20, 21, 30, 31,40 contd. | | |
|--|-----|--|
| | DDT | $l_1 = 7.2 \text{ cm}$ $t_1 = 10.5 \times 10^{-4} \text{ sec}$ $c_1 = 0.002659 \text{ kg/m}^3$ $T_1 = 3239 \text{ K}$ $l_2 = 9.6 \text{ cm}$ $t_2 = 11 \times 10^{-4} \text{ sec}$ $c_2 = 0.0029081 \text{ kg/m}^3$ $=T_1 = 3285 \text{ K}$ |
| | | $v = \frac{l_2 - l_1}{t_2 - t_1}$ $= \frac{9.6 - 7.2}{(11 - 10.5) \times 10^{-4}}$ $= \frac{2.4}{(0.5) \times 10^{-4}} \text{ cm/sec}$ $= 4.8 \times 10^4 \times 10^{-2} \text{ m/s}$ $= 4.8 \times 10^2 \text{ m/sec}$ $= 480 = 480 \text{ m/sec}$ |
| | DD | $l_1 = 9.3 \text{ cm}$ $t_1 = 11 \times 10^{-4} \text{ sec}$ $c_1 = 0.002908 \text{ kg/m}^3$ $T_1 = 3285 \text{ K}$ $l_2 = 11.8 \text{ cm}$ $t_2 = 11.5 \times 10^{-4} \text{ sec}$ $c_2 = 0.003088 \text{ kg/m}^3$ $=T_2 = 3350 \text{ K}$ |
| | | $v = \frac{l_2 - l_1}{t_2 - t_1}$ $= \frac{11.8 - 9.3}{(11.5 - 11) \times 10^{-4}}$ $= \frac{6.5}{(0.5) \times 10^{-4}} \text{ cm/s}$ $= 13.0 \times 10^4 \times 10^{-2} \text{ m/s}$ $= 13.0 \times 10^2 \text{ m/sec}$ $= 1300 \text{ m/sec}$ |
| R ₃₀ | LF | $l_1 = 0 \text{ cm}$ $t_1 = 0 \times 10^{-4} \text{ sec}$ $c_1 = 0.000 \text{ kg/m}^3$ $=T_1 = 2500 \text{ K}$ |
| | | $v = \frac{l_2 - l_1}{t_2 - t_1} =$ $= \frac{0}{(0) \times 10^{-4}} \text{ cm/sec}$ $= 0 \text{ m/sec.}$ |
| | FD | $l_1 = 1.0 \text{ cm}$ $t_1 = 2.1 \times 10^{-4} \text{ sec}$ $c_1 = 0.001856 \text{ kg/m}^3$ $T_1 = 3236 \text{ K}$ $l_2 = 1.2 \text{ cm}$ $t_2 = 2.25 \times 10^{-4} \text{ sec}$ $c_2 = 0.001876 \text{ kg/m}^3$ $=T_1 = 3235 \text{ K}$ |
| | | $v = \frac{l_2 - l_1}{t_2 - t_1}$ $= \frac{1.2 - 1.0}{(2.25 - 2.1) \times 10^{-4}}$ $= \frac{0.2}{(0.15) \times 10^{-4}} \text{ cm/sec}$ $= 1.33 \times 10^{-2} \text{ m/s}$ $= 1.33 \times 10^2 \text{ m/sec}$ $133 = 130 \text{ m/sec}$ |
| | DDT | $l_1 = 2.0 \text{ cm}$ $t_1 = 3.25 \times 10^{-4} \text{ sec}$ $c_1 = 0.002046 \text{ kg/m}^3$ $=T_1 = 3344 \text{ K}$ $l_2 = 5.3 \text{ cm}$ $t_2 = 4.0 \times 10^{-4} \text{ sec}$ $c_2 = 0.002583 \text{ kg/m}^3$ $=T_2 = 3430 \text{ K}$ |
| | | $v = \frac{l_2 - l_1}{t_2 - t_1}$ $= \frac{5.3 - 2.0}{(4.0 - 3.25) \times 10^{-4}}$ $= \frac{3.3}{(0.75) \times 10^{-4}} \text{ cm/s}$ $= 4.4 \times 10^4 \times 10^{-2} \text{ m/s}$ $= 4.4 \times 10^2 \text{ m/sec} = 440 = 440 \text{ m/sec}$ |

| Calculated flame speed of propane by kinetics for cases 20, 21, 30, 31,40 contd. | | | |
|--|-----|---|--|
| | DD | $l_1 = 10.8 \text{ cm}$ $t_1 = 4.8 \times 10^{-4} \text{ sec}$ $c_1 = 0.002804 \text{ kg/m}^3$ $=T_1 = 3344 \text{ K}$ $l_2 = 14.6 \text{ cm}$ $t_2 = 4.95 \times 10^{-4} \text{ sec}$ $c_2 = 0.004216 \text{ kg/m}^3$ $=T_2 = 3430 \text{ K}$ | $v = \frac{l_2 - l_1}{t_2 - t_1}$ $= \frac{14.6 - 10.8}{(4.95 - 4.80) \times 10^{-4}}$ $= \frac{3.8}{(0.15) \times 10^{-4}} \text{ cm/s}$ $= 25.3 \times 10^4 \times 10^{-2} \text{ m/s}$ $= 25.3 \times 10^2 \text{ m/sec}$ $= 2530 = 2530 \text{ m/sec}$ |
| R ₃₁ | LF | $l_1 = 0 \text{ cm}$ $t_1 = 0 \times 10^{-4} \text{ sec}$ $c_1 = 0.000 \text{ kg/m}^3$ $=T_1 = 2500 \text{ K}$ | $v = \frac{l_2 - l_1}{t_2 - t_1} =$ $= \frac{0}{(0) \times 10^{-4}} \text{ cm/sec}$ $= 0 \text{ m/sec.}$ |
| | FD | $l_1 = 0.85 \text{ cm}$ $t_1 = 5.45 \times 10^{-4} \text{ sec}$ $c_1 = 0.0002170 \text{ kg/m}^3$ $T_1 = 2504 \text{ K}$ $l_2 = 3 \text{ cm}$ $t_2 = 7.25 \times 10^{-4} \text{ sec}$ $c_2 = 0.001722 \text{ kg/m}^3$ $=T_1 = 3240 \text{ K}$ | $v = \frac{l_2 - l_1}{t_2 - t_1}$ $= \frac{3 - 0.85}{(7.25 - 5.45) \times 10^{-4}}$ $= \frac{2.15}{(1.8) \times 10^{-4}} \text{ cm/sec}$ $= 1.194 \times 10^{-2} \text{ m/s}$ $= 1.194 \times 10^2 \text{ m/sec}$ $119.4 = 120 \text{ m/sec}$ |
| | DDT | $l_1 = 2.1 \text{ cm}$ $t_1 = 8.2 \times 10^{-4} \text{ sec}$ $c_1 = 0.002311 \text{ kg/m}^3$ $=T_1 = 2500 \text{ K}$ $l_2 = 3.80 \text{ cm}$ $t_2 = 8.6 \times 10^{-4} \text{ sec}$ $c_2 = 0.002562 \text{ kg/m}^3$ $=T_2 = 2500 \text{ K}$ | $v = \frac{l_2 - l_1}{t_2 - t_1}$ $= \frac{3.8 - 2.1}{(8.6 - 8.2) \times 10^{-4}} \text{ cm/s}$ $= \frac{1.7}{(0.4) \times 10^{-4}} \text{ cm/s}$ $= 4.3 \times 10^4 \times 10^{-2} \text{ m/s}$ $= 4.3 \times 10^2 \text{ m/sec}$ $= 430 \text{ m/sec}$ |
| | DD | $l_1 = 10.3 \text{ cm}$ $t_1 = 9.4 \times 10^{-4} \text{ sec}$ $c_1 = 0.003521 \text{ kg/m}^3$ $=T_2 = 2500 \text{ K}$ $l_2 = 14.5 \text{ cm}$ $t_2 = 9.55 \times 10^{-4} \text{ sec}$ $c_2 = 0.003501 \text{ kg/m}^3$ $=T_2 = 2500 \text{ K}$ | $v = \frac{l_2 - l_1}{t_2 - t_1}$ $= \frac{14.5 - 10.3}{(9.55 - 9.4) \times 10^{-4}}$ $= \frac{4.2}{(0.15) \times 10^{-4}} \text{ cm/s}$ $= 28.0 \times 10^4 \times 10^{-2} \text{ m/s}$ $= 2800 = 2,800 \text{ m/sec}$ |

| Calculated flame speed of propane by kinetics for case studies 20, 21, 30, 31,40 | | | |
|--|-----|--|---|
| R ₄₀ | LF | $l_1 = 0 \text{ cm}$ $t_1 = 0 \times 10^{-4} \text{ sec}$ $c_1 = 0.000 \text{ kg/m}^3$ $=T_1 = 2500K$ | $v = \frac{l_2 - l_1}{t_2 - t_1} =$ $= \frac{0}{(0) \times 10^{-4}} \text{ cm/sec}$ $= 0 \text{ m/sec.}$ |
| | FD | $l_1 = 1.0 \text{ cm}$ $t_1 = 1.55 \times 10^{-4} \text{ sec}$ $c_1 = 0.001733 \text{ kg/m}^3$ $T_1 = 3254 \text{ K}$ $l_2 = 1.3 \text{ cm}$ $t_2 = 1.7 \times 10^{-4} \text{ sec}$ $c_2 = 0.001767 \text{ kg/m}^3$ $=T_1 = 3255 \text{ K}$ | $v = \frac{l_2 - l_1}{t_2 - t_1}$ $= \frac{1.3 - 1.0}{(1.7 - 1.55) \times 10^{-4}}$ $= \frac{0.3}{(0.15) \times 10^{-4}} \text{ cm/sec}$ $= \times 10^4 \times 10^{-2} \text{ m/s}$ $= 4.8 \times 10^2 \text{ m/sec}$ $= 480 = 480 \text{ m/sec}$ |
| | DDT | $l_1 = 10 \text{ cm}$ $t_1 = 7.5 \times 10^{-4} \text{ sec}$ $c_1 = 0.0029 \text{ kg/m}^3$ $T_1 = 3105 \text{ K}$ $l_2 = 12.4 \text{ cm}$ $t_2 = 8.0 \times 10^{-4} \text{ sec}$ $c_2 = 0.003041 \text{ kg/m}^3$ $=T_1 = 3613 \text{ K}$ | $v = \frac{l_2 - l_1}{t_2 - t_1}$ $= \frac{12.4 - 10.0}{(8 - 7.5) \times 10^{-4}}$ $= \frac{2.4}{(0.5) \times 10^{-4}} \text{ cm/sec}$ $= 2 \times 10^4 \times 10^{-2} \text{ m/s}$ $= 2 \times 10^2 \text{ m/sec}$ $= 200 = 200 \text{ m/sec}$ |
| | DD | $l_1 = 5.3 \text{ cm}$ $t_1 = 2.6 \times 10^{-4} \text{ sec}$ $c_1 = 0.002774 \text{ kg/m}^3$ $=T_1 = 4500K$ $l_2 = 11.7 \text{ cm}$ $t_2 = 2.85 \times 10^{-4} \text{ sec}$ $c_2 = 0.004744 \text{ kg/m}^3$ $=T_2 = 4500K$ | $v = \frac{l_2 - l_1}{t_2 - t_1}$ $= \frac{11.7 - 5.3}{(2.85 - 2.6) \times 10^{-4}} \text{ cm/s}$ $= \frac{6.4}{(0.25) \times 10^{-4}} \text{ cm/s}$ $= 25.6 \times 10^4 \times 10^{-2} \text{ m/s}$ $= 25.6 \times 10^2 \text{ m/sec}$ $= 2560 = 2,560 \text{ m/sec}$ |

Appendix 4: Calculated flame speed of effects of geometric configurations for cases block, step, wall

| Case Studies - H ₂ -O ₂ | Flames | Simulation results | Calculated flame speed of effects of geometric configuration on Explosion in H ₂ -O ₂ combustion |
|---|--------|--------------------|--|
| | | | |

| Calculated flame speed of effects of geometric configuration on H ₂ -O ₂ combustion for case studies block, step, wall contd. | | | |
|---|-----|---|---|
| Block | LF | $l_1 = 0 \text{ cm}$ $t_1 = 0 \times 10^{-4} \text{ sec}$ $c_1 = 0.000 \text{ kg/m}^3$ $=T_1 = 2500K$ | $v = \frac{l_2 - l_1}{t_2 - t_1} =$ $= \frac{0}{(0) \times 10^{-4}} \text{ cm/sec}$ $= 0 \text{ m/sec.}$ |
| | FD | $l_1 = 5.2 \text{ cm}$ $t_1 = 0.32 \times 10^{-4} \text{ sec}$ $c_1 = 0.007117 \text{ kg/m}^3$ $=T_1 = 4009K$ $l_2 = 5.25 \text{ cm}$ $t_2 = 0.34 \times 10^{-4} \text{ sec}$ $c_2 = 0.007454 \text{ kg/m}^3$ $=T_2 = 3994K$ | $v = \frac{l_2 - l_1}{t_2 - t_1}$ $= \frac{5.25 - 5.2}{(0.34 - 0.32) \times 10^{-4}}$ $= \frac{3.7}{(0.02) \times 10^{-4}} \text{ cm/sec}$ $= 2.5 \times 10^4 \times 10^{-2} \text{ m/s}$ $= 2.5 \times 10^2 \text{ m/sec}$ $= 250 = 250 \text{ m/sec}$ |
| | DDT | $l_1 = 6.58 \text{ cm}$ $t_1 = 0.38 \times 10^{-4} \text{ sec}$ $c_1 = 0.007132 \text{ kg/m}^3$ $=T_1 = 3988 K$ $l_2 = 6.67 \text{ cm}$ $t_2 = 0.4 \times 10^{-4} \text{ sec}$ $c_2 = 0.006800 \text{ kg/m}^3$ $=T_2 = 3982 K$ | $v = \frac{l_2 - l_1}{t_2 - t_1}$ $= \frac{6.67 - 6.58}{(0.4 - 0.38) \times 10^{-4}}$ $= \frac{0.09}{(0.02) \times 10^{-4}} \text{ cm/s}$ $= 4.5 \times 10^4 \times 10^{-2} \text{ m/s}$ $= 4.5 \times 10^2 \text{ m/sec}$ $= 450 = 450 \text{ m/sec}$ |
| | DD | $l_1 = 7.5 \text{ cm}$ $t_1 = 0.42 \times 10^{-4} \text{ sec}$ $c_1 = 0.009279 \text{ kg/m}^3$ $=T_1 = 4067 K$ $l_2 = 14.5 \text{ cm}$ $t_2 = 0.68 \times 10^{-4} \text{ sec}$ $c_2 = 0.008329 \text{ kg/m}^3$ $=T_2 = 4067 K$ | $v = \frac{l_2 - l_1}{t_2 - t_1}$ $= \frac{14.5 - 7.5}{(0.68 - 0.42) \times 10^{-4}}$ $= \frac{7.0}{(0.26) \times 10^{-4}} \text{ cm/s}$ $= 26.92 \times 10^4 \times 10^{-2} \text{ m/s}$ $= 26.92 \times 10^2 \text{ m/sec}$ $= 2692 \text{ m/sec} = 2,690 \text{ m/sec}$ |
| Step | LF | $l_1 = 0 \text{ cm}$ $t_1 = 0 \times 10^{-4} \text{ sec}$ $c_1 = 0.000 \text{ kg/m}^3$ $=T_1 = 300K$ | $v = \frac{l_2 - l_1}{t_2 - t_1} =$ $= \frac{0}{(0) \times 10^{-4}} \text{ cm/sec}$ $= 0 \text{ m/sec.}$ |

| | | | |
|--|----|--|---|
| Calculated flame speed of effects of geometric configuration on H ₂ -O ₂ combustion for cases block, step, wall contd. | | | |
| | DD | $l_1 = 4.7 \text{ cm}$ $t_1 = 0.02 \times 10^{-4} \text{ sec}$ $c_1 =$ $0.00000008493 \text{ kg/m}^3$ $=T_1 = 1341 \text{ K}$ $l_2 = 5.8 \text{ cm}$ $t_2 = 0.06 \times 10^{-4} \text{ sec}$ $c_2 = 0.009279 \text{ kg/m}^3$ $=T_2 = 3789 \text{ K}$ | $v = \frac{l_2 - l_1}{t_2 - t_1}$ $= \frac{5.8 - 4.7}{(0.06 - 0.02) \times 10^{-4}}$ $= \frac{1.1}{(0.04) \times 10^{-4}} \text{ cm/s}$ $= 27.5 \times 10^4 \times 10^{-2} \text{ m/s}$ $= 27.50 \times 10^2 \text{ m/sec}$ $= 2750 = 2,750 \text{ m/sec}$ |
| Wall | LF | $l_1 = 0 \text{ cm}$ $t_1 = 0 \times 10^{-4} \text{ sec}$ $c_1 = 0.000 \text{ kg/m}^3$ $=T_1 = 300 \text{ K}$ | $v = \frac{l_2 - l_1}{t_2 - t_1} =$ $= \frac{0}{(0) \times 10^{-4}} \text{ cm/sec}$ $= 0 \text{ m/sec.}$ |
| | DD | $l_1 = 5.7 \text{ cm}$ $t_1 = 0.01 \times 10^{-4} \text{ sec}$ $c_1 = 0.005481 \text{ kg/m}^3$ $=T_1 = 4474 \text{ K}$ $l_2 = 6.0 \text{ cm}$ $t_2 = 0.02 \times 10^{-4} \text{ sec}$ $c_2 = 0.005159 \text{ kg/m}^3$ $=T_2 = 4300 \text{ K}$ | $v = \frac{l_2 - l_1}{t_2 - t_1}$ $= \frac{6.0 - 5.7}{(0.02 - 0.01) \times 10^{-4}} \text{ cm/s}$ $= \frac{0.3}{(0.01) \times 10^{-4}} \text{ cm/s}$ $= 30 \times 10^4 \times 10^{-2} \text{ m/s}$ $= 30 \times 10^2 \text{ m/sec}$ $= 3,000 \text{ m/sec}$ |

Appendix 5: Calculated flame speed of effects of geometric configurations on Explosion for cases A, B, C.

| Case Studies - H ₂ -O ₂ | Flames | Simulation results | Calculated flame speed of effects of geometric configuration on H ₂ -O ₂ combustion for cases A, B, C. |
|---|--------|--|--|
| R _A | LF | $l_1 = 0 \text{ cm}$ $t_1 = 0 \times 10^{-4} \text{ sec}$ $c_1 = 0.000 \text{ kg/m}^3$ $=T_1 = 2,250 \text{ K}$ | $v = \frac{l_2 - l_1}{t_2 - t_1} =$ $= \frac{0}{(0) \times 10^{-4}} \text{ cm/sec}$ $= 0 \text{ m/sec.}$ |

| Calculated flame speed of effects of geometric configuration on H ₂ -O ₂ combustion for case studies A, B, C contd. | | |
|---|-----|---|
| | FD | $l_1 = 5.8 \text{ cm}$ $t_1 = 1.35 \times 10^{-4} \text{ sec}$ $c_1 = 0.01062 \text{ kg/m}^3$ $=T_1 = 3109 \text{ K}$ $l_2 = 6.3 \text{ cm}$ $t_2 = 1.65 \times 10^{-4} \text{ sec}$ $c_2 = 0.01010 \text{ kg/m}^3$ $=T_2 = 3183 \text{ K}$ |
| | | $v = \frac{l_2 - l_1}{t_2 - t_1}$ $= \frac{6.3 - 5.8}{(1.65 - 1.35) \times 10^{-4}}$ $= \frac{0.5}{(0.3) \times 10^{-4}} \text{ cm/sec}$ $= 1.667 \times 10^4 \times 10^{-2} \text{ m/s}$ $= 1.67 \times 10^2 \text{ m/sec}$ $= 167 = 170 \text{ m/sec}$ |
| | DDT | $l_1 = 6.0 \text{ cm}$ $t_1 = 1.65 \times 10^{-4} \text{ sec}$ $c_1 = 0.01010 \text{ kg/m}^3$ $=T_1 = 3243 \text{ K}$ $l_2 = 7.4 \text{ cm}$ $t_2 = 1.95 \times 10^{-4} \text{ sec}$ $c_2 = 0.009393 \text{ kg/m}^3$ $=T_2 = 3274 \text{ K}$ |
| | | $v = \frac{l_2 - l_1}{t_2 - t_1}$ $= \frac{7.4 - 6.0}{(1.95 - 1.65) \times 10^{-4}}$ $= \frac{1.4}{(0.3) \times 10^{-4}} \text{ cm/sec}$ $= 4.667 \times 10^4 \times 10^{-2} \text{ m/s}$ $= 4.67 \times 10^2 \text{ m/sec}$ $= 467 = 470 \text{ m/sec}$ |
| | DD | $l_1 = 10.5 \text{ cm}$ $t_1 = 2.15 \times 10^{-4} \text{ sec}$ $c_1 = 0.009032 \text{ kg/m}^3$ $=T_1 = 4136 \text{ K}$ $l_2 = 11.9 \text{ cm}$ $t_2 = 2.2 \times 10^{-4} \text{ sec}$ $c_2 = 0.00897 \text{ kg/m}^3$ $=T_2 = 4011 \text{ K}$ |
| | | $v = \frac{l_2 - l_1}{t_2 - t_1}$ $= \frac{11.7 - 10.5}{(2.2 - 2.15) \times 10^{-4}} \text{ cm/s}$ $= \frac{1.4}{(0.05) \times 10^{-4}} \text{ cm/s}$ $= 28 \times 10^4 \times 10^{-2} \text{ m/s}$ $= 28 \times 10^2 \text{ m/sec}$ $= 2,800 \text{ m/sec}$ |
| R _B | LF | $l_1 = 0 \text{ cm}$ $t_1 = 0 \times 10^{-4} \text{ sec}$ $c_1 = 0.000 \text{ kg/m}^3$ $=T_1 = 2,250 \text{ K}$ |
| | | $v = \frac{l_2 - l_1}{t_2 - t_1} =$ $= \frac{0}{(0) \times 10^{-4}} \text{ cm/sec}$ $= 0 \text{ m/sec.}$ |
| | FD | $l_1 = 5.5 \text{ cm}$ $t_1 = 1.45 \times 10^{-4} \text{ sec}$ $c_1 = 0.01044 \text{ kg/m}^3$ $=T_1 = 3153 \text{ K}$ $l_2 = 5.75 \text{ cm}$ $t_2 = 1.55 \times 10^{-4} \text{ sec}$ $c_2 = 0.01034 \text{ kg/m}^3$ $=T_2 = 3176 \text{ K}$ |
| | | $v = \frac{l_2 - l_1}{t_2 - t_1}$ $= \frac{5.75 - 5.5}{(1.95 - 1.65) \times 10^{-4}}$ $= \frac{0.25}{(0.1) \times 10^{-4}} \text{ cm/sec}$ $= 2.5 \times 10^4 \times 10^{-2} \text{ m/s}$ $= 2.5 \times 10^2 \text{ m/sec}$ $= 250 = 250 \text{ m/sec}$ |

| | | Calculated flame speed of effects of geometric configuration on H ₂ -O ₂ combustion for case studies A, B, C contd. | |
|----|-----|---|---|
| | DDT | $l_1 = 7.25 \text{ cm}$ $t_1 = 1.75 \times 10^{-4} \text{ sec}$ $c_1 = 0.009833 \text{ kg/m}^3$ $=T_1 = 3268 \text{ K}$ $l_2 = 7.7 \text{ cm}$ $t_2 = 1.85 \times 10^{-4} \text{ sec}$ $c_2 = 0.00953 \text{ kg/m}^3$ $=T_2 = 4012 \text{ K}$ | $v = \frac{l_2 - l_1}{t_2 - t_1}$ $= \frac{7.7 - 7.25}{(1.85 - 1.75) \times 10^{-4}}$ $= \frac{0.45}{(0.1) \times 10^{-4}} \text{ cm/s}$ $= 4.5 \times 10^4 \times 10^{-2} \text{ m/s}$ $= 4.5 \times 10^2 \text{ m/sec}$ $= 450 \text{ m/sec}$ |
| | DD | $l_1 = 9.5 \text{ cm}$ $t_1 = 1.9 \times 10^{-4} \text{ sec}$ $c_1 = 0.009443 \text{ kg/m}^3$ $=T_1 = 4202 \text{ K}$ $l_2 = 29.8 \text{ cm}$ $t_2 = 2.65 \times 10^{-4} \text{ sec}$ $c_2 = 0.008705 \text{ kg/m}^3$ $=T_2 = 3735 \text{ K}$ | $v = \frac{l_2 - l_1}{t_2 - t_1}$ $= \frac{29.8 - 9.5}{(2.65 - 1.9) \times 10^{-4}} \text{ cm/s}$ $= \frac{20.3}{(0.75) \times 10^{-4}} \text{ cm/s}$ $= 27.1 \times 10^4 \times 10^{-2} \text{ m/s}$ $= 27.1 \times 10^2 \text{ m/sec}$ $= 2,710 \text{ m/sec}$ |
| Rc | LF | $l_1 = 0 \text{ cm}$ $t_1 = 0 \times 10^{-4} \text{ sec}$ $c_1 = 0.000 \text{ kg/m}^3$ $=T_1 = 2000 \text{ K}$ | $v = \frac{l_2 - l_1}{t_2 - t_1}$ $= \frac{0}{(0) \times 10^{-4}} \text{ cm/sec}$ $= 0 \text{ m/sec.}$ |
| | FD | $l_1 = 7.3 \text{ cm}$ $t_1 = 3.65 \times 10^{-4} \text{ sec}$ $c_1 = 0.007481 \text{ kg/m}^3$ $=T_1 = 3092 \text{ K}$ $l_2 = 8.0 \text{ cm}$ $t_2 = 3.9 \times 10^{-4} \text{ sec}$ $c_2 = 0.007309 \text{ kg/m}^3$ $=T_2 = 3120 \text{ K}$ | $v = \frac{l_2 - l_1}{t_2 - t_1}$ $= \frac{8.0 - 7.3}{(3.9 - 3.65) \times 10^{-4}}$ $= \frac{1.4}{(0.25) \times 10^{-4}} \text{ cm/sec}$ $= 2.8 \times 10^4 \times 10^{-2} \text{ m/s}$ $= 2.8 \times 10^2 \text{ m/sec}$ $= 2.8 = 280 \text{ m/sec}$ |
| | DDT | $l_1 = 13.2 \text{ cm}$ $t_1 = 4.8 \times 10^{-4} \text{ sec}$ $c_1 = 0.006757 \text{ kg/m}^3$ $=T_1 = 3258 \text{ K}$ $l_2 = 14.4 \text{ cm}$ $t_2 = 5.05 \times 10^{-4} \text{ sec}$ $c_2 = 0.006564 \text{ kg/m}^3$ $=T_2 = 3303 \text{ K}$ | $v = \frac{l_2 - l_1}{t_2 - t_1}$ $= \frac{14.4 - 13.2}{(5.05 - 4.8) \times 10^{-4}}$ $= \frac{1.2}{(0.25) \times 10^{-4}} \text{ cm/s}$ $= 4.8 \times 10^4 \times 10^{-2} \text{ m/s}$ $= 4.8 \times 10^2 \text{ m/sec}$ $= 480 = 480 \text{ m/sec}$ |

| | | | |
|--|----|--|--|
| | | Calculated flame speed of effects of geometric configuration on H ₂ -O ₂ combustion for case studies A, B, C contd. | |
| | DD | $l_1 = 20.5 \text{ cm}$ $t_1 = 5.55 \times 10^{-4} \text{ sec}$ $c_1 = 0.006324 \text{ kg/m}^3$ $=T_1 = 3812 \text{ K}$ $l_2 = 49.6 \text{ cm}$ $t_2 = 6.65 \times 10^{-4} \text{ sec}$ $c_2 = 0.007291 \text{ kg/m}^3$ $=T_2 = 3689 \text{ K}$ | $v = \frac{l_2 - l_1}{t_2 - t_1}$ $= \frac{49.6 - 20.5}{(6.65 - 5.55) \times 10^{-4}} \text{ cm/s}$ $= \frac{29.1}{(1.10) \times 10^{-4}} \text{ cm/s}$ $= 26.5 \times 10^4 \times 10^{-2} \text{ m/s}$ $= 26.5 \times 10^2 \text{ m/sec}$ $= 2,650 \text{ m/sec.}$ |

Appendix 6: Calculated flame speed of geometric configuration effects for cases 20,21, 30, 30x,31,31x

| Case Studies -Propane | Flames | Simulation results | Calculated flame speed of effects of geometric configuration on Explosion in propane combustion |
|-----------------------|--------|--|--|
| R ₂₀ | LF | $l_1 = 0 \text{ cm}$ $t_1 = 0 \times 10^{-4} \text{ sec}$ $c_1 = 0.000 \text{ kg/m}^3$ $=T_1 = 3000 \text{ K}$ | $v = \frac{l_2 - l_1}{t_2 - t_1}$ $= \frac{0}{(0) \times 10^{-4}} \text{ cm/sec}$ $= 0 \text{ m/sec.}$ |
| | FD | $l_1 = 6.2 \text{ cm}$ $t_1 = 6.5 \times 10^{-4} \text{ sec}$ $c_1 = 0.002609 \text{ kg/m}^3$ $=T_1 = 3678 \text{ K}$ $l_2 = 7.7 \text{ cm}$ $t_2 = 7.0 \times 10^{-4} \text{ sec}$ $c_2 = 0.002766 \text{ kg/m}^3$ $=T_2 = 3806 \text{ K}$ | $v = \frac{l_2 - l_1}{t_2 - t_1}$ $= \frac{7.7 - 6.2}{(7.0 - 6.5) \times 10^{-4}}$ $= \frac{1.5}{(0.5) \times 10^{-4}} \text{ cm/sec}$ $= 3.0 \times 10^4 \times 10^{-2} \text{ m/s}$ $= 3 \times 10^2 \text{ m/sec}$ $= 300 = 300 \text{ m/sec}$ |
| | DDT | $l_1 = 7.7 \text{ cm}$ $t_1 = 7.0 \times 10^{-4} \text{ sec}$ $c_1 = 0.002766 \text{ kg/m}^3$ $=T_1 = 3806 \text{ K}$ $l_2 = 9.8 \text{ cm}$ $t_2 = 7.5 \times 10^{-4} \text{ sec}$ $c_2 = 0.002896 \text{ kg/m}^3$ $=T_2 = 3712 \text{ K}$ | $v = \frac{l_2 - l_1}{t_2 - t_1}$ $= \frac{9.8 - 7.7}{(7.5 - 7.0) \times 10^{-4}}$ $= \frac{2.1}{(0.5) \times 10^{-4}} \text{ cm/sec}$ $= 4.2 \times 10^4 \times 10^{-2} \text{ m/s}$ $= 4.2 \times 10^2 \text{ m/sec}$ $= 420 = 420 \text{ m/sec}$ |

| Calculated flame speed of effects of geometric configuration on H ₂ -O ₂ combustion for case studies 20, 21, 30, 30x, 31, 31x contd. | | | |
|--|-----|--|--|
| R ₂₁ | LF | $l_1 = 0 \text{ cm}$ $t_1 = 0 \times 10^{-4} \text{ sec}$ $c_1 = 0.000 \text{ kg/m}^3$ $=T_1 = 2500K$ | $v = \frac{l_2 - l_1}{t_2 - t_1}$ $= \frac{0}{(0) \times 10^{-4}} \text{ cm/sec} = 0 \text{ m/sec.}$ |
| | FD | $l_1 = 4.8 \text{ cm}$ $t_1 = 9.5 \times 10^{-4} \text{ sec}$ $c_1 = 0.002317 \text{ kg/m}^3$ $=T_1 = 3215 \text{ K}$ $l_2 = 6.0 \text{ cm}$ $t_2 = 10 \times 10^{-4} \text{ sec}$ $c_2 = 0.002453 \text{ kg/m}^3$ $=T_2 = 3223 \text{ K}$ | $v = \frac{l_2 - l_1}{t_2 - t_1}$ $= \frac{6.0 - 4.8}{(10 - 9.5) \times 10^{-4}}$ $= \frac{1.2}{(0.5) \times 10^{-4}} \text{ cm/s}$ $= 2.4 \times 10^4 \times 10^{-2} \text{ m/s}$ $= 2.4 \times 10^2 \text{ m/sec}$ $= 240 \text{ m/sec}$ |
| | DDT | $l_1 = 5.2 \text{ cm}$ $t_1 = 10 \times 10^{-4} \text{ sec}$ $c_1 = 0.002453 \text{ kg/m}^3$ $=T_1 = 3223 \text{ K}$ $l_2 = 9.3 \text{ cm}$ $t_2 = 11 \times 10^{-4} \text{ sec}$ $c_2 = 0.002876 \text{ kg/m}^3$ $=T_2 = 3237 \text{ K}$ | $v = \frac{l_2 - l_1}{t_2 - t_1}$ $= \frac{9.3 - 5.2}{(11 - 10) \times 10^{-4}}$ $= \frac{4.1}{(1.0) \times 10^{-4}} \text{ cm/sec}$ $= 4.1 \times 10^4 \times 10^{-2} \text{ m/s}$ $= 4.1 \times 10^2 \text{ m/sec} = 410 \text{ m/sec}$ |
| R ₃₀ | LF | $l_1 = 0 \text{ cm}$ $t_1 = 0 \times 10^{-4} \text{ sec}$ $c_1 = 0.000 \text{ kg/m}^3$ $=T_1 = 3000K$ | $v = \frac{l_2 - l_1}{t_2 - t_1}$ $v = \frac{l_2 - l_1}{t_2 - t_1}$ $= \frac{0}{(0) \times 10^{-4}} \text{ cm/sec}$ $= 0 \text{ m/sec.}$ |
| | FD | $l_1 = 5.5 \text{ cm}$ $t_1 = 4.0 \times 10^{-4} \text{ sec}$ $c_1 = 0.002587 \text{ kg/m}^3$ $=T_1 = 4036 \text{ K}$ $l_2 = 5.85 \text{ cm}$ $t_2 = 4.15 \times 10^{-4} \text{ sec}$ $c_2 = 0.002637 \text{ kg/m}^3$ $=T_2 = 4080 \text{ K}$ | $v = \frac{l_2 - l_1}{t_2 - t_1}$ $= \frac{5.85 - 5.5}{(4.15 - 4.0) \times 10^{-4}}$ $= \frac{0.35}{(0.15) \times 10^{-4}} \text{ cm/s}$ $= 2.3 \times 10^4 \times 10^{-2} /s$ $= 2.3 \times 10^2 \text{ m/sec} = 230$ $= 230 \text{ m/sec}$ |

| | | Calculated flame speed of effects of geometric configuration on H ₂ -O ₂ combustion for case studies 20, 21, 30, 30x, 31, 31x contd. | |
|------------------|-----|---|---|
| | DDT | $l_1 = 9.98 \text{ cm}$ $t_1 = 4.7 \times 10^{-4} \text{ sec}$ $c_1 = 0.002796 \text{ kg/m}^3$ $=T_1 = 3878 \text{ K}$ $l_2 = 10.2 \text{ cm}$ $t_2 = 4.75 \times 10^{-4} \text{ sec}$ $c_2 = 0.002834 \text{ kg/m}^3$ $=T_2 = 4453 \text{ K}$ | $v = \frac{l_2 - l_1}{t_2 - t_1}$ $= \frac{10.2 - 9.98}{(4.75 - 4.7) \times 10^{-4}}$ $= \frac{0.22}{(0.05) \times 10^{-4}} \text{ cm/sec}$ $= 4.4 \times 10^4 \times 10^{-2} \text{ m/s}$ $= 4.4 \times 10^2 \text{ m/sec}$ $= 440 = 440 \text{ m/sec}$ |
| | DD | $l_1 = 10.2 \text{ cm}$ $t_1 = 4.75 \times 10^{-4} \text{ sec}$ $c_1 = 0.002834 \text{ kg/m}^3$ $=T_1 = 4453 \text{ K}$ $l_2 = 14.2 \text{ cm}$ $t_2 = 4.9 \times 10^{-4} \text{ sec}$ $c_2 = 0.005389 \text{ kg/m}^3$ $=T_2 = 4364 \text{ K}$ | $v = \frac{l_2 - l_1}{t_2 - t_1}$ $= \frac{14.2 - 10.2}{(4.9 - 4.75) \times 10^{-4}}$ $= \frac{4.0}{(0.15) \times 10^{-4}} \text{ cm/sec}$ $= 26.667 \times 10^4 \times 10^{-2} \text{ m/s}$ $= 26.667 \times 10^2 \text{ m/sec}$ $= 2670 = 2670 \text{ m/s}$ |
| R _{30x} | LF | $l_1 = 0 \text{ cm}$ $t_1 = 0 \times 10^{-4} \text{ sec}$ $c_1 = 0.000 \text{ kg/m}^3$ $=T_1 = 3000 \text{ K}$ | $v = \frac{l_2 - l_1}{t_2 - t_1}$ $= \frac{0}{(0) \times 10^{-4}} \text{ cm/sec}$ $= 0 \text{ m/sec.}$ |
| | FD | $l_1 = 4.55 \text{ cm}$ $t_1 = 3.85 \times 10^{-4} \text{ sec}$ $c_1 = 0.002453 \text{ kg/m}^3$ $=T_1 = 3880 \text{ K}$ $l_2 = 5.0 \text{ cm}$ $t_2 = 4 \times 10^{-4} \text{ sec}$ $c_2 = 0.002587 \text{ kg/m}^3$ $=T_2 = 4035 \text{ K}$ | $v = \frac{l_2 - l_1}{t_2 - t_1}$ $= \frac{5.0 - 4.55}{(4 - 3.85) \times 10^{-4}} \text{ cm/s}$ $= \frac{0.45}{(0.15) \times 10^{-4}} \text{ cm/s}$ $= 3.0 \times 10^4 \text{ cm/s}$ $= 3.0 \times 10^4 \times 10^{-2} \text{ m/s}$ $= 3 \times 10^2 \text{ m/sec}$ $= 300 \text{ m/sec}$ |
| | DDT | $l_1 = 9.56 \text{ cm}$ $t_1 = 4.65 \times 10^{-4} \text{ sec}$ $c_1 = 0.002776 \text{ kg/m}^3$ $=T_1 = 3856 \text{ K}$ $l_2 = 9.8 \text{ cm}$ $t_2 = 4.7 \times 10^{-4} \text{ sec}$ $c_2 = 0.002796 \text{ kg/m}^3$ $=T_2 = 3878 \text{ K}$ | $v = \frac{l_2 - l_1}{t_2 - t_1}$ $= \frac{9.8 - 9.56}{(4.7 - 4.65) \times 10^{-4}}$ $= \frac{0.24}{(0.05) \times 10^{-4}} \text{ cm/s}$ $= 4.8 \times 10^4 \times 10^{-2} \text{ m/s}$ $= 480 = 480 \text{ m/sec}$ |

| | | Calculated flame speed of effects of geometric configuration on H ₂ -O ₂ combustion for case studies 20, 21, 30, 30x, 31, 31x contd. | |
|-----------------|-----|---|---|
| | DD | $l_1 = 12.4 \text{ cm}$ $t_1 = 4.75 \times 10^{-4} \text{ sec}$ $c_1 = 0.002834 \text{ kg/m}^3$ $=T_1 = 4453 \text{ K}$ $l_2 = 14.2 \text{ cm}$ $t_2 = 4.9 \times 10^{-4} \text{ sec}$ $c_2 = 0.005389 \text{ kg/m}^3$ $=T_2 = 4364 \text{ K}$ | $v = \frac{l_2 - l_1}{t_2 - t_1}$ $= \frac{14.2 - 12.4}{(4.9 - 4.75) \times 10^{-4}} \text{ cm/s}$ $= \frac{1.8}{(0.15) \times 10^{-4}} \text{ cm/s}$ $= 12 \times 10^4 \times 10^{-2} \text{ m/s}$ $= 12 \times 10^2 \text{ m/sec}$ $= 1,200 \text{ m/sec}$ |
| R ₃₁ | LF | $l_1 = 0 \text{ cm}$ $t_1 = 0 \times 10^{-4} \text{ sec}$ $c_1 = 0.000 \text{ kg/m}^3$ $=T_1 = 2500 \text{ K}$ | $v = \frac{l_2 - l_1}{t_2 - t_1}$ $v = \frac{l_2 - l_1}{t_2 - t_1}$ $= \frac{0}{(0) \times 10^{-4}} \text{ cm/sec} = 0 \text{ m/sec.}$ |
| | FD | $l_1 = 7.4 \text{ cm}$ $t_1 = 9.1 \times 10^{-4} \text{ sec}$ $c_1 = 0.002839 \text{ kg/m}^3$ $=T_1 = 3476 \text{ K}$ $l_2 = 7.55 \text{ cm}$ $t_2 = 9.15 \times 10^{-4} \text{ sec}$ $c_2 = 0.002791 \text{ kg/m}^3$ $=T_2 = 3495 \text{ K}$ | $v = \frac{l_2 - l_1}{t_2 - t_1}$ $= \frac{7.55 - 7.4}{(9.15 - 9.1) \times 10^{-4}} \text{ cm/s}$ $= \frac{0.15}{(0.05) \times 10^{-4}} \text{ cm/s}$ $= 3 \times 10^4 \text{ cm/s}$ $= 3 \times 10^4 \times 10^{-2} \text{ m/s}$ $= 3 \times 10^2 \text{ m/sec} = 300 = 300 \text{ m/sec}$ |
| | DDT | $l_1 = 8.56 \text{ cm}$ $t_1 = 9.25 \times 10^{-4} \text{ sec}$ $c_1 = 0.002839 \text{ kg/m}^3$ $=T_1 = 3521 \text{ K}$ $l_2 = 8.8 \text{ cm}$ $t_2 = 9.3 \times 10^{-4} \text{ sec}$ $c_2 = 0.002885 \text{ kg/m}^3$ $=T_2 = 3534 \text{ K}$ | $v = \frac{l_2 - l_1}{t_2 - t_1}$ $= \frac{8.8 - 8.56}{(9.3 - 9.25) \times 10^{-4}} \text{ cm/s}$ $= \frac{0.24}{(0.05) \times 10^{-4}} \text{ cm/s}$ $= 4.8 \times 10^4 \times 10^{-2} \text{ m/s}$ $= 4.8 \times 10^2 \text{ m/sec}$ $v = 480 = 480 \text{ m/sec}$ |
| | DD | $l_1 = 10 \text{ cm}$ $t_1 = 9.4 \times 10^{-4} \text{ sec}$ $c_1 = 0.002919 \text{ kg/m}^3$ $=T_1 = 4286 \text{ K}$ $l_2 = 14.45 \text{ cm}$ $t_2 = 9.55 \times 10^{-4} \text{ sec}$ $c_2 = 0.005499 \text{ kg/m}^3$ $=T_2 = 4334 \text{ K}$ | $v = \frac{l_2 - l_1}{t_2 - t_1}$ $= \frac{14.45 - 10}{(9.55 - 9.4) \times 10^{-4}} \text{ cm/s}$ $= \frac{4.45}{(0.15) \times 10^{-4}} \text{ cm/s}$ $= 29.667 \times 10^4 \times 10^{-2} \text{ m/sec}$ $= 29.667 = 2970 \text{ m/sec}$ |

| | | Calculated flame speed of effects of geometric configuration on propane combustion for case studies 20, 21, 30, 30x, 31, 31x contd. | |
|------------------|-----|--|--|
| R _{31X} | LF | $l_1 = 0 \text{ cm}$ $t_1 = 0 \times 10^{-4} \text{ sec}$ $c_1 = 0.000 \text{ kg/m}^3$ $=T_1 = 2500K$ | $v = \frac{l_2 - l_1}{t_2 - t_1}$ $= \frac{0}{(0) \times 10^{-4}} \text{ cm/sec}$ $= 0 \text{ m/sec.}$ |
| | FD | $l_1 = 5.3 \text{ cm}$ $t_1 = 8.75 \times 10^{-4} \text{ sec}$ $c_1 = 0.002566 \text{ kg/m}^3$ $=T_1 = 3377 \text{ K}$ $l_2 = 6.0 \text{ cm}$ $t_2 = 8.9 \times 10^{-4} \text{ sec}$ $c_2 = 0.002609 \text{ kg/m}^3$ $=T_2 = 3399 \text{ K}$ | $v = \frac{l_2 - l_1}{t_2 - t_1}$ $= \frac{6 - 5.3}{(8.9 - 8.75) \times 10^{-4}} \text{ cm/s}$ $= \frac{0.7}{(0.25) \times 10^{-4}} \text{ cm/s}$ $= 2.8 \times 10^4 \text{ cm/s}$ $= 2.8 \times 10^4 \times 10^{-2} \text{ m/sec}$ $= 280 \text{ m/sec}$ |
| | DDT | $l_1 = 7.0 \text{ cm}$ $t_1 = 9.1 \times 10^{-4} \text{ sec}$ $c_1 = 0.002702 \text{ kg/m}^3$ $=T_1 = 3445 \text{ K}$ $l_2 = 7.9 \text{ cm}$ $t_2 = 9.3 \times 10^{-4} \text{ sec}$ $c_2 = 0.002728 \text{ kg/m}^3$ $=T_2 = 3462 \text{ K}$ | $v = \frac{l_2 - l_1}{t_2 - t_1}$ $= \frac{7.9 - 7.0}{(9.3 - 9.1) \times 10^{-4}} \text{ cm/s}$ $= \frac{0.9}{(0.2) \times 10^{-4}} \text{ cm/s}$ $= 4.5 \times 10^4 \times 10^{-2} \text{ m/s}$ $= 4.50 \times 10^2 \text{ m/sec}$ $= 450 \text{ m/sec}$ |
| | DD | $l_1 = 8.6 \text{ cm}$ $t_1 = 9.35 \times 10^{-4} \text{ sec}$ $c_1 = 0.002762 \text{ kg/m}^3$ $=T_1 = 4239 \text{ K}$ $l_2 = 13.75 \text{ cm}$ $t_2 = 9.55 \times 10^{-4} \text{ sec}$ $c_2 = 0.004712 \text{ kg/m}^3$ $=T_2 = 4208 \text{ K}$ | $v = \frac{l_2 - l_1}{t_2 - t_1}$ $= \frac{13.75 - 8.6}{(9.55 - 9.35) \times 10^{-4}} \text{ cm/s}$ $= \frac{5.15}{(0.2) \times 10^{-4}} \text{ cm/s}$ $= 25.80 \times 10^4 \text{ cm/s}$ $= 25.80 \times 10^4 \times 10^{-2} \text{ m/sec}$ $= 2580 \text{ m/sec.}$ |

Appendix 7: Publications and Presentations

| S/No. | List of Publications |
|-------|--|
| 1 | Numerical investigation into fast deflagrations and deflagration-to-detonations in premixed gaseous H ₂ -O ₂ -N ₂ Mixtures – Joseph Adoghe ¹ , Weiming Liu ¹ , Jonathan Francis ¹ Journal of ASPCC 2019, Japan |
| 2 | Investigation into mechanisms of deflagration-to-detonation using Direct Numerical Simulations – Joseph Adoghe ¹ , Weiming Liu ¹ , Jonathan Francis ¹ and Akinola Adeniyi ¹ Journal of ICCHMT 2019, 128, 03002 (2019). Rome |
| 3 | Investigation into the propagation of fast combustion waves using Direct Numerical Simulations – Joseph Adoghe (2018). Fired-Up Programme 2018. Edinburgh, UK |
| 4 | Investigation into the propagations of fast combustion waves using Direct Numerical Simulations (Poster Presentation) – Joseph Adoghe. UCLAN Engineering EXPLO 2018. |
| 5 | Heavy-metal content of roadside gutter sediments in Ibadan, Nigeria – Joseph Adoghe ¹ ; P. C. Onianwa ¹ Journal of Environmental International, Vol. 23, No. 6, pp. 873-877. (1997). |